

***EXAMINING MECHANISMS AND FUNCTIONAL  
SIGNIFICANCE OF ADIPONECTIN STIMULATED AUTOPHAGY  
IN CARDIOMETABOLIC DISEASES***

WON SUK JAHNG

A DISSERTATION SUBMITTED TO THE FACULTY OF GRADUATE STUDIES IN  
PARTIAL FULFILMENT OF THE REQUIREMENTS OF THE DEGREE OF

**Doctor of Philosophy**

GRADUATE PROGRAM IN BIOLOGY  
YORK UNIVERSITY  
TORONTO, ONTARIO

AUGUST 2019

© Won Suk Jahng, 2019

## **ABSTRACT**

Unbalanced energy intake over expenditure causes obesity, and the prevalence and incidences of obesity have increased over last decades. People with obesity have a cluster of metabolic co-morbidities called metabolic syndrome which substantially increase the risk of diabetes and cardiovascular diseases. The pathophysiological mechanisms underlying metabolic syndrome are multifaceted and one contributing factor is altered adipokines profiles. Adiponectin is the most abundant adipokine in the circulation and a low serum adiponectin level is implicated in multiple diseases. Adiponectin acts on various tissues by improving energy metabolism and conferring protective effects. Majority of studies suggest adiponectin's beneficial effects are mediated through AMPK signaling.

AMPK is a master regulator of energy metabolism and activated upon low energy status. AMPK activates multiple cellular process to generate energy including autophagy. Autophagy is a conserved catabolic process which confers an adaptive force against stresses by mobilizing energy sources and preventing toxin accumulation. The studies presented here investigating molecular mechanism underlying adiponectin's pleiotropic effects, particularly focusing on its relation to autophagy.

In the first study, the effects of iron overload on autophagy in skeletal muscle were observed. Iron toxicity is associated with reduced circulating adiponectin level and increased the diabetes mellitus incidences. Chronic iron overload altered the autophagy regulatory signaling mTOR, which impaired autophagy lysosome reformation, a novel late stage autophagy process crucial for insulin sensitivity.

In the second and third studies, the changes in cardiac autophagy following pressure overload or myocardial infarction were monitored in mice lacking adiponectin. Adiponectin deficient mice exhibited exaggerated cardiac remodeling with evidence of autophagy impairments. With an advanced live-animal imaging system, a lower autophagy activity was observed in adiponectin knockout mice hearts after stresses. Cell culture experiments further validated that adiponectin directly stimulated autophagy flux and protected cardiomyocytes from cell death.

Taken together, the studies described here highlight that adiponectin is an important regulator of autophagy in skeletal muscle and hearts, and adiponectin signaling is a potential therapeutic target to modulate autophagy rates.

# TABLE OF CONTENTS

ABSTRACT .....	ii
LIST OF TABLES .....	vi
LIST OF FIGURES .....	vii
LIST OF ABBREVIATIONS .....	ix
CHAPTER 1: REVIEW OF LITERATURE .....	1
1.1 Metabolic Syndrome .....	1
1.2. Complications .....	1
1.2.1. Diabetes Mellitus .....	1
1.2.2. Cardiovascular Diseases .....	2
1.2.3. Iron Overload .....	3
1.3. Causes .....	3
1.3.1. Obesity .....	3
1.3.2. Leptin .....	4
1.3.3. Inflammatory Adipokines .....	4
1.4. Adiponectin .....	5
1.4.1. Diabetes Mellitus .....	5
1.4.2. Cardiovascular Disease .....	6
1.4.3. Iron Overload .....	6
1.5. Adiponectin Mechanisms of Actions .....	7
1.5.1. Structures .....	7
1.5.2. Genetic Regulations .....	8
1.5.2.1. PPAR $\gamma$ .....	8
1.5.2.2. FOXO1 .....	9
1.5.3. Adiponectin Signalling .....	10
1.5.3.1. Receptors [AdipoR1, AdipoR2, T-Cadherin] .....	10
1.5.3.2. Adaptors [APPL1, APPL2] .....	11
1.5.3.3. Signaling [PPAR $\alpha$ , AMPK] .....	12
1.6. Adiponectin Effects .....	14
1.6.1. Anti-Inflammatory .....	14

1.6.2. Anti-Diabetic .....	15
1.6.3. Cardioprotective .....	15
1.7. Autophagy .....	16
1.7.1. Definition .....	16
1.7.2. Classification .....	17
1.7.3. Process .....	17
1.7.4. Assessment .....	18
1.8. Metabolic Syndrome, Autophagy and Hypoadiponectinemia .....	20
1.9. Research Objective .....	21
CHAPTER 2: STUDY 1 .....	24
<i>“Iron Overload Inhibits Late Stage Autophagy Flux Leading to Insulin Resistance”</i>	
2.1 Abstract .....	24
2.2 Introduction .....	25
2.3 Materials and Methods .....	27
2.4 Results .....	36
2.5 Discussion .....	59
CHAPTER 3: STUDY 2 .....	62
<i>“Pressure Overload-Induced Cardiac Dysfunction in Aged Male Adiponectin Knockout Mice Is Associated with Autophagy Deficiency”</i>	
3.1 Abstract .....	62
3.2 Introduction .....	63
3.3 Materials and Methods .....	65
3.4 Results .....	70
3.5 Discussion .....	84
CHAPTER 4: STUDY 3 .....	88
<i>“Disrupted Autophagy Flux in Adiponectin Knockout Mice Exacerbates Ischemia-Induced Cardiomyocyte Cell Death”</i>	
4.1 Abstract .....	88

4.2 Introduction .....	89
4.3 Materials and Methods .....	91
4.4 Results .....	98
4.5 Discussion .....	112
CHAPTER 5: CONCLUSIONS .....	114
5.1 Summary of Research .....	114
5.2. Conclusions .....	115
5.3. Future Directions .....	116
REFERENCES .....	118
APPENDIX A: COPYRIGHT PERMISSION.....	135
APPENDIX B: REVIEW ARTICLE .....	136
APPENDIX C: STATEMENT OF CONTRIBUTION .....	147

## **LIST OF TABLES**

Table 1. Clinical Assessment of Metabolic Syndrome .....	1
Table 2. Body Mass Index Classification Set by Health Canada .....	3
Table 3. List of Primers Used in Study 1 .....	29

# LIST OF FIGURES

## CHAPTER 1

Figure 1.1 Adiponectin's biochemical property .....	8
Figure 1.2 Transcriptional regulation of adiponectin by upstream signals .....	10
Figure 1.3. Summary of Adiponectin signaling .....	14
Figure 1.4. A simplified process of autophagy .....	18
Figure 1.5. Detailed process of autophagy .....	20

## CHAPTER 2

Figure 2.1. Validation of Iron overload (IO) model and insulin resistance induction after IO in L6 muscle cells .....	46
Figure 2.2. Prevention of IO-induced insulin resistance in L6 cells with iron chelator .....	47
Figure 2.3. Iron treatment transiently induced autophagy yet led to flux inhibition at 24 h iron treatment .....	48
Figure 2.4. Chronic IO resulted in accumulation of abnormal autophagosomes despite normal proteolytic activity .....	49
Figure 2.5. Precipitous loss in autophagosome-free lysosome after IO .....	50
Figure 2.6. Iron treatment impaired mTOR restoration following autophagosomes degradation and enforced mTOR re-activation reversed autophagy defects and insulin resistance .....	51
Figure 2.7. Restoration of lysosomal pools following iron withdrawal reversed insulin resistance .....	52
Figure 2.8. Molecular mechanisms underlying IO-induced mTOR activity suppression .....	53
Figure 2.9. Molecular mechanisms underlying iron mediated mTOR suppression and restoration of lysosomal pools after iron withdrawal .....	54
Figure 2.10. Development of acute Iron Overload (IO) In Vivo model and validation of IO and insulin resistance in skeletal muscle .....	55
Figure 2.11. Evidence of ALR defects in skeletal muscles after acute IO .....	56
Figure 2.12. ALR defects in liver after iron overload .....	57
Figure 2.13. Schematic diagram of IO-mediated autophagy regulation .....	58

### CHAPTER 3

Figure 3.1. Temporal analysis of cardiac autophagy up to 3 weeks after thoracic aorta banding surgery .....	74
Figure 3.2. Development of cardiac hypertrophy after PO .....	75
Figure 3.3. Temporal analysis of progressive cardiac dysfunction up to 3 weeks after thoracic aorta banding surgery using echocardiography .....	76
Figure 3.4. Cardiac strain analysis by speckle tracking echocardiography to further investigate progressive cardiac dysfunction .....	77
Figure 3.5. Cardiac strain analysis by speckle tracking echocardiography to further investigate progressive cardiac dysfunction .....	78
Figure 3.6. Analysis of cardiac autophagy after PO in wt and Ad-KO mice .....	79
Figure 3.7. Mitochondria degradation after mTAB surgery in Ad-KO mice .....	80
Figure 3.8. Analysis of endoplasmic reticulum stress assessment after PO .....	81
Figure 3.9. Analysis of protein aggregates accumulation in heart tissue sections .....	82
Figure 3.10. Enhanced autophagic flux in H9c2 cells after treatment with fAd .....	83

### CHAPTER 4

Figure 4.1. Impaired autophagy in Ad-KO mice after ischemia .....	103
Figure 4.2. Reduced cathepsin D activity in Ad-KO mice hearts after ischemia .....	104
Figure 4.3. Exaggerated fibrosis, cell death and hypertrophy following ischemia in Ad-KO mice .....	105
Figure 4.4. Exacerbated cardiac remodeling in Ad-KO mice after ischemia .....	106
Figure 4.5. Validation of Cyto-ID and Magic Red assay to assess autophagy flux .....	107
Figure 4.6. Stimulation of autophagy flux upon adiponectin treatment .....	108
Figure 4.7. Adiponectin treatment enhanced autophagy flux in hypoxia .....	109
Figure 4.8. Adiponectin alleviates intrinsic apoptosis from mitochondria in H9c2 cells in hypoxia .....	110
Figure 4.9. AMPK- or Autophagy- inhibition abolished adiponectin's anti-apoptotic effect ...	111

## LIST OF ABBREVIATIONS

<u>Abbreviation</u>	<u>Definitions</u>
ACC	acetyl CoA carboxylase
ACO	acetyl CoA oxidase
Acrp30	adipocyte complement-related protein of 30 kDa
AdipoQ	adiponectin gene
AdipoR1	adiponectin receptor 1
AdipoR2	adiponectin receptor 2
AKT	protein kinase B
ALR	autophagy lysosome reformation
AMP	adenosine monophosphate
AMPK	AMP activated protein kinase
apM1	adipose most abundant gene transcript 1
APPL1	adaptor protein, phosphotyrosine with pH domain Leucine zipper 1
APPL2	adaptor protein, phosphotyrosine with pH domain Leucine zipper 2
ASCVD	atherosclerotic cardiovascular disease
ATG	autophagy
ATP	adenosine triphosphate
BMI	body mass index
BSA	bovine serum albumin
BW	body weight
C1q	complement component 1q
CAL	coronary artery ligation
CD36	fatty acid translocase
CHD	coronary heart disease
CMA	chaperone mediated autophagy
CPT1	carnitine palmitoyltransferase I
CQ	chloroquine
DAPI	4',6-diamidino-2-phenylindole
db/db	leptin receptor knockout mice
EF	ejection fraction

eIF2	eukaryotic initiation factor 2
eNOS	endothelial NO synthase
ER	endoplasmic reticulum
fAd	full length adiponectin
FBS	fetal bovine serum
FMT	fluorescence molecular tomography
FOXO1	forkhead box O1
FT	ferritin
gAd	globular adiponectin
GAPDH	glyceraldehyde 3-phosphate dehydrogenase
GBP-28	gelatin binding protein 28
GLUT4	glucose transporter type 4
HDL-c	high density lipoprotein cholesterol
HF	heart failure
HFD	high fat diet
HMW	high molecular weight
IGF-1	insulin like growth factor 1
IL-6	interleukin 6
IO	iron overload
Ire1 $\alpha$	inositol-requiring enzyme 1 $\alpha$
IRS1	insulin receptor substrate 1
kDa	kilo dalton
LAMP1	lysosomal-associated membrane protein 1
LC3B	microtubule-associated proteins 1A/1B light chain 3B
LIR	LC3 interacting region
LMW	low molecule weight
LV	left ventricle
MCP1	monocyte chemoattractant protein 1
MetS	metabolic syndrome
MI	myocardial infarction
MMW	middle molecular weight
mTAB	minimally invasive transverse aortic banding

mTOR	mammalian target of rapamycin
NAD	nicotinamide adenine dinucleotide
NCEP-ATP	national cholesterol education program's adult treatment panel
NF- $\kappa$ B	nuclear factor kappa-light-chain-enhancer of activated B cells
NO	nitric oxide
NTBI	non-transferrin bound labile iron
ob/ob	leptin knockout mice
p38 MAPK	p38 mitogen activated protein kinase
PAQR	progesterone and adiponectin Q receptor
PE	phosphatidylethanolamine
PGC1 $\alpha$	peroxisome proliferator-activated receptor gamma coactivator 1-alpha
PGSK	phen green SK
PPAR $\alpha$	peroxisome proliferator-activated receptor alpha
PPAR $\gamma$	peroxisome proliferator-activated receptor gamma
PPRE	peroxisome proliferator response element
PVDF	polyvinylidene difluoride
RHEB	ras homolog enriched in brain
S1P	sphingosine 1 phosphatase
S6K	ribosomal protein S6 kinase beta 1
SDS-PAGE	sodium dodecyl sulfate polyacrylamide gel electrophoresis
Sirt1	sirtuin 1
SQSTM1	sequestosome 1
T1D	type I diabetes
T2D	type II diabetes
TEM	transmission electron microscopy
TF	transferrin
TFR1	transferrin receptor 1
TG	triglycerides
TNF $\alpha$	tumor necrosis factor $\alpha$
TSC2	tuberous sclerosis complex 2
TZD	thiazolidinediones
UBD	ubiquitin binding domain

UCP	uncoupling protein I
ULK1	Unc-51 like autophagy activating kinase
UVRAG	UV radiation resistance associated gene
WHO	world health organization
WT	Wild type

# CHAPTER 1

## 1.1 Metabolic Syndrome

Metabolic syndrome (MetS) is a combination of metabolic comorbidities which increase the risk of diabetes and cardiovascular disease, and the first clinical guideline was postulated by The World Health Organization (WHO) in 1998 [1]. The most widely used criteria is defined by The National Cholesterol Education Program's Adult Treatment Panel (NCEP-ATP) III, and one is diagnosed with MetS if he or she meets at least three of the following conditions (Table 1). MetS has increased the economic burden in Canada, and it is estimated that \$4.3 billion dollars were spent annually on healthcare costs related to multitudinous pathologies [2, 3].

<b>Risk Factor</b>	<b>Defining Level</b>
<i>Abdominal obesity (Waist circumferences)</i>	
Men	> 102 cm (> 40 in)
Women	> 88 cm (> 35 in)
<i>Triglycerides (TG)</i>	≥ 150 mg/dL
<i>High Density Lipoprotein Cholesterol (HDL-c)</i>	
Men	< 40 mg/dL
Women	< 50 mg/dL
<i>Blood Pressure</i>	≥ 130 / 85 mm Hg
<i>Fasting Glucose</i>	≥ 110 mg/dL

Table 1 Clinical Assessment of Metabolic Syndrome set by NCEP-ATP III Criteria [4, 5].

## 1.2. Disease Complications

### 1.2.1. Diabetes Mellitus

Diabetes is the mishandling of serum glucose levels due to insulin deficiency (T1D, Type I Diabetes) or insulin resistance (T2D, Type II Diabetes), and people with MetS are first diagnosed as pre-diabetic, an intermediate state between normal and diabetic, clinically defined by fasting glucose (100 to 125 mg/dL). Approximately 70% of pre-diabetic patients progress toward T2D

[6] and it takes 29 months to convert toward T2D on average [7]. The incidences of T2D is five to six-fold for people with MetS [2, 5].

### *1.2.2. Cardiovascular Disease*

Every criterion for MetS independently increases the risk of atherosclerotic cardiovascular disease (ASCVD), the leading cause of death worldwide. ASCVD is primarily caused by dyslipidemia, high TG and low HDL-c levels, which promotes plaque formation and enhances a pro-thrombosis state. Blood clots following plaque rupture can narrow or block blood vessels and cause ischemic heart attack.

High blood pressure or hypertension can lead to ASCVD via vascular remodeling. Increased systemic pressure put forces on blood vessels, which undergo thickening of walls and cause ischemic diseases. On the same note, hypertension directly causes structural remodeling in the heart, known as cardiac remodeling. It is a broad term describing dynamic changes in the heart such as gene expression, cellular and molecular alterations in response to stresses. The heart initially undergoes adaptive remodeling featuring compensated hypertrophy yet converts to pathological remodelling featuring with decompensated hypertrophy, fibrosis and inflammation, which eventually causes heart failure (HF) [8].

Hyperglycemia indirectly increases the incidence of ASCVD by increasing circulating insulin levels. Sustained hyperglycemic conditions will cause the body to respond by releasing more insulin, yet people with insulin resistance can't correct hyperglycemia and respond excessively by secreting more insulin, an event referred to as "compensatory hyperinsulinemia."

Hyperinsulinemia acts on the kidney enhancing sodium re-absorption and leading to hypertension and activation renin-angiotensin system [9].

### *1.2.3. Iron Overload*

Iron is an essential element involved in multiple cellular process such as DNA synthesis and heme synthesis, and body iron level is tightly regulated. Under the conditions of excessive iron uptake or failed iron regulatory system, NTBIs (non-transferrin bound labile iron) exit out of circulation and cause toxic damage to peripheral tissues. Iron overload (IO) leads to local iron deposition in tissues, resulting in increased ferritin levels in the circulation.

Emerging evidence suggests increased serum ferritin level is strongly associated with MetS. The serum ferritin was the second strongest determinant of blood glucose next to obesity [10, 11] and IO is strongly associated with high blood pressure and high TG [12-14].

## **1.3. Causes**

### *1.3.1. Obesity*

MetS is primarily caused by caloric imbalance due to lack of physical activity [15], sedentary lifestyles [16, 17] and overnutrition [18]. Excessive energy intake over energy expenditure will be stored into body fat, and obesity is the central cause of MetS [19]. According to WHO, the incidence of obesity tripled since 1975, and the trend continuously increases worldwide. In Canada, approximately 25 % of adults are obese [20]. Obesity is defined by BMI (Body Mass Index, calculated by weight over square of height) greater than 30 kg/m<sup>2</sup>, and there are further three classes at obese depending on severity of BMI.

<b>BMI (kg / m<sup>2</sup>)</b>	<b>Category</b>
< 18.5	Underweight
18.5 – 24.9	Normal Weight
25.0 – 29.9	Overweight
30.0 – 34.9	Obese – Class I

35.0 – 39.5	Obese – Class II
≥ 40.0	Obese – Class III

Table 2. Body Mass Index Classification set by Health Canada [21].

Obesity is associated with numerous diseases including cancer, T2D, stroke, and CVD, and fat deposition in the abdominal cavity has been recognized as a distinguishing feature due to increased health risks [22, 23].

### 1.3.2. *Leptin*

Fat cells or adipocytes were traditionally considered an inert storage site for TG yet metabolic morbidities in obesity can't be solely explained by fat storage roles. In 1970s, Douglas Coleman identified the first secreted appetite mediator from two murine models, obese (ob/ob) and diabetes (db/db) mice, the first genetic models of obesity [24]. Jeffery Friedman's group successfully cloned the ob gene, encoding leptin, and found out that adipocytes are the predominant source of leptin [25]. Leptin controls the appetite by acting on receptors (expressed by db gene) in the hypothalamus, and leptin sensitivity decreased in obesity and T2D [26]. Since then, adipocytes have been more recognized as a secretory organ which releases numerous "adipo-cytokines" or "adipokines", and exerts strong hormonal effects at different tissues [27].

### 1.3.3. *Inflammatory Adipokines*

In 1993, it was first reported that adipocytes from obese animals or humans can release the pro-inflammatory cytokine TNF- $\alpha$  (Tumor Necrosis Factor Alpha), and TNF- $\alpha$  can directly impair insulin action on liver and skeletal muscles [28, 29]. Follow-up studies further identified other diabetic cytokines such as MCP-1, IL-6 from adipocytes in obesity patients or animals [30]. However, patients with lipoatrophy (adipocyte deficiency) are diabetic [31], and adipose tissue transplantation to lipoatrophic animal models reversed diabetes. Intriguingly, the same amount of adipose tissue transplantation from obese animals to lipoatrophic animal models worsened

diabetes [32, 33]. It was later found that normal adipose tissue secretes an anti-diabetic adipokine called adiponectin, and adiponectin exists at low levels in ob/ob or db/db mice. The replenishment of adiponectin in lipoatrophic animals successfully reversed diabetes [34-36].

#### **1.4. Adiponectin**

Adiponectin was independently identified by four different groups, named differently as Acrp30 [37], AdipoQ [38], GBP-28 [39], apM1 [40], and adiponectin's expression is limited to adipocytes. Adiponectin is the most abundant adipokine in the circulation (5-10  $\mu\text{g/ml}$ ) and the serum adiponectin level is inversely correlated with the degree of obesity, particularly abdominal adiposity [41, 42].

Inflammation is a key mechanism to suppress adiponectin levels, and inflammatory cytokines associated with obesity such as TNF- $\alpha$  and IL-6 downregulate adiponectin expression and secretion from adipose tissues [43, 44]. Reduced adiponectin level is strongly associated with the incidence of T2D, CVD, and IO. [45-47]

##### *1.4.1. Diabetes Mellitus*

Adiponectin's anti-diabetic effect is well established in numerous epidemiological and clinical studies. According to large-scale epidemiological studies (10,275 participants), the hazard ratios for developing diabetes mellitus was 57%, 39% and 18% for individuals in the second, third and fourth quartile of adiponectin levels [48]. Reduction in serum adiponectin level precedes T2D occurrence, and individuals with low adiponectin levels have a two-fold increase in T2D development [49, 50]. The adiponectin level is positively associated with insulin-stimulated glucose disposal rates and insulin receptor signaling in skeletal muscle [51]. In addition, serum

adiponectin level is strongly associated with beta cell function and glucose disposal rate in T1D patients as well [52, 53].

#### *1.4.2. Cardiovascular Disease*

Hypoadiponectinemia or adiponectin deficiency has been implicated in conditions of dyslipidemia and coronary heart disease (CHD). The serum adiponectin level is positively correlated with serum TG and negatively correlated with serum HDL-C [54-56]. Importantly, people in the highest quartile of adiponectin levels have a 40% lower chance of developing CHD, myocardial infarction (MI), and CHD mediated mortality compared to people in the lowest quartile [57-59].

The serum adiponectin level is also strongly associated with blood pressure. According to a large-scale epidemiological study (21,100 participants) in Japan, serum adiponectin was negatively associated with systolic and diastolic blood pressure [60]. In Hong Kong, 600 non-diabetic subjects were monitored for changes in adiponectin level and blood pressure over 5 years. The study reported people with the lowest quartile of adiponectin level had a 3-fold increased chance of developing hypertension (140/90 mm Hg) [61]. Taken together, hypoadiponectinemia is strongly associated with both ischemic and non-ischemic CVD.

#### *1.4.3. Iron Overload*

In 1989, the potential association between diabetes and serum ferritin level [62] was first reported, and emerging evidence suggests a strong association between diabetes and IO [11, 63]. Iron chelation therapy or dietary iron restriction in ob/ob mice significantly enhanced the insulin sensitivity and beta cell function [64]. IO in adipocytes reduced adiponectin expression and contributed to diabetes development [47]. Multiple clinical studies suggest IO is strongly

associated with hypoadiponectinemia [65-68], hence adiponectin is an important mediator in IO mediated metabolic dysfunctions.

## **1.5. Adiponectin Actions**

### *1.5.1. Structures*

Adiponectin is made up of 244 amino acids with a 30 kDa (kiloDaltons) of molecular weight (Fig 1.1). It is composed of signaling N-terminal hypervariable domain, collagenous domain and C-terminal catalytic globular C1q (Complement component 1q) like domain [69].

Biological adiponectin undergoes post-translational modification and oligomerization.

Adiponectin contains four lysine residues in the collagenous domain for hydroxylation and glycosylation [70]. Mutation of these residues resulted in failed oligomerization and reduced biological function by adiponectin [71].

Adiponectin oligomerization leads to formation of three isoforms: low molecular weight (LMW), middle-molecular weight (MMW) and high-molecular weight (HMW). LMW is formed with three adiponectin monomers, MMW with six monomers, HMW with twelve to eighteen monomers. The combination of LMW, MMW and HMW is referred to as full-length adiponectin (fAd), while the C-terminal globular domain is referred to as globular adiponectin (gAd). gAd can be found in circulation and its cleavage is mediated by immune cells [72, 73]. Both forms of adiponectin can exert metabolic actions such as increasing insulin sensitivity or decreasing TG in HFD (High Fat Diet) fed mice [36].

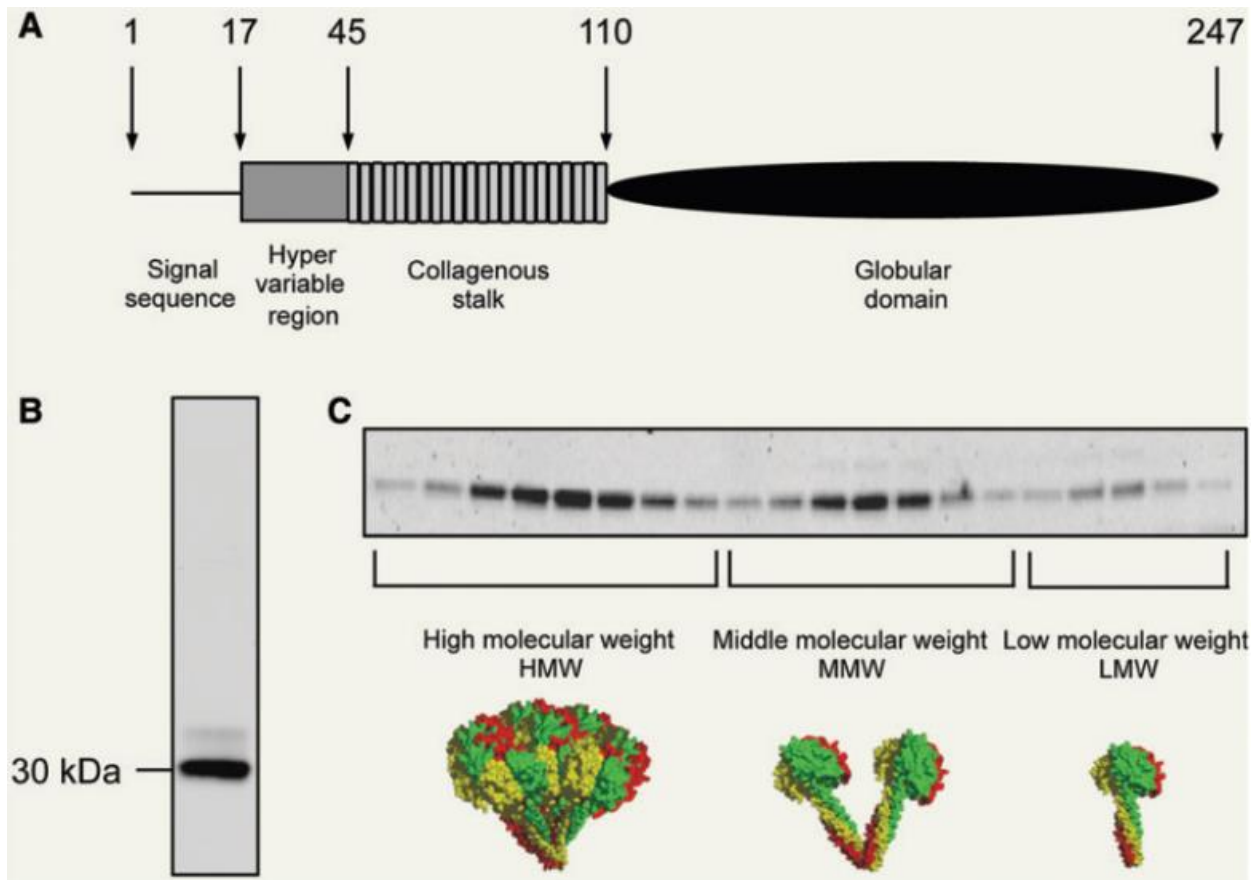


**Figure 1.1 Adiponectin's biochemical property.**

**A** adiponectin structure **B-C** adiponectin's molecular weight is 30kDa and exists in three different multimers: HMW, MMW, LMW. Adapted from Wang and Scherer [74] with copyright permission.

However, the HMW form of fAd is considered the most biologically effective form. Failure in fAd oligomerization led to insulin resistance in liver [75], and the HMW fAd level best reflects the changes in metabolic risk factors and the prevalence of diseases like diabetes and CVD in clinical settings. associated with increased obesity [46, 76, 77].

### 1.5.2. Genetic Regulations

#### 1.5.2.1. PPAR $\gamma$

PPAR $\gamma$  (Peroxisome Proliferation-Activated Receptor Gamma) is a central regulator of adipogenesis, and adiponectin transcription increases by 100 times upon adipocyte differentiation [78]. PPAR $\gamma$  directly binds to the promoter region of adiponectin, containing

PPRE (Peroxisome Proliferation Response Element) putative sites (Fig 1.2) . Adipocyte specific deletion of the PPAR $\gamma$  gene in mice resulted in decreased adiponectin levels and caused dyslipidemia and insulin resistance [79]. TZD (Thiazolidinediones) are approved drugs against T2D, and act as PPAR  $\gamma$  agonists altering transcriptions of multiple genes. Adiponectin transcription is directly stimulated by TZD, and TZD-induced adiponectin is a crucial factor to treat T2D [80, 81]. The ability of TZDs to improve insulin sensitivity is abolished in Ad-KO (Adiponectin Knock Out) mice [82].

#### 1.5.2.2. FOXO1

FOXO1 (Forkhead Box O1) is a transcription factor playing important roles in insulin action and adipogenesis [83]. It undergoes various post-translational modifications such as phosphorylation or de-acetylation which controls its sub-cellular localization and transcriptional activity of FOXO1. FOXO1 phosphorylation is mainly mediated by insulin or IGF-1 (Insulin-like Growth Factor 1) and decreased transcriptional activity by cytosolic localization of FOXO1 [84]. On the other hand, FOXO1 de-acetylation is mainly mediated by NAD (Nicotinamide Adenine Dinucleotide) dependent de-acetylase SIRT1 (Sirtuin 1) and increased transcriptional activity by nuclear localization of FOXO1 [85]. Resveratrol, a natural polyphenol compound found in red wine, enhances FOXO1 activity via increasing SIRT1 expression, which also enhances adiponectin expression [86]. Transgenic SIRT1 overexpressing mice improved metabolic profiles and prevents diabetes by increased adiponectin levels while knockdown of FOXO1 decreased adiponectin expression and worsened the metabolic profiles response after high fat diet challenge [86, 87].

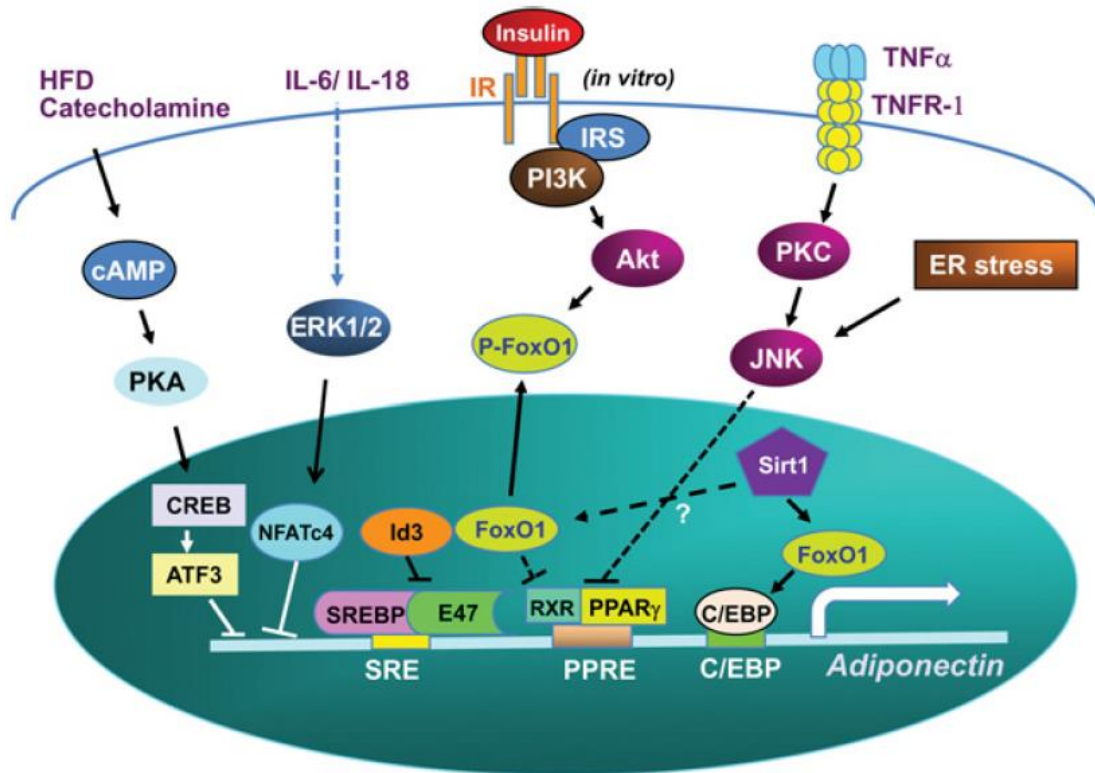


**Figure 1.2 Transcriptional regulation of adiponectin by upstream signals.**

The schematic diagram of adiponectin expression regulation by different transcription factors. The detailed transcriptional mechanism by other factors besides PPAR $\gamma$  and FOXO1 is Liu and Liu [88].

### 1.5.3. Adiponectin Signalling

#### 1.5.3.1. Receptors [AdipoR1, AdipoR2, T-Cadherin]

Adiponectin receptors, AdipoR1 and AdipoR2 (Adiponectin Receptor 1 and Adiponectin Receptor 2), were first cloned by the Kadowaki groups in Japan, and are integral membrane proteins with seven transmembrane domains belong to the PAQR (Progesterone and Adiponectin Q Receptor) family [89]. The expression of AdipoR1 and AdipoR2 are regulated by FOXO1. Incubation of hepatocytes or myocytes with insulin resulted in reductions in AdipoR1 and AdipoR2 expression, and ob/ob mice with hyperinsulinemia had lower adipoR1 and adipoR2 expression [90, 91].

Both forms of receptors are ubiquitously expressed in different tissues. AdipoR1 is highly expressed in skeletal muscle and AdipoR2 is highly expressed in liver [89]. AdipoR1 has stronger binding affinity for gAd while AdipoR2 has equal binding affinity for fAd and gAd [89]. Both receptors are essential in conveying adiponectin's metabolic effects. AdipoR1 activates AMPK signaling, enhancing glucose uptake, fatty acid oxidation, mitochondrial function, and increasing type 1 skeletal muscle fiber abundance. AdipoR2 enhances PPAR $\alpha$  activity, which facilitates lipid metabolism and inhibits gluconeogenesis in liver [92]. When AdipoR1 and AdipoR2 were over-expressed in ob/ob mice, AMPK and PPAR $\alpha$  activities were enhanced, ameliorating diabetic and atherosclerotic conditions in ob/ob mice. On the other hand, simultaneous deletion of AdipoR1 and AdipoR2 resulted in increased TG, inflammation, and insulin resistance [92].

T-cadherin is an unconventional adiponectin receptor, reported to have binding affinity for HMW and MMW fAd [93]. T-cadherin is a member of the cadherin cell adhesion molecules, which has no transmembrane or cytoplasmic domains to transmit signaling. T-cadherin is highly expressed in the heart and blood vessels, and T-cadherin deficient mice failed to activate adiponectin-dependent AMPK signaling, resulting in severe cardiac dysfunction after pressure overload or myocardial infarction [94].

#### 1.5.3.2. Adaptors [APPL1, APPL2]

APPL1 (Adaptor protein, Phospho-tyrosine interacting with pH domain Leucine zipper 1) is an adaptor protein that directly binds to AdipoR1 and transmits adiponectin signaling. APPL1 activates adiponectin mediated downstream signaling, AMPK and p38 MAPK (Mitogen Activated Protein Kinase), which enhanced glucose uptake in skeletal muscle by locating GLUT4 on all membranes [95, 96]. Mechanistically, APPL1 translocates LKB1 (Liver Kinase

B1) to the cytoplasm from the nucleus, which activates AMPK by phosphorylation at position T172. Over-expression of APPL1 enhanced adiponectin-stimulated AMPK activation while APPL1 downregulation reduced adiponectin-stimulated AMPK activation [97, 98]. APPL1 knockout mice showed insulin resistance [97], and transgenic APPL1 overexpressing mice showed better insulin sensitivity and reduced hepatic gluconeogenesis [99, 100].

APPL2 (Adaptor protein, Phospho-tyrosine interacting with pH domain Leucine zipper 2) is an adaptor protein and has 54% amino acid sequence homology to APPL1. It forms a dimer with APPL1, and the APPL1-APPL2 complex competitively inhibits the AdipoR1-APPL1 interaction. APPL2 downregulation resulted in enhanced adiponectin stimulated signaling, glucose uptake and fatty acid oxidation [101]. On the other hand, APPL2 over-expression resulted in reduced insulin stimulated glucose clearance [102].

#### 1.5.3.3. Signaling [PPAR $\alpha$ , AMPK]

The major signaling pathways activated by adiponectin are PPAR $\alpha$  and AMPK (Fig 1.3). PPAR $\alpha$  is a nuclear receptor protein, a member of the PPAR transcription factor family, and plays a central role in lipid metabolism. PPAR $\alpha$  is activated under energy deprived conditions and stimulates fatty acid oxidation to refuel energy systematically [103]. Synthetic PPAR  $\alpha$  agonists effectively lower serum TG and raise HDL-c, and they have been routinely used to treat dyslipidemia in clinical settings [104].

PPAR $\alpha$  regulates gene transcription involved in lipid metabolism. Adiponectin injection or transgenic adiponectin over-expressing mice have higher PPAR $\alpha$  activity, which resulted in CD36 overexpression, enhancing fatty acids uptake [36]. Adiponectin treatment enhanced expression of PPAR $\alpha$  target genes such as ACO (Acetyl CoA oxidase), CPT1 (carnitine palmitoyltransferase 1), and UCP (uncoupling protein), which are involved in acetyl co-A

formation and mitochondrial fatty acid beta oxidation [105]. Adiponectin deficient mice have lower hepatic insulin sensitivity and a reduced response to PPAR $\alpha$  agonists [82].

AMPK is an energy sensor molecule and plays a central role in energy homeostasis. AMPK is activated upon increased AMP to ATP ratios when energy is used up. Activation of AMPK inhibits ATP catabolism and enhances ATP production by mobilizing energy sources [106], and phosphorylation of AMPK $\alpha$  subunit at T172 position activates downstream signaling pathways to improve energy status [107].

Adiponectin phosphorylates AMPK T172 via LKB cytosolic translocation [97]. Adiponectin injection or transgenic adiponectin overexpressing mice showed robustly enhanced AMPK phosphorylation in skeletal muscle and liver, and adiponectin knockout mice had lower AMPK activity [36, 108]. Phosphorylated AMPK suppresses lipogenesis-associated genes and enhances fatty acid oxidation by inhibiting ACC (Acetyl-CoA Carboxylase) activity [109-111]. AMPK also promotes p38 MAPK mediated GLUT4 translocation and enhances glucose uptake [95, 96, 105]. Adiponectin stimulated AMPK increases NO (nitric oxide) production via activating eNOS (endothelial NO synthase). NO ameliorates pro-atherosclerotic status by reducing inflammation and promoting vasodilation at vessels [112, 113]. Adiponectin stimulated AMPK enhances SIRT1 activity by increasing NAD to NADH ratios, and SIRT1 activates PGC-1 $\alpha$  expression [114]. PGC-1 $\alpha$  is a master regulator of mitochondria biogenesis, and the suppression of adiponectin action resulted in decreased exercise endurance due to reduced mitochondrial content and oxidative type I myofibers [115, 116]. Taken together, AMPK confers adiponectin's metabolic improvement (Fig 1.3).

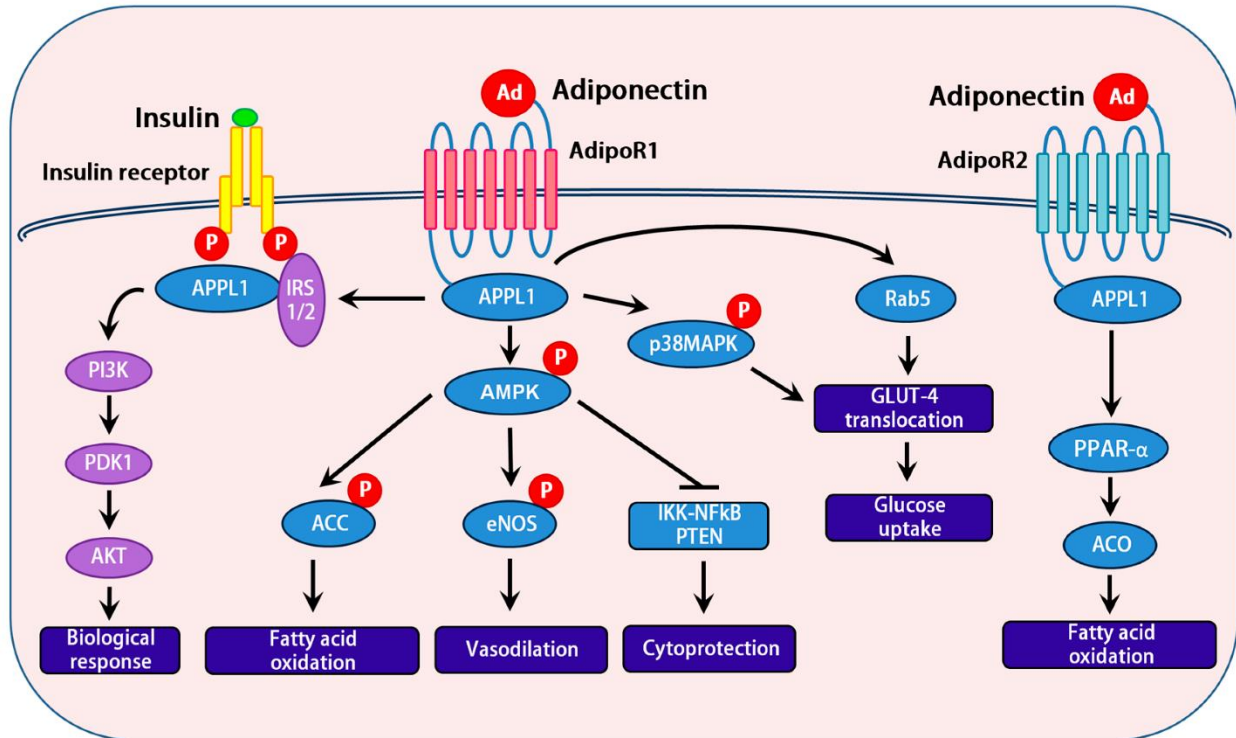


**Figure 1.3. Summary of Adiponectin signaling.** Schematic representation of adiponectin signaling transduction system. The figure is adapted from Achari and Jain [117].

## 1.6. Adiponectin Effects

### 1.6.1. Anti-Inflammatory

The circulating adiponectin level is strongly associated with the degree of inflammation. The serum adiponectin level is inversely correlated with key inflammatory cytokines such as c-reactive proteins and IL-6, IL-18 levels [118, 119]. Ad-KO mice had increased TNF $\alpha$ , IL-6, and MCP-1 levels [120, 121] while enhancing adiponectin levels by TZD decreased IL-6, TNF $\alpha$ , and MCP-1 levels [122]. When ob/ob mice were crossed with transgenic adiponectin overexpressing mice, their weight did not decrease, but metabolic profiles improved with decreased inflammatory cytokines [123]. In cell culture experiments, adiponectin promoted macrophage polarization from the pro-inflammatory phenotype M1 to the anti-inflammatory phenotype M2, which secretes anti-inflammatory cytokines such as Arginase-1 and IL-10 [121].

### *1.6.2. Anti-Diabetic*

Adiponectin's anti-diabetic effect is well established and adiponectin reduces the incidences of both forms of diabetes, T1D and T2D. Serum adiponectin level is strongly associated with beta cell function in T1D patients [52, 53], and adiponectin protects beta cells from cell death by lipotoxicity via enhancing S1P (Sphingosine 1 Phosphatase) activity [123-125].

Adiponectin enhances insulin mediated glucose clearance to ensure normal insulin sensitivity. Ad-KO mice showed lower insulin stimulated glucose and fatty acid clearance [120, 126], while adiponectin replenishment restored insulin sensitivity [36, 120, 127, 128]. In cultured cells, adiponectin treatment stimulated GLUT4 translocation to the membrane and enhanced fatty acid oxidation via the AMPK pathway [95, 96, 105]. Blocking AMPK activity compromised adiponectin's anti-diabetic effects [109].

Adiponectin regulates serum glucose levels by blocking hepatic glucose production. Injection of adiponectin in ob/ob mice resulted in blood glucose reduction not owing to increased insulin levels. In liver, adiponectin robustly suppressed gluconeogenesis [129]. Adiponectin treatment of primary hepatocytes reduced glucose synthesis by suppressing gluconeogenesis enzymes expression [75, 130], and this was dependent on AMPK signaling. When LKB1 was knocked out in liver, it impaired adiponectin mediated regulation of gluconeogenic gene expression. [109, 131].

### *1.6.3. Cardioprotective*

Cardioprotective effects by adiponectin have been noted in multiple studies. Low serum adiponectin level is strongly associated with dyslipidemia and incidence of coronary heart disease [55-59, 132]. Adiponectin exerts strong lipid clearance effects by enhancing lipoprotein lipase activity and fatty oxidation [72, 108]. Adiponectin supplementation protected from

atherosclerosis by reducing endothelial inflammation and inflammatory cytokine levels while adiponectin deficiency increased atherosclerosis events due to arterial wall thickening by oxidative stress and inflammation [133-136].

Adiponectin directly acts on the heart and confers anti-hypertrophic and anti-apoptotic effects via the AMPK pathway. Pharmacological or genetic overexpression of adiponectin protected HFD mediated cardiac hypertrophy and cardiac dysfunction [137]. Angiotensin-II infused or pressure overload induced hypertrophy was exacerbated in Ad-KO mice, while adiponectin replenishment reversed hypertrophy by enhancing angiogenesis, ameliorating oxidative stress, and suppressing hypertrophy related gene expression via the AMPK pathway [138-142].

Adiponectin-AMPK mediated ROS regulation is a key mechanism to enhance cardiomyocyte survival. Ad-KO mice developed greater injury after surgical myocardial infarction due to diminished AMPK dependent angiogenesis and increased endothelial oxidative stress [143-146]. On the other hand, adiponectin administration protected hearts from various stresses by enhancing antioxidant activity and decreasing inflammation in the heart [125, 147, 148]. In cultured cell experiments, adiponectin enhanced cell survival via the AMPK pathway [149, 150].

## **1.7. Autophagy**

### *1.7.1. Definition*

Autophagy or self-eating is an evolutionarily conserved mechanism for bulk degradation of protein aggregates or organelles by transporting them to lysosomes (Fig 1.4). It was first reported by Christian de Duve in 1967 when he observed the degraded intracellular structures within lysosomes in rat livers [151]. Dr. Yoshinori Oshumi characterized the morphology and key genes involved in autophagy [152], and he won a Nobel Prize in Physiology or Medicine in 2016 for

his discoveries of autophagy mechanisms. Autophagy is implicated in a broad range of diseases and is essential for cellular homeostasis [153].

### *1.7.2. Classifications*

Autophagy is classified into three types (Macroautophagy, Microautophagy and Chaperone Mediated Autophagy, CMA) depending on delivery methodologies. Macroautophagy delivers targets by encapsulating them into double membraned vesicles, called autophagosomes, delivered to and fused with lysosomes for degradation. Microautophagy occurs by direct engulfment of targets via invagination of lysosomal membranes and degraded at lysosomes. In CMA, targets are translocated across the lysosomal membranes via chaperon proteins which unfold and degrade targets within lysosomes [154].

### *1.7.3. Autophagy Process*

Autophagy occurs by multiple steps, regulated by different signaling and autophagy proteins (Fig 1.5). Autophagy initiates by pinching small portions of double lipid layers membranes called phagophores from ER (Endoplasmic Reticulum), Trans-Golgi or endosomes, which get separated from their sources and elongated until they are enclosed to become a ring-like structure called an autophagosomes [155, 156]. In the stage of phagophore elongation, autophagosomes recognize the target by adaptor proteins, and the name of autophagy is called differently depending on targets such as mitophagy for mitochondria, lipophagy for lipid, or ERphagy for ER. Once autophagosomes are loaded, they fuse with lysosomes, becoming autophago-lysosomes, a transient single membraned structures that degrade targets with lysosomal proteolytic enzymes. Once degraded, products or amino acids are released and re-fuel the cell [156].

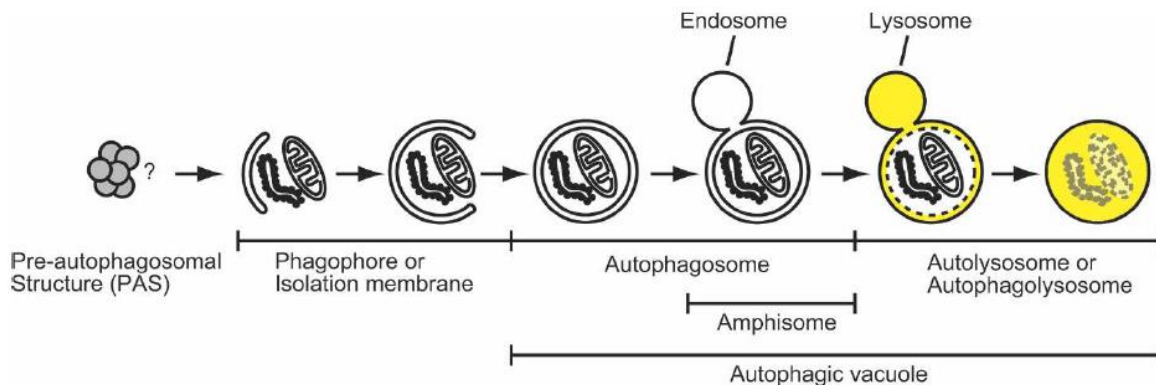


**Figure 1.4. A simplified process of autophagy.** Phagophores are generated from double lipid membrane sources, which continuously elongated to encapsulate cargo targets, becoming autophagosomes. Autophagosomes are fused with lysosomes for degradation. Adapted from Mizushima [156]

#### 1.7.4. Assessments

##### *Autophagy Induction*

Autophagy induction starts from ATG1 or ULK1/2, a serine/threonine kinase, the most upstream component of autophagy machinery (Fig 1.5). ATG1 or ULK1/2 forms a complex with ATG13 or mATG13 and ATG17 or FIP200, and this complex induces phagophore formation [157].

Depending on cellular energy status, two counteracting signaling molecules, mTOR and AMPK, regulate ULK1 complex formation and control autophagy induction.

mTOR, mammalian target of rapamycin, is a member of the PI3 kinase signaling pathways and regulates multiple processes such as cell growth, proliferation, and survival. It is composed of two complex units: mTORC1 and mTORC2. mTORC1 is activated by cellular nutrients such as amino acids and inhibits autophagy induction by phosphorylating ATG13 and ULK1 to disrupt ATG1-ATG13-ATG17 or ULK1/2-ATG17-FIP200 complex [158, 159].

AMPK, as described earlier, is activated upon energy deprived condition, which initiates autophagic catabolism to re-fuel the system to restore ATP. AMPK directly phosphorylates ULK1 to promote complex formation and induces autophagy [160, 161].

### *Autophagosome formation*

Ubiquitination is a central process in the autophagy process, and there are two ubiquitin like systems: ATG5-ATG12 conjugation and LC3 processing. The former complex serves as a final ubiquitinating enzyme for LC3 processing. ATG12 is conjugated to ATG5 by ATG7 and ATG10, and ATG5-ATG12 forms a complex with ATG16L, which process LC3B to induce phagophore elongation. LC3B, microtubule-associated protein light chain 3, is processed from LC3B-I to LC3B-II during autophagosome formation. LC3B is ubiquitously expressed in most cell types and undergoes proteolytic cleavage to generate LC3B-I by ATG4 upon autophagy induction. Activated LC3B-I is transferred to ATG3 and phosphatidylethanolamine (PE) is conjugated to generate LC3-II. LC3-II is integrated on growing autophagosomes and the conversion of LC3-I to LC3-II is used as a marker protein for autophagosomes [162].

### *Cargo Degradation*

Autophagy was initially viewed as a random degradation of cytosolic compartments, yet growing evidence suggests that autophagy degradation can be selective. Multiple “adaptor” molecules were identified which guide targets for autophagy degradation. p62 or SQSTM1 is a multi-functional adaptor protein which recognizes poly-ubiquitinated targets by binding to UBD (ubiquitin binding domain) and connects to LIR (LC3-interacting region) in autophagosome [163, 164]. p62 is generally used as an indicator of autophagy flux or autophagosome turnover. When the key autophagy genes such as ATG5 or ATG7 is deleted, p62 levels increased [165-167].

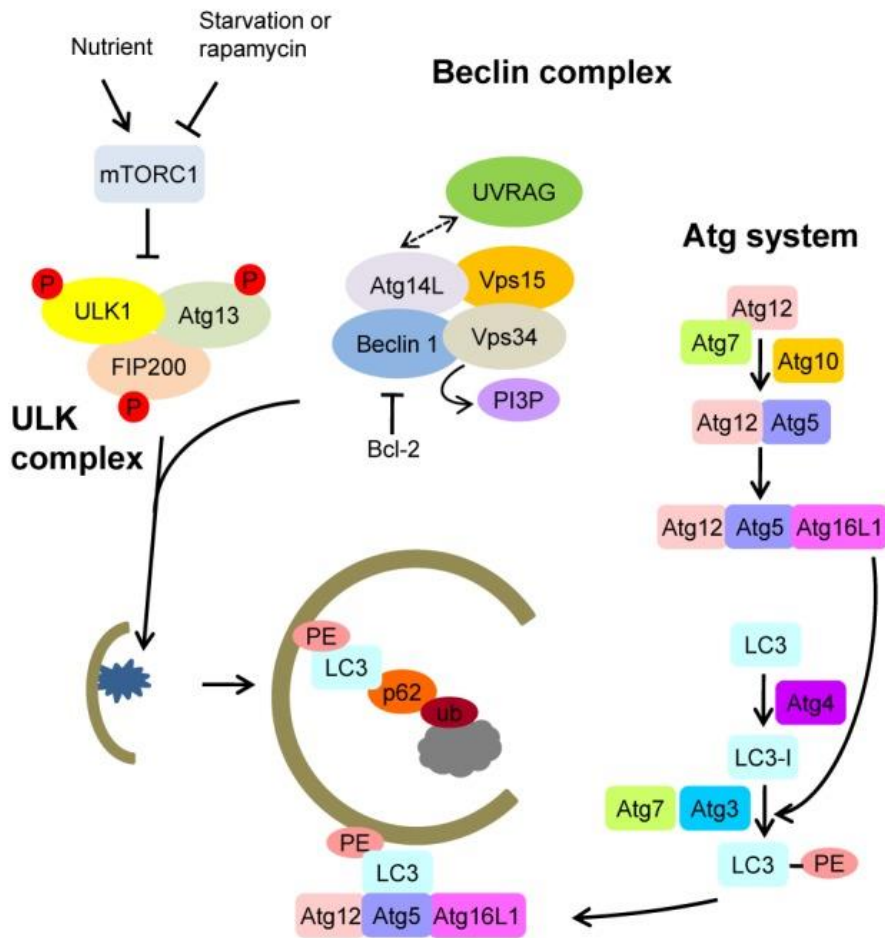


**Figure 1.5. Detailed process of autophagy.**

Autophagy is regulated by energy sensing molecules mTORC1, which directly phosphorylate ULK1 and promote the ULK complex, an autophagy initiation signaling molecule. Atg proteins regulate autophagosome elongation by lipidating LC3, which binds to polyubiquitinated p62 on cargo targets. Adapted from Quan and Lee [168]

### 1.8. Metabolic Syndrome, Autophagy and Hypoadiponectinemia

As mentioned earlier, autophagy initiation is affected by energy status, and overnutrition inhibits autophagy due to enhanced mTOR activity. Mice fed with HFD exhibited enhanced mTOR activity and reduced autophagy rates in insulin acting tissues such as skeletal muscle, adipocytes, and hyperinsulinemia reduced autophagy gene expression and impaired autophagy flux [169-172]. Ob/ob or db/db mice showed suppressed key ATG proteins in the liver, and restoration of

ATG gene expression by adenovirus improved metabolic profiles [173]. On the other hand, undernutrition enhances autophagy due to enhanced AMPK activity. Caloric restriction or intermittent fasting enhanced AMPK and SIRT1 activity and enhanced autophagy activity in a number of tissues, which improved metabolic profiles such as increased insulin sensitivity, lean body mass [174]. Caloric restriction or exercise training increased serum adiponectin levels and improved metabolic profiles [175, 176].

Adiponectin is a potent AMPK inducer, and autophagy defects under MetS are associated with reduced AMPK activity. Multiple lines of evidence suggest autophagy is regulated by adiponectin. HFD resulted in reduced AMPK activity, decreased autophagy related gene expression, and increased p62 levels, and this result was aggrandized in Ad-KO mice. However, pharmacological activation of AMPK ameliorated metabolic dysfunction in both WT and Ad-KO mice [177, 178]. Our lab recently reported that adiponectin can stimulate autophagy in skeletal muscle In Vivo and In Vitro. Adiponectin replenishment in Ad-KO mice enhanced autophagy related gene expression and LC3-II level, and decreased p62 level. Adiponectin treatment in L6 myoblasts activated AMPK mediated ULK1 complex formation, increased autophagosomes and lysosomal degradation [171, 179].

## **1.9. Research Objectives**

Obesity is pandemic and the incidence is predicted to increase continuously for the next several decades. Low serum adiponectin level is implicated in numerous metabolic complications, and adiponectin's molecular effects are huge therapeutic interests. Adiponectin's beneficial effects are pre-dominantly dependent on AMPK signaling, which regulates autophagy. Throughout my doctoral training at York University, I aimed to investigate the molecular mechanism underlying adiponectin mediated metabolic effects, focusing their relation to autophagy.

*Study 1: Iron overload impairs autophagy in skeletal muscle, leading to insulin resistance*

My first study was to investigate molecular mechanisms underlying IO induced T2D. IO is strongly associated with hypoadiponectinemia, yet the causative relationship with insulin resistance is not clear [180]. We previously reported that adiponectin signaling is important in autophagy to maintain insulin sensitivity in skeletal muscle [179], yet no studies examined the changes in autophagy upon IO and its effects on insulin sensitivity in skeletal muscle. I developed and characterized IO-induced insulin resistance models both in vitro and in vivo.

*Study 2: Adiponectin deficiency exacerbates PO-induced cardiac remodeling due to autophagy impairment*

My second study was to characterize cardiac autophagy after PO in aged mice. To characterize the relationship between adiponectin and autophagy response after PO, mTAB (minimally invasive transverse aortic banding) surgery was performed on wild type (WT) and Ad-KO mice. Temporal changes in cardiac function were monitored by echocardiography and cardiac autophagy was analyzed by measuring key autophagy protein expressions and ultrastructural morphology of hearts at the end point. In vitro experiments with H9c2 cells were performed to see if adiponectin can stimulate autophagy.

*Study 3: Adiponectin signaling stimulates protective AMPK mediated autophagy during ischemia*

In the course of MI, the heart experiences ischemia and reperfusion. Protective AMPK-dependent autophagy is activated during ischemia, yet detrimental AMPK-independent autophagy is activated during reperfusion. To identify the contribution of AMPK-dependent autophagy by adiponectin, CAL (coronary artery ligation) surgery was performed without

reperfusion, and cardiac autophagy was characterized after 7 days. To accurately measure autophagy activity, we adopted a novel FMT (fluorescent molecular tomography) technique which enabled us to monitor lysosomal enzyme activity in live animals. In vitro experiments with autophagy deficient H9c2 cells were performed to identify the significance of adiponectin stimulated autophagy.

## **CHAPTER 2**

### **2.1. Abstract**

Iron overload (IO), a common clinical occurrence, is implicated in the metabolic syndrome (MetS) although the contributing pathophysiological mechanisms are not fully defined. We show that prolonged IO resulted in an autophagy defect associated with accumulation of dysfunctional autolysosomes and loss of free lysosomes in skeletal muscle. These autophagy defects contributed to impaired insulin-stimulated glucose uptake and insulin signaling. Mechanistically, we observed IO led to a decrease in: Akt-mediated repression of tuberous sclerosis complex (TSC2), Rheb-mediated mTORC1 activation on autolysosomes, and autophagic lysosomal regeneration (ALR). Constitutive activation of mTORC1 or iron withdrawal replenished lysosomal pools via increased mTORC1-UVRAG signaling, which restored insulin sensitivity. Induction of IO via intravenous iron-dextran delivery in mice also resulted in insulin resistance accompanied by abnormal autophagosome accumulation, lysosomal loss and decreased mTORC1-UVRAG signaling in muscle. Collectively, our results show that chronic IO leads to a profound autophagy defect through mTORC1-UVRAG inhibition and provides new mechanistic insight into Mets-associated insulin resistance.

## 2.2. Introduction

Iron is an essential element involved in multiple cellular processes such as erythropoiesis, mitochondrial respiration and growth/differentiation [181-183]. The total amount of labile iron must be precisely regulated and in circulation iron typically exists bound to transferrin (TF) [184, 185]. However, when iron exceeds TF capacity, iron homeostasis becomes imbalanced [186] and non-TF bound iron contributes to pathophysiological processes, including insulin resistance and diabetes [180, 187-189]. Interventions to reduce iron have been reported to improve insulin sensitivity and delay the onset of type 2 diabetes (T2D). These include the use of chelators [190-192], blood-letting [11, 193, 194] and iron restriction diet [64]. However, the molecular mechanisms linking iron overload (IO) to T2D are poorly understood. Cellular labile iron, which contains chelatable redox-active  $\text{Fe}^{2+}/\text{Fe}^{3+}$ , has been implicated in iron-mediated cellular toxicity by increasing oxidative stresses. Excess accumulation of intracellular iron leads to the generation of reactive oxygen species (ROS) and tissue damage [182, 195].

We have previously shown that autophagy plays an important role in regulating insulin sensitivity and metabolism in skeletal muscle [179]. Autophagy is a stress-sensitive cellular degradative process capable of clearing and recycling potential substrates such as damaged mitochondria and protein aggregates [196]. Indeed, autophagy is generally considered to play a protective role against T2D, recycling nutrients to maintain energy homeostasis and remove damaged organelles [197, 198]. IO has been described to regulate the activity of both AMP-activated protein kinase (AMPK) and mTOR complex 1 (mTORC1) [199, 200], which are both established upstream regulators of the autophagy pathway [158, 160]. However, the potential mechanisms linking IO-mediated autophagy to insulin resistance remain to be elucidated.

Here we established *in vitro* and *in vivo* models to examine direct effects of IO on autophagy flux in skeletal muscle and its significance in insulin resistance. We describe a mechanistic link between chronic IO and autophagy dysfunction, which alters insulin sensitivity in skeletal muscle. We identified the regulation of mTORC1 by IO as a double-edged sword that initially leads to transient autophagy activation, but ultimately causes an autophagy defect through loss of autophagic-lysosomal regeneration (ALR), a newly discovered membrane recycling mechanism that to date has not been identified as a contributor to pathophysiology [201]. The data presented here provide new mechanistic knowledge to enhance our understanding of the pathogenic mechanisms of IO, which may have widespread consequences in insulin resistance, metabolic dysfunction and beyond.

## 2.3. Materials and Methods

### *Materials*

The cell culture medium ( $\alpha$ -minimal essential medium [ $\alpha$ -MEM]), fetal bovine serum (FBS) and antibiotics/antimycotic solution were purchased from Wisent (St Bruno, QC, Canada).

Cytochalasin B (Sigma) and Human insulin (Humulin) were purchased from Eli Lilly (Toronto, ON, Canada) and deoxy-D-[2-3H] glucose was purchased from PerkinElmer (Woodbridge, ON, Canada). Ferrous Sulfate heptahydrates ( $\text{FeSO}_4 \cdot 7\text{H}_2\text{O}$ , Cat#310077), Torin-1 (Cat# 475991) Monoclonal Anti-Vinculin (Cat#V9131) and beta-Actin antibody (Cat#A5441 clone AC-15) were purchased from Sigma Aldrich (Ottawa, ON, Canada). AKT inhibitor MK-2206 was purchased from Selleck Chemicals. S6K (Cat#ab32529), LAMP1 (Cat#ab25630) and Alexa 647 conjugated antibody (goat anti-rabbit, Cat#ab15007) were purchased from Abcam (Cambridge, MA, USA). LC3B (Cat#2775), GAPDH (Cat#2118), Tubulin (Cat#2148) antibodies and phospho-specific antibodies (phosphorylation sites) for AKT (T308, Cat#4056), phospho-S6K (T389, Cat#9234), phospho-ULK1 (S757, Cat#14202), mTOR (Cat#2983) phospho-mTOR (S2448, Cat#2971), TSC2 (Cat#4308T) phospho-TSC2 (T1462, Cat#3617T) ) phospho-AKT (Ser473 Cat#4060) total AKT (Cat#4691) , horseradish peroxidase-conjugated secondary antibodies (anti-rabbit-IgG, Cat# #7074 and anti-mouse-IgG, Cat#7076) were purchased from Cell Signaling Technology (Beverly, MA, USA). UVRAG phospho-specific (S550, Cat# S307D) and UVRAG antibody (Cat# S323D) was provided from MRC PPU at The University of Dundee. Anti-Transferrin Receptor (Tfr1) monoclonal antibody (Cat#13-6800 clone H68.4), phospho-specific antibody for anti-IRS-1 (Y612, Cat#44-816G), Alexa555 conjugated antibody (donkey anti-rat, Cat#A-21434), Lipofectamine 2000 (Cat# 11668019), ProLong Gold (Cat#P36930) were purchased from Thermo Fisher Scientific (Burlington, ON, Canada). Anti-

LC3B (Cat#PM036) and Anti-p62 (Cat# M162-3) were purchased from MBL. Anti-Ferritin heavy chain (Cat#NBP1-31944) was purchased from Novus Biologicals. Anti-Myc (Cat# 9E10) was purchased from Alzforum. LAMP1 (Cat#sc-19992, Santa Cruz) antibody and iron-dextran dextran (a ferric hydroxide,  $\text{Fe}(\text{OH})^3$ , complex with low molecular weight dextran, Cat#9004-66-4) was purchased from Santa Cruz Biotechnology Inc. VECTASHIELD Antifade Mounting Medium with DAPI (Cat# H-1200) was purchased from Vector Laboratories. Polyvinylidene difluoride membrane was from Bio-Rad Laboratories, Inc (Burlington, ON, Canada), and chemiluminescence reagent plus was from PerkinElmer (Boston, MA). Concanamycin A was purchased from BioShop Canada Inc. (Cat# FOL202, Burlington, ON, Canada). All other reagents and chemicals used were of the highest purity available.

#### ***Cell Culture and generation of L6 cell line stably overexpressing gene of interest***

L6 skeletal muscle cell line (ATCC® CRL-1458™ tested mycoplasma free) were grown to confluency in  $\alpha$ -MEM supplemented with 10% (volume/volume (v/v)) FBS and 1% (v/v) antibiotic/antimycotic solution under a humidified atmosphere of 95% air and 5%  $\text{CO}_2$  at 37°C. During treatment or iron withdrawal, the cells were switched to medium containing 0.5% (volume/volume (v/v)) FBS and 1% (v/v) antibiotic/antimycotic. During iron treatment, ferrous iron stock, prepared by dissolving ferrous sulfate heptahydrate ( $\text{FeSO}_4 \cdot 7\text{H}_2\text{O}$ ) in sterile distilled water at 10mM, was dissolved in treatment medium at appropriate concentration. L6-GLUT4 cells stably transfected to overexpress myc-tagged GLUT4 were a gift from Dr Amira Klip, The Hospital for Sick Children, Toronto. IRE-CFP L6 cells stably transfected to overexpress IRE-CFP were a gift from Dr.s' James R Connor and Stephanie Patton, Penn State Hershey Medical Center, USA [202]. eGFP-mCherry-LC3B, eGFP-mCherry-p62 stables, and myc-tagged RHEB

Q64L mutant L6 cells were infected with lentivirus and a stable polyclonal population was obtained through puromycin (1 µg/ml) selection for stable integration.

***Determination of intracellular iron***

Intracellular iron concentration was estimated by ferrozine-based assay as described previously [203]. PhenGreen SK (PGSK) diacetate dyes [204] was used to determine the degree of di-valent ions. Iron specific probe-1 (IP-1) [205, 206] was a kind gift from Dr Christopher J. Chang, University of California, Berkeley) was used to determine labile iron levels in cells.

***Gene expression analysis***

Quantitative Polymerase Chain Reaction (qPCR) was performed as previously described [179]. Total RNA was extracted with RNEasy Mini Kit (Qiagen, Toronto, Canada), then converted to cDNA with GoScript reverse transcriptase (Promega). PCR cycle was performed with iTaq™ Universal SYBR® green mixture (Bio-Rad) at following condition: 2 minutes at 95C, followed by 40 cycles of 15 seconds each at 95C, 60C, 72C. Relative gene expression levels were normalized to 18s rRNA. Primers used in this study are summarized in Table 3.

<b>Name</b>	<b>Kind</b>	<b>Segeunce (5' - 3')</b>
FTH	Forward	CTTTGCAACTTCGTCGCTCC
	Reverse	AGTCATCACGGTCAGGTTTCTTT
FTL	Forward	AGACCCTCACCTCTGTGACT
	Reverse	GGCGGTTACAAAGCTGCCTA
SLC40A1	Forward	CGTGCTATCTCCGGTTCCTC
	Reverse	TGTCAAGAGGAGGCCGTTTC
TFRC	Forward	AGCCAGATCAGCATTCTCTAACT
	Reverse	GCCTTCATGTTATTGTTCGGCAT
18srRNA	Forward	CCATAAACGATGCCGACTG
	Reverse	CGCTCCACCAACTAAGAAC

**Table 3. List of Primers used in Study 1.**

### ***Western blotting***

Lysates were prepared as we described before [207]. SDS-PAGE was performed, and proteins were transferred to PVDF membrane then incubated with blocking buffer (3% BSA or 5% skim milk in TBS-T), washed with TBS-T five times and incubated with primary antibodies (1:1000 in TBS-T 2% BSA) overnight at 4°C. Next, membranes were incubated in appropriate horseradish peroxidase-conjugated secondary antibody (1:10000 in TBS-T 2% BSA or skim milk) for one hour at room temperature. Quantitation of each specific protein band was determined by densitometric scanning with correction for the respective loading control.

### ***Insulin Sensitivity Test***

Glucose uptake was determined by measuring uptake of 2-deoxy-d-[<sup>3</sup>H] glucose exactly as described previously [208]. L6-GLUT4 cells were incubated with insulin (10 nM and 100 nM) for 20 min after treatment with or without iron as described. Phosphorylation of IRS1 (Y612) and AKT (T308) were determined in cells incubated with insulin (10nM or 100nM) for 5 min after appropriate treatment.

### ***Transmission Electron Microscope (TEM)***

TEM was performed as described previously [207]. Briefly, samples were fixed in fixative (2% formaldehyde, 2% glutaldehyde in 0.1M sodium cacodylate buffer) for 2 hours at room temperature. After washing three times with sodium cacodylate buffer, samples were fixed in 1% osmium tetroxide for 1 hour at room temperature. After dehydration with ascending concentration of ethanol in series (50%-100%), cells were embedded in Spurr's Epoxy resin. Thin sections (60-80nm) were cut with ultramicrotome and mounted on copper mesh grids. The

sections were then contrasted with 1% uranyl acetate and lead citrate and examined with a FEI CM100 TEM and Kodak Megaplug Camera.

### ***In Vitro Autophagy Analysis***

Activity of the autophagy pathway was monitored by western blot and immunofluorescence-based puncta quantification of LC3B. Flux assay was performed by measuring levels of LC3B-I and LC3B-II from cell lysates after appropriate treatment co-treated with lysosomal inhibitor (chloroquine, 30  $\mu$ M). LC3B immunofluorescence was performed as described previously [209]. Briefly, cells were fixed, permeabilized and blocked with PBS solution containing 1% BSA and 2% goat serum. After blocking, cells were incubated with blocking solution containing LC3B (Cat#PM036, MBL, conjugated with Cy3 Alexa Fluor 555 1:1000) and mouse anti-LAMP1 (Cat#A11029, 1:500). Cells were incubated with anti-mouse Alexa Fluor488 secondary antibody ((Cat#ab25630, Thermo Fisher Scientific, 1:200) at room temperature for 1h. After incubation, cells were mounted with DPAI after washes. Deconvoluted images were captured with an Apotome enabled Zeiss AxioObserver.Z1. For live cell imaging L6 cells stably expressing eGFP-mCherry-LC3B or eGFP-mCherry-p62 were seeded in Ibidi chambers and treated with iron ( $\text{FeSO}_4$ , 250  $\mu$ M) or starvation medium (without amino acid). Treatments were carried out in FluorBright<sup>TM</sup> phenol red-free DMEM (Invitrogen) supplemented with GlutaMAX. Images were acquired and deconvoluted using an environmental chamber control (DeltaVision Elite-Olympus IX-71 with FemtoJet Microinjector) microscopy.

### ***Lysosome Dynamics Analysis***

L6 cells were co-transfected with LAMP1-RFP and LC3-GFP using Lipofectamine 2000 as per manufacturer's specifications. Following 8 h of transfection, cells were incubated in treatment medium then imaged live. During live-cell imaging, cells were maintained in an environment set to 5% CO<sub>2</sub> and 37 °C. We used a Quorum Discovery spinning disc confocal microscope system equipped with a Leica DMI8 microscope and connected to an Andor Zyla Megapixel sCMOS camera. Microscope and acquisition settings were controlled using Quorum Wave FX powered by MetaMorph software (Quorum Technologies, Guelph, ON). For time-lapse imaging and determination of lysosomal dynamics, images were acquired every 3 seconds for 3 minutes. For determination of lysosomal numbers, images were acquired along the z-plane at a defined interval of 0.3 μm.

For image analysis, lysosomal numbers were unbiasedly determined using particle detection tools in Volocity 6.3.0 software (PerkinElmer). Lysosomal numbers were determined in at least 15 cells per condition per experiment, where we repeated each experiment at least three independent times. For lysosomal track analysis, movies were analyzed using particle detection tools in Imaris (Bitplane) image analysis software. Lysosome particles were defined as having a minimum of 0.5 μm in diameter and tracked using the software's autoregressive motion track analysis function. To minimize mis-tracking of particles, tracks were restricted to particles that moved a maximum distance of 1 μm between frames and with no more than a maximum gap distance of 3 frames. This analysis was completed for at least 6 cells per trial per condition with more than 100 tracks per cell. Track mean speed and displacement, which is defined as the distance between start and endpoints, were calculated.

### ***Cathepsin Activity Assay***

We used Magic Red Cathepsin L kit (BioRad Technologies, Cat# ICT941) and performed experiments as follows. After 24 h IO treatment, IO and control cells were incubated with 1x magic red cathepsin L reagent, concurrently or in the absence of 1uM ConA, for 1 hour, prior to live cell imaging. Using spinning-disc confocal microscopy, confocal slices were acquired with a 0.3-micron interval between slices. For image analysis, the total magic red fluorescence for MR-positive puncta was determined and compared to the control counterpart.

### ***Lysosomal $\beta$ -Glucosidase Activity Assay***

L6 Cells were plated on ibidi 8 well m-Slide (Ibidi, Cat# 80826) overnight and treated with iron (FeSO<sub>4</sub>, 250uM) for 24h. Cells were then incubated in AMEM containing the  $\beta$ -glucosidase substrate (5uM) for an hour (Marker Gene Technologies, Cat# M2775). Then cells were washed 3 times with PBS prior to the addition of Opti-Klear™ Live Cell Imaging Buffer. Images were acquired and deconvolved using an environmental chamber control (DeltaVision Elite-Olympus IX-71 with FemtoJet Microinjector) microscopy.

### ***Cyto-ID Autophagy Detection Assay***

L6 Cells were plated on ibidi 8 well m-Slide (Ibidi, Cat# 80826) overnight and treated with iron (FeSO<sub>4</sub>, 250uM). Cells were then incubated in AMEM without phenol red containing Cyto-ID autophagy detection stain (Enzo, ENZ-KIT175-0050) for 30 minutes with/without iron, then washed with PBS. Images were acquired and deconvolved using an environmental chamber control (DeltaVision Elite-Olympus IX-71 with FemtoJet Microinjector) microscopy.

### ***Iron Overload Animals, Glucose Tolerance Tests (GTT), and Insulin Tolerance Tests (ITT)***

Animal facilities met the guidelines of Canadian Council on Animal Care, and the York University Animal Care Committee approved the experimental protocols. Animals were fed ad libitum on regular chow diet and kept in temperature and humidity-control rooms ( $21 \pm 2$  °C, 35-40%) with a daily 12:12h light-dark cycle. Groups (n = 6) of 2-month-old C57/BL6 male mice were randomized into 2 groups and injected with iron-dextran dextran intravenously (15mg per kg, diluted in PBS to make 150  $\mu$ l injection volume) three times at 2 hours interval or with only PBS as control. After 24hr post first injection GTT and ITT were performed, without blinding, as described previously [210]. For phosphorylation of insulin signaling molecules analysis, mice were injected with 4 units of insulin per kg before sacrifice.

### ***Tissue Immunofluorescence***

Paraffin-embedded sections were deparaffinized and rehydrated with descending concentrations of ethanol and then brought into double distilled water. The antigens were retrieved in citrate buffer pH6.0 in autoclave for 15min. After three washes with PBS, sections then were permeabilized with Triton X-100 (0.3% Triton X-100 in PBS) and blocked with 2% BSA and 5% goat serum in PBS for 90 minutes. Sections were incubated with LAMP1 (Santa Cruz) and LC3B (MBL) at 1:100 in 2% BSA in PBS, followed by Alexa secondary antibody conjugated fluorophores (Alexa 555 donkey anti-rat and Alexa 647 goat anti-rabbit). Sections were mounted on coverslips with ProLong Gold and VECTASHIELD antifade mounting medium with DAPI and images were captured with Zeiss LSM 700. The number of Lamp1 puncta were determined by setting pre-set threshold “momentum” in ImageJ, and counted the puncta ( $>0.6$   $\mu$ m diameter,  $>0.35$  circularity) per field of views.

### *Statistical Analysis*

Data are expressed as mean  $\pm$  standard error mean (SEM) from at least three separate experiments. The differences between groups were analyzed using Prism 5.0 (GraphPad Software Inc., San Diego, CA, USA) with one-way analysis of variance (ANOVA) followed by Student t-test; with  $p < 0.05$  considered as statistically significant. Quantification of endogenous lysosome and autophagosome number was performed using Perkin Elmer Volocity software for unbiased identification and quantification of objects. Vesicle numbers and individual vesicle sizes were identified from a minimum of nine representative cells, with a minimum of 40 vesicles per condition. Samples were compared using Student's t-test. Autophagosome mobility was determined by blinded vesicle tracking using a minimum of 11 time points to track an average of 10 autophagosomes per sample. Mean velocity was calculated for each autophagosome and sample sets across multiple conditions were compared using Student's t-test.

## 2.4. Results

### *Iron overload (IO) induced insulin resistance in L6 cells*

Skeletal muscle is a primary consumer of glucose, yet the effects of IO on glucose uptake and insulin sensitivity are not known. Therefore, we first sought to determine if IO induces insulin resistance in rat L6 skeletal myoblasts. An experimental model of IO was established by treating cells with ferrous labile iron for up to 24 h. The extent of IO was then determined via dose and temporal analysis using biochemical intracellular iron measurement (Fig 2.1A). The concentration selected for subsequent use, 250  $\mu$ M, is intended to mimic IO and is consistent with iron concentrations used in literature for other cell types [205, 211]. Conventional iron overload response [185] by skeletal muscle cells was monitored by using an iron response element (IRE) driven reporter construct tagged with cyan fluorescence protein (CFP) transfected in L6 cells as well as the use of fluorescence-based indicators of iron levels (IP-1). We observed that iron treatment for 24 h increased the expression of CFP and fluorescence of iron probe IP-1 without adversely affecting viability (Fig 2.1B and Fig 2.2A). Analyzing increased intracellular iron via quenching of the iron-sensitive fluorescent probe phen green SK (PGSK) we confirmed elevated iron in our model and that it could be effectively blocked by the iron chelator, 2,2' di-pyridyl (DPD) (Fig 2.1C). We further tested iron-responsive transcription by performing qPCR against ferritin (FTH and FTL, H- heavy and L-light chain), Ferroportin (SLC40A1) and Tfr1 (Transferrin receptor 1, TFRC). Iron treatment for 24 h significantly increased the expression of ferritins, ferroportin and decreased the expression of Tfr1 (Fig 2.1D). Transcriptional changes aligned with protein levels indicating that iron treatment significantly increased ferritin heavy chain and decreased Tfr1 expression (Fig 2.1E). Together, these results indicate that our *in vitro* IO-model in skeletal muscle line recapitulates the key hallmarks of IO [212].

We next analyzed insulin sensitivity after IO measuring glucose uptake and phosphorylation of insulin signaling molecules (IRS-1 Y612 and AKT T308) after insulin stimulation. Iron treatment for 24 h significantly reduced glucose uptake following insulin stimulation (Fig 2.1F). Additionally, insulin-stimulated phosphorylation of IRS-1 and AKT were significantly reduced after 24 h iron treatment (Fig 2.1G). Furthermore, we determined that insulin resistance was due to intracellular iron accumulation since DPD significantly reduced the intracellular iron accumulation at 24 h iron treatment, and restored insulin stimulated glucose uptake and insulin signaling phosphorylation (Fig 2.2B-E). Taken together our results indicate that IO directly caused insulin resistance in skeletal muscle.

### ***Prolonged iron treatment causes autophagy flux defects in skeletal muscle cells***

We have previously established that autophagy is an important regulator of insulin sensitivity in skeletal muscle [179]. Thus, we analyzed the temporal effect of iron treatment on autophagosome production and fusion with lysosomes by imaging L6 cells stably expressing LC3B-eGFP-mCherry. In this assay, eGFP fluorescence was quenched by low pH after autophagosome fusion with the lysosome whereas mCherry is not [213]. We observed a rapid increase in the number of autophagosome puncta after iron treatment, which was corroborated by western blot analysis of LC3B that showed the lipidated form of LC3B (LC3-II) was significantly increased after iron treatment (Fig 2.3A-B, Fig 2.4A). Consistent with our analysis of LC3B we found that p62 puncta formation and protein clearance was rapidly increased by iron treatment (Fig 2.3C, Fig 2.4B-C). Surprisingly, while we observed p62 protein levels decreased significantly at early time points after iron treatment, we found they were significantly stabilized

at 24 h post treatment (Fig 2.3C). p62 stabilization under prolonged iron treatment potentially indicates a blockage of autophagic flux at later time points. To further analyze autophagy flux, we quantified the accumulation of lipidated LC3B in the presence of a late stage autophagy inhibitor (CQ, chloroquine). At 4 h after iron treatment, LC3-II significantly increased with CQ, indicating an induction in autophagy (Fig 2.3D). However, 24 h after iron treatment LC3-II levels were elevated but unchanging, indicating a lack of autophagy flux despite the presence of a large pool of autophagosomes (Fig 2.3E).

We also observed autophagosomes under prolonged IO were morphologically abnormal, with a mean diameter nearly three times those in the untreated samples (Fig 2.3F-G). Enlarged LC3-positive vesicles are often observed in autophagy-deficient backgrounds including cells with knock outs in: ULK1/2 (Fig 2.4D-E), Beclin-1[209], FIP200[214] and ATG14L1[215]. We next performed live cell imaging to analyze autophagosome mobility that, in addition to autophagosome number, is positively correlated with autophagic flux [216]. As expected, amino acid starvation increased autophagosome motility to 78 nanometers per second compared to 44 nm/s in untreated samples indicating an increase in autophagy rates. In contrast, autophagosomes observed in cells with IO were nearly static, moving an average of 6.4 nm/s (Fig 2.3H).

Ultrastructure analysis by transmission electron microscopy (TEM) showed that chronic IO resulted in a striking accumulation of enlarged vesicles, characteristic of autolysosomes (Fig 2.3I). To further characterize the blockage of autophagy that accompanies insulin resistance under chronic IO we sought to determine if lysosomal fusion with autophagosomes was inhibited at this time point [213, 217]. We immunostained for endogenous LC3B and LAMP1 and observed large dual positive structures, which indicated that lysosomal fusion was not inhibited in the accumulated autolysosomes under prolonged IO (Fig 2.3J). This was confirmed by

additional markers for both autophagosomes and lysosomes (Fig 2.4F). Moreover, we found that chronic IO did not inhibit the proteolytic activity of lysosomal enzymes ( $\beta$ -glucosidase and cathepsin B) that were still active in autolysosomes under chronic IO, indicating that autophagy defects were not caused by an inhibition of lysosomal fusion or lysosomal enzyme activity (Fig 2.4G-I). However, we also observed that under IO there was a precipitous loss of ‘free’ lysosomes (defined as LAMP1-positive, LC3B-negative), with nearly all LAMP1 staining detected on autophagosomes (Fig 2.3J, Fig2.5A-B). Taken together our data indicates that IO overload results in a temporary increase in autophagy rates, followed by an accumulation in non-functional autolysosomes and autophagy inhibition.

#### ***IO inhibits reactivation of mTOR following autophagosome degradation***

The nature of the lysosomal and autophagosomal defects described above could be consistent with attenuation of the recently described membrane recycling event termed autophagic-lysosome regeneration (ALR) [218, 219]. ALR is essential to sustain prolonged periods of autophagic induction [218]. ALR is an mTOR-dependent process where membrane from the spent autophagosome is extruded, followed by scission to form protolysosomes that then mature into new lysosomes. mTORC1 promotes this scission after being activated by nutrients generated from the degradation of autophagic cargo. Importantly, this function of mTORC1 acts to promote autophagy under prolonged stress through the production of lysosomes and is independent of the autophagy-suppressive effects mTORC1 exerts under basal conditions [218]. Therefore, we next sought to monitor mTORC1 activity in iron treated samples. Temporal analysis of mTORC1 target phosphorylation (p-S6K T389 and p-ULK1 S757) upon FBS withdrawal showed a partial rescue at 8 h that was absent in the iron treated samples (Fig 2.6A-

B). This indicates that IO may prevent reactivation of mTORC1 from nutrients generated by the autolysosomes.

We next tested whether maintenance of mTORC1 activation under chronic IO was sufficient to rescue the autophagic defects observed. To do so, L6 cells were transiently transfected with a Myc-tagged RHEB (Ras Homology Enriched in Brain) GTPase, which is contained the Q64L mutation to remain GTP bound and can directly maintain mTORC1 activity [220, 221].

Transfected cells were treated with iron for 24 h, then stained for anti-LC3B antibodies to identify autophagosomal aggregates and anti-Myc antibodies to mark cells transfected with Myc-RHEB mutant. We found that cells with forced activation of mTORC1 exhibited a dramatic absence of large autolysosome accumulation under chronic iron treatment (Fig 2.6C, Box1) when compared to cells that were not transfected under the same conditions (Fig 2.6C, Box2).

We next generated stable cell lines over expressing RHEB mutant (RHEB Q64L L6) and compared to wt (wild type) cells after treating with iron. As a control we tested intracellular iron levels in RHEB Q64L and wt cells after 24 h iron treatment and found them comparable (Fig 2.6D). After 24 h iron treatment, wt cells developed autophagosomal aggregates and compromised LC3B-free lysosomal pools as previously observed. Conversely, RHEB Q64L cells did not accumulate large autophagosomes and total lysosomal content was comparable with/without iron treatment (Fig 2.6E-F). Ultrastructure analysis by TEM further confirmed that RHEB Q64L stable cells did not develop abnormal autophagosomal structures after iron treatment, when compared to control (Fig 2.6G). To examine the functional significance of these observations, we tested if maintenance of mTORC1 activity affected IO-induced insulin resistance. In RHEB Q64L cells, we observed improved insulin signalling (p-IRS-1 Y612 and p-

AKT T308) under IO (Fig 2.6H-I). Taken together, these data suggest that loss of mTORC1 activity during chronic IO is responsible for autophagy defects and insulin resistance.

***IO induced insulin resistance and autophagy defects are reversed upon iron withdrawal***

In the clinic, IO-induced insulin resistance can be improved by iron restricted diets or iron chelation therapy [64, 222]. Therefore, we examined whether IO-induced insulin resistance could be rescued by withdrawing iron from treatment medium following iron treatment for 24 h. 24 h withdrawal resulted in alleviation of IO, by significantly reducing intracellular iron levels as indicated by PGSK and ferrozine based colorimetric assay (Fig 2.7A-B). The recovery from IO occurred concurrently with insulin sensitivity restoration. Phosphorylation of insulin signaling molecules after insulin stimulation significantly recovered after 24 h withdrawal (Fig 2.7C-D). We next analyzed the effects of iron withdrawal after iron overload on autophagosome and lysosomal populations. We observed that iron withdrawal after chronic IO resulted in clearance of autolysosome accumulation and a restoration of LC3B-negative lysosomes (Fig 2.7E-F). Iron overload has been described to inhibit the targeting of ferritin to autophagosomes. Therefore, we looked at ferritin protein levels under IO and after iron wash off. As expected, ferritin was stabilized by chronic IO consistent with a block in autophagic clearance and was cleared significantly by 24 h after media replacement without excess iron (Fig 2.7G). Taken together our data shows that iron removal results in clearance of abnormal autophagosomes, restoration of lysosomes, and increased insulin sensitivity.

### ***Chronic IO blocks mTORC1 reactivation on autolysosomes and signaling to UVRAG***

We next sought to determine the mechanism underlying IO-induced autophagic defects. We previously determined that forced mTORC1 activation was sufficient to block autolysosome accumulation (Fig 2.6C, Fig 2.6G). Therefore, we first sought to characterize the effects of prolonged IO regulated on regulatory phosphorylation of mTORC1. L6 cells were treated with iron for 24 h, or 24 h plus iron withdrawal. mTORC1 was monitored by phosphorylation at S2448, which correlates with mTORC1 activity [223, 224]. We observed mTORC1 phosphorylation was greatly diminished at 24 h IO and recovered after 4h of iron withdrawal (Fig 2.8A). mTORC1 phosphorylation at S2448 is dependent on localization to the lysosome or autolysosome for activation by the Rheb-GTPase activity, which is in turn regulated by tuberous sclerosis complex (TSC)-AKT signaling [225, 226]. We stained cells for endogenous mTOR and LC3B and found that mTOR was localized to autolysosomes under prolonged IO, indicating localization defects are likely not the cause of mTORC1 activity loss (Fig 2.9A). Therefore, we next looked at the effect of IO on AKT-mediated inhibition of TSC2. We observed a decrease in inhibitory phosphorylation of TSC2 under IO, which was dramatically reversed upon wash off (Fig 2.8B). However, when iron withdrawal media was supplemented with AKT inhibitor, mTORC1 was not re-activated upon iron removal (Fig 2.8B). Together these data demonstrate that IO results in a decrease in AKT-mediated repression of TSC2, resulting in a potent repression of Rheb and mTORC1.

The lysosomal loss, mTORC1 inhibition, and autophagy defect we observe under IO are all consistent with a defect in ALR. mTORC1 promotes ALR through scission of the autolysosome activity via direct phosphorylation of UVRAG, a component of the VPS34 lipid kinase complex [219]. Phospholipid production by UVRAG-containing VPS34 complexes is essential for the

scission of the auto-lysosomal membrane. mTORC1-mediated phosphorylation of UVRAG on serine S550 was monitored in L6 cells transfected with FLAG-UVRAG that were treated with iron as indicated followed by immunoprecipitation of FLAG-UVRAG-containing VPS34 complexes (Fig 2.8C). Interestingly, at 4 h iron treatment we saw a slight increase in mTORC1-mediated UVRAG phosphorylation, which indicates that mTORC1 can be activated at the autolysosome even when global mTORC1 activity (as measured by S6K phosphorylation) is low (Fig 2.6A). This is consistent with the relatively normal functioning of autophagosomes and lysosomes that we observe at this time point (Fig 2.4C-D). However, at 24 h iron treatment we observed a dramatic loss in mTORC1-mediated phosphorylation of UVRAG (Fig 2.8C); indicating mTORC1 is incapable of efficiently promoting ALR under chronic iron treatment despite an overabundance substrate (mature autolysosomes). Additionally, the removal of iron resulted in a partial recovery of mTORC1-mediated UVRAG phosphorylation, indicating that IO-induced stress was responsible for the loss of ALR signaling (Fig 2.8C). We then used Torin-1, a well-established mTOR inhibitor [227, 228], and found that in its presence recovery of UVRAG signaling was completely abolished, confirming that mTORC1 ALR signaling is regulated by IO (Fig 2.8D). Based on the recovery of mTORC1 signaling to UVRAG upon iron withdrawal we hypothesized that treatment of cells with Torin-1 would be sufficient to block lysosomal recovery following iron withdrawal. To validate our hypothesis, we monitored lysosomal number and trafficking using cells transfected with RFP-LAMP1 to determine if inhibition of mTORC1 was sufficient to ablate the rescue of lysosomes upon iron withdrawal after chronic IO. RFP-LAMP1 was present on enlarged autolysosomes similar to endogenous LAMP1 (Fig 2.9B). At basal conditions, the number of lysosomes ranged from 100 to 300 per cell, and continuously trafficked and underwent fusion events (Fig 2.8E). On the other hand, iron

treatment significantly reduced the number of lysosomes (Fig 2.8E) and the motility of LAMP1 particles was reduced significantly (Fig 2.8F-G). The lysosomal pools were significantly recovered near basal levels after 4 h withdrawal. However, as predicted the addition of Torin-1 abolished recovery of lysosomal pools and lysosomal motility following iron withdrawal (Fig 2.8E-F). Collectively, these data demonstrate that prolonged IO results in lysosomal loss due to ablation of mTORC1-reactivation on autolysosomes caused by alterations in AKT-TSC-Rheb signaling (Fig 2.8H).

### ***Induction of IO in mice and development of insulin resistance following IO***

As in previous studies which have adopted injections to induce IO [229, 230], we delivered iron intravenously at 15 mg per kg, a dose with minimal toxicity [231], via three injections at 2 h intervals (Fig 2.10A). 24 h after first administration, animals were sacrificed, and tissue iron accumulation examined with Perls Prussian Blue staining. As expected, a robust increase in hepatic iron staining and more modest increase in skeletal muscle iron content was apparent (Fig 2.10B). Western blotting indicated that skeletal muscle ferritin levels increased while TfR1 levels decreased significantly in IO mice (Fig 2.10C-D). IO mice exhibited signs of peripheral insulin resistance, as shown upon examination of glucose handling via insulin and glucose tolerance tests (Fig 2.10E-H). To directly investigate changes in skeletal muscle insulin sensitivity we examined insulin-stimulated phosphorylation of IRS-1 (Y612) and AKT (T308) and observed significantly attenuated insulin-induced phosphorylation in IO mice (Fig 2.10J-K). Collectively, these data that our intravenous iron injection regimen recapitulated key aspects of iron-induced insulin resistance in skeletal muscle from our L6 cell culture model.

***IO caused reduced lysosomal pools with reduced UVRAG signaling and inhibited autophagy flux***

To measure ALR events *in vivo*, we performed LC3B and LAMP1 immunofluorescence on tissue sections and observed a pronounced difference between control and IO groups (Fig 2.11A). In control mice, there was a minimal complement of autophagosomes (LC3B puncta) yet numerous lysosomes (LAMP1 puncta), quantitatively 200 to 300 puncta per field of view (Fig 2.11B). In IO mice, the number of autophagosomes increased yet the number of lysosomes decreased significantly, less than 100 puncta per field of view was observed. TEM analysis of muscle tissue from control group confirmed the predominant appearance of lysosomes as single membrane clear structures, with occasional observation of autophagosomes (Fig 2.11C). On the other hand, TEM analysis of muscle from Iron group showed very sparse lysosomal content, with much smaller size than lysosomal structures observed in wt group. Also present in IO samples were tubular projections that are characteristic of reduced activity of UVRAG-containing VPS34 complexes [219] (Fig 2.11C). We further analyzed autophagy flux and ALR by western blotting of phosphorylation of UVRAG, and LC3B and p62 expression. In iron-treated mice, phosphorylation of UVRAG at S550 significantly decreased, matching *in vitro* data. Moreover, both LC3B-II and p62 expression in the IO group increased, indicating impaired autophagy flux, compared to control groups (Fig 2.11E-F). These changes were also observed in liver, indicating that IO-induced ALR defects are not limited to skeletal muscle and may have widespread highly significant pathophysiological implications (Fig 2.12A-E). Taken together, we have identified that IO induces an mTORC1 reactivation defect in skeletal muscle of mice leading to an ALR defect, which represents a new mechanistic link connecting disturbed iron homeostasis to insulin resistance and metabolic dysfunction.

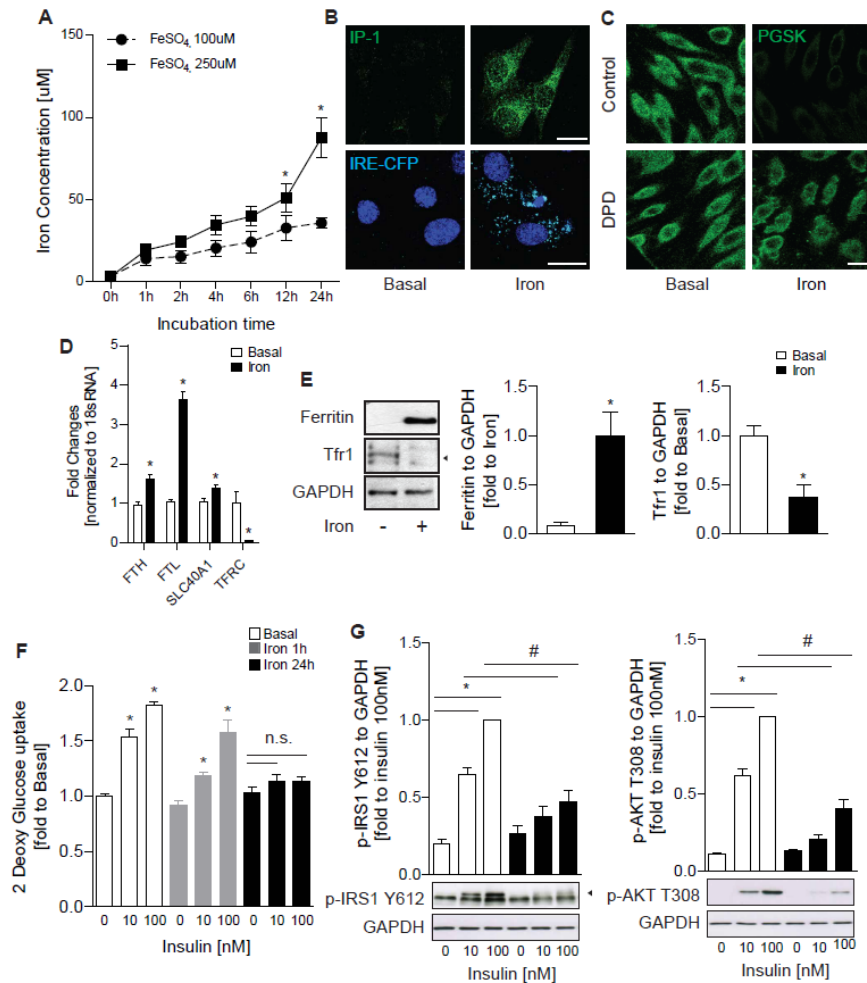


**Figure 2.1. Validation of Iron overload (IO) model and insulin resistance induction after IO in L6 muscle cells**

**A** Ferrozine-based intracellular iron concentration measurement in L6 cells after temporal analysis of iron treatment at 100 or 250  $\mu\text{M}$  for multiple time points. **B** Representative confocal microscope images of L6 cells stained with IP-1 (Iron Probe 1) or transfected with IRE-CFP (Iron Regulatory Element) reporter after iron treatment ( $\text{FeSO}_4$ , 250  $\mu\text{M}$ ) for 24 h. **C** Representative confocal images of L6 cells using iron-sensitive fluorescent PGSK dye after iron treatment (250  $\mu\text{M}$ , 24 h) with iron chelator DPD (500  $\mu\text{M}$ ). **D** Relative gene expressions – ferritin heavy chain (FTH), ferritin light chain (FTL), ferroportin (SLC40A1, transferrin receptor 1 (tfr1, TFRC) – normalized to 18sr RNA expression after iron treatment ( $\text{FeSO}_4$ , 250  $\mu\text{M}$ ) for 24 h. **E** Representative western blot images and quantification of ferritin (heavy chain) and tfr1 over GAPDH after iron treatment (250  $\mu\text{M}$ , 24 h). **F** Glucose uptake of L6 cells with insulin stimulation (10 nM or 100 nM, 20 min) after iron treatment (250  $\mu\text{M}$ , 1 h or 24 h) **G** Representative western blot images and quantification of phospho-IRS1 (Y612) and phospho-AKT (T308) over GAPDH with insulin stimulation (10 nM or 100 nM, 5 min) after iron treatment (250  $\mu\text{M}$ , 24 h). All experiments were repeated five times. Data are expressed as means  $\pm$  SEM. \* $P < 0.05$  relative to control (basal without insulin). # $P < 0.05$  relative to basal with matched insulin stimulation at 10nM or 100nM, respectively. Scale bar = 20  $\mu\text{m}$ .

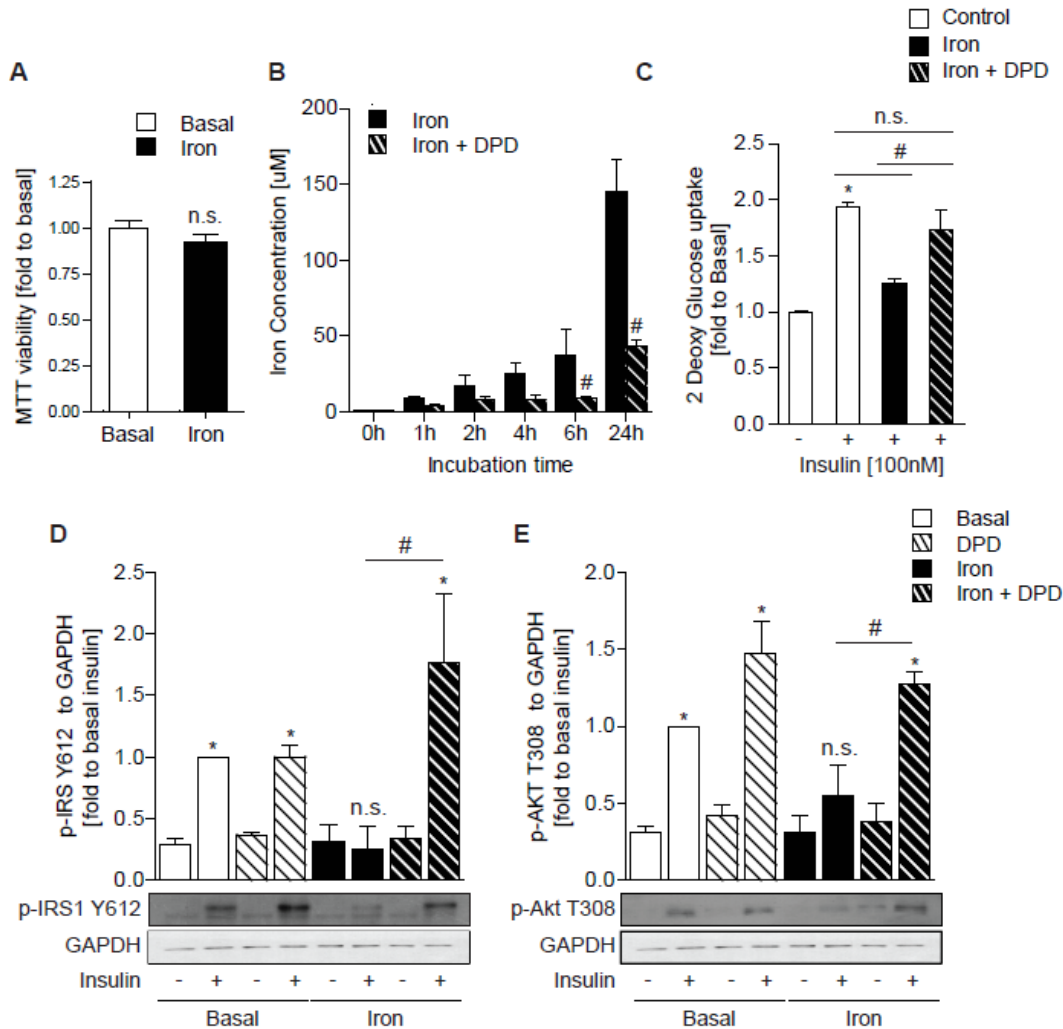


**Figure 2.2. Prevention of IO-induced insulin resistance in L6 cells with iron chelator**

**A** MTT viability assay in L6 cells after iron treatment (FeSO<sub>4</sub>, 250 μM) for 24 h **B** Time course measurement of intracellular iron concentration in L6 cells after iron treatment (250 μM) with iron chelator DPD (500 nM) for multiple time points. **C** Glucose uptake of L6 cells with insulin stimulation (100 nM, 20 min) after iron treatment (250 μM, 24 h) with DPD (500 nM). **D** Representative western blot images and quantification of phospho-IRS-1 Y612 over GAPDH in L6 cells with insulin stimulation (100 nM, 5 min) after iron treatment (250 μM, 24 h) with DPD (500 nM). **E** Representative western blot images and quantification of pAKT T308 over GAPDH in L6 cells with insulin stimulation (100nM, 5min) after iron treatment (250 μM, 24 h) with DPD (500 nM). All experiments were repeated three times. Results are represented mean +/- SEM. \*p<0.05 compared to control groups (without insulin stimulation). #P < 0.05 compared to iron treatment with insulin stimulation (100nM). n.s. p-value is not significant.

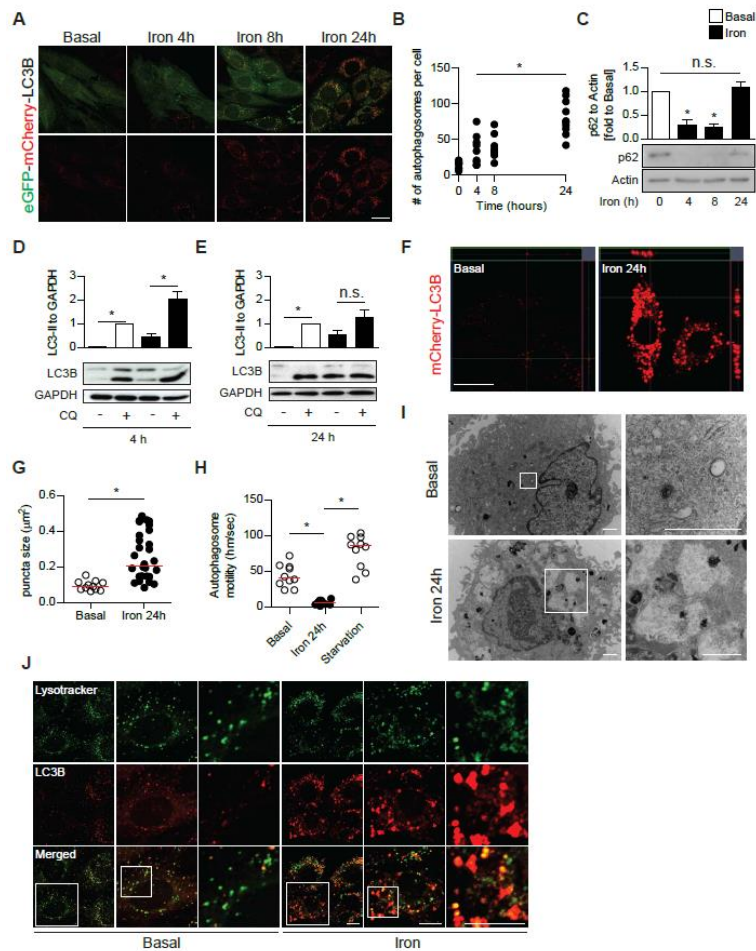


**Figure 2.3. Iron treatment transiently induced autophagy yet led to flux inhibition at 24 h iron treatment**

**A** Representative confocal microscope image of L6 cells stably expressing tandem fluorescent-eGFP-mCherry LC3B treated with iron ( $\text{FeSO}_4$ ,  $250 \mu\text{M}$ ) for the indicated time points (4 h, 8 h, 24 h). **B** Quantification of mean LC3B puncta per cell from Fig 2A. **C** Representative western blot images and quantification of p62 to actin in L6 cells after iron treatment ( $\text{FeSO}_4$ ,  $250 \mu\text{M}$ ) at multiple time points. **D** Representative western blot images and quantification of LC3B-II to GAPDH in L6 cells after 4h iron treatment stimulated with chloroquine (CQ,  $30 \mu\text{M}$ ). **E** Representative western blot images and quantification of LC3B-II to GAPDH in L6 cells after 24 h iron treatment stimulated with CQ  $30 \mu\text{M}$ . **F** Representative confocal microscope z-stack image of mCherry-LC3B L6 cells after iron treatment ( $250 \mu\text{M}$ , 24 h). **G** Quantification of LC3B puncta size from Fig 2.3F. **H** Quantification of autophagosomes motility from live cell microscopy from mCherry-LC3B L6 cells under basal, iron ( $250 \mu\text{M}$ , 24 h) and starvation (amino acid free) condition. **I** Representative TEM images of autophagosome and autophagolysosomes in L6 cells after iron treatment ( $250 \mu\text{M}$ , 24 h). **J** Representative confocal microscope images of eGFP-mCherry-LC3B L6 cells with Lysotracker DeepRed after iron treatment ( $250 \mu\text{M}$ , 24 h). Data are expressed as means  $\pm$  SEM. \* $P < 0.05$  compared to basal. Western blot and confocal image analysis were performed three times. Scale bar (confocal microscope) =  $10 \mu\text{m}$ . Scale bar (electron microscope) =  $1 \mu\text{m}$ .

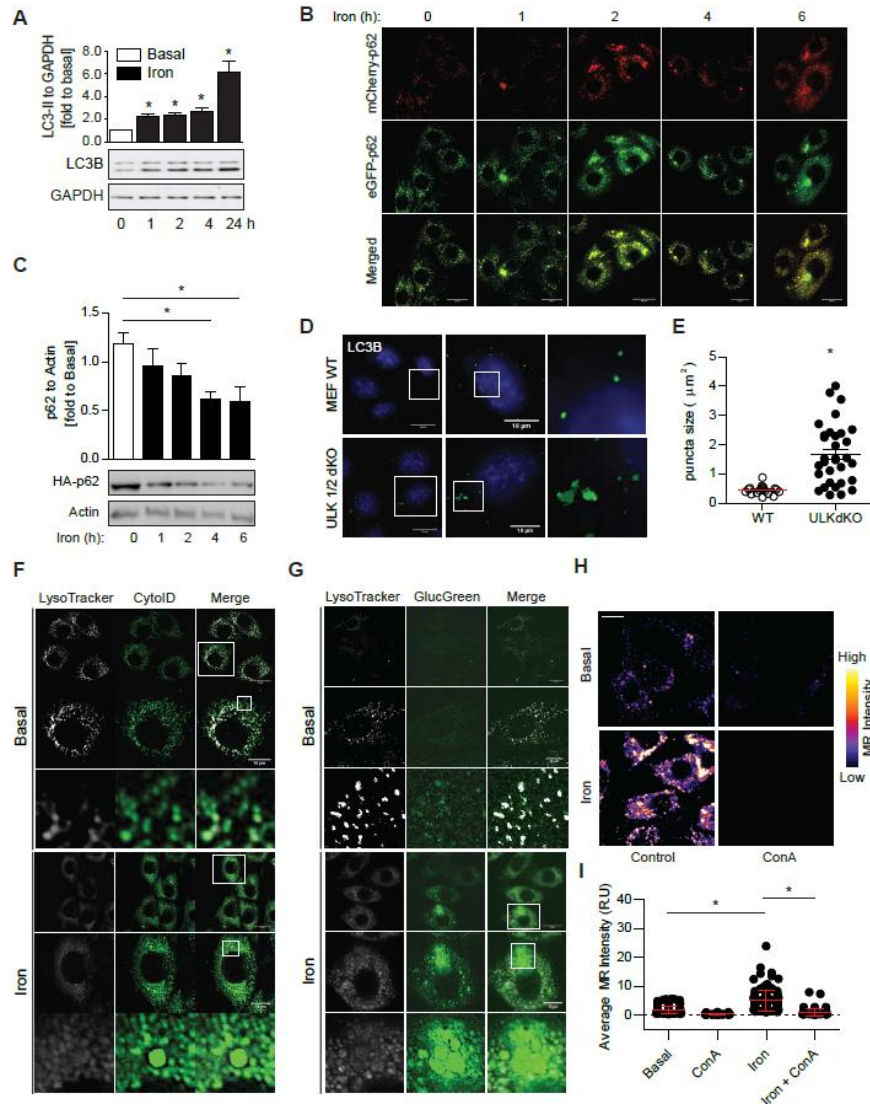


**Figure 2.4. Chronic IO resulted in accumulation of abnormal autophagosomes despite normal proteolytic activity**

**A** Representative western blot images and quantification of LC3B-II to GAPDH in L6 cells after iron treatment (FeSO<sub>4</sub>, 250  $\mu$ M) for multiple time points. **B** Representative epi-fluorescent images of p62 puncta in L6 cells stably expressing mCherry-eGFP p62, after iron treatment (250  $\mu$ M) at time points indicated. **C** Representative western blot images and quantification of L6 transfected with HA-p62 after iron treatment (250  $\mu$ M) at time points indicated. **D** Representative epi-fluorescent images of MEF cells ( wild type, and ULK1 and ULK2 dKO) immuno-stained against LC3B. **E** Quantification of LC3B puncta size from Fig EV2D. **F** Representative epi-fluorescent images of autophagosomes (CytoID) and lysosome (LysoTracker) in L6 cells after iron (FeSO<sub>4</sub>, 250  $\mu$ M) for 24h. **G** Representative epi-fluorescent images of beta-glucosidase (GlucGreen) and lysosome (LysoTracker) in L6 cells after iron (FeSO<sub>4</sub>, 250  $\mu$ M) for 24h. **H** Representative confocal microscope images of L6 cells pulsed with Magic Red L after iron treatment (250  $\mu$ M, 24 h) with 1  $\mu$ M concanamycin A. **I** Quantification mean fluorescence intensity from magic red signals in 3D puncta in Fig 2.4H. Data are expressed as means  $\pm$  SEM. \*P < 0.05 compared to basal or wild type. Western blot and confocal image analysis were performed three times. Scale bar = 15  $\mu$ m

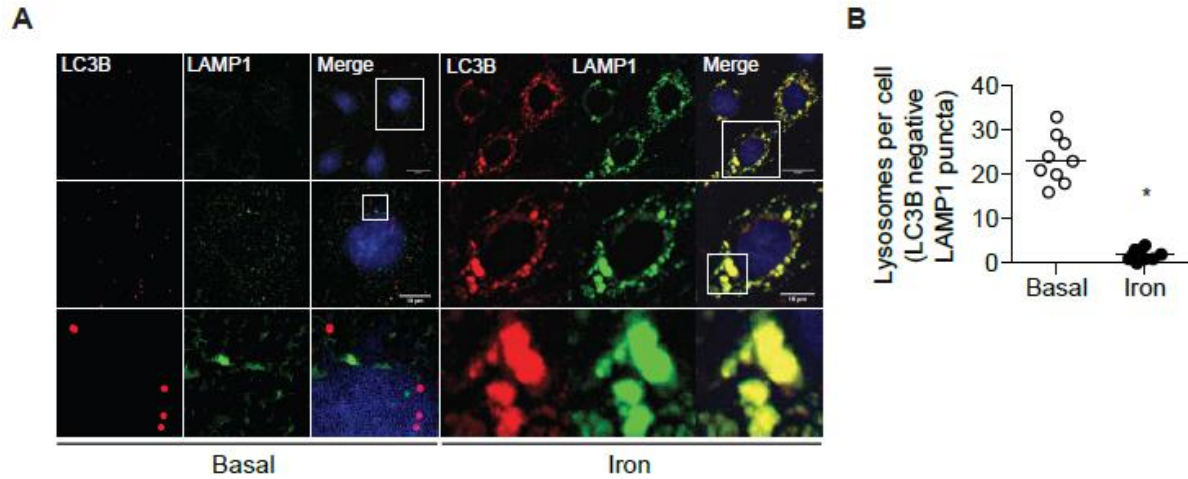


**Figure 2.5. Precipitous loss in autophagosome-free lysosome after IO**

**A** Representative epi-fluorescent microscope images of L6 cells immuno-stained against LC3B (autophagosomes) and LAMP1 (lysosome) in L6 cells in response to iron treatment (250  $\mu$ M, 24 h) **B** quantification of number of autophagosome-free lysosomes per cell. Scale bar = 20 , 10 and 5  $\mu$ m.

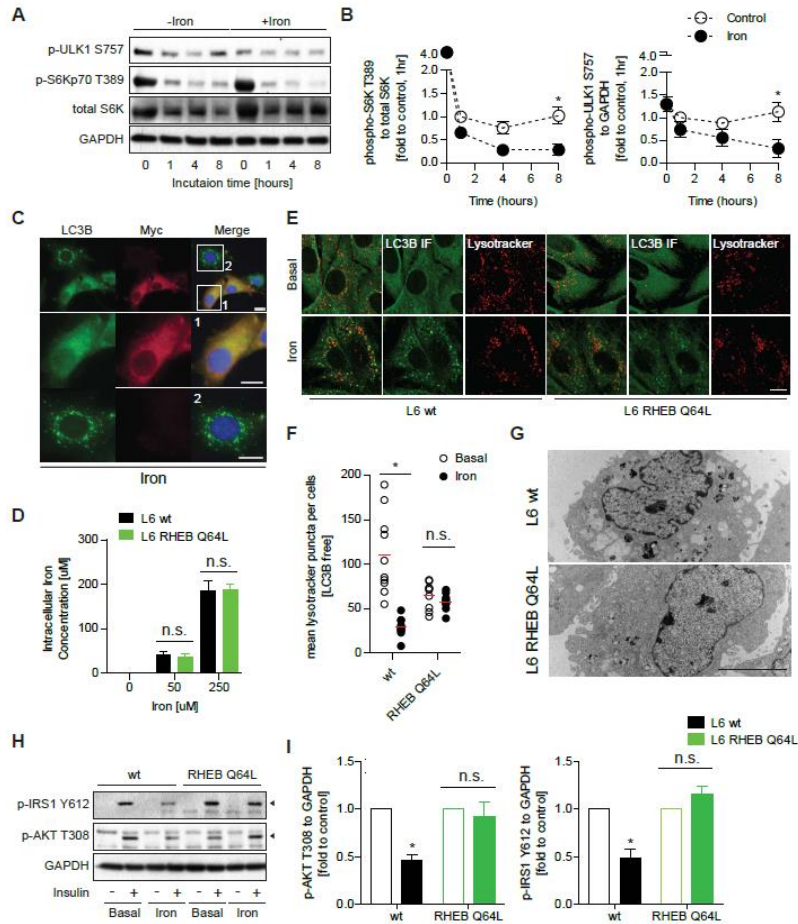


**Figure 2.6. Iron treatment impaired mTOR restoration following autophagosomes degradation and enforced mTOR re-activation reversed autophagy defects and insulin resistance**

**A** Representative western blot images of phospho-ULK1 (S757), phospho-S6Kp70 (T389), total S6K, GAPDH after iron treatment (FeSO<sub>4</sub>, 250 μM) for multiple time points. **B** Quantification of mTORC1 activity analyzed through phosphorylation of S6K T389 to total S6k and ULK1 S757 to GAPDH after iron treatment (FeSO<sub>4</sub>, 250 μM) for multiple time points. **C** Representative epi-immunofluorescent images of L6 cells transfected with myc-RHEB Q46L and immuno-stained against LC3B and myc after iron treatment (FeSO<sub>4</sub>, 250 μM) for 24 h. **D** Ferrozine-based colorimetric measurement of intracellular iron in wild-type (wt) L6 and RHEB-Q64L L6 cells after iron treatment (50 μM or 250 μM) for 24 h. **E** Representative confocal images of wt L6 and RHEB-Q64L L6 cells pulsed with Lysotracker Deep Red and immuno-stained against LC3B after iron treatment (250 μM, 24 h). **F** Quantification of LC3B-free lysosome numbers in Fig 2.6E **G** Representative TEM images of wt L6 and RHEB-Q64L cells after iron treatment (250 μM, 24 h). **H-I** Representative western blot images and quantifications of phospho-IRS1 (Y612) and AKT (T308) to GAPDH in wt and RHEB-Q64L L6 cells stimulated with insulin (100 nM, 5 min) after iron treatment (250 μM, 24 h). All experiments were performed three times. Data are expressed as means ± SEM. \*P < 0.05 relative to control. Scale bar (confocal microscope) = 10 μm, (electron microscope) = 5 μm, and (epi-immunofluorescent microscope) = 25 and 5 μm

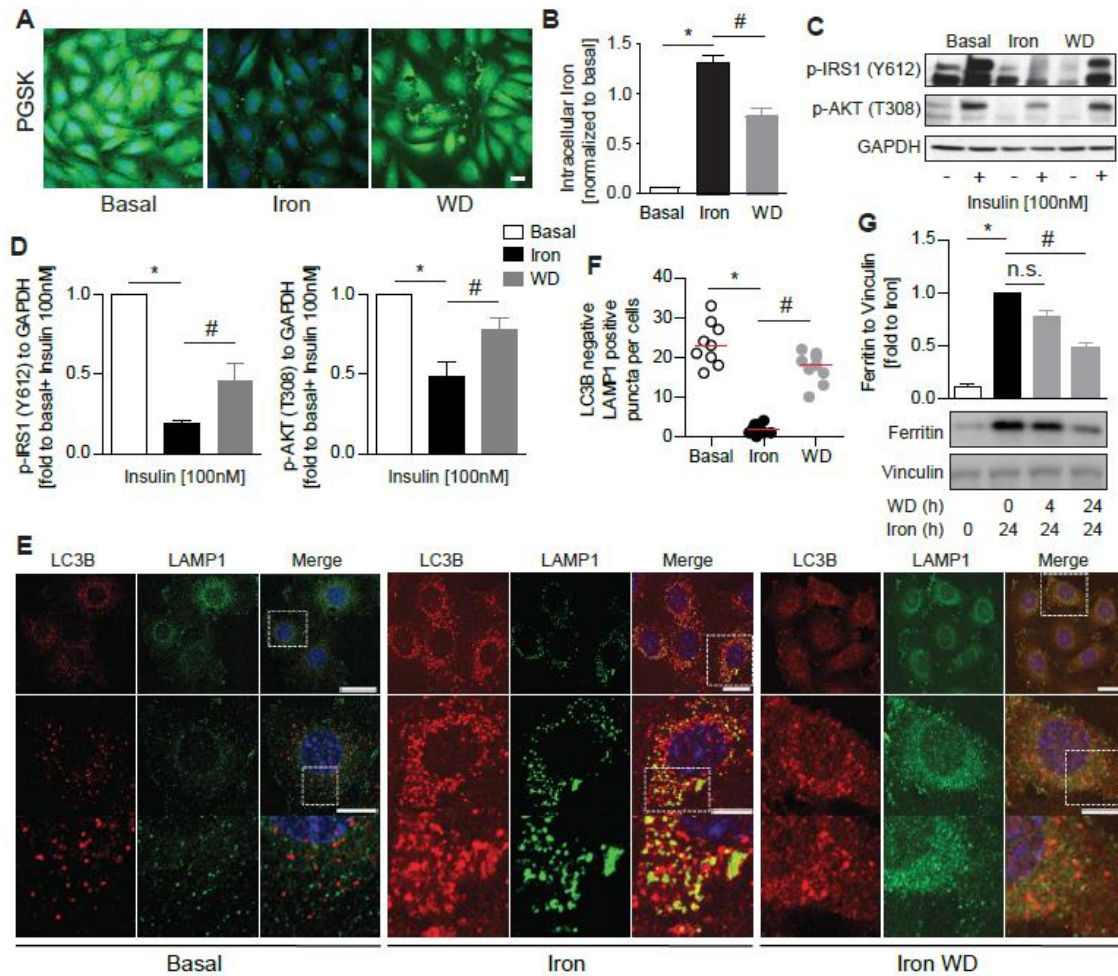


**Figure 2.7. Restoration of lysosomal pools following iron withdrawal reversed insulin resistance**

**A** Representative confocal microscope images of L6 cells pulsed with PGSK dye after iron treatment (250  $\mu$ M, 24 h) followed by 24 h iron withdrawal. **B** Ferrozine based colorimetric measurement of intracellular iron in L6 cells after iron treatment (250  $\mu$ M, 24 h) followed by 24 h withdrawal. **C-D** Representative western blot images and quantification of phospho-IRS1 (Y612) and phospho-AKT (T308) to GAPDH in L6 cells iron treatment (250  $\mu$ M, 24 h) followed by 24 h withdrawal. **E** Representative epi-immunofluorescent microscope images of L6 cells immuno-stained against LC3B and LAMP1 after iron treatment (250  $\mu$ M, 24 h) followed by 3 h withdrawal. **F** Quantification of autophagosome-free lysosomes in Fig 2.7E. **G** Representative western blot images and quantification of ferritin to vinculin in L6 cells after iron treatment (250  $\mu$ M, 24 h) followed by withdrawal for 4 h or 24 h. All experiments were performed three times. Data are expressed as means  $\pm$  SEM. \* $P$  < 0.05 relative to Basal or Control (insulin stimulation). # $P$  < 0.05 relative to Iron. Scale bar = (confocal microscope) 10  $\mu$ m and (epi-immunofluorescent microscope) = 20, 10 and 5  $\mu$ m

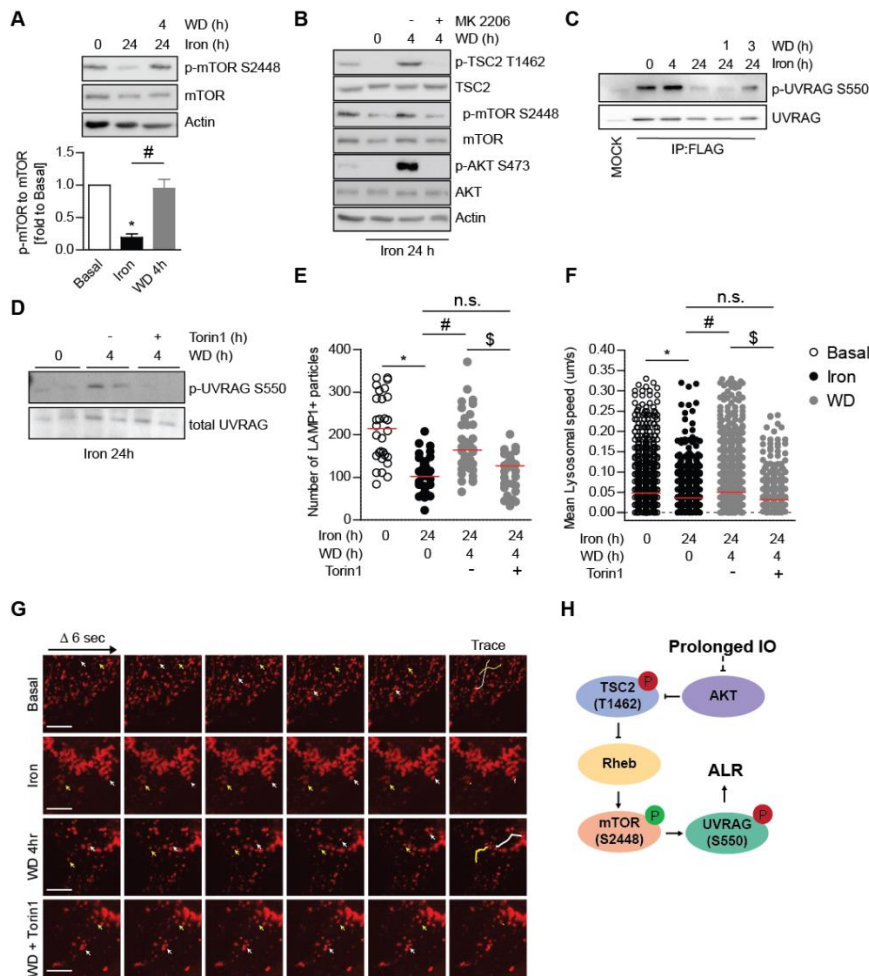


**Figure 2.8. Molecular mechanisms underlying IO-induced mTOR activity suppression**

**A** Representative western blot images and quantification of phospho-mTOR S2448, total mTOR and actin in L6 cells after iron treatment (250  $\mu$ M, 24 h) followed by withdrawal for 4 h. **B** Representative western blot images of phospho-mTOR S2448, total mTOR, phospho-TSC2 T1462, total TSC2, phospho-mTOR S2448, total mTOR, phospho-AKT S473, total AKT, actin in L6 cells after iron treatment (250  $\mu$ M, 24 h) followed by withdrawal for 4 h with or without MK2206 (AKT inhibitor.) **C** Representative western blot images of phospho-UVRAG S550 and total UVRAG in L6 cells transfected with FLAG-UVRAG and FLAG pulldown after iron treatment (250  $\mu$ M, 4 h and 24 h) followed by withdrawal for 1 h and 3 h. **D** Representative western blot images of endogenous phospho-UVRAG S550, total and UVRAG expression in L6 cells after iron treatment (250  $\mu$ M, 24 h) followed by withdrawal for 4 h with or without torin1 (200 nM). **E** Live cell imaging analysis of L6 cells transfected with LAMP1-RFP from lysosomal number (E) and speed (F) in L6 cells after iron treatment (250  $\mu$ M, 24 h) followed by withdrawal for 4 h with or without Torin1 (200 nM). **G** Representative confocal images of time-lapse captures of lysosomes at 6 sec intervals for 30 sec. **H** Schematic diagram of mTOR signaling regulation by IO. \* $p < 0.05$  compared to Basal. # $p < 0.05$  compared to Iron. \$ $p < 0.05$  compared to WD 4hr. Scale bar = 10  $\mu$ m.

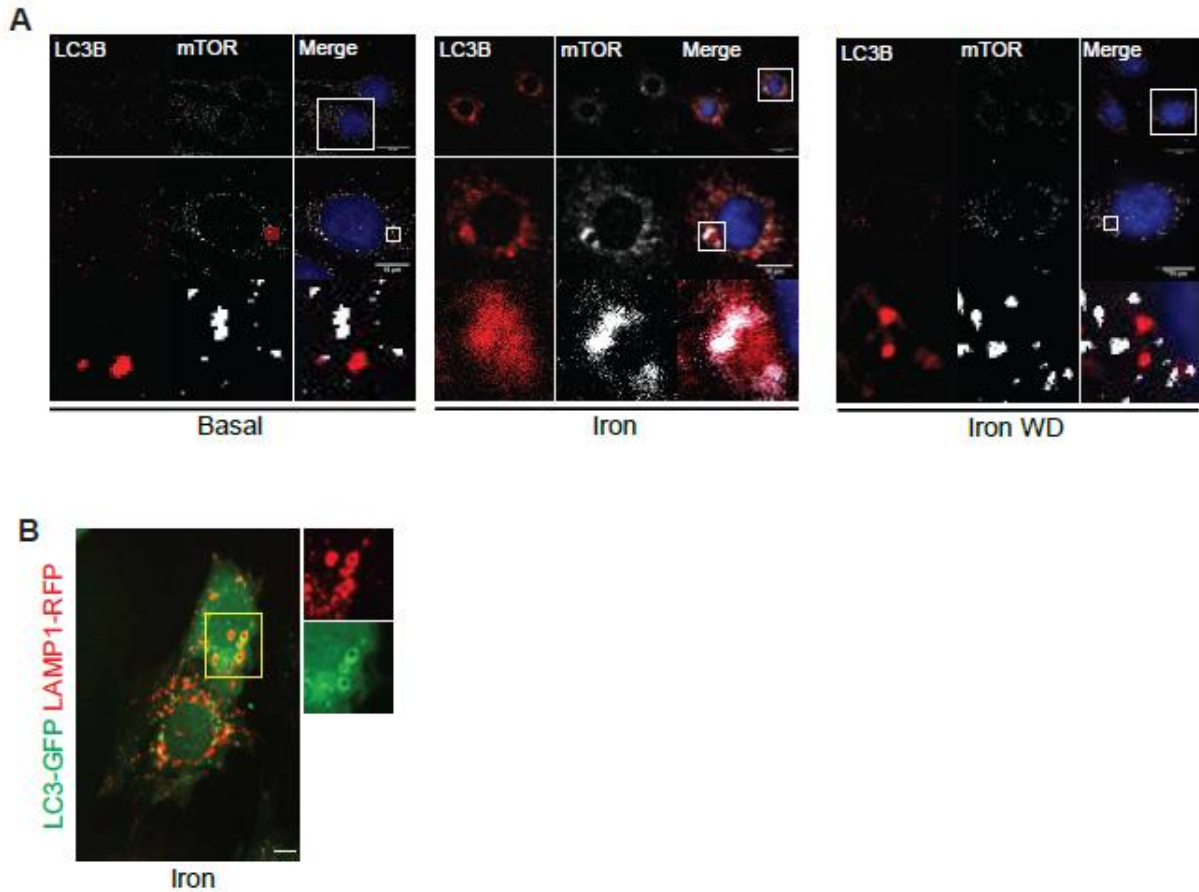


**Figure 2.9. Molecular mechanisms underlying iron mediated mTOR suppression and restoration of lysosomal pools after iron withdrawal**

**A** Representative epi-fluorescent microscope images of L6 cells immuno-stained against LC3B and mTOR after iron treatment (250  $\mu$ M, 24 h) followed by withdrawal for 4 h. **B** Representative confocal images of L6 cells transfected with LC3-GFP and LAMP1-RFP after 24 h iron treatment (250  $\mu$ M). Scale bar (confocal microscope) = 10  $\mu$ m and (epi-immunofluorescent microscope) = 20, 10 and 5  $\mu$ m

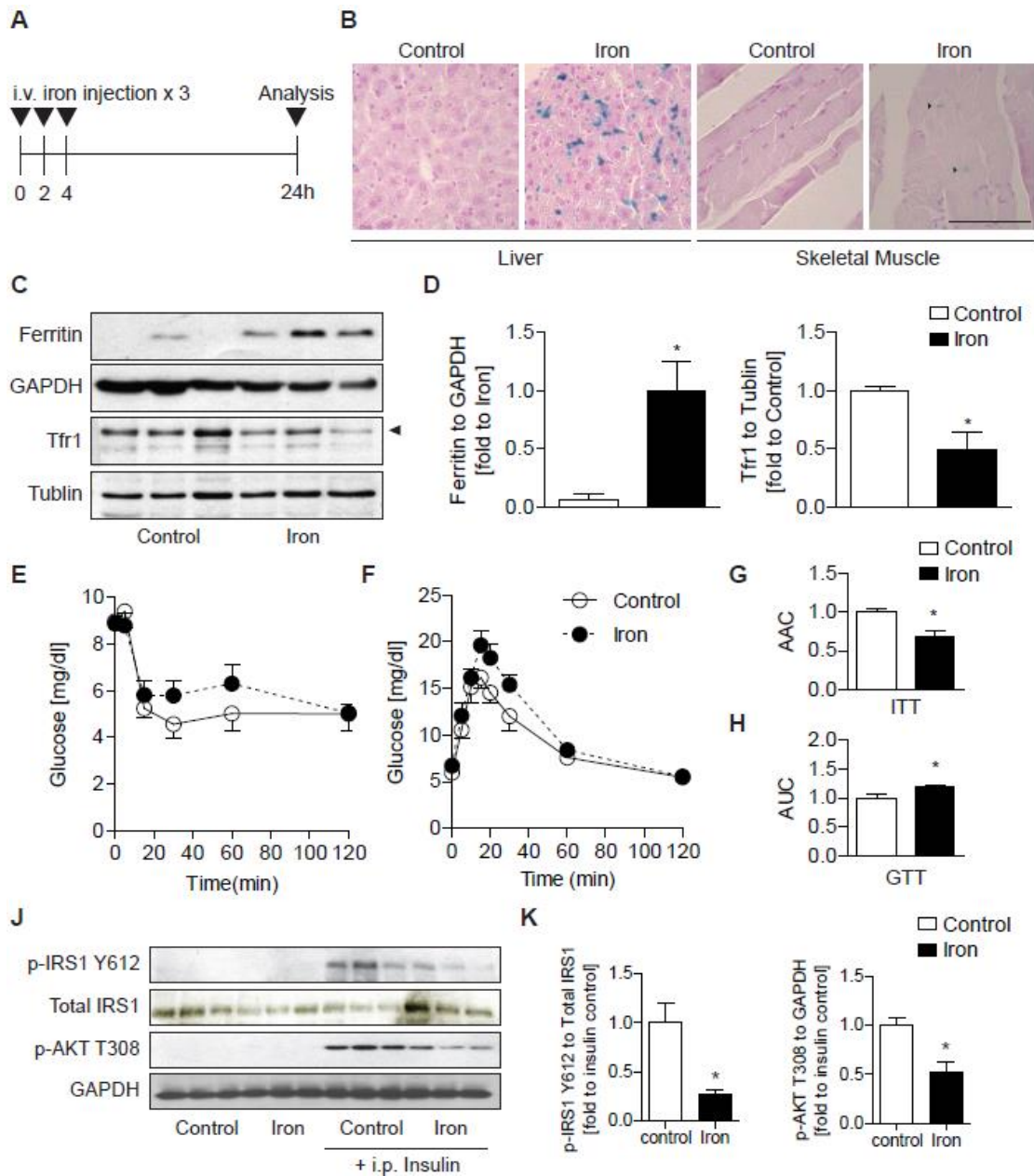


**Figure 2.10. Development of acute Iron Overload (IO) In Vivo model and validation of IO and insulin resistance in skeletal muscle**

**A** Schematic diagram of iron-dextran injections experimental plan. **B** Prussian Perl blue staining in liver and skeletal muscle after iron injections. **C-D** Representative western blot images and quantification of ferritin and tfr1 to tubulin in skeletal muscles 24 h after iron injections. **E** Insulin tolerance test 24 h after iron injections. **F** Glucose tolerance test (GTT) 24 h after iron injections. **G** Quantification of area under curve in ITT. **H** Quantification of area under curve for panel F. **I-J** Representative western blot images and quantification of phospho-IRS1 (Y612) and phospho-AKT (T308) to GAPDH in skeletal muscles 24 h after iron injection followed by i.p. insulin injection. n=6 for ITT and GTT. n=3 for western blot analysis. \*p<0.05 compared to control. Scale bar = 50  $\mu$ m.

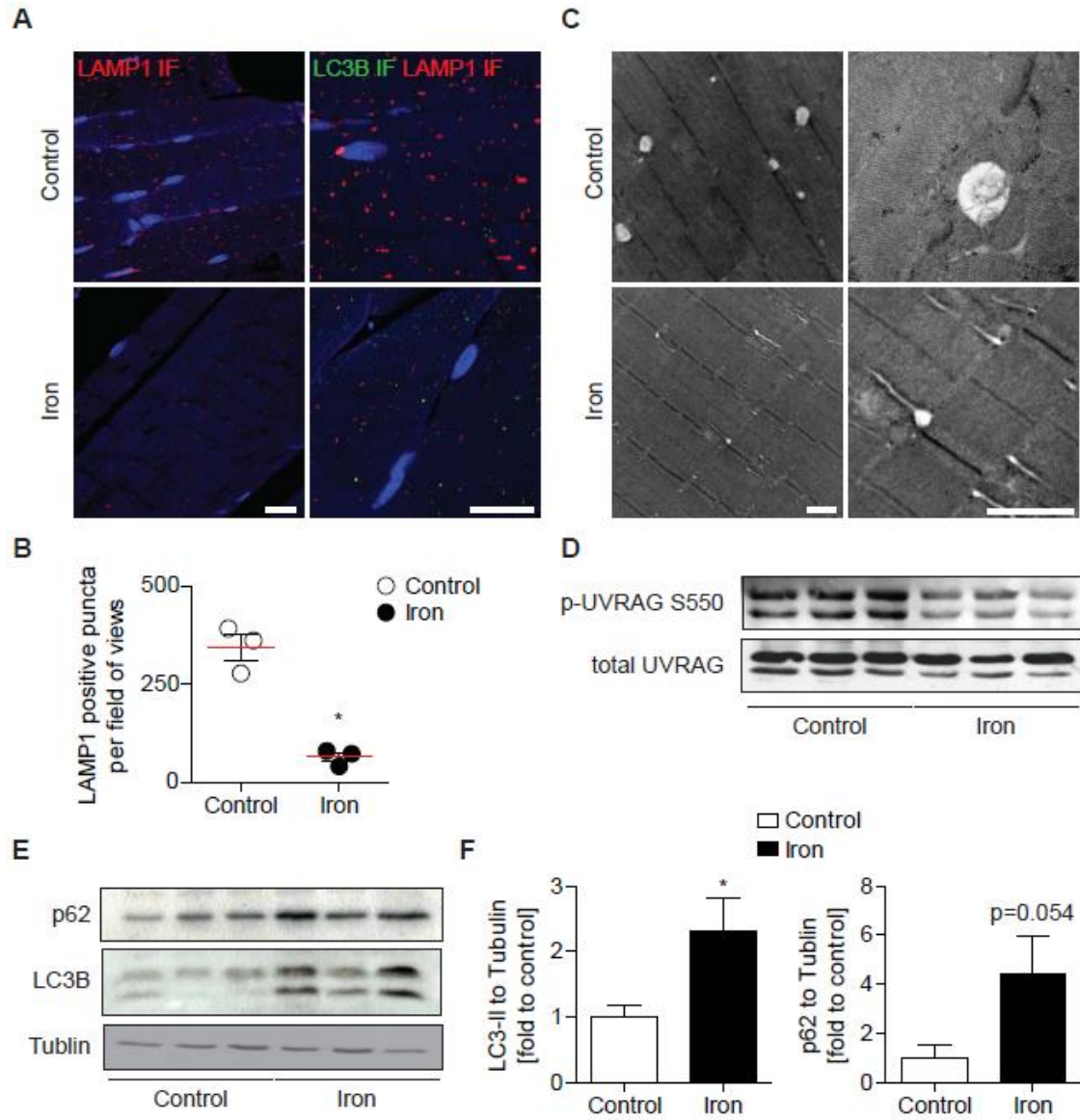


**Figure 2.11. Evidence of ALR defects in skeletal muscles after acute IO**

**A** Representative confocal microscope images of skeletal muscle tissue sections immuno-stained against LC3B (Alexa 647) and LAMP1 (Alexa 555) **B** Quantification of lysosomes (LAMP1 puncta) in skeletal muscles 24 h after iron injections. **C** Representative TEM images of skeletal muscle 24 h after iron injections. **D** Representative western blot images of phospho-UVRAG S550 and total UVRAG in skeletal muscle 24 h after iron injections. **E-F** Representative western blot images and quantification of LC3-B and p62 to tubulin in skeletal muscles 24 h after iron injections.  $n=3$ . Results are presented in mean  $\pm$  SEM. \* $p<0.05$  compared to control. Scale bar (confocal microscope) 20  $\mu\text{m}$ . Scale bar (electron microscope) = 500 nm.

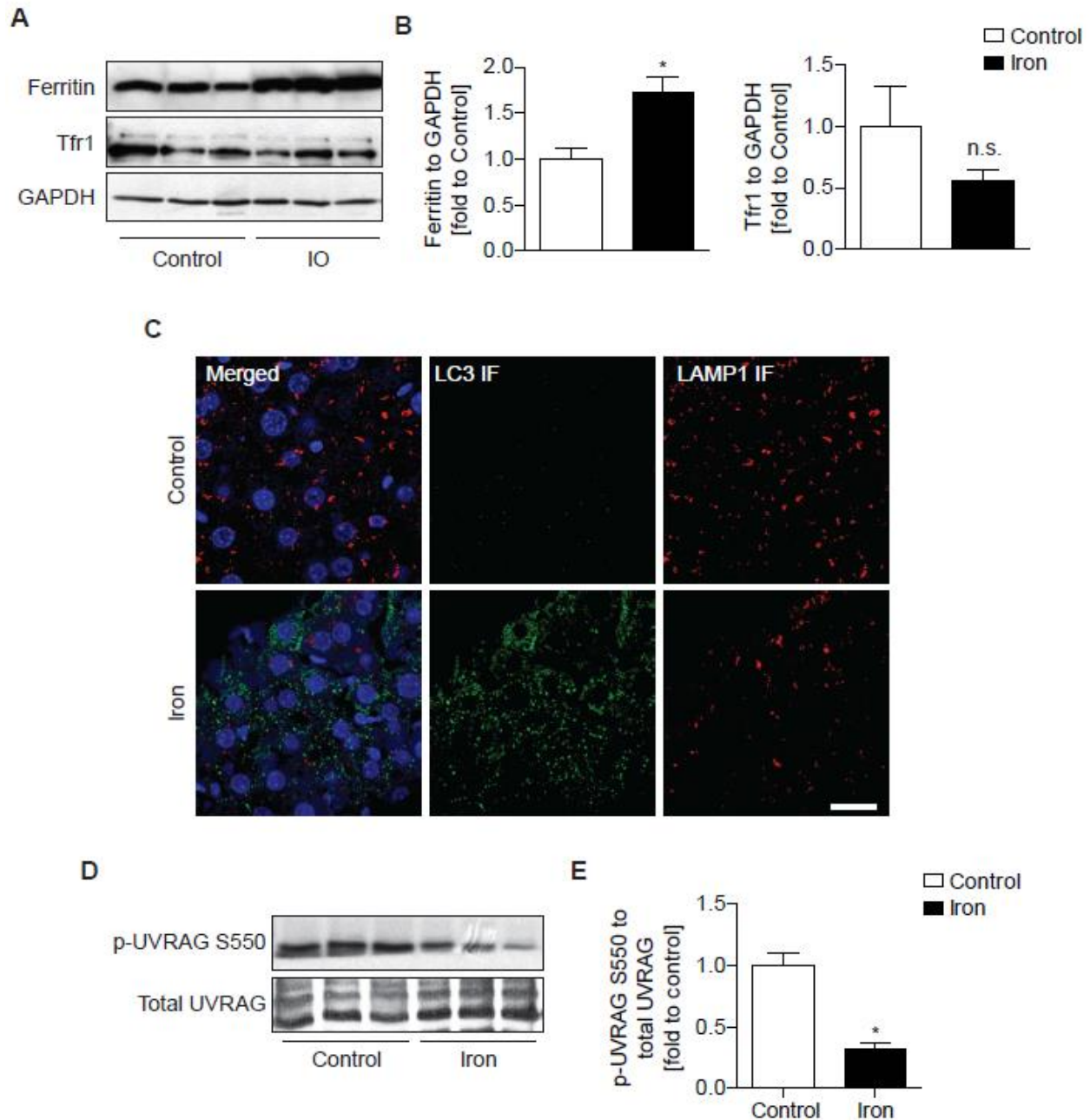


**Figure 2.12. ALR defects in liver after iron overload**

**A-B** Representative western blot and quantification of ferritin and tfrq to GAPDH in liver 24 h after iron injections. **C** Confocal microscope images of liver tissue sections immuno-stained with against LC3B (Alexa 647) and LAMP1 (Alexa 555) **D-E** Representative western blot images and quantification of phospho-UVRAG S550 to total UVRAG in liver 24 h after iron injections. n=3. \*p<0.05 compared to Control.

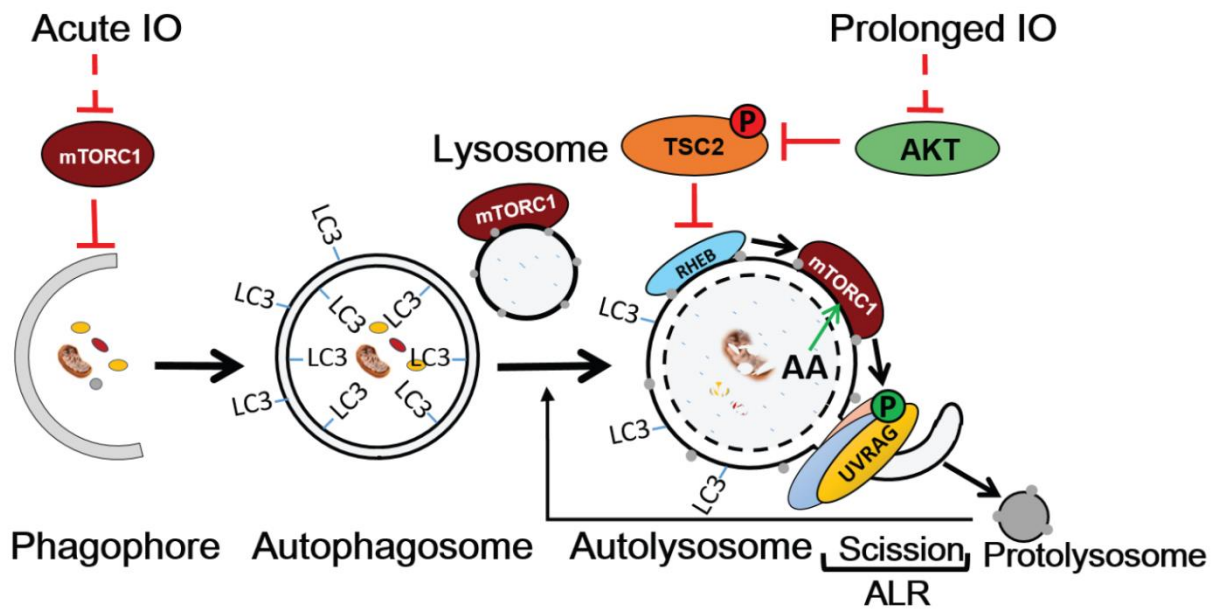


**Figure 2.13. Schematic diagram of IO-mediated autophagy regulation**

Working model of autophagy regulation by IO. Acute IO leads to inhibition of mTORC1 leading to autophagy induction. Prolonged IO prevents ALR-mediated production of new lysosomes through AKT-TSC-Rheb-mTORC1-UVRAG signaling defects. The lack of free lysosomes contributes to autophagy inhibition and insulin resistance in skeletal muscle.

## 2.5 Discussion

IO is a devastating and complex condition that most notably arises in individuals with beta thalassemia that require frequent blood transfusions or those with hereditary hemochromatosis, while IO in metabolic syndrome is also a common finding [189]. The pathophysiological mechanism underlying IO-induced diabetes is complicated as both insulin deficiency and insulin resistance contribute [180]. The causative relationship between IO and insulin secretion defects is well established [232], yet the precise mechanisms whereby iron can elicit insulin resistance are complicated and we believe that IO in skeletal muscle is underappreciated [192, 233]. Here we used an *In Vitro* model using L6 cells and translated this to analysis of mouse skeletal muscle using an *In Vivo* model of iron overload. In both, we observed that skeletal muscle insulin sensitivity was significantly compromised after IO. We found that preventing excess free iron levels in L6 cells using an iron chelator could prevent IO-induced insulin resistance and metabolic dysfunction, which is in keeping with the fact that clinical interventions to reduce free iron improved insulin sensitivity and can delay onset of T2D [190-192].

We and others have recently focused on the role of autophagy in regulation of metabolism at various levels [171, 179, 234]. For example, we have previously shown that stimulation of autophagy by adiponectin was of functional significance in improving insulin sensitivity and metabolism in skeletal muscle [179]. Interestingly, IO-induced insulin resistance has been described to involve reduced adiponectin expression in adipocytes. However, systematic IO did not always translate to insulin resistance because adipocytes could enhance iron excretion to avoid intracellular iron overload [47].

The relationship between IO and autophagy has been examined, where acute IO was observed to stimulate autophagy [235, 236]. Indeed, this is in agreement with our own observations in that IO

exposure for up to eight hours stimulates autophagy. This increase in autophagy is likely the result of a compensatory cellular response upon detection of cellular stress. Acute IO activation of autophagy is also consistent with the observed rapid inhibition of mTORC1, the single most potent repressor of autophagy in mammals that responds to a large number of stressors including nutrient starvation and ER stress [237-240]. Yet, there are several problems with these conditions. First, acute IO does not reflect clinical reality of individuals that suffer from IO – chronic IO treatments and their pathophysiological effects are a more realistic case study. Second, initiation of autophagy is only the first step in a much more elaborate series of events that evolved to resolve stress and promote cell survival. Following autophagy, autophagosomes mature by fusing with lysosomes to degrade cargo and this is then followed by a third stage, whereby autolysosomal membranes are resorbed back into the endomembrane system, including reformation of lysosomes using a process now referred to as ALR. ALR is thus critical for cells to regain their degradative capacity and autophagic proficiency under prolonged stress. We now show for the first time that chronic IO causes autolysosomes to accumulate while depleting cells of free lysosomes, suggesting a defect in ALR.

Importantly, we have determined that IO prevents the reactivation of mTORC1 on autolysosomes thereby causing a precipitous loss of a distinct lysosomal compartment. Normally, degradation of autophagic cargo locally stimulates mTORC1 on matured autolysosomes, even when the majority of mTORC1 remains inactive and is not bound to lysosomes. This localized reactivation of mTORC1 then promotes lysosomal reformation from the spent autolysosomes [219]. However, since IO prevents mTORC1 activation, lysosome reformation is impaired and lysosome numbers are depleted. Conversely, iron withdrawal restored mTORC1 activity, downstream UVRAG signaling, lysosomal numbers, and insulin

signaling. Furthermore, forced activation of mTORC1 by expressing the constitutively active Rheb-GTPase not only prevented autophagosome accumulation with minimal lysosomal loss, but also restored insulin sensitivity in cells exposed to IO. Altogether, these data strongly indicate that the block of mTORC1 activation on autolysosomes by IO is a contributor of insulin resistance.

Overall, our study adds important new knowledge on a novel molecular mechanisms contributing to insulin resistance in response to IO and presents the first *in vivo* model to show an ALR defect [201]. Mechanistically, we observed that chronic IO led to a decrease in Akt-mediated repression of TSC2, resulting in a potent repression of Rheb and mTORC1, with consequent loss of ALR. Furthermore, our data indicates that mTOR-UVRAG dependent lysosomal pool regeneration is an important contributor in maintaining autophagic flux and insulin sensitivity in skeletal muscle. Together, our data uncover a previously undocumented mechanism via which chronic IO limits autophagic capacity and leads to metabolic dysfunction. This observation may have implications in a wide range of disease states where cellular IO plays a pathogenic role.

## CHAPTER 3

### 3.1 Abstract

Heart failure is a leading cause of death, especially in the elderly or obese and diabetic populations. Various remodeling events have been characterized, which collectively contribute to the progression of heart failure. Of particular interest, autophagy has recently emerged as an important determinant of cardiac remodeling and function. Here, we used aged, 13-month-old, male adiponectin knockout (Ad-KO) or wild-type (wt) mice subjected to aortic banding to induce pressure overload (PO). Cardiac strain analysis using speckle tracking echocardiography indicated significant dysfunction at an earlier stage in Ad-KO than wt. Analysis of autophagy by Western blotting for Light Chain 3 or microtubule-associated proteins 1B and Sequestosome 1 together with transmission electron microscopy of left ventricular tissue indicated a lack of PO-induced cardiac autophagy in Ad-KO compared with wt mice. Associated with this was mitochondrial degeneration and evidence of enhanced endoplasmic reticulum stress. Western blotting for Light Chain 3 or microtubule-associated proteins 1B, examination of flux using tandem fluorescent tagged-Light Chain 3, and analysis of lysosomal activity in H9c2 cardiac myoblasts treated with adiponectin indicated that adiponectin enhanced autophagy flux. In conclusion, adiponectin directly stimulates autophagic flux and the lack of autophagy in response to PO in aged mice lacking adiponectin may contribute to cellular events which exacerbate the development of cardiac dysfunction.

### **3.2 Introduction**

Cardiovascular disease, including heart failure, is the leading cause of death worldwide, especially in the elderly or obese and diabetic populations [241-243]. Accordingly, there have been extensive efforts to investigate the various cellular and structural changes which occur in the failing heart [9, 244]. Well-established remodeling events that contribute to the progressive development of heart failure include alterations in fibrosis, hypertrophy, and metabolism [9, 245]. Recently, autophagy has emerged as an important determinant of cardiac remodeling and function [246-249], and we now must understand more clearly the changes in autophagic flux which occur in relevant animal models of heart failure. Indeed, various studies have shown that surgical induction of pressure overload (PO) in mice elevated cardiac autophagy [250-252], and studies in autophagy-deficient mice have implicated this process in reversal of hypertrophy and improvement in function after alleviation of cardiac stress [253, 254]. Furthermore, maintenance of adequate tonic levels of autophagy is critical in maintaining optimal cardiac structure and function and lack of autophagy will cause age-related cardiomyopathy [255]. As can be seen from these examples, autophagy can clearly influence cardiac structure and function, and its precise role, as well as physiological regulatory mechanisms, must be fully understood. An important potential pathophysiological mechanism of heart failure in obesity and diabetes is due to altered circulating adipokine profiles [9]. In particular, adiponectin is one of the most abundant proteins in the circulation of normal individuals, yet levels are reduced in obese and/or diabetic individuals [256]. Importantly, numerous clinical studies have established correlations between adiponectin and various aspects of heart failure [257]. Adiponectin knockout (Ad-KO) mice have proven to be highly informative as a model to delineate the role of adiponectin, with these mice typically showing exaggerated

cardiac remodeling and dysfunction in response to various cardiac stressors [257]. Previous work has established anti-hypertrophic, anti-fibrotic, anti-inflammatory, anti-apoptotic, and beneficial metabolic effects of adiponectin, which together may all contribute to its cardioprotective effects [257]. Almost all of these studies were performed in young mice and very few studies have examined changes in aged Ad-KO mice. However, one very recent study has shown that high-fat diet induced more cardiac endoplasmic reticulum (ER) stress in 11-month-old Ad-KO vs wild-type (wt) mice [258]. Here, we used aged Ad-KO mice and subjected them to aortic banding, or sham, surgery to induce PO. Temporal analysis of cardiac cellular, structural and functional changes was performed 3 days, 1, 2, and 3 weeks after surgery. Echocardiography with strain rate analysis indicated earlier and more significant cardiac dysfunction in Ad-KO mice after PO, which, as expected, was associated with enhanced cardiomyocyte hypertrophy. An important new observation from this work was the lack of autophagy in response to PO in hearts of Ad-KO mice and concomitant development of elevated endoplasmic reticulum stress and gross mitochondrial dysfunction (Figure 3.1).

### **3.3. Materials and Methods**

#### ***Animals and minimally invasive transverse aortic banding to induce PO***

We used male Ad-KO mice [120] at 13 months of age. Animal facilities met the guidelines of the Canadian Council on Animal Care and all protocols used were approved by the Animal Care Committee, York University. Left ventricular (LV) PO was induced by subjecting mice to minimally invasive transverse aortic banding or PO as validated [259] and described [260] previously. Briefly, mice are placed under general anesthesia (ip; xylazine 0.15 mg/g; ketamine 0.03 mg/g) in supine position, and skin is sterilized with betadine after shaving. Medial cranio-caudal incision is made through the skin from neck to the sternum, and an incision is made through the suprasternal notch, 2-3mm down the rib cage. Transverse aorta is visualized under low magnification between the innominate and left common carotid arteries. Titanium micro ligation clip is applied across the transverse aorta using banding calipers calibrated to a 27-g needle. Sham surgery is performed as outlined above without placement of ligation clip. Upon completion of procedure, rib cage and skin are closed with silk suture. Mice are injected with Buprenorphine (sc 0.05 mg/ kg) and placed face down on a warming pad until awake.

#### ***Analysis of cardiac function using echocardiography***

Echocardiography was performed as we previously described [261, 262] using the Vevo2100 system (Visual Sonics) equipped with an MS550D transducer. Mice were lightly anesthetized using 2.0% isoflurane mixed with 100% O<sub>2</sub> during the time of imaging. M-mode images of the parasternal short-axis view at papillary level were used to calculate the cardiac systolic functions of ejection fraction, fractional shortening and cardiac output. Speckle-tracking cardiac strain analysis was performed using VevoStrain software and movie files acquired from the B-mode

and M-mode view. All parameters were averaged over at least 3 cardiac cycles for analysis. Histological analysis of cardiac structure Animals were sacrificed through cervical dislocation and hearts were quickly isolated and perfused with ice-cold cardioplegic solution (30 mM KCl in PBS) to arrest the heart in diastole. Hearts were sliced at midventricular level and stored in 10% neutral buffered formalin for fixation at room temperature for 24 hours before paraffin embedding and serially sectioned (10 µm slices).

#### ***Wheat germ agglutinin (WGA) staining***

Paraffin-embedded sections were deparaffinized and rehydrated first with descending concentrations of ethanol and then brought into double distilled water. The sections then were incubated with WGA (Alexa Fluor 488 conjugated; Life Technologies) for 2 hours in the dark, briefly washed with PBS, and then mounted on coverslips using ProLong Gold (Life Technologies). The images were captured with an Olympus confocal microscope and analyzed with NIH ImageJ software (v.147). Quantitative data from at least 100 cells were determined per group from representative triplicate experiments.

#### ***Detection of aggresome with p62 (sequestosome 1[SQSTM1]) immunofluorescence***

Paraffin-embedded sections were deparaffinized and rehydrated first with descending concentrations of ethanol and then brought into double distilled water. The sections then were permeabilized with phosphate buffered saline with Triton X-100 (0.3% Triton X-100 in PBS) and blocked with 5% goat serum in phosphate buffered saline with Triton X-100 for 90 minutes. After an overnight incubation with p62 (1:100) primary antibody, tissue sections were incubated with secondary antibody conjugated with Alexa Fluor 488. Tissue sections were further stained

with the ProteoStat Aggresome Detection kit according to the manufacturer's instruction [263], then mounted on coverslips using ProLong Gold (Life Technologies). The images were captured with an Olympus confocal microscope.

### ***Transmission electron microscopy (TEM)***

TEM was performed as described previously [263]. Briefly, LV tissues from sham-operated or banded mice were cut into small pieces (roughly 1 mm<sup>3</sup>) and immediately fixed in 2.5% glutaraldehyde in 0.1M sodium cacodylate buffer followed by post fixation with 1% osmium tetroxide for 1 hour at room temperature. The specimens were then dehydrated with ascending concentrations of ethanol in series (50% to 100%) and embedded in Spurr's Epoxy resin. Afterwards, thin sections (60-80 nm) were cut with an ultramicrotome and mounted on copper mesh grids. The sections were then contrasted with 1% uranyl acetate and lead citrate and examined with a FEI CM100 TEM and Kodak Megaplug camera. For this qualitative ultrastructural analysis, 10 to 15 random fields of view from at least 3 to 4 mice from each group were used.

### ***Western blot analysis***

LV heart tissue was snap frozen and then pulverized with mortar and pestle in liquid nitrogen. The powdered tissue was then suspended in lysis buffer as we previously described [264], and proteins were separated by reducing SDS-PAGE. After proteins were transferred to polyvinylidene fluoride, the quantification of signals was performed by densitometry of scanned autoradiographs with the aid of Image J (version 1.47v). The next antibodies were used for the immunoblot analysis: LC3B (1:1000), cytochrome c oxidase complex 4 (Cox IV) (1:1000),

eukaryotic initiation factor 2 subunit (peIF2)-Ser51 (1:1000), Beclin1 (1:1000), and Glyceraldehyde-3-phosphate dehydrogenase (GAPDH) (1:2000) from Cell Signaling Technology and Inositol-Requiring Enzyme 1 pIRE -Ser724 (1:1000) from Novus Biologicals and cathepsin D (1:1000) from Santa Cruz Biotechnology, Inc and p62 (1:1000) from BD Transduction Laboratories.

### ***Cell culture***

H9c2 rat embryonic cardiac myoblasts from American Type Culture Collection were grown in DMEM supplemented with 10% fetal bovine serum and 1% (vol/vol) streptomycin/penicillin (Gibco, Invitrogen) at 37°C, 5% CO<sub>2</sub>. When cells reached approximately 80% confluence, they were incubated in 1.0% fetal bovine serum-DMEM with or without 5 or 10 µg/mL of full-length adiponectin (fAd).

### ***Analysis of endogenous LC3B expression by immunofluorescence***

H9c2 cells were cultured in 12-well plates, after treatment with or without 10 µg/mL of fAd for 2 hours. Cells were fixed in 4% paraformaldehyde (PFA), quenched with 1% glycine, and permeabilized with 0.1% Triton X-100. After blocking with 3% BSA, cells were incubated with LC3B primary antibody (1:500), and Alexa Fluor 488 goat antirabbit IgG (Life Technologies) at 1:200. Images were taken using a 60 objective with confocal microscope (Olympus, BX51).

### ***Analysis of autophagy flux by transfecting cells with tandem fluorescence LC3B***

H9c2 cells were transduced with Premo autophagy tandem sensor Red Fluorescent Protein-Green Fluorescent Protein (RFP GFP)-LC3B (Life technologies) according to manufacturer's protocol, to monitor autophagic flux with or without fAd [265]. Cells were treated with or without 5 or 10  $\mu\text{g}/\text{mL}$  of fAd for 2 hours, fixed in 4% PFA, quenched with 1% glycine before mounting on a glass slide. Confocal images were taken using a 60 objective (Olympus, BX51 Microscope). Overlapping coefficient and Manders' coefficient were calculate using ImageJ with the JACoP plug-in to quantify the extent of GFP and RFP overlap.

#### ***Magic red assay of lysosomal cathepsin activity***

H9c2 cells were cultured in 12-well plates, after treatment with or without 5 or 10  $\mu\text{g}/\text{mL}$  of fAd for 2 hours, cells were loaded with Magic Red cathepsin B reagents (ImmunoChemistry Technologies LLC) according to manufacturer's protocol. Cells were fixed in 4% PFA, quenched with 1% glycine before monitoring on a glass slide. Images were taken using a60 objective with confocal microscope (Olympus, BX51). The number of red puncta and nuclei were counted using ImgaeJ.

#### ***Statistical analysis***

All data were calculated as mean  $\pm$  SEM. Statistical analyses were performed using GraphPad Prism (version 5). Temporal changes in echocardiographic data between sham and PO, and protein fold increase between genotype and surgery were analyzed using one-way ANOVA with Dunnett's post test and un-paired t tests (GraphPad Prism). Differences were considered statistically significant at  $P < 0.05$ .

### **3.4 Results**

#### ***Development of cardiac hypertrophy after PO in aged wt and Ad-KO mice***

Wt and Ad-KO mice were subjected to aortic banding to induce PO or sham surgery. Three weeks after surgery, the gross size of excised hearts was significantly higher in both wt and Ad-KO mice with PO vs sham surgery. Body weight (BW) was unaltered by surgery or genotype where heart weight (HW) was significantly increased by PO in both wt and Ad-KO mice, with a more significant change in HW to BW ratio in Ad-KO mice (Figure 3.2A). WGA staining showed that there was significant cardiomyocyte hypertrophy evaluated by cellular sectional area after PO and that this was more pronounced in Ad-KO mice compared with wt mice (Figure 3.2C). Similarly, echocardiography analysis showed that Ad-KO mice with PO developed a significant increase in posterior wall thickness 1 week after PO, whereas wt mice developed a significant increase 2 weeks after PO (Figure 3.2B).

#### ***Temporal analysis of cardiac dysfunction induced by PO***

The cardiac function of aged wt and Ad-KO mice was evaluated by echocardiography 3 days, 1 week, 2 weeks, and 3 weeks after PO or sham surgery. Both ejection fraction (EF) and fractional shortening (FS) were significantly decreased compared with time-matched sham-operated mice, indicating significant cardiac dysfunction (Figure 3.3A). By 3 weeks, cardiac output was also significantly reduced (Figure 3.3A). On the other hand, in wt mice only EF at 3 weeks post surgery was significantly decreased in when compared with sham-operated mice (Figure 3.3A). As visualized clearly in representative short axis images of M-mode echocardiography taken 3 weeks after the surgery, PO-induced mice showed a dilated pattern of ventricular wall

constriction, whereas sham-operated Ad-KO mice showed a clear and normal contractile pattern of systole and diastole (Figure 3.3B).

### ***Temporal analysis of myocardial strain rate using speckle tracking echocardiography***

To provide additional details on regional cardiac dysfunction induced by PO, we used speckle tracking echocardiography to calculate 2-dimensional strain rate, an indicator of how much the myocardial tissue has physically disabled. VevoStrain analysis indicated that diastolic and systolic circumferential strain rate of endocardium in aged Ad-KO mice with PO dropped significantly compared with sham (Figure 3.4A). Especially at diastole, circumferential strain rate in Ad-KO mice dropped significantly 1 week after PO whereas in wt mice dropped significantly 3 weeks after PO. At systole, only in Ad-KO hearts showed a significant decrease in circumferential strain rate, 2 and 3 weeks after PO (Figure 3.4A). Similarly, at diastole, longitudinal strain rate in Ad-KO mice dropped significantly earlier at 1 week, whereas wt mice dropped at 3 weeks compared with sham mice. However, there were no significant changes in radial strain rate between wt and Ad-KO mice (Figure 3.5). Additionally, as visualized clearly in representative images of circumferential strain rate of 6 segmented wall regions, the synchronicity of 2 opposing segments (anterior/posterior) of endocardium were disturbed (Figure 3B.4) in Ad-KO mice 2 weeks after PO, whereas the synchronicity was maintained in wt mice.

### ***Assessment of autophagy after PO***

Autophagic flux was first assessed by examining cardiac protein expression levels of Beclin1, LC3B, p62, and cathepsin D. Representative Western blotting (Figure 3.6A) and quantitation (Figure 3.6B) showed that the protein level of Beclin1 and p62 were significantly increased after

PO in both genotypes, yet the conversion of LC3-I to LC3-II was compromised after PO in aged Ad-KO mouse hearts compared with wt. Similarly, although the level of cathepsin D was significantly increased after PO in wt mice, but this was not observed in Ad-KO mice (Figure 3.6A). The goal of this work was to compare the effect of PO in each genotype, and 1 minor limitation is we did not compare sham vs PO directly on Western blotting. TEM showed that cardiomyocytes from Ad-KO mice exhibited that electron- dense, lysosome-like structures were more frequently observed in sham-operated mice heart compared with minimally invasive transverse aortic banding (mTAB)-operated PO-induced mice heart. On the other hand, such dark vacuoles were absent in cardiomyocytes from wt mice (Figure 3.6C). Such observation is supported by Western blotting of LC3B and cathepsin D (Figure 3.6B).

#### ***Evidence of mitochondrial degradation induced by PO in Ad-KO mice***

TEM analysis also provided evidence that mitochondria were differentially affected by surgery depending on the genotype. In Ad-KO mice, 3 weeks of PO severely degraded mitochondria, disrupting outer membrane and clearing cristae, whereas PO caused less marked effects on mitochondria in wt mice hearts (Figure 3.7A). Asterisks indicate mitochondria in mTAB-operated aged Ad-KO mice hearts which were significantly damaged with evidence of ruptured membrane and cristae clearance. Furthermore, Western blotting of heart homogenates demonstrated that expression of Cox IV, a mitochondrial outer-membrane protein, was comparable in wt mice with or without PO, but significantly reduced in Ad-KO mice hearts after PO vs sham (Figure 3.7B).

#### ***Indicators of ER stress were elevated by PO***

The extent of ER stress was assessed using well-established indicators, namely specific components of the unfolded protein response. Phosphorylation of Inositol-Requiring Enzyme 1 and eif2 $\alpha$  were assessed by Western blotting (Figure 3.8A), and p-eif2 $\alpha$  was increased by PO in both genotypes. However, although IRE phosphorylation was increased by PO in wt mice, there was no change in Ad-KO (Figure 3.8B). The extent of protein aggregation was measured by aggresome detection kit, which become strongly fluorescent upon binding to the tertiary structure of aggregated proteins, and cardiomyocytes undergone PO in both genotypes showed strong red fluorescent signals. These protein aggregates strongly colocalized with p62, indicating that they are subject to autophagic degradation (Figure 3.9).

#### ***Enhanced autophagic flux in H9c2 cardiomyoblasts after adiponectin treatment***

To examine whether adiponectin regulates cellular autophagic flux, H9c2 cardiomyoblasts were treated with fAd, and autophagic flux was assessed at multiple stages. Representative Western blotting and quantification (Figure 3.10A) of LC3-II levels indicated that there was a significant increase in autophagosome contents after fAd treatment. To observe whether this is due to increase in autophagosome formation or inhibition of flux, the fusion of autophagosome and lysosome was analyzed using the tandem fluorescent GFP-RFP construct. Colocalization analysis using ImageJ software indicated that both overlapping coefficient and M2 coefficient (the frequency of overlapped puncta out of total red puncta) significantly decreased after fAd treatment (Figure 3.10B). This significant increase in lysosomal GFP quenching after fAd treatment compared with control suggested increased autophagy flux. Examination of lysosomal cathepsin activity by Magic Red assay indicated that fAd treatment significantly increased cathepsin B activity (Figure 3.10C).

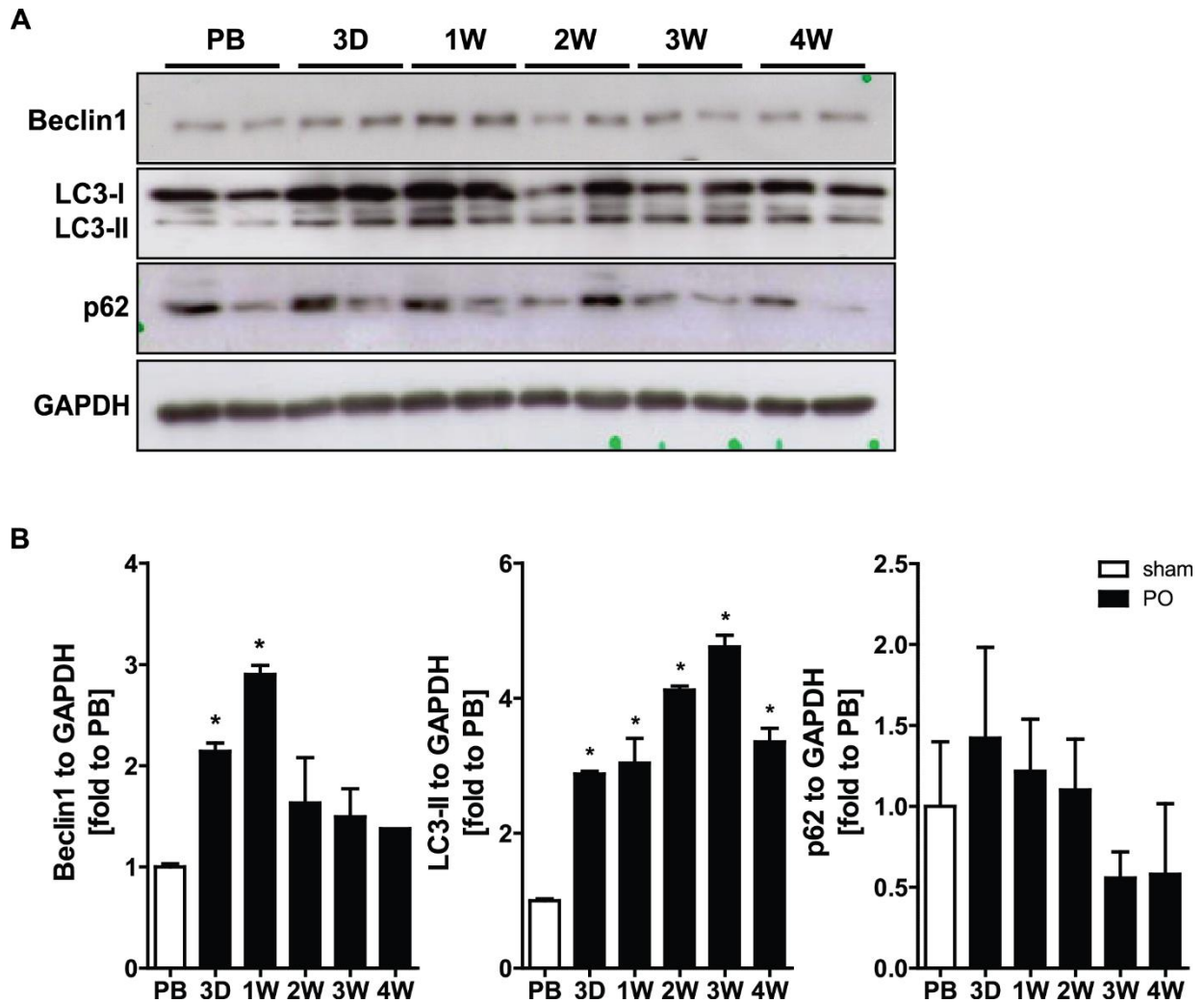


**Figure 3.1. Temporal analysis of cardiac autophagy up to 3 weeks after thoracic aorta banding surgery.**

A: representative images of Western blot analysis of Beclin1, LC3B, p62 in the heart before (PB) and after 3 days (3D), 1 week (1W), 2 weeks (2W), and 3 weeks (3W) of banding. B:

Densitometry analysis of the ratio of Beclin1, LC3- II, and p62 to GAPDH. Results are presented as mean  $\pm$  SEM (n=3 per each group). \*P<0.05 versus pre-banding.

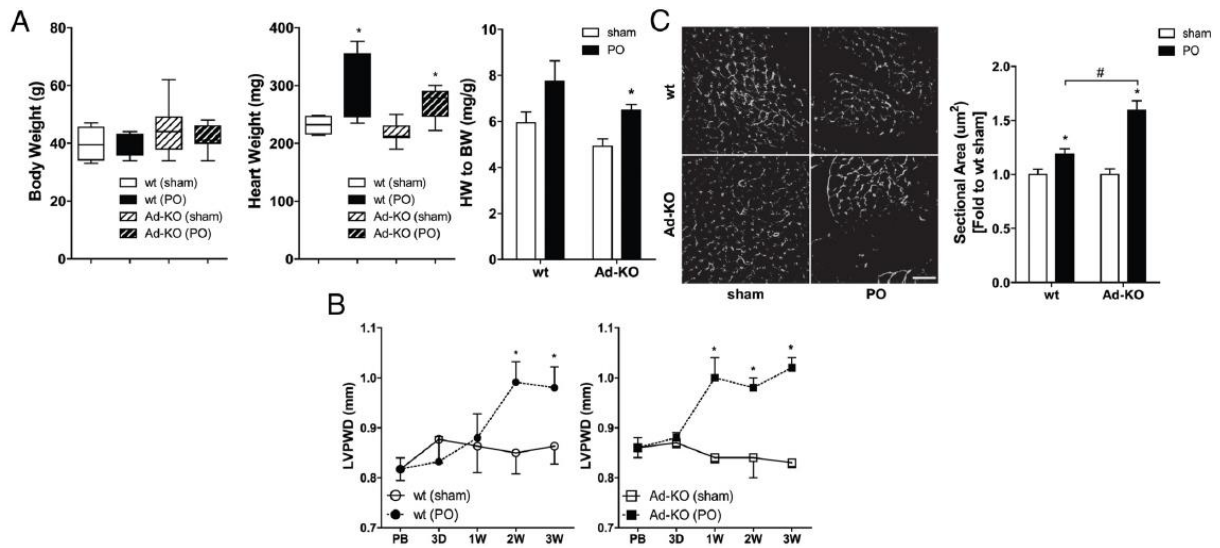


**Figure 3.2. Development of cardiac hypertrophy after PO.**

A, BW (left) and HW (right) were analyzed 3 weeks after PO or sham surgery. B, LV posterior wall diameter (LVPWD) measured by echocardiography before surgery and at 3 days (3D), 1 week (1W), 2 weeks (2W), and 3 weeks (3W) after banding. C, Representative images of heart tissue sections after WGA staining and quantitative analysis of cell size. All data are mean  $\pm$  SEM ( $n = 7$  for Ad-KO and  $n = 5$  for wt mice). Scale bar, 50  $\mu\text{m}$ . \* $P < 0.05$  vs corresponding sham; # $P < 0.05$  vs wt (PO).

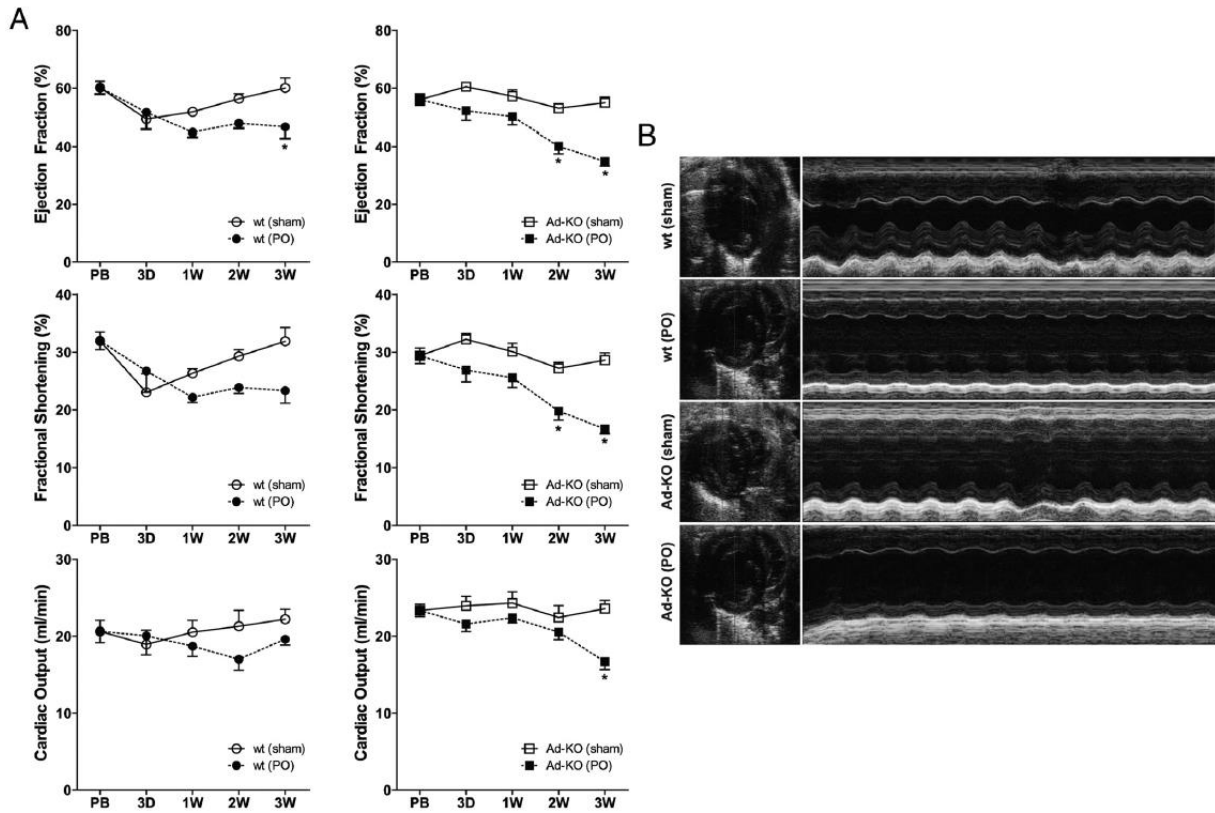


**Figure 3.3. Temporal analysis of progressive cardiac dysfunction up to 3 weeks after thoracic aorta banding surgery using echocardiography.**

A, Functional parameters (EF, FS, and cardiac output) measured before PO and at 3 days (3D), 1 week (1W), 2 weeks (2W), and 3 weeks (3W) after PO or sham surgery in wt (left) and Ad-KO (right) mice. B, Representative M-mode images of short-axis view of LV. All data are mean  $\pm$  SEM (n=7 for Ad-KO and n=5 for wt mice). \*P<0.05 vs corresponding sham.

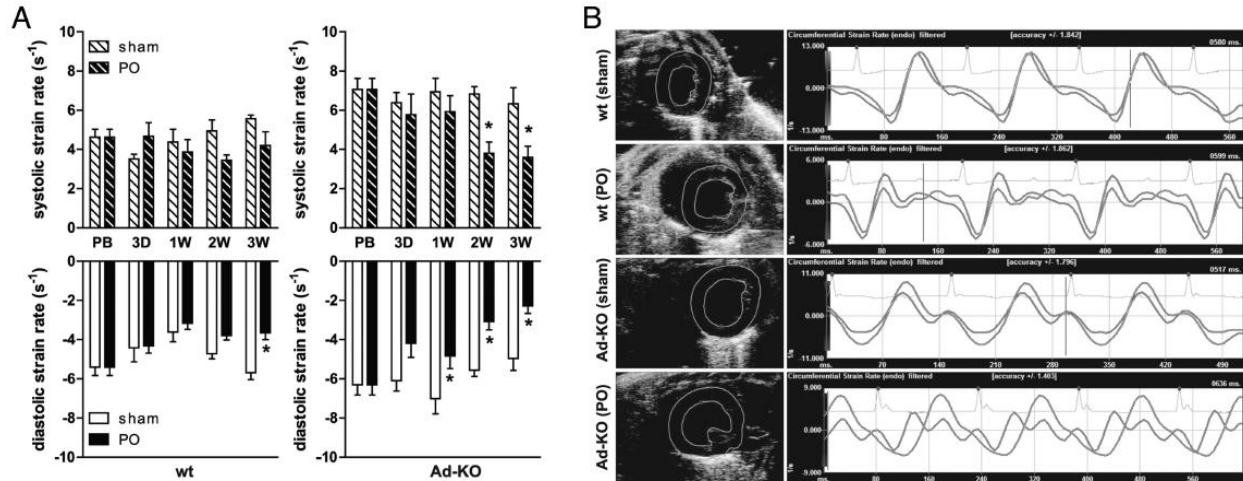


**Figure 3.4. Cardiac strain analysis by speckle tracking echocardiography to further investigate progressive cardiac dysfunction.**

A, Peak circumferential strain rate (/s) was measured and calculated at systole and diastole before PO, then 3 days (3D), 1 week (1W), 2 weeks (2W), and 3 weeks (3W) after PO in wt (left) and Ad-KO (right) mice. B, Representative images of circumferential strain rate change between 2 segments (anterior/posterior apex) during 4 cardiac cycles, \* $P < 0.05$  vs corresponding sham.

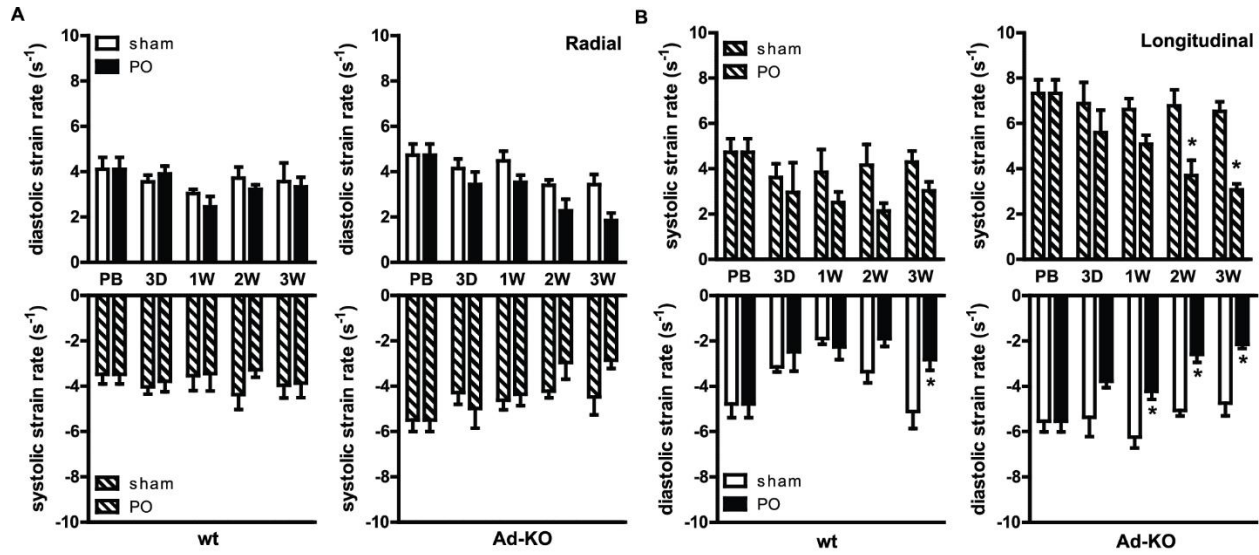


**Figure 3.5. Cardiac strain analysis by speckle tracking echocardiography to further investigate progressive cardiac dysfunction.**

A: Radial strain rate (/s) was measured and calculated at systole and diastole before PO, then 3 days (3D), 1 week (1W), 2 weeks (2W) and 3 weeks (3W) after PO in wt (left) and Ad-KO (right) mice. B: longitudinal strain rate (/s) was measured and calculated at systole and diastole before PO, then 3 days (3D), 1 week (1W), 2 weeks (2W) and 3 weeks (3W) after PO in wt (left) and Ad-KO (right) mice;  $P < 0.05$  versus corresponding sham.

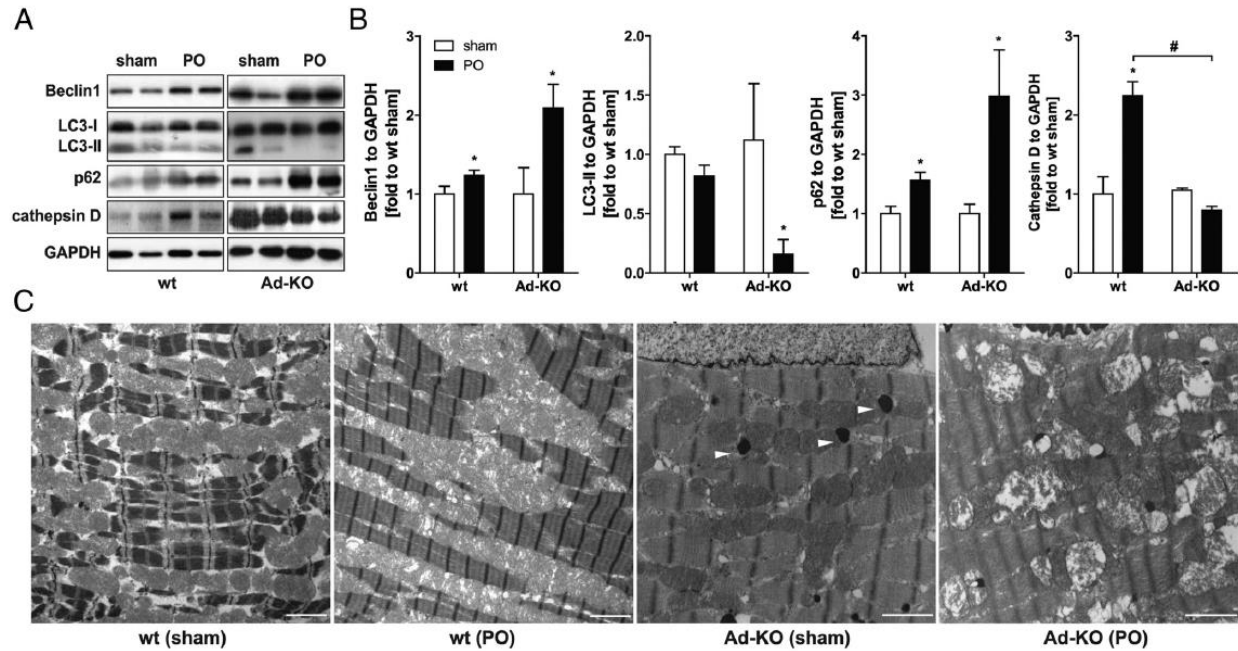


**Figure 3.6. Analysis of cardiac autophagy after PO in wt and Ad-KO mice.**

A, representative images of Western blot analysis of Beclin1, LC3B, p62, and cathepsin D in the heart after 3 weeks of banding. B, Densitometry analysis of the ratio of Beclin1, LC3-II, p62, and cathepsin D to GAPDH. C, TEM microscopy of ventricular cardiomyocytes from wt and Ad-KO mice. White arrowheads indicate homogeneously electron-dense vesicles. Results are presented as mean  $\pm$  SEM (n = 5 to n = 7 per each group). \*P<0.05 verse corresponding sham; #P<0.05 vs wt (PO). Scale bar, 2= $\mu$ m.

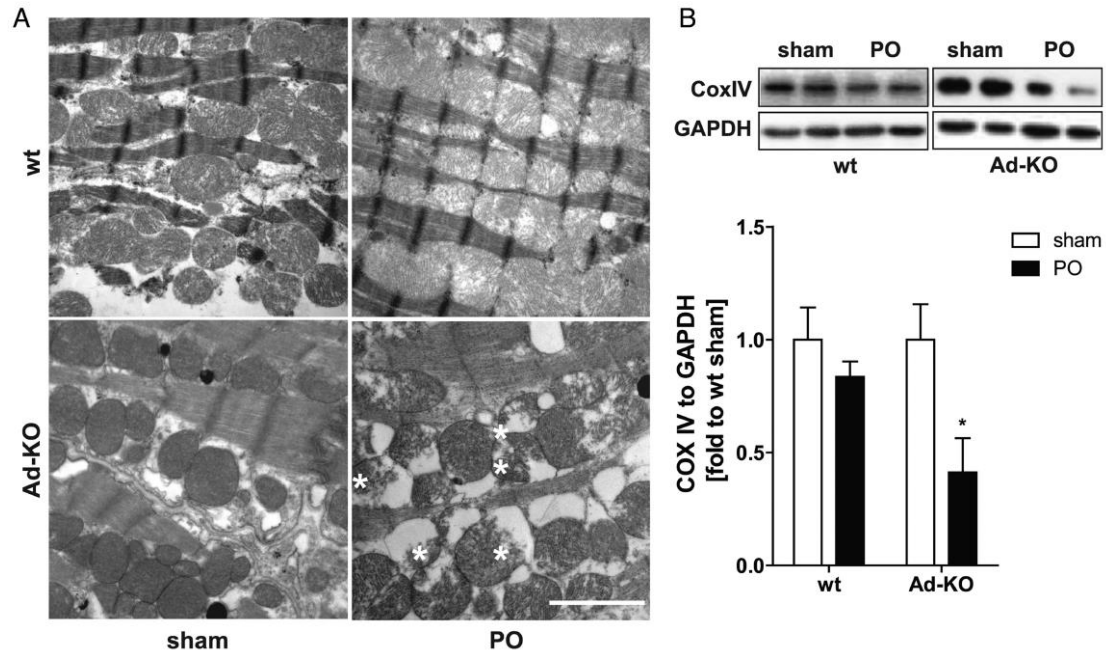


**Figure 3.7. Mitochondria degradation after mTAB surgery in Ad-KO mice.**

A, TEM micrographs of ventricular cardiomyocytes from sham and mTAB-operated wt and Ad-KO mice. B, top, Western blot analysis of Cox IV in the heart after 3 weeks of banding. B, bottom, Densitometric analysis of the Cox IV to GAPDH. Results are presented as mean  $\pm$  SEM (n = 5 to n = 7 per each group). \* $P < 0.05$  vs corresponding sham. Scale bar = 2  $\mu$ m.

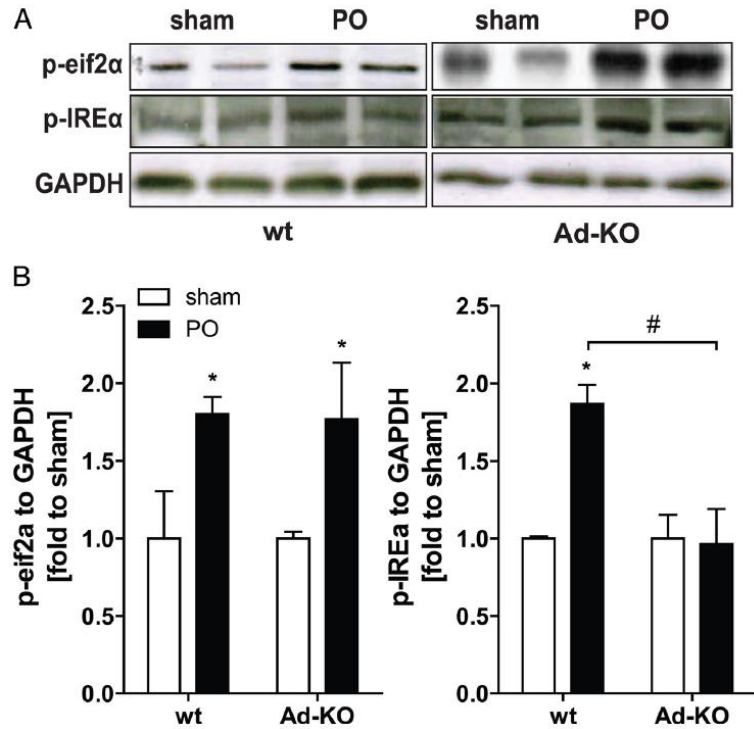


**Figure 3.8. Analysis of endoplasmic reticulum stress assessment after PO.**

A, Representative Western blot analysis of p-eif2 $\alpha$  and p-IRE $\alpha$  in the heart after 3 weeks of PO. B, Densitometric analysis of p-eif2 $\alpha$  and p-IRE $\alpha$  levels relative to GAPDH. Results are presented as mean  $\pm$  SEM (n = 5 to n = 7 per each group). \*,  $P < 0.05$  vs corresponding sham; #,  $P < 0.05$  vs wt (PO).

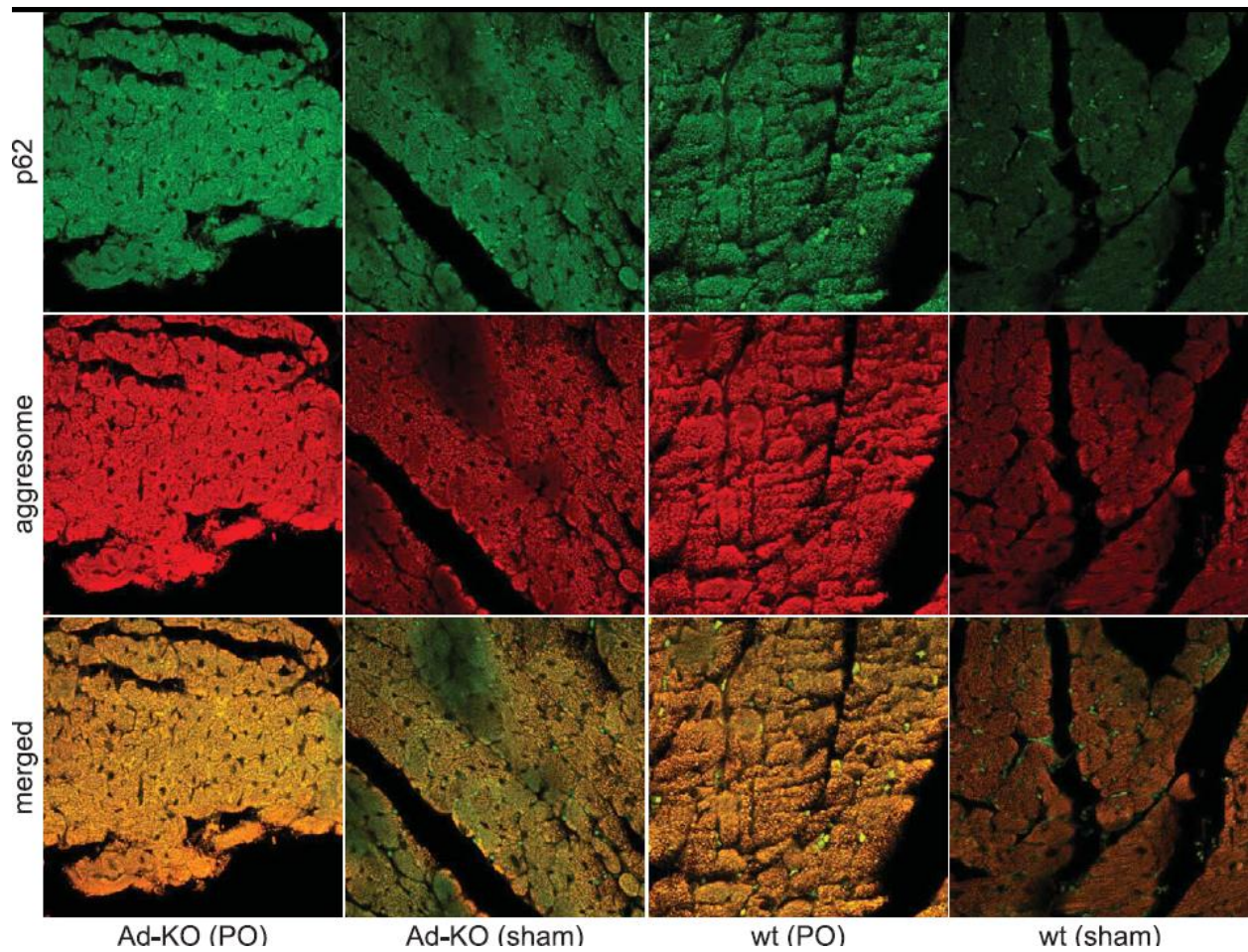


**Figure 3.9. Analysis of protein aggregates accumulation in heart tissue sections.** Representative immunofluorescent images of heart tissue sections from wt and Ad-KO mice after 3 weeks of sham and PO surgery. Paraffin-embedded sections were de-paraffinized and stained with p62 (green) and ProteoStat aggresome detection reagent (red). Scale bar = 50  $\mu$ m.

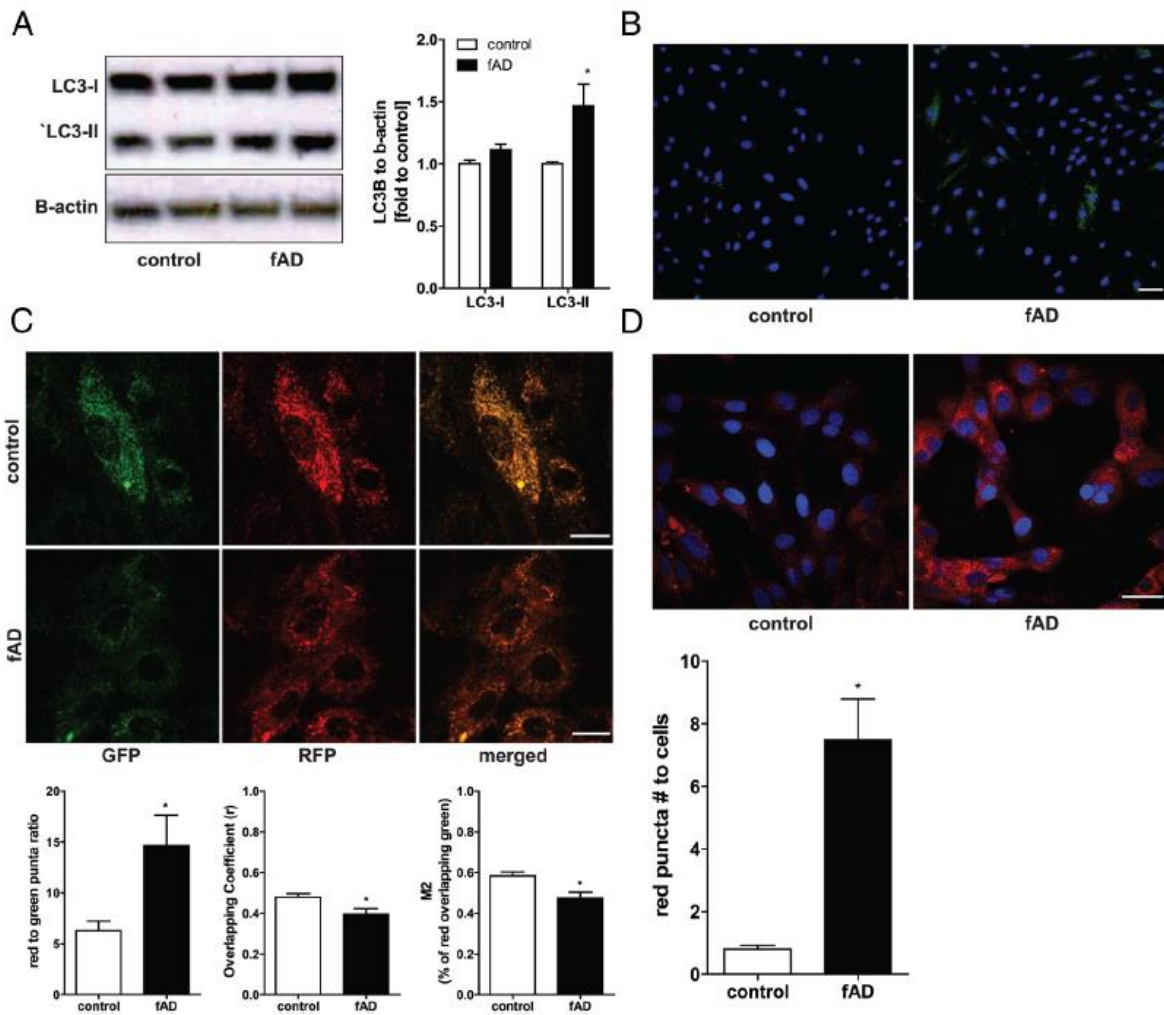


**Figure 3.10. Enhanced autophagic flux in H9c2 cells after treatment with fAd.**

A, left, Western blot analysis of LC3B in H9c2 cell lysates after 2 hours of treatment with fAd (10  $\mu$ g/mL). A, right, Densitometry analysis of LC3B to  $\beta$ -actin. B, Representative confocal images of endogenous LC3B immunofluorescence in H9c2 cells treated with fAd. C, top, Representative confocal images of tandem fluorescent-GFP-RFP-LC3 in H9c2 cells after fAd treatment. C, bottom, Quantitative and statistical analysis of red to green puncta ratio and colocalization coefficients using ImageJ. D, Representative confocal images of magic red assay in H9c2 cells after fAd treatment. Experiments were performed at least 3 times and results are presented as mean  $\pm$  SEM. \*,  $P < 0.05$  vs control. Scale bar, 20 =  $\mu$ m.

### **3.5 Discussion**

Understanding mechanisms contributing to the diverse pathophysiology of heart failure, especially in the elderly and obese populations, is of great importance given the global impact on human health [9, 243, 244]. Myocardial remodeling encompasses a wide array of cellular events which may contribute to altered performance, including alterations in metabolism, hypertrophy, fibrosis, and cell death [9, 244]. Numerous adipokines have been shown to be important regulators of cardiac remodeling and adiponectin has emerged as an important mediator of the progression of heart failure. Clinical, animal model and in vitro studies have primarily, but not exclusively, documented cardioprotective effects of adiponectin [257]. Studies in Ad-KO mice hearts have shown them to have exaggerated hypertrophy, fibrosis, apoptosis and metabolic dysfunction in response to cardiac stressors, including surgery and angiotensin-II. Strategies to administer adiponectin to these mice, including use of adenovirus or recombinant protein, could prevent or reverse the exaggerated remodeling phenotype of Ad-KO mice [257]. As expected, almost all of these studies were conducted in mice between 6 and 12 weeks of age with one very recent study using 11-month-old mice [258]. The focus of our manuscript was to study Ad-KO mice aged to 13 months. Cardiac function of aged wt and Ad-KO mice was first evaluated by conventional echocardiography 3 days and 1, 2, and 3 weeks after PO or sham surgery. The indices of cardiac systolic functions (EF and FS) were significantly decreased in Ad-KO mice 2 weeks after PO compared with sham mice. Cardiac output was also significantly reduced 3 weeks after PO operation. In contrast, wt mice only showed reduction of EF at 3 weeks post surgery when compared with sham-operated mice. Cardiac performance was further evaluated by speckle tracking echocardiography to provide additional details of regional cardiac functions. We found that both diastolic and systolic circumferential strain rate in endocardium of Ad-KO mice

decreased significantly after PO compared with sham mice. Particularly, circumferential strain rate at diastole decreased significantly in Ad-KO mice 1 week after PO whereas this rate was decreased in wt mice at 3 weeks after PO. Furthermore, only Ad-KO mice showed a significant decrease in circumferential strain rate at systole 2 weeks after PO, whereas wt mice had no significant changes compared with sham mice. Similarly, at diastole, longitudinal strain rate in Ad-KO mice dropped significantly earlier at 1 week, whereas wt mice dropped at 3 weeks compared with sham mice. Finally, the synchronicity of 2 opposing segments (anterior/posterior) of endocardium was disturbed in Ad-KO mice 2 weeks after PO, whereas the synchronicity was maintained in wt mice.

Our data demonstrated that Ad-KO mice had earlier, and worse cardiac dysfunction compared with wt mice after PO stress. Previous reports have suggested that adiponectin deficiency enhanced adverse cardiac remodeling [266] and led to increased mortality after PO [142]. Additionally, increased myocardial infarct size, apoptosis, and TNF-expression were observed in Ad-KO mice compared with wt mice after ischemia-reperfusion injury [146]. Our results corroborated previous studies, but the exact mechanism of adiponectin to influence the cardiac function after PO needs to be further investigated. An important novel feature of this study was to elucidate how autophagy is altered in aged mice in response to PO and whether the lack of adiponectin influences changes in autophagy. We used LV tissue and analyzed markers of autophagy by Western blotting and TEM and observed that in Ad-KO mice cardiac autophagy was deficient after PO. This correlated with cardiac dysfunction and is in keeping with recent studies which have established that sufficient levels of basal cardiac autophagy are crucial for maintaining optimal cardiac function [252, 255]. Again, the existing literature using young mice has clearly established that PO in mice increased various indices of cardiac autophagy [251,

252], and we confirmed that the PO resulted in increase in autophagy markers (Figure 2.1A). The fact that we observed the reversed response at autophagosome maturation stage in aged Ad-KO mice suggests that lack of adiponectin renders these mice unable to elicit an appropriate processing of protein aggregates or damaged organelle by autophagic flux and that loss of this protective mechanism contributes to more severe cardiac dysfunction we observed. This is in keeping with studies in genetic mouse models of autophagy deficiency, which have shown that lack of induction of autophagic flux exacerbates development of heart failure [252, 255].

However, our data provide the first evidence that aged Ad-KO mice lack an appropriate PO-induced increase in autophagic flux, suggesting that adiponectin may be a critical mediator of cardiomyocyte autophagy under these conditions. This may contribute to the exacerbation of PO-induced cardiac dysfunction which we and others have observed in Ad-KO mice [257], because the prevailing dogma is that induction of autophagy is an innate mechanism in response to various stressors, which protects against progression of cardiac remodeling and heart failure postinfarction [255, 267]. It should also be borne in mind that excessive or inadequate levels of autophagy are both associated with heart failure [179, 255]. Regulation of mitophagy, a distinct form of autophagy, may be an important determinant of myocardial metabolic dysfunction [268]. Mitochondria are particularly predominant and critical in the heart due to high-energy demands, yet mitochondria must also be tightly regulated due to reactive oxygen species production [269].

Our data suggested that PO induced mitochondrial dysfunction in wt mice, which was exacerbated in Ad-KO mice, and we hypothesized that this may be due to lack of adequate mitophagy in Ad-KO mice, which would normally be expected to clear and recycle damaged mitochondria. We speculate that lack of adiponectin signaling via AMPK in our model may underlie these effects, because AMPK is well established as a mediator of many of adiponectin

physiological effects, as an important inducer of autophagy and disruption of AMPK signaling will result in reduced mitophagy [160, 270, 271].

Our study also found that ER stress was significantly increased in the myocardium of aged wt and Ad-KO mice after PO, which is in keeping with literature in young mice [272]. Interestingly, we observed partial activation of the unfolded protein response, involving protein kinase-like endoplasmic reticulum kinase and eIF2 phosphorylation. This is consistent with a very recent report, which showed that whereas Ad-KO mice had elevated basal ER stress levels, detected by IRE1 and eif2, compared with wt mice, subjecting mice to stress such as high-fat diet resulted in increased growth arrest and DNA damage protein 34 and eif2 dephosphorylation but no change in IRE1 phosphorylation [258]. The diminished autophagy capacity of Ad-KO mice may also contribute to excess ER stress, which we also observed as enhanced accumulation of protein aggregates, which colocalized with p62 upon immunofluorescent analysis. It is likely that this ER stress can subsequently lead to cardiac dysfunction via several potential mechanisms, including cell death and insulin resistance [272, 273]. In summary, lack of adiponectin in aged mice was associated with deficient PO-induced cardiac autophagy, which was observed in wt mice. This is likely of major significance, because it has been shown that induction or maintenance of cardiac autophagy is crucial in maintaining normal heart functions under stress or upon aging. Potential cellular events related to lack of sufficient autophagy in Ad-KO mice after PO include mitochondrial dysfunction and ER stress. Together these manifests as cardiac dysfunction detected by echocardiography. Our studies suggest that the increased susceptibility of Ad-KO mice to stimulus-induced cardiac dysfunction may be at least in part due to autophagy deficiency.

## Chapter 4

### 4.1 Abstract

Autophagy is an evolutionarily conserved catabolic process acting protective during ischemia yet detrimental during reperfusion in myocardial infarction induced cardiac remodeling. Adiponectin is the most abundant adipokine in circulation, and it is cardioprotective with potent AMPK inducing capacity. We investigated the role of adiponectin signaling in regulating cardiac autophagy during ischemia by ligating coronary artery without reperfusion. After 7 days ischemia, the infarct regions of Ad-KO mice hearts showed decreased phosphorylation of AMPK T172-ULK1 S555, decreased LC3-II and increased p62 expression. We adopted a novel FMT (Fluorescence Molecular Tomography) technique with CT scan to examine pan-cathepsin activity (ProSense® 680) in live animals hearts after 7 days ischemia. Ischemia robustly increased lysosomal activity in hearts after ischemia but not in Ad-KO mice hearts. In vitro experiments with H9c2 cardiomyoblasts showed adiponectin robustly induced autophagy via the AMPK-ULK1 pathway and enhanced autophagy flux in hypoxia conditions. Adiponectin's antioxidant and anti-apoptotic effects were blunted by AMPK inhibitor or in autophagy deficient cells (ATG5K130R-H9c2). Overall, our study suggests that adiponectin is an important mediator of cardiac autophagy during ischemia.

## 4.2 Introduction

Cardiovascular disease (CVD) is the leading cause of deaths worldwide, and coronary heart disease (CHD) accounts for the biggest portion of deaths by CVD [274]. CHD is primarily caused by dyslipidemia which leads to myocardial infarction (MI) [9], which causes structural and functional changes in hearts [275].

Mechanisms underlying MI induced cardiac remodeling are multifaceted, and one contributing factor is an altered adiponectin profile. Adiponectin is the most abundant adipokine in the circulation [9], and it is inversely correlated with the degree of adiposity and the inflammatory status [41, 276]. Low serum adiponectin level is implicated in various CVDs, and numerous studies have established adiponectin's cardio-protective effects [58, 59, 257, 277].

The level of adiponectin is inversely correlated with MI risk [278] and MI in adiponectin knockout (Ad-KO) mice resulted in exacerbated left ventricle dilation and hypertrophy with increased apoptosis and interstitial fibrosis [144, 146]. Adiponectin ameliorates MI-induced remodeling by reducing inflammation and oxidative stress via enhancing AMP kinase (AMPK) signaling [58, 137, 279-282].

AMPK is an energy sensing molecule which activates various catabolic processes including autophagy to balance cellular energy levels [283]. Autophagy is a bulk degradation of cellular components such as protein aggregates or organelles to recycle energy sources. Cardiac autophagy is important to maintain normal heart function and an adaptive response against stresses [255, 284]. Autophagy is generally considered a protective mechanism against MI-induced remodeling [285-289] yet excessive autophagy could be detrimental in certain circumstances [290-292]. Recently, several studies suggested that adiponectin is associated with autophagy rates in different tissues including the heart [177, 207, 264, 293, 294].

In the present study, we investigated the significance of adiponectin stimulated autophagy in hearts during ischemia and hypoxia. By subjecting wt and Ad-KO mice to permanent coronary artery ligation, we observed the changes in autophagy related protein expression and lysosomal activity. We further studied the autophagy stimulating capacity of adiponectin in H9c2 cardiomyoblasts and identified its significance in hypoxic stresses.

### **4.3 Materials and Methods**

#### **Animals**

In house bred adiponectin knockout (Ad-KO) mice [120] and age matched C57BL/6J (wild type, wt) mice (The Jackson Laboratory, USA) were fed *ad libitum* on regular chow diet until 9-10 weeks of age and were randomly separated into treatment groups (n=6 per group). All animals were kept in temperature and humidity-control led rooms ( $21 \pm 2^{\circ}\text{C}$ , 35-40%) with a daily 12:12 hr light-dark cycle in the animal care facility of York University in accordance with the guidelines of the Canadian Council on Animal Care. All study protocols were approved by the Animal Care Committee of York University.

#### **Coronary artery ligation surgery**

MI was induced by coronary artery ligation (CAL) surgery as previously described [295]. Briefly, the left anterior descending coronary artery was ligated with a 8-O suture at 3mm distal to the tip of the left atrium for 7 days. Sham animals underwent the same procedure except for the suture ligation around the coronary artery. Mice were sacrificed 7 days after MI.

#### **Echocardiography**

Echocardiography was performed as we previously described [207] using the Vevo2100 system (Visual Sonics, Canada) equipped with an MS550D transducer. Mice were lightly anesthetized using 2.0~3.0% isoflurane mixed with 100% O<sub>2</sub> during the time of imaging. M-mode images of the parasternal short-axis view at the papillary level were used to calculate cardiac functions. B-mode movie files of the parasternal short-axis view were used to perform speckle-tracking

cardiac strain rate analysis. All parameters were averaged over at least 3 cardiac cycles for analysis.

### **Immunofluorescence staining (LC3B and p62)**

Paraffin embedded heart tissue sections were de-paraffinized and antigen retrieval was performed in sodium citrate buffer (pH 6.0). Heart sections were permeablized with PBST (PBS + 0.3% Triton X-100) for 90min and blocked with blocking buffer (2% BSA + 5% goat + 5% donkey serum) for 60min. Then, the slides were kept in primary antibody (Rabbit anti-LC3B, MBL #PM036, and Mouse anti-p62, MBL #M162-3) at 1:200 overnight at 4 Celsius degree. The slides were kept in secondary antibody (Goat anti-Rabbit Alexa 488 and Donkey anti-Mouse Alexa 555, Invitrogen #A27034 and # A-31570) at 1:1000 for 1 hour at room temperature after three washes. Slides were mounted in DAPI containing medium after three washes, and slides were visualized with a Zeiss LSM700 confocal microscope at 20X or 40X.

### **Western blot**

The ischemic zone of LV heart tissue was snap frozen and pulverized with a mortar and pestle in liquid nitrogen. The powdered tissue was then suspended in RIPA lysis buffer with Laemmli loading dye [264]. Total cell lysates were prepared directly with Laemmli buffer with inhibitors. Proteins were separated by reducing SDS-PAGE. After proteins were transferred to polyvinylidene difluoride, the quantification of signals was performed by densitometry of scanned autoradiographs with the aid of ImageJ (version 1.4v). The following antibodies were used in this study: Atg5 (Novus Biologicals #NB110-53818), adiponectin (Signalway Antibody #FAO1-2) Caspase 3 (Cell Signaling Technology, CST #9662), BAX (CST #2772), Beclin 1

(CST #3738), Bcl-2 (CST #3498), LC3B (CST #2775), GAPDH (CST #2118), p-ULK1 S555 (CST #5869), p-AMPK T172 (CST #2531),  $\beta$ -Actin (CST #4970), p62 (CST #5114), anti-rabbit or anti-mouse IgG HRP-linked antibodies (CST #7074, CST #7076).

### **Fluorescent Molecular Tomography (FMT) imaging in mice**

Two nanomoles of pan-cathepsin protease sensor (ProSense® 680, Perkin Elmer, MA, USA) was infused into mice via tail vein for the assessment of autophagy. Probes were delivered 24 hours (ProSense® 680) prior to beginning of in vivo imaging. The intensity of fluorescence was visualized with FMT using a VisEn FMT 2500 LX Quantitative Tomography System (Perkin Elmer, MA USA) [296]. Mice were shaved prior to scanning and placed in the supine position in a plexiglass holder and the scan region was established to capture the upper half of the mouse (i.e. nose to above the liver) using an in-plane resolution of  $1 \times 1 \text{ mm}^2$ . After cathepsin images were captured, mice were transferred for micro-computed tomography (CT) imaging (eXplore Ultra, GE Healthcare, London, Canada) while maintained under light anesthesia. FMT and CT images were reconstructed, merged, and 3D images were constructed by software Amide (Amide's Medical Imaging Data Examiner).

### **Ex vivo fluorescent molecular tomography imaging of mouse hearts**

Hearts were isolated from mice after FMT scanning and placed on an opaque resin block in the FMT plexiglass mouse holder and imaged at 680nm. Epifluorescence images were captured for each mouse heart, and analysis of ex-vivo images was performed using the FMT System software (TrueQuant 4.0).

### **Masson's Trichrome / TUNEL / WGA staining**

Five-micrometer-thick paraffin embedded heart sections were subjected to TUNEL (*In Situ* Cell Death Detection kit, Roche #11684795910) or Masson Trichrome staining (Abcam #ab150686) or WGA staining (ThermoFisher, #W11261) according to manufacturer's suggested protocol and visualized using an Olympus IX71 inverted fluorescent microscope (Olympus Canada, Richmond Hill, ON, Canada).

### **Cell culture**

H9c2 rat embryonic cardiac myoblasts (ATCC® CRL-1446™) were grown in Dulbecco's Modified Eagle's Medium (DMEM, Gibco #11885076) supplemented with 10% fetal bovine serum (FBS, WISENT #080-110) and 1% (vol/vol) Penicillin-Streptomycin (Gibco #15140122) at 37°C and 5% CO<sub>2</sub>. When cells reached 80-90% confluence, media were switched to serum free DMEM. Globular adiponectin (gAd) was produced as we previously described [297].

Hypoxia condition was achieved by placing cells in a hypoxic chamber filled with a pre-analyzed gas mixture of 5% CO<sub>2</sub>, 95% N<sub>2</sub>. Compound C was purchased from Calbiochem Inc (#CAS 866405-64-3).

### **Autophagy Flux assay with Cyto-ID and Magic Red**

H9c2 cells or rat adult cardiomyocytes [298] were seeded on glass coverslips incubated with appropriate treatment conditions. Cells were incubated with Cyto-ID (Enzo Life Sciences, #ENZ-51031) and Magic Red Cathepsin B Assay (Immunohistochemistry Technologies, #937) at 37°C according to manufacturer's instructions. After 30 min incubation, cells were washed

with PBS and fixed with 4% PFA and visualized with a confocal microscope (Zeiss LSM700) with 48x objective.

### **Transmission electron microscopy (TEM)**

TEM was performed as described previously[262]. Briefly, cells were fixed in 2.5% glutaraldehyde in 0.1M sodium cacodylate buffer followed by post-fixation with 1% osmium tetroxide for 1 hour at room temperature. The specimens were then dehydrated with ascending concentrations of ethanol in series (50%–100%) and embedded in Spurr's Epoxy resin. Afterwards, thin sections (60–80 nm) were cut with an ultramicrotome and mounted on copper mesh grids. The sections were then contrasted with 1% uranyl acetate and lead citrate and examined with a FEI CM100 TEM and Kodak Megaplug camera.

### **Analysis of autophagic degradation by DQ-BSA assay**

Cells were cultured in 6 well plate, and DQ™ green BSA (Life Technologies Inc.) was added to each well at 20 µg/mL and incubated for 15 minutes after appropriate treatment. Cells were harvested and fixed with 4% PFA, and run in a flow cytometer machine (Gallios™, Beckman Coulter Inc.) to analyze brightness of green fluorescent (BODIPY) in each cell. 100,000 cells were analyzed, and fluorescent intensity was plotted. Mean, median and geo-mean of fluorescence were calculated using Flowing Software 2[299].

### **Analysis of intrinsic apoptosis pathway**

H9c2 cells were treated with appropriate treatment conditions. Cells were fixed in 4% PFA, and permeabilized with 0.3% Triton X-100. Cells were blocked with 3% BSA and incubated with

antibodies to TOM20 (Santa Cruz #sc-11415) and cytochrome C (Abcam #ab110325) at 1:200 for 2 hours followed by secondary antibody (Goat Anti-Rabbit Alexa Fluor® 546, ThermoFisher #A-11010, Goat Anti-Mouse, Alexa Fluor® 488, ThermoFisher #A28175) at 1:1000 for 1 hour. Images were taken using a 60x objective with confocal microscope (Olympus, BX51), and co-localization between green and red fluorescence were calculated with the ImageJ JACOP plugin.

### **Analysis of apoptosis by Caspase 3/7 substrate degradation**

After treatments, cells were pulsed with CellEvent® Caspase-3/7 Green Detection Reagent according to manufacturer's protocol. Cells were fixed in 4% PFA, then quenched with 1% glycine before mounting. Nuclei of cells were counter-stained with with DAPI (Vector Laboratories). Images were taken using a 60x objective with a confocal microscope (Olympus, BX51). The dead cells, with green fluorescent nuclei, were counted in 20 images randomly taken.

### **Immunofluorescence of p-AMPK**

H9c2 cell were treated with appropriate treatment conditions and fixed in 4% PFA. Cells were permeabilized with 0.3% Triton X-100 and blocked with 3% BSA. Cells were incubated with primary antibody (p-AMPK T172, CST #2531) at 1:200 for 2 hours, then incubated with secondary antibody (Goat Anti-Rabbit Alexa Fluor® 546, ThermoFisher #A-11010) at 1:1000 for 1 hour. Images were taken using a confocal microscope (Zeiss LSM700) with 48x objective.

### **Generation of autophagy deficient (H9c2-ATG5K130R) cell lines**

To generate H9c2 cells stably over-expressing mutant ATG5 proteins (ATG5K130R), H9c2 cells were transduced with retroviral vector carrying pmCherry-ATG5K130R [210]. Cells stably expressing ATG5K130R were selected with puromycin (1.0  $\mu\text{g}/\text{mL}$ ) in growth medium (DMEM with 10% FBS), and single cells were cloned, cultured, and used for experiments.

### **Statistics**

Data was presented as mean  $\pm$  SEM. Statistical significance between surgery/treatment groups was calculated with unpaired Student's t-test. For comparing more than two groups, One Way ANOVA with multiple comparisons was performed to adjust multiple comparisons. P value less than 0.05 was considered statistically significant.

## **4.4 Results**

### **Disrupted autophagy flux in Ad-KO mice**

wt and Ad-KO mice were subjected to CAL surgery without reperfusion to induce ischemia and paraffin embedded mid-heart sections were stained against LC3B and p62. Autophagosomes, indicated by LC3B puncta, were generated near the infarct zone in wt-mice hearts but not in Ad-KO mice (Figure 4.1A). The changes in autophagy were further assessed by measuring proteins expressions involved in autophagy in the apex of hearts (infarct zone): Beclin1, ATG5-ATG12 complex, LC3B, and p62 (Figure 4.1B). Beclin1 expression significantly increased in both genotypes after ischemia yet the increase was aggrandized in Ad-KO mice. The ATG5-ATG12 complex expression significantly increased in both genotypes after ischemia yet the increase was significantly greater in Ad-KO mice. The expression of LC3-II, indicative of autophagosomes, significantly decreased in Ad-KO mice after ischemia while the expression of LC3-II between sham and ischemia were comparable in wt mice. The expression of p62, an indicator for protein aggregates destined to autophagy degradation, significantly increased in Ad-KO mice after ischemia but not in WT mice (Figure 4.1C).

Adiponectin is reported to accumulate in the heart following MI up to 4 days [300]. To investigate if adiponectin locally accumulated after ischemia, total adiponectin levels were assessed by western blot and compared to systemic adiponectin level, measured by ELISA. After ischemia, cardiac adiponectin level significantly increased yet the systemic adiponectin level was not affected (Figure 4.1D-E).

### **Reduced lysosomal activities in Ad-KO mice hearts after ischemia**

The live lysosomal activity in vivo was measured by Fluorescence Molecular Tomography scanning of pan-cathepsin activatable fluorophore (680nm), and signals from hearts were localized by aligning FMT scan images with CT scan images (Figure 4.2A). Ischemia resulted in enhanced cathepsin activity compared to sham surgery group in wt mice (Figure 4.2B). Ex vivo fluorescence analysis showed that the cathepsin activity in hearts with ischemia was significantly higher in wt mice than Ad-KO mice (Figure 4.2C).

### **Greater fibrosis, apoptosis and inflammation in Ad-KO mice after ischemia**

MI resulted in bigger fibrotic scars and more apoptosis in AdKO mice hearts (Figure 4.3A-C). Western blotting analysis of apoptosis markers (BAX, Bcl-2, cleaved caspase 3) indicated that the ischemia surgery increased pro-apoptosis markers in both genotypes, yet exacerbated changes in Ad-KO mice. The cleavage of caspase-3 and BAX expressions increased in both genotypes after ischemia while the expression of Bcl-2, an anti-apoptotic protein, decreased in both genotypes after CAL surgery (Figure 4.3D-E). In addition to that, the local and systemic serum lipocalin 2 levels significantly increased after ischemia in Ad-KO mice (Figure 4.3F-G).

### **Exacerbated cardiac remodeling in Ad-KO mice after ischemia**

Ad-KO mice developed worse ejection fraction and fractional shortening compared to wt mice after ischemia (Figure 4.4A). To provide regional changes in contractions, the changes in strain in radial and longitudinal directions were calculated in three cardiac cycles. The average strain of six cardiac segments in the radial and longitudinal directions significantly decreased after ischemia only in Ad-KO mice (Figure 4.4B-C). In addition to that, ischemia resulted in cardiac

hypertrophy in both WT and Ad-KO mice, yet the degree was greater in Ad-KO mice (Figure 4.3D-E).

### **Autophagy flux enhanced by adiponectin in H9c2 cells**

H9c2 cells were treated with adiponectin (Ad, globular adiponectin at 1 $\mu$ g/mL) for 30 min and phosphorylation of autophagy signaling molecules and autophagosome markers were assessed. Phosphorylation of ULK1 at S555 and AMPK at T172 significantly increased after 30 min Ad treatment (Figure 4.6A-B). Autophagosome turnover and lysosomal activity were monitored by the combination of cyto-ID and Magic Red. They successfully co-localized with autophagosome and lysosomes (Figure 4.5). Adiponectin treatment enhanced the number of autophagosomes and lysosomal degradation. The increased autophagosomes number remain up to 4 hours (Figure 4.6C-E).

### **Adiponectin enhanced autophagy flux in hypoxia**

H9c2 cells were subject to short term hypoxia for 2 hours with or without adiponectin, and the change in autophagy flux was assessed at three stages: autophagosome formation, autophagosome-lysosome fusion, and lysosomal degradation. Western blotting analysis for LC3B indicated that Ad treatment significantly increased the expression of LC3-I and LC3-II in hypoxia, but not in normoxia (Figure 4.7A-B). The degree of degradation was assessed by DQ-BSA, a fluorophore (BODIPY) conjugated substrate which releases fluorescence upon degradation at endosome or lysosomes. The intensity of green fluorescence in 10,000 cells was analyzed by flow cytometry and plotted on histogram. Mean, median and geometric values of fluorescence significantly decreased in hypoxia condition whereas adiponectin treatment significantly increased all values

(Figure 4.7C). TEM ultrastructure analysis indicated that the autophago-lysosome structures (dark, double-membraned vesicles) were more prevalent in hypoxia with adiponectin treatment compared to hypoxia alone (Figure 4.7D).

### **Alleviation of intrinsic apoptosis activation from mitochondria by adiponectin**

H9c2 cells were subjected to a longer duration of hypoxia (48 hours), and the incidence of apoptosis was assessed. The intrinsic apoptosis activation was assessed by subcellular localization of cytochrome c with immunofluorescence assay. H9c2 cells were stained with cytochrome C (green) and counter stained with mitochondria markers (TOM20 IF, red). Long term hypoxia resulted in a significant decrease in co-localization between cytochrome C and mitochondria, indicating cytochrome c release. However, adiponectin treatment significantly increased co-localization between cytochrome C and mitotracker (Figure 4.8A-B).

Phosphorylation of AMPK at T172 significantly increased after long term hypoxia, and the degree of increase was comparable between treatments with or without adiponectin. Cleaved caspase 3 expression significantly increased after long term hypoxia, yet adiponectin treatment significantly decreased cc3 expression (Figure 4.8C).

### **Abolishment of anti-apoptotic effects by adiponectin in the presence of AMPK inhibitor or in autophagy deficient cells**

Adiponectin's anti-apoptotic effects were investigated in the presence of AMPK inhibitor or in autophagy deficient cells. Caspase activity was assessed in H9c2 cells after long term hypoxia with or without adiponectin in the presence of AMPK inhibitor, Compound C at 5  $\mu$ M.

Phosphorylation of AMPK at T172 significantly decreased even in hypoxia when adiponectin is

co-treated with compound c. Adiponectin co-treatment with Compound C in hypoxia resulted in the apoptosis, indicated by green fluorescence co-localization with nuclei DAPI staining (Figure 4.9A). Cleaved caspase 3 expression significantly increased when compound c was co-treated with adiponectin in hypoxia (Figure 4.9B).

Autophagy deficient cells (ATG5K130R-H9c2) were generated by retroviral infection of H9c2 cells, resulting in over-expression of mutant ATG5 (ATG5K130R) proteins. Cells transduced with empty vector were used as control. The cleaved caspase 3 expression increased significantly after long term hypoxia and decreased significantly with Ad treatment in Ev-H9c2 cells.

However, in ATG5K130R-H9c2 cells, the cc3 expression was further increased compared to EV-H9c2 cells in hypoxia, and adiponectin treatment did not decrease cc3 expression (Figure 4.9C). Caspase activity was assessed in EV- and ATG5K130R-H9c2 cells after long term hypoxia with or without Ad. Hypoxia caused near 100% apoptosis in ATG5K130R-H9c2 cells and Ad treatment had no effect on reversing apoptosis (Figure 4.9D).

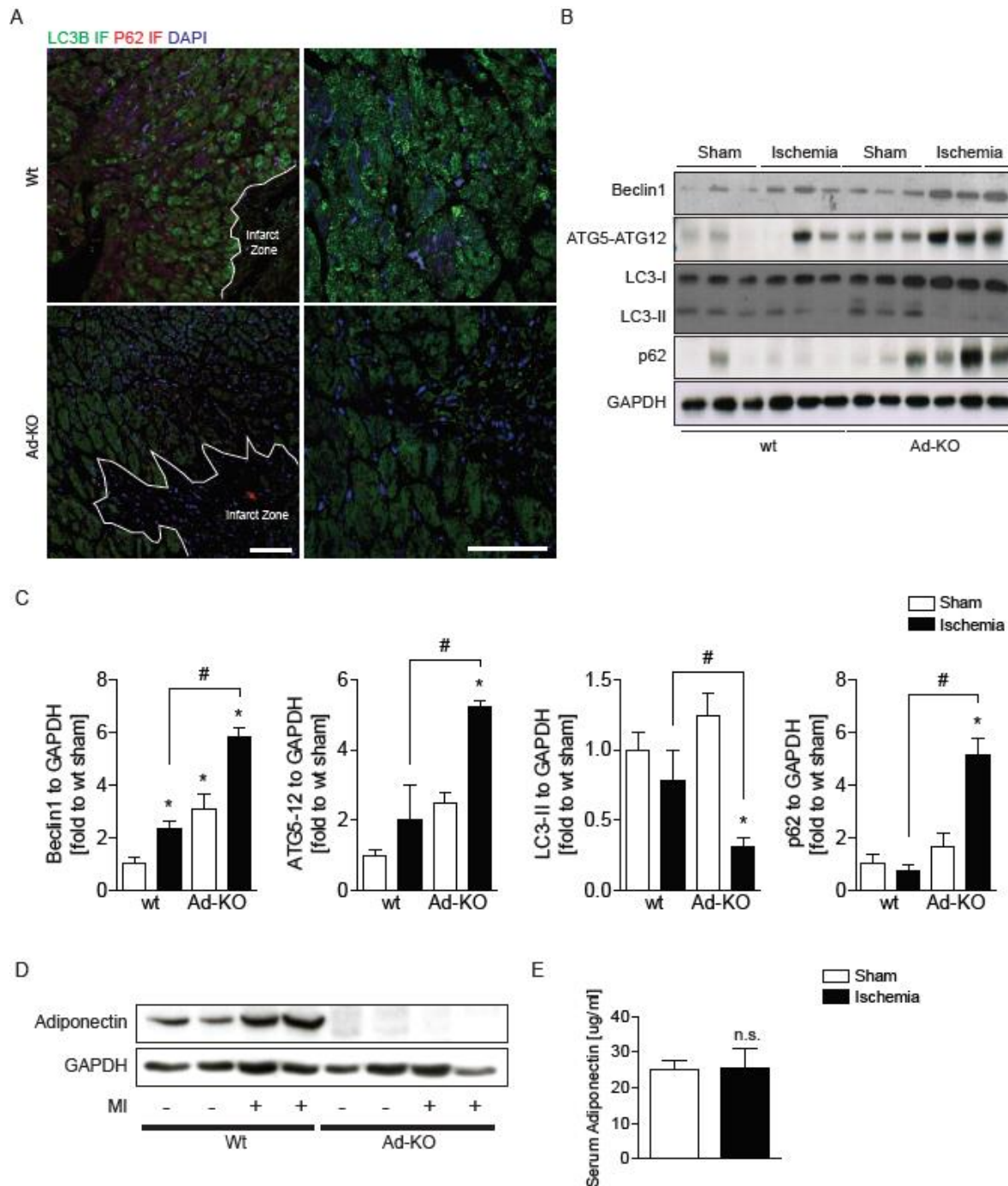
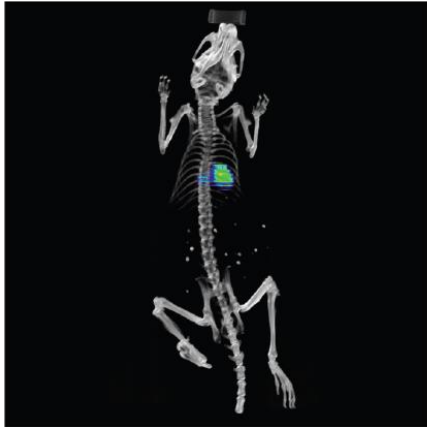


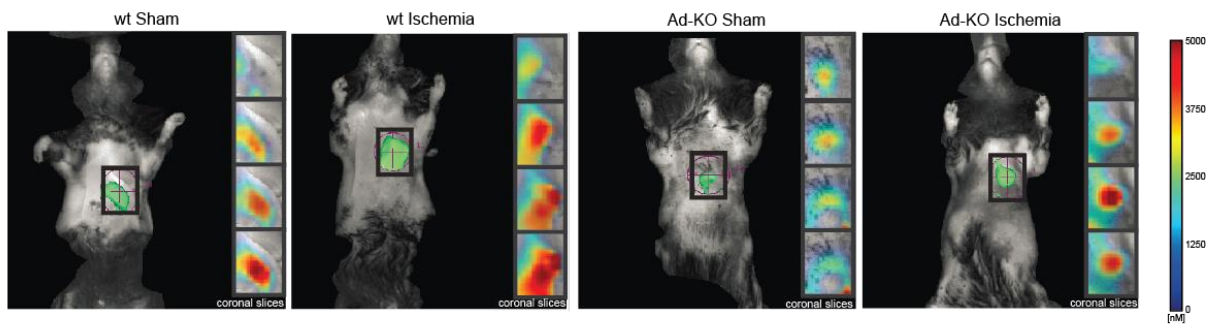
**Figure 4.1. Impaired autophagy in Ad-KO mice after ischemia.**

**A** Representative confocal immunofluorescent microscope against LC3B (green) and p62 (Red) in paraffin heart sections. **B** Representative western blot images of Beclin-1, ATG5-ATG12, LC3B, p62, and GAPDH from apical heart homogenates **C** Densitometric analysis of Beclin1, ATG5-ATG12, LC3-II, p62 to GAPDH from **B**. **D** Representative western blot images of adiponectin, GAPDH from apical heart homogenates **E** ELISA quantification of serum adiponectin in wt mice after ischemia. Results are presented as mean  $\pm$  SEM (n=6 each). \*P<0.05 versus corresponding sham. #P<0.05 versus wt Ischemia. Scale bar = 50  $\mu$ m.

A



B



C

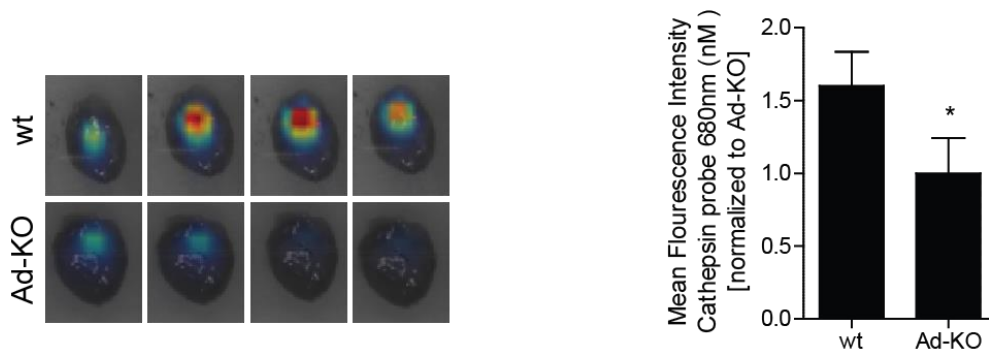


**Figure 4.2. Reduced cathepsin D activity in Ad-KO mice hearts after ischemia.**

**A** Representative in-vivo FMT (Cathepsin-680nm) image superimposed with CT scan image to locate signal from hearts. **B** Representative FMT images of mice with or without ischemia surgery. **C** Representative ex-vivo FMT (Cathepsin-680nm) scan images of hearts after ischemia, and quantification of mean fluorescence intensity. Results are presented as mean  $\pm$  SEM (n=3 each for FMT). \*P<0.05 versus wt Ischemia.

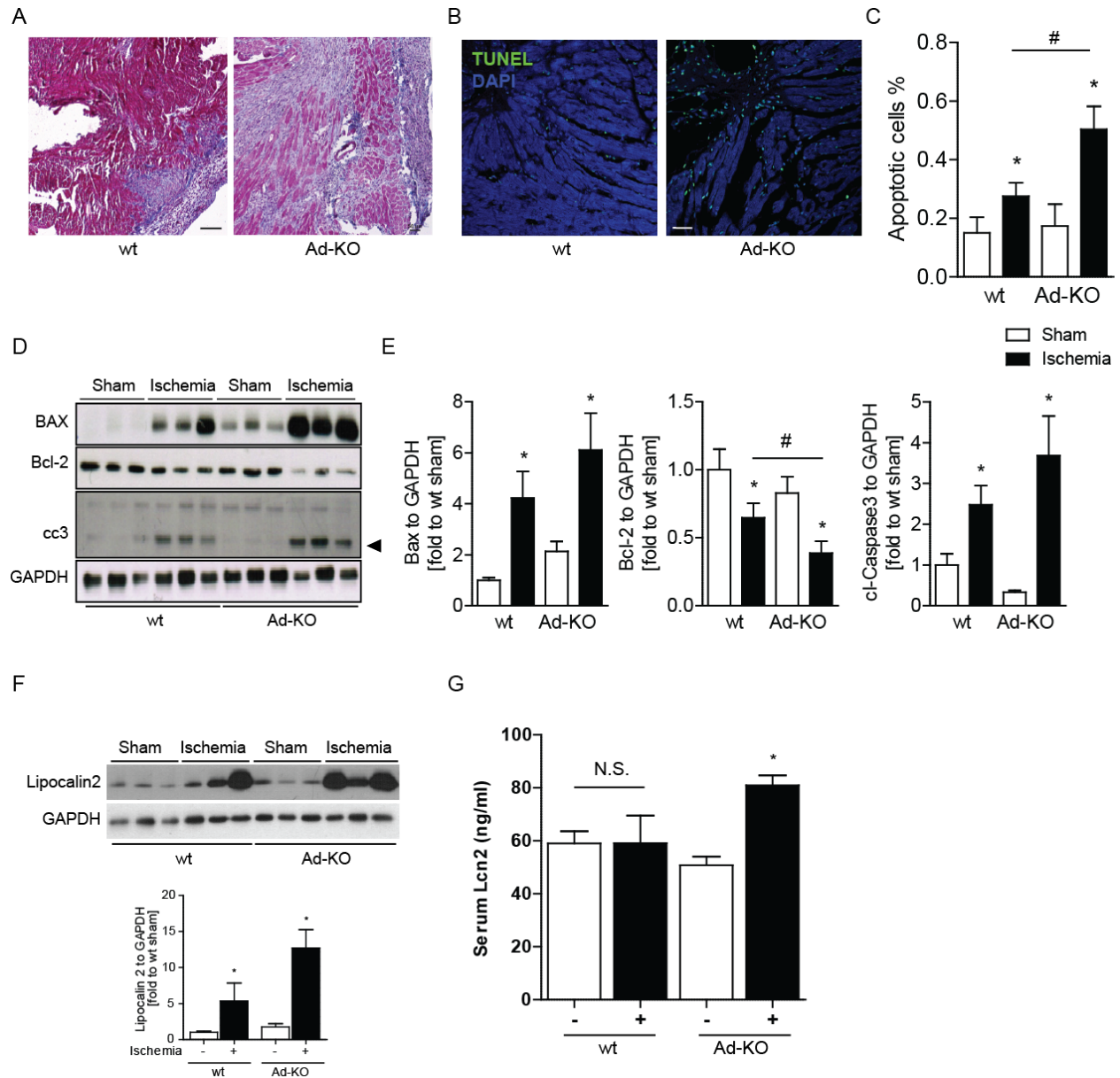
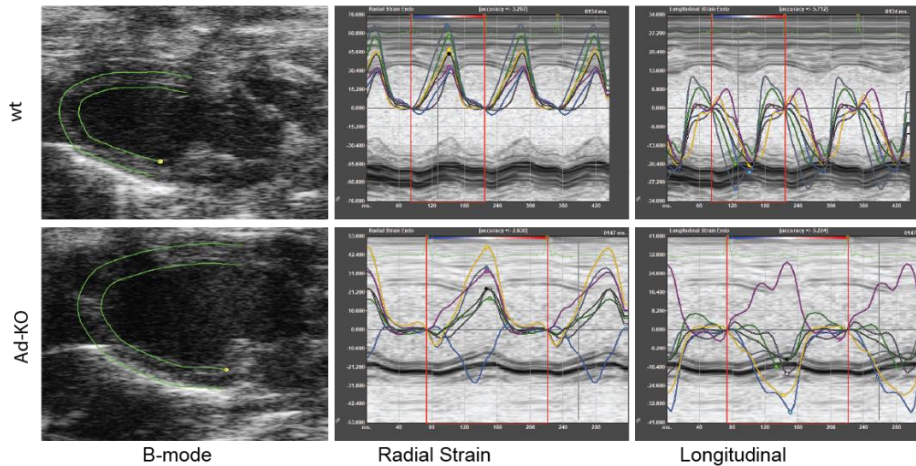


**Figure 4.3. Exaggerated fibrosis, cell deaths and inflammation in Ad-KO mice with MI.** **A** Representative Masson trichrome staining images on heart sections after Ischemia. **B-C** Representative TUNEL staining images and quantification of TUNEL positive nuclei in heart sections from wt and Ad-KO mice with or without ischemia surgery. **D** Representative western blot images of BAX, Bcl-2, caspase 3, GAPDH levels in hearts with or without ischemia surgery. **E** Densitometry analysis of BAX, Bcl-2, cleaved caspase 3 expressions relative to GAPDH levels. **F** Representative western blot images of lipocalin2 and GAPDH, and quantification of lipocalin2 to GAPDH expression on hearts after ischemia. **G** ELISA quantification of serum lipocalin 2 levels in wt and Ad-KO mice after ischemia. Results are presented as mean  $\pm$  SEM (n=6). Scale bar = 50  $\mu$ m. \*P<0.05 versus corresponding sham. #P<0.05 versus wt Ischemia.

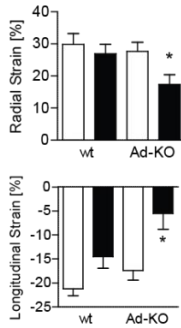
A

	wt		Ad-KO	
	Sham	Ischemia	Sham	Ischemia
LVEDD (mm)	2.32 ± 0.130	2.79 ± 0.175 <sup>a</sup>	2.51 ± 0.117	3.27 ± 0.101 <sup>a</sup>
LVEDD (mm)	3.59 ± 0.0794	3.97 ± 0.137 <sup>a</sup>	3.95 ± 0.0963 <sup>b</sup>	4.47 ± 0.107 <sup>a,c</sup>
LVESV (ul)	18.9 ± 2.42	30.5 ± 5.13	22.9 ± 2.58	43.7 ± 3.49 <sup>a,c</sup>
LVEDV (ul)	54.3 ± 2.89	69.5 ± 5.74 <sup>a</sup>	68.3 ± 3.94 <sup>b</sup>	91.7 ± 5.38 <sup>a,c</sup>
SV (ul)	35.4 ± 1.46	38.9 ± 2.38	45.3 ± 1.90 <sup>b</sup>	47.9 ± 2.10
EF (%)	65.6 ± 3.31	57.3 ± 3.55	66.7 ± 2.23	52.7 ± 1.09 <sup>a</sup>
FS (%)	35.5 ± 2.59	29.9 ± 2.20	36.5 ± 1.69	26.9 ± 0.659 <sup>a</sup>
CO (mL/min)	16.9 ± 0.713	18.3 ± 1.08	20.6 ± 1.29 <sup>b</sup>	21.9 ± 0.791

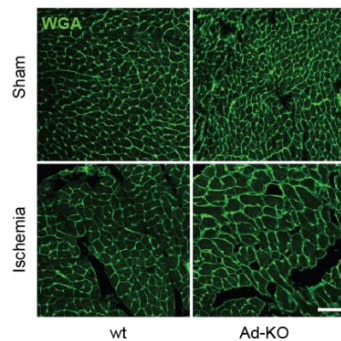
B



C



D



E

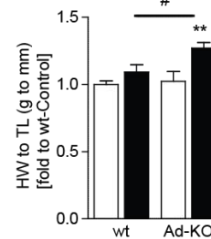
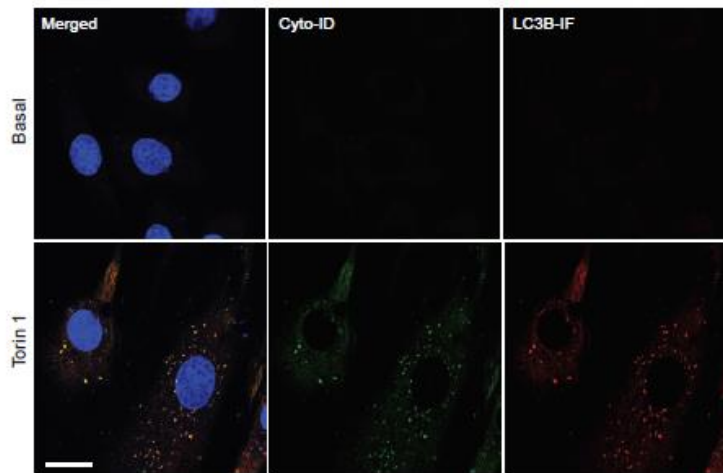


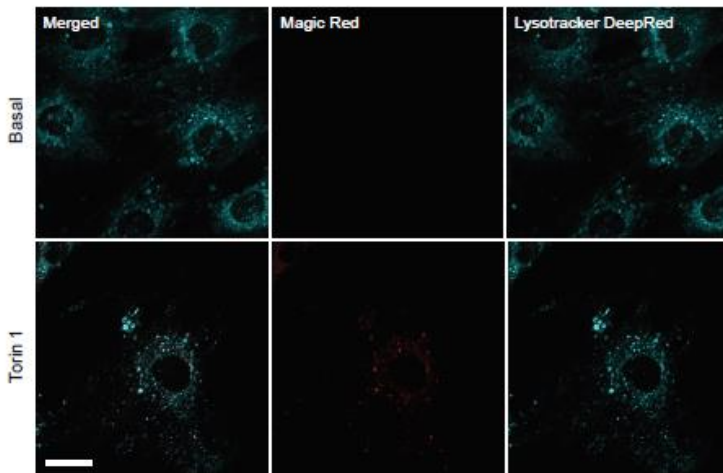
### Figure 4.4. Exacerbated cardiac remodeling in Ad-KO mice after ischemia.

**A** Summary of Cardiac parameters and functions analyzed in hearts of wt and Ad-KO mice with or without ischemia surgery. **B** Representative images of changes in strains over three cardiac cycles in radial and longitudinal directions from hearts with or without ischemia surgery. **C** Average strains from 6 segments of cardiac walls at long axis in longitudinal and radial directions from hearts with or without ischemia surgery. **D** Representative images of WGA staining on paraffin embedded hearts after ischemia **E** Gross heart weight to tibial length ratio. Results are presented as mean ± SEM (n=6). \*P<0.05 versus corresponding sham. <sup>a</sup>P<0.05 versus corresponding sham <sup>b</sup>P<0.05 versus wt Sham <sup>c</sup>P<0.05 versus wt Ischemia. Scale bar = 20 μm.

A



B



C

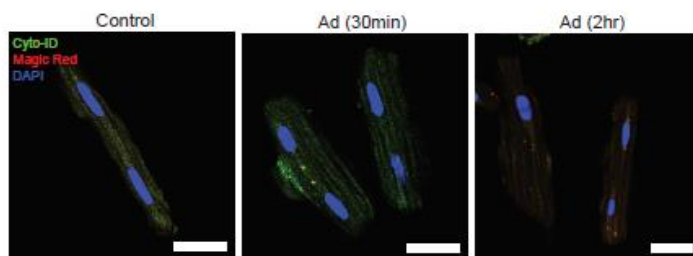


**Figure 4.5. Validation of Cyto-ID and Magic Red assay to assess autophagy flux.**

**A** Representative confocal image of H9c2 cells stained with Cyto-ID (green) and LC3B IF (red) after Torin 1 treatment (200nM, 1hr). **B** Representative confocal image of H9c2 cells stained with Lysotracker DeepRed (Cyan) and Magic Red (Red) after Torin 1 treatment (200nM, 1hr). **C** Representative confocal images of primary rat cardiomyocytes after adiponectin treatment (gAd, 2ug) at 30 min, 2 hr and stained with Cyto-ID and Magic Red. Scale bar = 10  $\mu$ m.

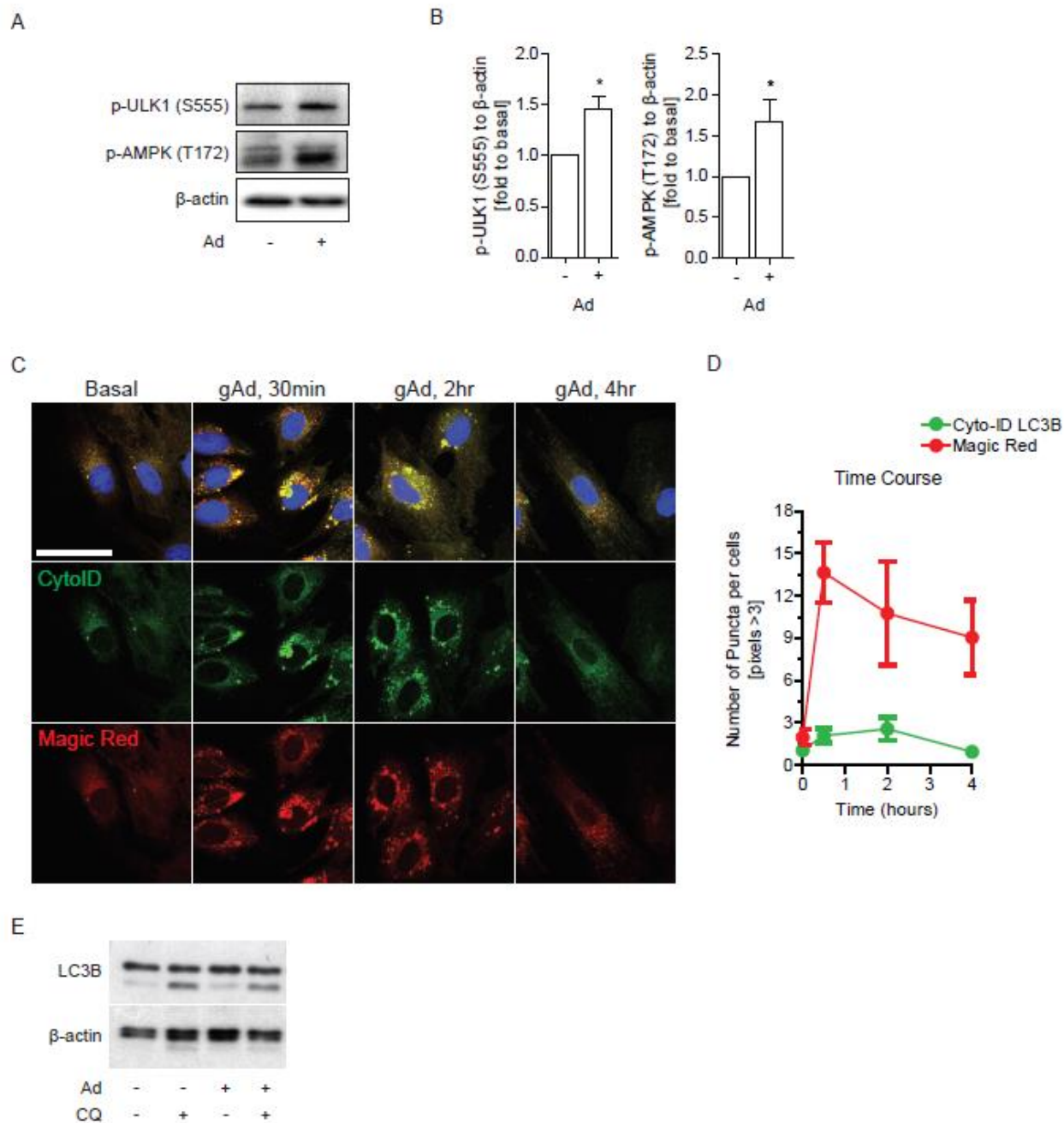


**Figure 4.6. Stimulation of autophagy flux upon adiponectin treatment.**

**A** Representative western blot images of p-ULK1 S555, p-AMPK T172, and  $\beta$ -actin in H9c2 cells after adiponectin stimulation (gAd  $1\mu\text{g/mL}$ , 30min). **B** Quantification of p-ULK1 S555 and p-AMPK T172 to  $\beta$ -actin from **A**. **C** Representative confocal microscope image of H9c2 stained with Cyto-ID and Magic Red after adiponectin treatment (gAd  $1\mu\text{g/mL}$ ) for 30 min, 2 hr and 4hr. **D** Quantification of Cyto-ID and Magic-Red puncta at each time points from **C**. **E** Representative images of LC3B and  $\beta$ -actin after 4 hr adiponectin treatment (gAd  $1\mu\text{g/mL}$ ) with chloroquine (CQ,  $60\mu\text{M}$ ). Results are shown in Mean  $\pm$  SEM ( $n=3$ ). Scale bar =  $20\mu\text{m}$ .

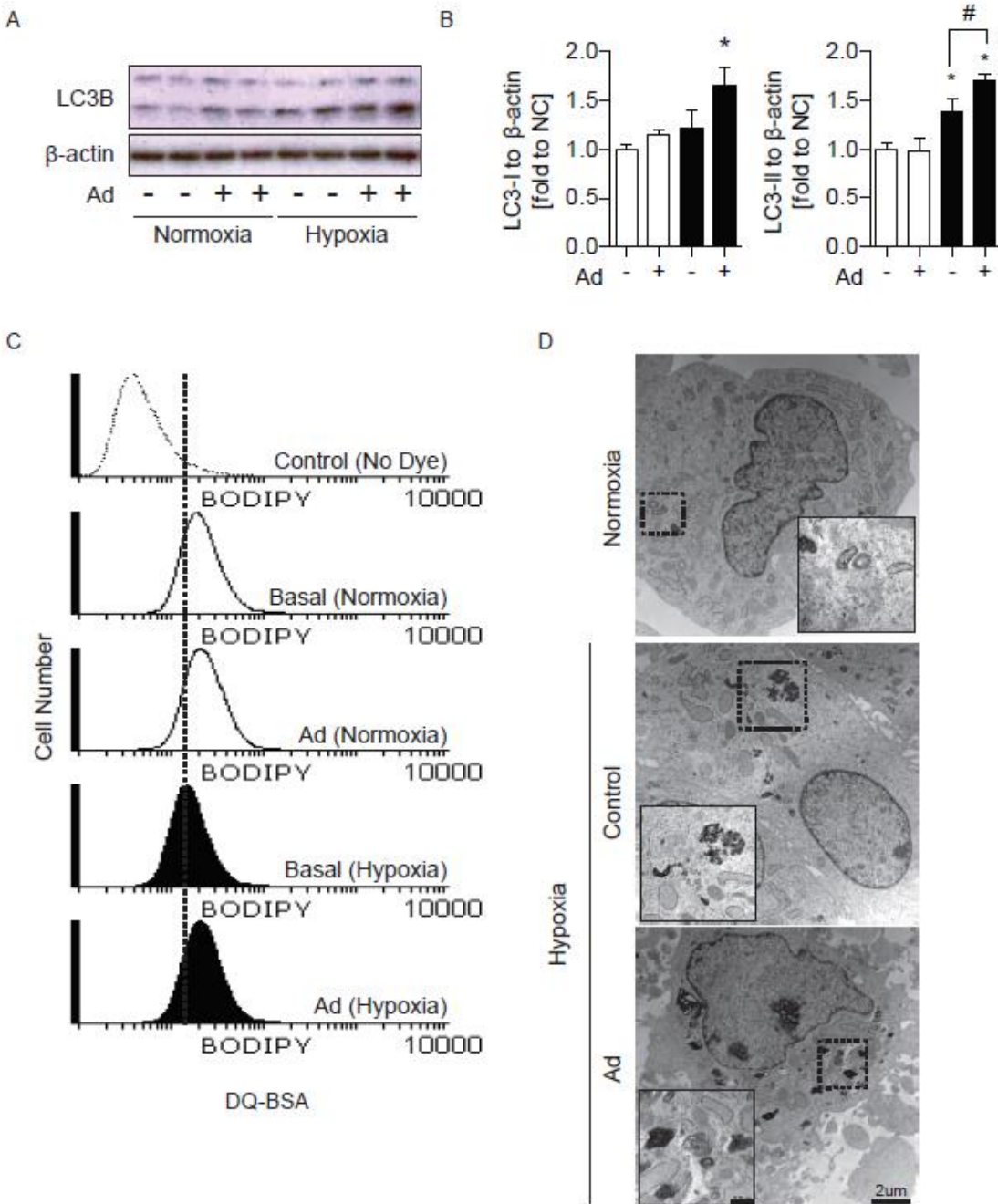


**Figure 4.7. Adiponectin treatment enhanced autophagy flux in Hypoxia.**

**A** Representative western blot images of LC3B and  $\beta$  actin expression in H9c2 in normoxia or hypoxia with Ad for 2 hr. **B** Densitometric analysis of LC3-II to  $\beta$  actin from **A**. **C** BODIPY-Green fluorescence distribution graph in H9c2 cells in normoxia or hypoxia with or without Ad. **D** Representative TEM images H9c2 cells in normoxia or hypoxia with or without Ad. Experiments were performed at least three times and results are presented as mean  $\pm$  SEM. Scale bar = 2 $\mu$ m. \*P<0.05 versus corresponding normoxia control. #P<0.05 versus hypoxia control.

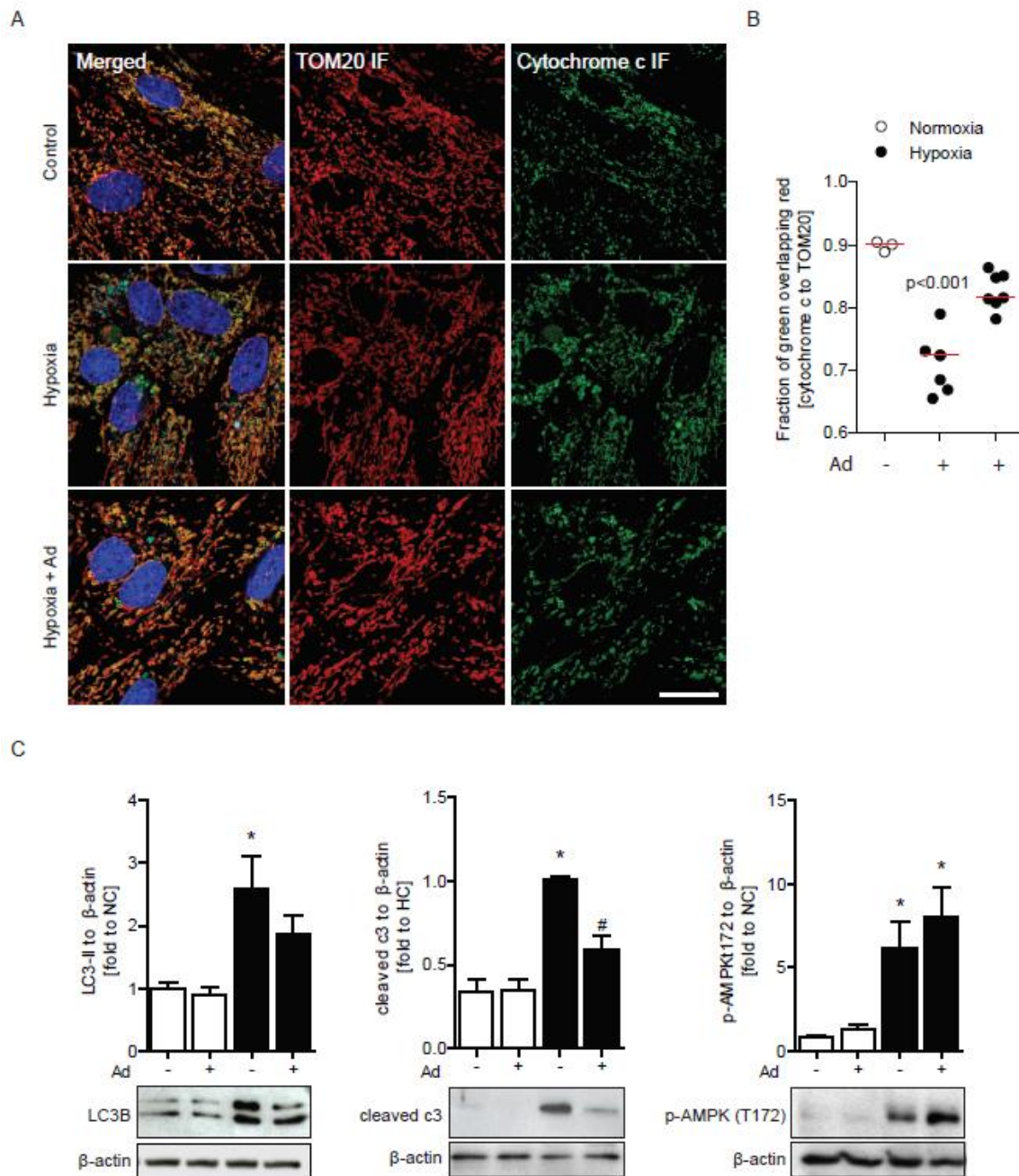


**Figure 4.8. Adiponectin alleviates intrinsic apoptosis from mitochondria in H9c2 cells in Hypoxia.**

**A** Representative confocal images of H9c2 cells labeled with TOM20 and cytochrome C after long term hypoxia with or without Ad. **B** Co-localization analysis from A, a proportion of cytochrome c signals (green) localized to mitochondria (red). **C** Representative western blot images and densitometry analysis of LC3B, phosphor-AMPK (T172) and cleaved caspase 3 to  $\beta$ -actin expression in H9c2 cell lysates after long term hypoxia with or without Ad. Experiments were performed three times and results are presented as mean  $\pm$  SEM. \* $P < 0.05$  versus normoxia control. # $P < 0.05$  versus hypoxia control. Scale bar = 20  $\mu$ m.

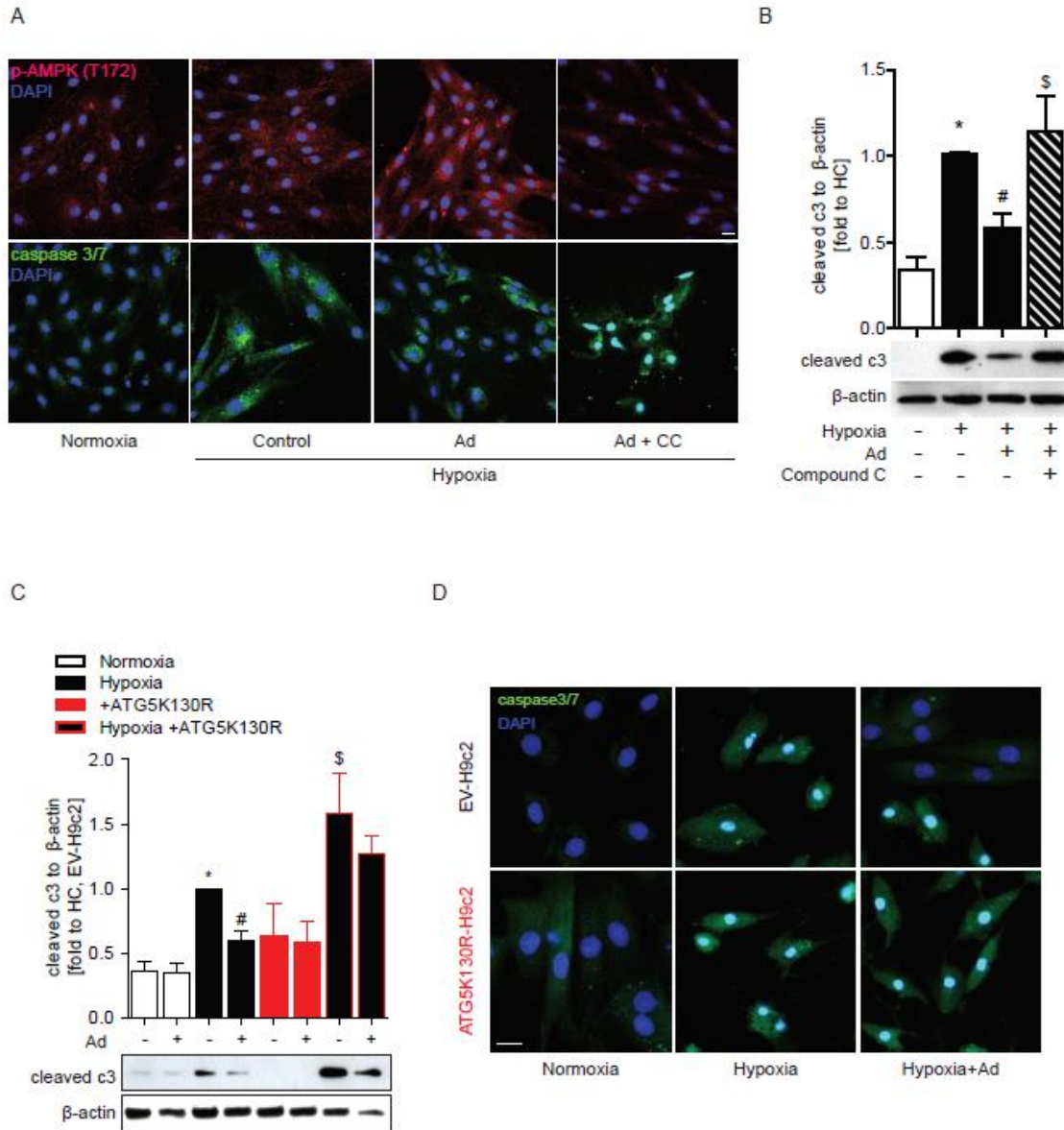


**Figure 4.9. AMPK- or Autophagy- inhibitions abolished adiponectin's anti-apoptotic effect.**

**A** Representative confocal immunofluorescence (anti-p-AMPK T172, red) and caspase 3/7 assay images of H9c2 cells after long term hypoxia (48hr) with or without Ad (gAd, 1ug/mL) in the presence of absence of compound c (5uM). **B** Representative western blot images and densitometry analysis of cleaved caspase 3 to β-actin expression in H9c2 cell lysates after long term hypoxia with or without Ad in the presence of absence of compound c. **C** Representative western blot image and densitometry analysis of cleaved caspase 3 to B-actin in H9c2 cells (EV or ATG5K130R overexpressing) in hypoxia treated with or without Ad. **D** Representative confocal images of EV- or ATG5K130R- H9c2 cells treated with caspase3/7 substrate after long-term hypoxia with or without Ad. CC= Compound C. EV = Empty Vector. Experiments were performed three times and results are presented as mean ± SEM. \*P<0.05 versus normoxia control. #P<0.05 versus hypoxia control. \$P<0.05 versus hypoxia Ad. Scale bar = 20 μm.

## 4.5 Discussion

In the present study, we examined the functional significance of adiponectin stimulated autophagy in cardiomyocytes during ischemia or hypoxia. Low adiponectin level is implicated in cardiovascular disease and emerging evidence suggests adiponectin is associated with decreased autophagy response [171, 179, 207]. Adiponectin was reported to accumulate at the infarct zone following myocardial infarction [300], and AMPK associated autophagy was activated during ischemia [291]. Adiponectin has a potent AMPK inducing capacity in cardiomyocytes [98, 149, 297] thus we examined changes in autophagy after myocardial infarction without reperfusion up to 7 days in wt and Ad-KO mice.

Ischemia robustly stimulated autophagy via phosphorylation of ULK1 S555, activated by AMPK [160] after MI, and autophagosomes robustly formed near the border-zone in wt mice. However, AMPK activity and autophagic response were abolished in Ad-KO mice. Importantly, Ad-KO mice hearts with ischemia had significantly lower lysosomal activity and increased p62 levels, a sign of autophagy defects [247]. Overall Ad-KO mice hearts had compromised autophagy response after ischemia and developed worse cardiac dysfunction with greater hypertrophy and fibrotic scars aligning with previous reports [301, 302]. Interestingly, ischemia surgery resulted in cell deaths and accumulation of lipocalin 2 in hearts in Ad-KO mice. We previously reported that lipocalin 2 causes cell death by enhancing oxidative stress and reducing autophagy flux in cardiomyocytes [298, 299, 303], and Ad-KO mice after ischemia not only had significantly increased lipocalin 2 in hearts but also in the circulation.

Consistent with our animal experiments, we observed a robust autophagy stimulatory effect by adiponectin in H9c2 cells. Short-term globular adiponectin has a stronger binding affinity to AdipoR1-AMPK signaling [105, 109], and we observed gAd enhanced phosphorylation of

AMPK T172 and ULK1 S555, along with an increased number of autophagosomes and lysosomal activity in H9c2 cells. During hypoxia, where the clearance of autophagosomes was partially impaired [304], adiponectin treatment enhanced autophagosome clearance and increased degradation activity at endosomes/lysosomes. A longer duration of hypoxia caused the accumulation of autophagosomes and induced cell deaths via intrinsic apoptosis, which were ameliorated by adiponectin treatment. Adiponectin's anti-apoptotic effects were abolished in the presence of AMPK inhibitor or in autophagy deficient cells (ATG5K130R-H9c2).

In summary, our study showed that adiponectin is an important mediator of cardiac autophagy, and the lack of adiponectin signaling impaired autophagy stimulation via the AMPK pathway during ischemia, which resulted in more cell death and pathological remodeling. Our study also found that adiponectin accumulation in hearts could last up to 7 days if MI was induced without reperfusion. Intriguingly, Ad-KO mice hearts significantly increased Beclin1 expression after MI, a feature of maladaptive autophagy response leading to excessive autophagy cell deaths [290, 291, 305, 306]. However, we concluded autophagy activity was impaired in spite of enhanced Beclin1 expression due to increased p62 levels and decreased lysosomal activity. Our study reported an unprecedented case of autophagy impairment with Beclin1 overexpression and capitalized the cardiac autophagy stimulatory effect by adiponectin during ischemia.

## Chapter 5

### 5.1 Research Summary

#### *Study 1 “Iron overload inhibits late stage autophagy flux leading to insulin resistance”*

The causative relationship between IO and diabetes is elusive because IO induced diabetes are contributed by both T1D and T2D. In spite of the strong association between IO and the prevalence of diabetes, the genetic model of hemochromatosis IO has increased insulin sensitivity and exhibits T1D [180, 232]. My study has added an important mechanistic insight underlying IO induced T2D by examining insulin sensitivity in skeletal muscle, a major site for glucose disposal, after IO. IO robustly induced insulin resistance, in which autophagy defects concomitantly occurred. Autophagy defects are caused by inhibiting mTOR reactivation for a novel lysosomal genesis process, ALR, in which very few in vivo studies have been reported to date [201].

#### *Study 2 “Pressure Overload-Induced Cardiac Dysfunction in Aged Male Adiponectin Knockout Mice Is Associated with Autophagy Deficiency”*

The cardioprotective effects of adiponectin are well established yet adiponectin’s role in regulating cardiac autophagy has not been investigated. At the time of this study’s publication, very few studies addressed the potential link between adiponectin signalling and autophagy rates in different tissues [177, 179, 307]. We examined changes in cardiac autophagy after PO in wt and Ad-KO mice, older than 12 months in which ageing did not affect changes in autophagy protein expression. However, autophagy response against PO in Ad-KO mice was compromised with a significant accumulation of protein aggregates or damaged mitochondria. Overall, this study uncovered that adiponectin signaling is a critical mediator of cardiac autophagy response against hemodynamic stress.

### *Study 3 “Disrupted Autophagy Flux in Adiponectin Knockout Mice Exacerbates Ischemia-Induced Cardiomyocyte Cell Death”*

Autophagy can act as a protective and a detrimental response during MI-induced cardiac remodeling. During ischemia, AMPK induced autophagy is protective which prevents cardiomyocytes from death and mitigates infarct size. During reperfusion, excessive beclin1-mediated autophagy with an unknown mechanism causes autophagic cell death, worsening dysfunction [291]. Our study adds a potential mechanism underlying switching from AMPK to Beclin-1 mediated autophagy during MI-induced cardiac remodelling. We observed a robust increase in AMPK-ULK1 autophagy induction following MI without reperfusion, which was abolished in Ad-KO mice. Instead, Ad-KO mice hearts exhibited significantly increased Beclin-1 expression, which aligns with my second study [276], with increased cell death and exaggerated remodeling after MI. Beclin1 is associated with autophagy cell death and Beclin1 heterozygous KO mice (homozygous KO is lethal) protects from PO and reperfusion induced autophagy cell death [290, 291]. However, Beclin-1 overexpression is not associated with increased autophagy rates since p62 level increased and lysosomal enzymatic activity decreased in Ad-KO mice. Nevertheless, this study strongly suggests adiponectin is an important regulator of protective autophagy during ischemia.

## **5.2 Conclusion**

Overall, the studies described above underscored a critical role of autophagy in skeletal muscle and heart during diabetes and CVDs. IO is associated with hypoadiponectinemia, and our study discovered an unconventional form of autophagy defects in IO induced skeletal muscle which led to insulin resistance. Adiponectin deficiency not only worsened diabetes but also exaggerated

heart diseases. My thesis added an important aspect of adiponectin signaling in autophagy regulation, an indispensable component of normal heart function and stress response. In summary, adiponectin is a key mediator to enhance autophagy response under dysfunctional cardiometabolic conditions.

### **5.3 Future Direction**

The predominant cause of death by IO complications is HF, and IO induced cardiomyopathy is well established [308, 309]. We recently published that adiponectin ameliorates IO-induced autophagy defects and insulin resistance in H9c2 cells [294, 310]. It will be interesting to look at the effects of IO on Ad-KO mice and to characterize autophagy changes in both skeletal muscle and hearts after IO.

With respect to analyzing autophagy, it is important to assess mitophagy. Heart and muscles are heavily loaded with mitochondria, which are sources of ROS contributing to oxidative damage and a wide range of pathologies [311]. Mitochondrial degradation by autophagy is an important quality control system and mitophagy defects are implicated in many diseases [153].

In the second and third studies, we observed an accumulation of damaged mitochondria in Ad-KO mice hearts after PO or MI. Adiponectin's cardioprotective effect is strongly associated with its anti-oxidative effect, and it will be interesting to assess if adiponectin stimulated autophagy is related to mitophagy. To do so, it is important to replenish adiponectin signaling in Ad-KO mice, either injecting adiponectin receptor agonist [312] or adenovirus mediated adiponectin over-expression [111]. Ad-KO mice are now being crossed with tamoxifen inducible cardiomyocyte specific autophagy-deficient mice (ATG7<sup>flox/flox</sup>;αMHC-MerCreMer) to generate mice lacking autophagy in cardiomyocytes on the Ad-KO background. The purpose of these mice was to see if

adiponectin replenishment could exert similar cardioprotective effects between Ad-KO mice and Ad-KO mice lacking cardiac autophagy.

Metabolic heart failure is a common and devastating event. My research contributes new knowledge to our understanding of the potential causes of HF associated with obesity and diabetes, and highlights adiponectin signaling as a potential therapeutic strategy to enhance cardiac autophagy. Only when we accurately understand causes of heart failure at the molecular level, we will be able to identify opportunities for therapeutic exploitation and improved health care.

## References

1. Balkau, B. and M.A. Charles, *Comment on the provisional report from the WHO consultation. European Group for the Study of Insulin Resistance (EGIR)*. Diabet Med, 1999. **16**(5): p. 442-3.
2. Scholze, J., et al., *Epidemiological and economic burden of metabolic syndrome and its consequences in patients with hypertension in Germany, Spain and Italy; a prevalence-based model*. BMC Public Health, 2010. **10**: p. 529.
3. Katzmarzyk, P.T. and I. Janssen, *The economic costs associated with physical inactivity and obesity in Canada: an update*. Can J Appl Physiol, 2004. **29**(1): p. 90-115.
4. National Cholesterol Education Program Expert Panel on Detection, E. and A. Treatment of High Blood Cholesterol in, *Third Report of the National Cholesterol Education Program (NCEP) Expert Panel on Detection, Evaluation, and Treatment of High Blood Cholesterol in Adults (Adult Treatment Panel III) final report*. Circulation, 2002. **106**(25): p. 3143-421.
5. American Heart, A., et al., *Diagnosis and management of the metabolic syndrome. An American Heart Association/National Heart, Lung, and Blood Institute Scientific Statement. Executive summary*. Cardiol Rev, 2005. **13**(6): p. 322-7.
6. Nathan, D.M., et al., *Impaired fasting glucose and impaired glucose tolerance: implications for care*. Diabetes Care, 2007. **30**(3): p. 753-9.
7. Fonseca, V.A., *Defining and characterizing the progression of type 2 diabetes*. Diabetes Care, 2009. **32 Suppl 2**: p. S151-6.
8. Schirone, L., et al., *A Review of the Molecular Mechanisms Underlying the Development and Progression of Cardiac Remodeling*. Oxid Med Cell Longev, 2017. **2017**: p. 3920195.
9. Abel, E.D., S.E. Litwin, and G. Sweeney, *Cardiac remodeling in obesity*. Physiol Rev, 2008. **88**(2): p. 389-419.
10. Fernandez-Real, J.M., et al., *Serum ferritin as a component of the insulin resistance syndrome*. Diabetes Care, 1998. **21**(1): p. 62-8.
11. Fernandez-Real, J.M., A. Lopez-Bermejo, and W. Ricart, *Cross-talk between iron metabolism and diabetes*. Diabetes, 2002. **51**(8): p. 2348-54.
12. Piperno, A., et al., *Increased serum ferritin is common in men with essential hypertension*. J Hypertens, 2002. **20**(8): p. 1513-8.
13. Williams, M.J., R. Poulton, and S. Williams, *Relationship of serum ferritin with cardiovascular risk factors and inflammation in young men and women*. Atherosclerosis, 2002. **165**(1): p. 179-84.
14. Bozzini, C., et al., *Prevalence of body iron excess in the metabolic syndrome*. Diabetes Care, 2005. **28**(8): p. 2061-3.
15. Lakka, T.A. and D.E. Laaksonen, *Physical activity in prevention and treatment of the metabolic syndrome*. Appl Physiol Nutr Metab, 2007. **32**(1): p. 76-88.
16. Ford, E.S., et al., *Sedentary behavior, physical activity, and the metabolic syndrome among U.S. adults*. Obes Res, 2005. **13**(3): p. 608-14.
17. Bankoski, A., et al., *Sedentary activity associated with metabolic syndrome independent of physical activity*. Diabetes Care, 2011. **34**(2): p. 497-503.
18. Grundy, S.M., *Overnutrition, ectopic lipid and the metabolic syndrome*. J Investig Med, 2016. **64**(6): p. 1082-6.

19. Grundy, S.M., *Adipose tissue and metabolic syndrome: too much, too little or neither*. Eur J Clin Invest, 2015. **45**(11): p. 1209-17.
20. Bancej, C., et al., *Evidence Brief--Trends and projections of obesity among Canadians*. Health Promot Chronic Dis Prev Can, 2015. **35**(7): p. 109-12.
21. Lemieux, S., et al., *Health Canada's new guidelines for body weight classification in adults: challenges and concerns*. CMAJ, 2004. **171**(11): p. 1361-3.
22. Hamdy, O., S. Porramatikul, and E. Al-Ozairi, *Metabolic obesity: the paradox between visceral and subcutaneous fat*. Curr Diabetes Rev, 2006. **2**(4): p. 367-73.
23. Nomura, K., et al., *Visceral fat accumulation and metabolic risk factor clustering in older adults*. J Am Geriatr Soc, 2010. **58**(9): p. 1658-63.
24. Coleman, D.L., *Obese and diabetes: two mutant genes causing diabetes-obesity syndromes in mice*. Diabetologia, 1978. **14**(3): p. 141-8.
25. Zhang, Y., et al., *Positional cloning of the mouse obese gene and its human homologue*. Nature, 1994. **372**(6505): p. 425-32.
26. Pan, H., J. Guo, and Z. Su, *Advances in understanding the interrelations between leptin resistance and obesity*. Physiol Behav, 2014. **130**: p. 157-69.
27. Rasouli, N. and P.A. Kern, *Adipocytokines and the metabolic complications of obesity*. J Clin Endocrinol Metab, 2008. **93**(11 Suppl 1): p. S64-73.
28. Hotamisligil, G.S., N.S. Shargill, and B.M. Spiegelman, *Adipose expression of tumor necrosis factor-alpha: direct role in obesity-linked insulin resistance*. Science, 1993. **259**(5091): p. 87-91.
29. Kern, P.A., et al., *The expression of tumor necrosis factor in human adipose tissue. Regulation by obesity, weight loss, and relationship to lipoprotein lipase*. J Clin Invest, 1995. **95**(5): p. 2111-9.
30. Wellen, K.E. and G.S. Hotamisligil, *Obesity-induced inflammatory changes in adipose tissue*. J Clin Invest, 2003. **112**(12): p. 1785-8.
31. Sasaki, T., et al., *Lipoatrophic diabetes*. J Dermatol, 1992. **19**(4): p. 246-9.
32. Gavrilova, O., et al., *Surgical implantation of adipose tissue reverses diabetes in lipoatrophic mice*. J Clin Invest, 2000. **105**(3): p. 271-8.
33. Colombo, C., et al., *Transplantation of adipose tissue lacking leptin is unable to reverse the metabolic abnormalities associated with lipoatrophy*. Diabetes, 2002. **51**(9): p. 2727-33.
34. Proffit, W.R., *Muscle pressures and tooth position: North American whites and Australian aborigines*. Angle Orthod, 1975. **45**(1): p. 1-11.
35. Yamauchi, T., et al., *The mechanisms by which both heterozygous peroxisome proliferator-activated receptor gamma (PPARgamma) deficiency and PPARgamma agonist improve insulin resistance*. J Biol Chem, 2001. **276**(44): p. 41245-54.
36. Yamauchi, T., et al., *The fat-derived hormone adiponectin reverses insulin resistance associated with both lipoatrophy and obesity*. Nat Med, 2001. **7**(8): p. 941-6.
37. Scherer, P.E., et al., *A novel serum protein similar to C1q, produced exclusively in adipocytes*. J Biol Chem, 1995. **270**(45): p. 26746-9.
38. Hu, E., P. Liang, and B.M. Spiegelman, *AdipoQ is a novel adipose-specific gene dysregulated in obesity*. J Biol Chem, 1996. **271**(18): p. 10697-703.
39. Nakano, Y., et al., *Isolation and characterization of GBP28, a novel gelatin-binding protein purified from human plasma*. J Biochem, 1996. **120**(4): p. 803-12.

40. Maeda, K., et al., *cDNA cloning and expression of a novel adipose specific collagen-like factor, apM1 (adipose most abundant gene transcript 1)*. 1996. *Biochem Biophys Res Commun*, 2012. **425**(3): p. 556-9.
41. Arita, Y., et al., *Paradoxical decrease of an adipose-specific protein, adiponectin, in obesity*. *Biochem Biophys Res Commun*, 1999. **257**(1): p. 79-83.
42. Sirbu, A.E., et al., *Adiponectin expression in visceral adiposity is an important determinant of insulin resistance in morbid obesity*. *Endokrynol Pol*, 2018. **69**(3): p. 252-258.
43. McArdle, M.A., et al., *Mechanisms of obesity-induced inflammation and insulin resistance: insights into the emerging role of nutritional strategies*. *Front Endocrinol (Lausanne)*, 2013. **4**: p. 52.
44. Chung, S., et al., *Preadipocytes mediate lipopolysaccharide-induced inflammation and insulin resistance in primary cultures of newly differentiated human adipocytes*. *Endocrinology*, 2006. **147**(11): p. 5340-51.
45. Abdelgadir, M., et al., *Low serum adiponectin concentrations are associated with insulin sensitivity independent of obesity in Sudanese subjects with type 2 diabetes mellitus*. *Diabetol Metab Syndr*, 2013. **5**(1): p. 15.
46. Aso, Y., et al., *Comparison of serum high-molecular weight (HMW) adiponectin with total adiponectin concentrations in type 2 diabetic patients with coronary artery disease using a novel enzyme-linked immunosorbent assay to detect HMW adiponectin*. *Diabetes*, 2006. **55**(7): p. 1954-60.
47. Gabrielsen, J.S., et al., *Adipocyte iron regulates adiponectin and insulin sensitivity*. *J Clin Invest*, 2012. **122**(10): p. 3529-40.
48. Duncan, B.B., et al., *Adiponectin and the development of type 2 diabetes: the atherosclerosis risk in communities study*. *Diabetes*, 2004. **53**(9): p. 2473-8.
49. Lai, H., et al., *Association between the level of circulating adiponectin and prediabetes: A meta-analysis*. *J Diabetes Investig*, 2015. **6**(4): p. 416-29.
50. Lindsay, R.S., et al., *Adiponectin and development of type 2 diabetes in the Pima Indian population*. *Lancet*, 2002. **360**(9326): p. 57-8.
51. Stefan, N., et al., *Plasma adiponectin concentration is associated with skeletal muscle insulin receptor tyrosine phosphorylation, and low plasma concentration precedes a decrease in whole-body insulin sensitivity in humans*. *Diabetes*, 2002. **51**(6): p. 1884-8.
52. Pham, M.N., et al., *Serum adipokines as biomarkers of beta-cell function in patients with type 1 diabetes: positive association with leptin and resistin and negative association with adiponectin*. *Diabetes Metab Res Rev*, 2013. **29**(2): p. 166-70.
53. Blaslov, K., et al., *Relationship between Adiponectin Level, Insulin Sensitivity, and Metabolic Syndrome in Type 1 Diabetic Patients*. *Int J Endocrinol*, 2013. **2013**: p. 535906.
54. Matsubara, M., S. Maruoka, and S. Katayose, *Decreased plasma adiponectin concentrations in women with dyslipidemia*. *J Clin Endocrinol Metab*, 2002. **87**(6): p. 2764-9.
55. Cnop, M., et al., *Relationship of adiponectin to body fat distribution, insulin sensitivity and plasma lipoproteins: evidence for independent roles of age and sex*. *Diabetologia*, 2003. **46**(4): p. 459-69.
56. Nakamura, Y., et al., *Implications of plasma concentrations of adiponectin in patients with coronary artery disease*. *Heart*, 2004. **90**(5): p. 528-33.

57. Laughlin, G.A., et al., *Association of adiponectin with coronary heart disease and mortality: the Rancho Bernardo study*. Am J Epidemiol, 2007. **165**(2): p. 164-74.
58. Pischon, T., et al., *Plasma adiponectin levels and risk of myocardial infarction in men*. JAMA, 2004. **291**(14): p. 1730-7.
59. Hotta, K., et al., *Plasma concentrations of a novel, adipose-specific protein, adiponectin, in type 2 diabetic patients*. Arterioscler Thromb Vasc Biol, 2000. **20**(6): p. 1595-9.
60. Baden, M.Y., et al., *Association of adiponectin with blood pressure in healthy people*. Clin Endocrinol (Oxf), 2013. **78**(2): p. 226-31.
61. Chow, W.S., et al., *Hypoadiponectinemia as a predictor for the development of hypertension: a 5-year prospective study*. Hypertension, 2007. **49**(6): p. 1455-61.
62. Cutler, P., *Deferoxamine therapy in high-ferritin diabetes*. Diabetes, 1989. **38**(10): p. 1207-10.
63. Forouhi, N.G., et al., *Elevated serum ferritin levels predict new-onset type 2 diabetes: results from the EPIC-Norfolk prospective study*. Diabetologia, 2007. **50**(5): p. 949-56.
64. Cooksey, R.C., et al., *Dietary iron restriction or iron chelation protects from diabetes and loss of beta-cell function in the obese (ob/ob lep<sup>-/-</sup>) mouse*. Am J Physiol Endocrinol Metab, 2010. **298**(6): p. E1236-43.
65. Wlazlo, N., et al., *Iron metabolism is associated with adipocyte insulin resistance and plasma adiponectin: the Cohort on Diabetes and Atherosclerosis Maastricht (CODAM) study*. Diabetes Care, 2013. **36**(2): p. 309-15.
66. Ku, B.J., et al., *Serum ferritin is inversely correlated with serum adiponectin level: population-based cross-sectional study*. Dis Markers, 2009. **27**(6): p. 303-10.
67. Aregbesola, A., et al., *Serum adiponectin/Ferritin ratio in relation to the risk of type 2 diabetes and insulin sensitivity*. Diabetes Res Clin Pract, 2018. **141**: p. 264-274.
68. Aso, Y., et al., *Relation between serum high molecular weight adiponectin and serum ferritin or prohepcidin in patients with type 2 diabetes*. Diabetes Res Clin Pract, 2010. **90**(3): p. 250-5.
69. Swarbrick, M.M. and P.J. Havel, *Physiological, pharmacological, and nutritional regulation of circulating adiponectin concentrations in humans*. Metab Syndr Relat Disord, 2008. **6**(2): p. 87-102.
70. Wang, Y., et al., *Hydroxylation and glycosylation of the four conserved lysine residues in the collagenous domain of adiponectin. Potential role in the modulation of its insulin-sensitizing activity*. J Biol Chem, 2002. **277**(22): p. 19521-9.
71. Wang, Y., et al., *Post-translational modifications of the four conserved lysine residues within the collagenous domain of adiponectin are required for the formation of its high molecular weight oligomeric complex*. J Biol Chem, 2006. **281**(24): p. 16391-400.
72. Fruebis, J., et al., *Proteolytic cleavage product of 30-kDa adipocyte complement-related protein increases fatty acid oxidation in muscle and causes weight loss in mice*. Proc Natl Acad Sci U S A, 2001. **98**(4): p. 2005-10.
73. Waki, H., et al., *Generation of globular fragment of adiponectin by leukocyte elastase secreted by monocytic cell line THP-1*. Endocrinology, 2005. **146**(2): p. 790-6.
74. Wang, Z.V. and P.E. Scherer, *Adiponectin, the past two decades*. J Mol Cell Biol, 2016. **8**(2): p. 93-100.
75. Pajvani, U.B., et al., *Structure-function studies of the adipocyte-secreted hormone Acrp30/adiponectin. Implications for metabolic regulation and bioactivity*. J Biol Chem, 2003. **278**(11): p. 9073-85.

76. Almeda-Valdes, P., et al., *Total and high molecular weight adiponectin have similar utility for the identification of insulin resistance*. Cardiovasc Diabetol, 2010. **9**: p. 26.
77. Hara, K., et al., *Measurement of the high-molecular weight form of adiponectin in plasma is useful for the prediction of insulin resistance and metabolic syndrome*. Diabetes Care, 2006. **29**(6): p. 1357-62.
78. Shao, X., et al., *Peroxisome Proliferator-Activated Receptor-gamma: Master Regulator of Adipogenesis and Obesity*. Curr Stem Cell Res Ther, 2016. **11**(3): p. 282-9.
79. He, W., et al., *Adipose-specific peroxisome proliferator-activated receptor gamma knockout causes insulin resistance in fat and liver but not in muscle*. Proc Natl Acad Sci U S A, 2003. **100**(26): p. 15712-7.
80. Iwaki, M., et al., *Induction of adiponectin, a fat-derived antidiabetic and antiatherogenic factor, by nuclear receptors*. Diabetes, 2003. **52**(7): p. 1655-63.
81. Yu, J.G., et al., *The effect of thiazolidinediones on plasma adiponectin levels in normal, obese, and type 2 diabetic subjects*. Diabetes, 2002. **51**(10): p. 2968-74.
82. Nawrocki, A.R., et al., *Mice lacking adiponectin show decreased hepatic insulin sensitivity and reduced responsiveness to peroxisome proliferator-activated receptor gamma agonists*. J Biol Chem, 2006. **281**(5): p. 2654-60.
83. Nakae, J., et al., *The forkhead transcription factor FoxO1 regulates adipocyte differentiation*. Dev Cell, 2003. **4**(1): p. 119-29.
84. Guo, S., et al., *Phosphorylation of serine 256 by protein kinase B disrupts transactivation by FKHR and mediates effects of insulin on insulin-like growth factor-binding protein-1 promoter activity through a conserved insulin response sequence*. J Biol Chem, 1999. **274**(24): p. 17184-92.
85. van der Heide, L.P. and M.P. Smidt, *Regulation of FoxO activity by CBP/p300-mediated acetylation*. Trends Biochem Sci, 2005. **30**(2): p. 81-6.
86. Wang, A., et al., *Up-regulation of adiponectin by resveratrol: the essential roles of the Akt/FOXO1 and AMP-activated protein kinase signaling pathways and DsbA-L*. J Biol Chem, 2011. **286**(1): p. 60-6.
87. Banks, A.S., et al., *Sirt1 gain of function increases energy efficiency and prevents diabetes in mice*. Cell Metab, 2008. **8**(4): p. 333-41.
88. Liu, M. and F. Liu, *Transcriptional and post-translational regulation of adiponectin*. Biochem J, 2009. **425**(1): p. 41-52.
89. Yamauchi, T., et al., *Cloning of adiponectin receptors that mediate antidiabetic metabolic effects*. Nature, 2003. **423**(6941): p. 762-9.
90. Tsuchida, A., et al., *Insulin/Foxo1 pathway regulates expression levels of adiponectin receptors and adiponectin sensitivity*. J Biol Chem, 2004. **279**(29): p. 30817-22.
91. Cui, X.B., et al., *Insulin decreases myocardial adiponectin receptor 1 expression via PI3K/Akt and FoxO1 pathway*. Cardiovasc Res, 2012. **93**(1): p. 69-78.
92. Yamauchi, T., et al., *Targeted disruption of AdipoR1 and AdipoR2 causes abrogation of adiponectin binding and metabolic actions*. Nat Med, 2007. **13**(3): p. 332-9.
93. Hug, C., et al., *T-cadherin is a receptor for hexameric and high-molecular-weight forms of Acrp30/adiponectin*. Proc Natl Acad Sci U S A, 2004. **101**(28): p. 10308-13.
94. Denzel, M.S., et al., *T-cadherin is critical for adiponectin-mediated cardioprotection in mice*. J Clin Invest, 2010. **120**(12): p. 4342-52.
95. Mao, X., et al., *APPL1 binds to adiponectin receptors and mediates adiponectin signalling and function*. Nat Cell Biol, 2006. **8**(5): p. 516-23.

96. Niu, W., et al., *Maturation of the regulation of GLUT4 activity by p38 MAPK during L6 cell myogenesis*. J Biol Chem, 2003. **278**(20): p. 17953-62.
97. Deepa, S.S. and L.Q. Dong, *APPL1: role in adiponectin signaling and beyond*. Am J Physiol Endocrinol Metab, 2009. **296**(1): p. E22-36.
98. Fang, X., et al., *An APPL1-AMPK signaling axis mediates beneficial metabolic effects of adiponectin in the heart*. Am J Physiol Endocrinol Metab, 2010. **299**(5): p. E721-9.
99. Chandrasekar, B., et al., *Adiponectin blocks interleukin-18-mediated endothelial cell death via APPL1-dependent AMP-activated protein kinase (AMPK) activation and IKK/NF-kappaB/PTEN suppression*. J Biol Chem, 2008. **283**(36): p. 24889-98.
100. Cheng, K.K., et al., *APPL1 potentiates insulin-mediated inhibition of hepatic glucose production and alleviates diabetes via Akt activation in mice*. Cell Metab, 2009. **9**(5): p. 417-27.
101. Wang, C., et al., *Yin-Yang regulation of adiponectin signaling by APPL isoforms in muscle cells*. J Biol Chem, 2009. **284**(46): p. 31608-15.
102. Cheng, K.K., et al., *The adaptor protein APPL2 inhibits insulin-stimulated glucose uptake by interacting with TBC1D1 in skeletal muscle*. Diabetes, 2014. **63**(11): p. 3748-58.
103. Kersten, S., et al., *Peroxisome proliferator-activated receptor alpha mediates the adaptive response to fasting*. J Clin Invest, 1999. **103**(11): p. 1489-98.
104. Mandard, S., M. Muller, and S. Kersten, *Peroxisome proliferator-activated receptor alpha target genes*. Cell Mol Life Sci, 2004. **61**(4): p. 393-416.
105. Yoon, M.J., et al., *Adiponectin increases fatty acid oxidation in skeletal muscle cells by sequential activation of AMP-activated protein kinase, p38 mitogen-activated protein kinase, and peroxisome proliferator-activated receptor alpha*. Diabetes, 2006. **55**(9): p. 2562-70.
106. Viollet, B., et al., *Physiological role of AMP-activated protein kinase (AMPK): insights from knockout mouse models*. Biochem Soc Trans, 2003. **31**(Pt 1): p. 216-9.
107. Viollet, B. and F. Andreelli, *AMP-activated protein kinase and metabolic control*. Handb Exp Pharmacol, 2011(203): p. 303-30.
108. Combs, T.P., et al., *A transgenic mouse with a deletion in the collagenous domain of adiponectin displays elevated circulating adiponectin and improved insulin sensitivity*. Endocrinology, 2004. **145**(1): p. 367-83.
109. Yamauchi, T., et al., *Adiponectin stimulates glucose utilization and fatty-acid oxidation by activating AMP-activated protein kinase*. Nat Med, 2002. **8**(11): p. 1288-95.
110. Tomas, E., et al., *Enhanced muscle fat oxidation and glucose transport by ACRP30 globular domain: acetyl-CoA carboxylase inhibition and AMP-activated protein kinase activation*. Proc Natl Acad Sci U S A, 2002. **99**(25): p. 16309-13.
111. Satoh, H., et al., *Adenovirus-mediated adiponectin expression augments skeletal muscle insulin sensitivity in male Wistar rats*. Diabetes, 2005. **54**(5): p. 1304-13.
112. Chen, H., et al., *Adiponectin stimulates production of nitric oxide in vascular endothelial cells*. J Biol Chem, 2003. **278**(45): p. 45021-6.
113. Lam, K.S. and A. Xu, *Adiponectin: protection of the endothelium*. Curr Diab Rep, 2005. **5**(4): p. 254-9.
114. Suwa, M., et al., *Endurance exercise increases the SIRT1 and peroxisome proliferator-activated receptor gamma coactivator-1alpha protein expressions in rat skeletal muscle*. Metabolism, 2008. **57**(7): p. 986-98.

115. Iwabu, M., et al., *Adiponectin and AdipoR1 regulate PGC-1alpha and mitochondria by Ca(2+) and AMPK/SIRT1*. Nature, 2010. **464**(7293): p. 1313-9.
116. Liang, H. and W.F. Ward, *PGC-1alpha: a key regulator of energy metabolism*. Adv Physiol Educ, 2006. **30**(4): p. 145-51.
117. Achari, A.E. and S.K. Jain, *Adiponectin, a Therapeutic Target for Obesity, Diabetes, and Endothelial Dysfunction*. Int J Mol Sci, 2017. **18**(6).
118. Ouchi, N., et al., *Reciprocal association of C-reactive protein with adiponectin in blood stream and adipose tissue*. Circulation, 2003. **107**(5): p. 671-4.
119. Esposito, K., et al., *Effect of weight loss and lifestyle changes on vascular inflammatory markers in obese women: a randomized trial*. JAMA, 2003. **289**(14): p. 1799-804.
120. Maeda, N., et al., *Diet-induced insulin resistance in mice lacking adiponectin/ACRP30*. Nat Med, 2002. **8**(7): p. 731-7.
121. Ohashi, K., et al., *Adiponectin promotes macrophage polarization toward an anti-inflammatory phenotype*. J Biol Chem, 2010. **285**(9): p. 6153-60.
122. Sharma, A.M. and B. Staels, *Review: Peroxisome proliferator-activated receptor gamma and adipose tissue--understanding obesity-related changes in regulation of lipid and glucose metabolism*. J Clin Endocrinol Metab, 2007. **92**(2): p. 386-95.
123. Kim, J.Y., et al., *Obesity-associated improvements in metabolic profile through expansion of adipose tissue*. J Clin Invest, 2007. **117**(9): p. 2621-37.
124. Ye, R., et al., *Adiponectin is essential for lipid homeostasis and survival under insulin deficiency and promotes beta-cell regeneration*. Elife, 2014. **3**.
125. Holland, W.L., et al., *Receptor-mediated activation of ceramidase activity initiates the pleiotropic actions of adiponectin*. Nat Med, 2011. **17**(1): p. 55-63.
126. Kerr, J.W., *The practising allergist in the United Kingdom and Europe, prospects for the next twenty years*. Clin Exp Allergy, 1991. **21 Suppl 1**: p. 119-22.
127. Zhao, L., et al., *Globular adiponectin ameliorates metabolic insulin resistance via AMPK-mediated restoration of microvascular insulin responses*. J Physiol, 2015. **593**(17): p. 4067-79.
128. Otabe, S., et al., *Overexpression of human adiponectin in transgenic mice results in suppression of fat accumulation and prevention of premature death by high-calorie diet*. Am J Physiol Endocrinol Metab, 2007. **293**(1): p. E210-8.
129. Berg, A.H., et al., *The adipocyte-secreted protein Acrp30 enhances hepatic insulin action*. Nat Med, 2001. **7**(8): p. 947-53.
130. Combs, T.P., et al., *Endogenous glucose production is inhibited by the adipose-derived protein Acrp30*. J Clin Invest, 2001. **108**(12): p. 1875-81.
131. Miller, R.A., et al., *Adiponectin suppresses gluconeogenic gene expression in mouse hepatocytes independent of LKB1-AMPK signaling*. J Clin Invest, 2011. **121**(6): p. 2518-28.
132. Suzuki, M., Y. Akiyama, and J. Hamuro, *A change in monokine requirements for proliferation during thymocyte maturation: co-stimulating activity of interleukin 6 in the proliferation of LYT2- and L3T4- thymocytes*. Dev Comp Immunol, 1991. **15**(1-2): p. 83-92.
133. Yamauchi, T., et al., *Globular adiponectin protected ob/ob mice from diabetes and ApoE-deficient mice from atherosclerosis*. J Biol Chem, 2003. **278**(4): p. 2461-8.

134. Wang, Y., et al., *Adiponectin inhibits tumor necrosis factor-alpha-induced vascular inflammatory response via caveolin-mediated ceramidase recruitment and activation*. *Circ Res*, 2014. **114**(5): p. 792-805.
135. Kubota, N., et al., *Disruption of adiponectin causes insulin resistance and neointimal formation*. *J Biol Chem*, 2002. **277**(29): p. 25863-6.
136. Wang, X., et al., *Adiponectin abates atherosclerosis by reducing oxidative stress*. *Med Sci Monit*, 2014. **20**: p. 1792-800.
137. Amin, R.H., et al., *Endogenously produced adiponectin protects cardiomyocytes from hypertrophy by a PPARgamma-dependent autocrine mechanism*. *Am J Physiol Heart Circ Physiol*, 2010. **299**(3): p. H690-8.
138. Shimano, M., et al., *Adiponectin deficiency exacerbates cardiac dysfunction following pressure overload through disruption of an AMPK-dependent angiogenic response*. *J Mol Cell Cardiol*, 2010. **49**(2): p. 210-20.
139. Fujita, K., et al., *Adiponectin protects against angiotensin II-induced cardiac fibrosis through activation of PPAR-alpha*. *Arterioscler Thromb Vasc Biol*, 2008. **28**(5): p. 863-70.
140. Essick, E.E., et al., *Adiponectin mediates cardioprotection in oxidative stress-induced cardiac myocyte remodeling*. *Am J Physiol Heart Circ Physiol*, 2011. **301**(3): p. H984-93.
141. Wang, C., et al., *Globular adiponectin inhibits angiotensin II-induced nuclear factor kappaB activation through AMP-activated protein kinase in cardiac hypertrophy*. *J Cell Physiol*, 2010. **222**(1): p. 149-55.
142. Shibata, R., et al., *Adiponectin-mediated modulation of hypertrophic signals in the heart*. *Nat Med*, 2004. **10**(12): p. 1384-9.
143. Shibata, R., et al., *Adiponectin stimulates angiogenesis in response to tissue ischemia through stimulation of amp-activated protein kinase signaling*. *J Biol Chem*, 2004. **279**(27): p. 28670-4.
144. Shibata, R., et al., *Adiponectin protects against the development of systolic dysfunction following myocardial infarction*. *J Mol Cell Cardiol*, 2007. **42**(6): p. 1065-74.
145. Tao, L., et al., *Adiponectin cardioprotection after myocardial ischemia/reperfusion involves the reduction of oxidative/nitrative stress*. *Circulation*, 2007. **115**(11): p. 1408-16.
146. Shibata, R., et al., *Adiponectin protects against myocardial ischemia-reperfusion injury through AMPK- and COX-2-dependent mechanisms*. *Nat Med*, 2005. **11**(10): p. 1096-103.
147. Kondo, K., et al., *Impact of a single intracoronary administration of adiponectin on myocardial ischemia/reperfusion injury in a pig model*. *Circ Cardiovasc Interv*, 2010. **3**(2): p. 166-73.
148. Yi, W., et al., *Reduced cardioprotective action of adiponectin in high-fat diet-induced type II diabetic mice and its underlying mechanisms*. *Antioxid Redox Signal*, 2011. **15**(7): p. 1779-88.
149. Park, M., et al., *Globular adiponectin, acting via AdipoR1/APPL1, protects H9c2 cells from hypoxia/reoxygenation-induced apoptosis*. *PLoS One*, 2011. **6**(4): p. e19143.
150. Konishi, M., et al., *Adiponectin protects against doxorubicin-induced cardiomyopathy by anti-apoptotic effects through AMPK up-regulation*. *Cardiovasc Res*, 2011. **89**(2): p. 309-19.

151. Deter, R.L. and C. De Duve, *Influence of glucagon, an inducer of cellular autophagy, on some physical properties of rat liver lysosomes*. J Cell Biol, 1967. **33**(2): p. 437-49.
152. Nakatogawa, H., et al., *Dynamics and diversity in autophagy mechanisms: lessons from yeast*. Nat Rev Mol Cell Biol, 2009. **10**(7): p. 458-67.
153. Levine, B. and G. Kroemer, *Autophagy in the pathogenesis of disease*. Cell, 2008. **132**(1): p. 27-42.
154. Glick, D., S. Barth, and K.F. Macleod, *Autophagy: cellular and molecular mechanisms*. J Pathol, 2010. **221**(1): p. 3-12.
155. Simonsen, A. and S.A. Tooze, *Coordination of membrane events during autophagy by multiple class III PI3-kinase complexes*. J Cell Biol, 2009. **186**(6): p. 773-82.
156. Mizushima, N., *Autophagy: process and function*. Genes Dev, 2007. **21**(22): p. 2861-73.
157. Diaz-Troya, S., et al., *The role of TOR in autophagy regulation from yeast to plants and mammals*. Autophagy, 2008. **4**(7): p. 851-65.
158. Kim, J., et al., *AMPK and mTOR regulate autophagy through direct phosphorylation of Ulk1*. Nat Cell Biol, 2011. **13**(2): p. 132-41.
159. Jung, C.H., et al., *mTOR regulation of autophagy*. FEBS Lett, 2010. **584**(7): p. 1287-95.
160. Egan, D.F., et al., *Phosphorylation of ULK1 (hATG1) by AMP-activated protein kinase connects energy sensing to mitophagy*. Science, 2011. **331**(6016): p. 456-61.
161. Shang, L. and X. Wang, *AMPK and mTOR coordinate the regulation of Ulk1 and mammalian autophagy initiation*. Autophagy, 2011. **7**(8): p. 924-6.
162. Hanada, T., et al., *The Atg12-Atg5 conjugate has a novel E3-like activity for protein lipidation in autophagy*. J Biol Chem, 2007. **282**(52): p. 37298-302.
163. Pankiv, S., et al., *p62/SQSTM1 binds directly to Atg8/LC3 to facilitate degradation of ubiquitinated protein aggregates by autophagy*. J Biol Chem, 2007. **282**(33): p. 24131-45.
164. Bjorkoy, G., et al., *p62/SQSTM1 forms protein aggregates degraded by autophagy and has a protective effect on huntingtin-induced cell death*. J Cell Biol, 2005. **171**(4): p. 603-14.
165. Komatsu, M., et al., *Impairment of starvation-induced and constitutive autophagy in Atg7-deficient mice*. J Cell Biol, 2005. **169**(3): p. 425-34.
166. Komatsu, M., et al., *Homeostatic levels of p62 control cytoplasmic inclusion body formation in autophagy-deficient mice*. Cell, 2007. **131**(6): p. 1149-63.
167. Johansen, T. and T. Lamark, *Selective autophagy mediated by autophagic adapter proteins*. Autophagy, 2011. **7**(3): p. 279-96.
168. Quan, W. and M.S. Lee, *Role of autophagy in the control of body metabolism*. Endocrinol Metab (Seoul), 2013. **28**(1): p. 6-11.
169. Li, S., M.S. Brown, and J.L. Goldstein, *Bifurcation of insulin signaling pathway in rat liver: mTORC1 required for stimulation of lipogenesis, but not inhibition of gluconeogenesis*. Proc Natl Acad Sci U S A, 2010. **107**(8): p. 3441-6.
170. Liu, H.Y., et al., *Hepatic autophagy is suppressed in the presence of insulin resistance and hyperinsulinemia: inhibition of FoxO1-dependent expression of key autophagy genes by insulin*. J Biol Chem, 2009. **284**(45): p. 31484-92.
171. Ahlstrom, P., et al., *Adiponectin improves insulin sensitivity via activation of autophagic flux*. J Mol Endocrinol, 2017. **59**(4): p. 339-350.

172. Newgard, C.B., et al., *A branched-chain amino acid-related metabolic signature that differentiates obese and lean humans and contributes to insulin resistance*. *Cell Metab*, 2009. **9**(4): p. 311-26.
173. Yang, L., et al., *Defective hepatic autophagy in obesity promotes ER stress and causes insulin resistance*. *Cell Metab*, 2010. **11**(6): p. 467-78.
174. Escobar, K.A., et al., *Autophagy and aging: Maintaining the proteome through exercise and caloric restriction*. *Aging Cell*, 2019. **18**(1): p. e12876.
175. Ding, Q., et al., *Caloric restriction increases adiponectin expression by adipose tissue and prevents the inhibitory effect of insulin on circulating adiponectin in rats*. *J Nutr Biochem*, 2012. **23**(8): p. 867-74.
176. Rogozina, O.P., et al., *Effect of chronic and intermittent calorie restriction on serum adiponectin and leptin and mammary tumorigenesis*. *Cancer Prev Res (Phila)*, 2011. **4**(4): p. 568-81.
177. Guo, R., et al., *Adiponectin knockout accentuates high fat diet-induced obesity and cardiac dysfunction: role of autophagy*. *Biochim Biophys Acta*, 2013. **1832**(8): p. 1136-48.
178. Guo, R., et al., *Adiponectin deficiency rescues high-fat diet-induced hepatic injury, apoptosis and autophagy loss despite persistent steatosis*. *Int J Obes (Lond)*, 2017. **41**(9): p. 1403-1412.
179. Liu, Y., et al., *Adiponectin stimulates autophagy and reduces oxidative stress to enhance insulin sensitivity during high-fat diet feeding in mice*. *Diabetes*, 2015. **64**(1): p. 36-48.
180. Simcox, J.A. and D.A. McClain, *Iron and diabetes risk*. *Cell Metab*, 2013. **17**(3): p. 329-41.
181. Evstatiev, R. and C. Gasche, *Iron sensing and signalling*. *Gut*, 2012. **61**(6): p. 933-52.
182. Wang, J. and K. Pantopoulos, *Regulation of cellular iron metabolism*. *Biochem J*, 2011. **434**(3): p. 365-81.
183. Zimmermann, M.B. and R.F. Hurrell, *Nutritional iron deficiency*. *Lancet*, 2007. **370**(9586): p. 511-20.
184. Hentze, M.W., et al., *Two to tango: regulation of Mammalian iron metabolism*. *Cell*, 2010. **142**(1): p. 24-38.
185. Pantopoulos, K., et al., *Mechanisms of mammalian iron homeostasis*. *Biochemistry*, 2012. **51**(29): p. 5705-24.
186. Sebastiani, G. and K. Pantopoulos, *Disorders associated with systemic or local iron overload: from pathophysiology to clinical practice*. *Metallomics*, 2011. **3**(10): p. 971-86.
187. Brissot, P., et al., *Non-transferrin bound iron: a key role in iron overload and iron toxicity*. *Biochim Biophys Acta*, 2012. **1820**(3): p. 403-10.
188. Zhuang, T., H. Han, and Z. Yang, *Iron, oxidative stress and gestational diabetes*. *Nutrients*, 2014. **6**(9): p. 3968-80.
189. McClain, D.A., et al., *High prevalence of abnormal glucose homeostasis secondary to decreased insulin secretion in individuals with hereditary haemochromatosis*. *Diabetologia*, 2006. **49**(7): p. 1661-9.
190. Wongjaikam, S., et al., *Current and future treatment strategies for iron overload cardiomyopathy*. *Eur J Pharmacol*, 2015. **765**: p. 86-93.
191. Rajpathak, S.N., et al., *The role of iron in type 2 diabetes in humans*. *Biochim Biophys Acta*, 2009. **1790**(7): p. 671-81.

192. Datz, C., et al., *Iron homeostasis in the metabolic syndrome*. Eur J Clin Invest, 2013. **43**(2): p. 215-24.
193. Bofill, C., et al., *Response to repeated phlebotomies in patients with non-insulin-dependent diabetes mellitus*. Metabolism, 1994. **43**(5): p. 614-20.
194. Abraham, D., et al., *Increased insulin secretory capacity but decreased insulin sensitivity after correction of iron overload by phlebotomy in hereditary haemochromatosis*. Diabetologia, 2006. **49**(11): p. 2546-51.
195. Galaris, D. and K. Pantopoulos, *Oxidative stress and iron homeostasis: mechanistic and health aspects*. Crit Rev Clin Lab Sci, 2008. **45**(1): p. 1-23.
196. Mizushima, N. and M. Komatsu, *Autophagy: renovation of cells and tissues*. Cell, 2011. **147**(4): p. 728-41.
197. Yang, J.S., et al., *Autophagy and its link to type II diabetes mellitus*. Biomedicine (Taipei), 2017. **7**(2): p. 8.
198. Sarparanta, J., M. Garcia-Macia, and R. Singh, *Autophagy and Mitochondria in Obesity and Type 2 Diabetes*. Curr Diabetes Rev, 2017. **13**(4): p. 352-369.
199. Zheng, Q., et al., *Iron overload promotes mitochondrial fragmentation in mesenchymal stromal cells from myelodysplastic syndrome patients through activation of the AMPK/MFF/Drp1 pathway*. Cell Death Dis, 2018. **9**(5): p. 515.
200. Watson, A., et al., *Iron depletion suppresses mTORC1-directed signalling in intestinal Caco-2 cells via induction of REDD1*. Cell Signal, 2016. **28**(5): p. 412-424.
201. Chen, Y. and L. Yu, *Development of Research into Autophagic Lysosome Reformation*. Mol Cells, 2018. **41**(1): p. 45-49.
202. Henderson, R.J., S.M. Patton, and J.R. Connor, *Development of a fluorescent reporter to assess iron regulatory protein activity in living cells*. Biochim Biophys Acta, 2005. **1743**(1-2): p. 162-8.
203. Riemer, J., et al., *Colorimetric ferrozine-based assay for the quantitation of iron in cultured cells*. Anal Biochem, 2004. **331**(2): p. 370-5.
204. Esposito, B.P., et al., *A review of fluorescence methods for assessing labile iron in cells and biological fluids*. Anal Biochem, 2002. **304**(1): p. 1-18.
205. Au-Yeung, H.Y., et al., *Molecular imaging of labile iron(II) pools in living cells with a turn-on fluorescent probe*. J Am Chem Soc, 2013. **135**(40): p. 15165-73.
206. Aron, A.T., A.G. Reeves, and C.J. Chang, *Activity-based sensing fluorescent probes for iron in biological systems*. Curr Opin Chem Biol, 2018. **43**: p. 113-118.
207. Jahng, J.W., et al., *Pressure Overload-Induced Cardiac Dysfunction in Aged Male Adiponectin Knockout Mice Is Associated With Autophagy Deficiency*. Endocrinology, 2015. **156**(7): p. 2667-77.
208. Palanivel, R., et al., *Regulation of insulin signalling, glucose uptake and metabolism in rat skeletal muscle cells upon prolonged exposure to resistin*. Diabetologia, 2006. **49**(1): p. 183-90.
209. Russell, R.C., et al., *ULK1 induces autophagy by phosphorylating Beclin-1 and activating VPS34 lipid kinase*. Nat Cell Biol, 2013. **15**(7): p. 741-50.
210. Liu, Q., et al., *Effect of carvedilol on cardiomyocyte apoptosis in a rat model of myocardial infarction: a role for toll-like receptor 4*. Indian J Pharmacol, 2013. **45**(5): p. 458-63.
211. Xu, G., et al., *Lipocalin-2 induces cardiomyocyte apoptosis by increasing intracellular iron accumulation*. J Biol Chem, 2012. **287**(7): p. 4808-17.

212. Varghese, J., et al., *Increased intracellular iron in mouse primary hepatocytes in vitro causes activation of the Akt pathway but decreases its response to insulin*. *Biochim Biophys Acta Gen Subj*, 2018. **1862**(9): p. 1870-1882.
213. Kimura, S., T. Noda, and T. Yoshimori, *Dissection of the autophagosome maturation process by a novel reporter protein, tandem fluorescent-tagged LC3*. *Autophagy*, 2007. **3**(5): p. 452-60.
214. Hara, T., et al., *FIP200, a ULK-interacting protein, is required for autophagosome formation in mammalian cells*. *J Cell Biol*, 2008. **181**(3): p. 497-510.
215. Matsunaga, K., et al., *Two Beclin 1-binding proteins, Atg14L and Rubicon, reciprocally regulate autophagy at different stages*. *Nat Cell Biol*, 2009. **11**(4): p. 385-96.
216. Zhang, Y., et al., *Defective autophagosome trafficking contributes to impaired autophagic flux in coronary arterial myocytes lacking CD38 gene*. *Cardiovasc Res*, 2014. **102**(1): p. 68-78.
217. Kao, J.K., et al., *Chronic Iron Overload Results in Impaired Bacterial Killing of THP-1 Derived Macrophage through the Inhibition of Lysosomal Acidification*. *PLoS One*, 2016. **11**(5): p. e0156713.
218. Yu, L., et al., *Termination of autophagy and reformation of lysosomes regulated by mTOR*. *Nature*, 2010. **465**(7300): p. 942-6.
219. Munson, M.J., et al., *mTOR activates the VPS34-UVRAG complex to regulate autolysosomal tubulation and cell survival*. *EMBO J*, 2015. **34**(17): p. 2272-90.
220. Parmar, N. and F. Tamanoi, *Rheb G-Proteins and the Activation of mTORC1*. *Enzymes*, 2010. **27**: p. 39-56.
221. Li, Y., K. Inoki, and K.L. Guan, *Biochemical and functional characterizations of small GTPase Rheb and TSC2 GAP activity*. *Mol Cell Biol*, 2004. **24**(18): p. 7965-75.
222. Fernandez-Real, J.M., et al., *Blood letting in high-ferritin type 2 diabetes: effects on insulin sensitivity and beta-cell function*. *Diabetes*, 2002. **51**(4): p. 1000-4.
223. Chiang, G.G. and R.T. Abraham, *Phosphorylation of mammalian target of rapamycin (mTOR) at Ser-2448 is mediated by p70S6 kinase*. *J Biol Chem*, 2005. **280**(27): p. 25485-90.
224. Holz, M.K. and J. Blenis, *Identification of S6 kinase 1 as a novel mammalian target of rapamycin (mTOR)-phosphorylating kinase*. *J Biol Chem*, 2005. **280**(28): p. 26089-93.
225. Inoki, K., et al., *Rheb GTPase is a direct target of TSC2 GAP activity and regulates mTOR signaling*. *Genes Dev*, 2003. **17**(15): p. 1829-34.
226. Inoki, K., et al., *TSC2 is phosphorylated and inhibited by Akt and suppresses mTOR signalling*. *Nat Cell Biol*, 2002. **4**(9): p. 648-57.
227. Thoreen, C.C., et al., *An ATP-competitive mammalian target of rapamycin inhibitor reveals rapamycin-resistant functions of mTORC1*. *J Biol Chem*, 2009. **284**(12): p. 8023-32.
228. Liu, Q., et al., *Discovery of 1-(4-(4-propionylpiperazin-1-yl)-3-(trifluoromethyl)phenyl)-9-(quinolin-3-yl)benz o[h][1,6]naphthyridin-2(1H)-one as a highly potent, selective mammalian target of rapamycin (mTOR) inhibitor for the treatment of cancer*. *J Med Chem*, 2010. **53**(19): p. 7146-55.
229. Martin, L.E., et al., *The pharmacology of an iron-dextran intramuscular haematinic*. *Br J Pharmacol Chemother*, 1955. **10**(3): p. 375-82.

230. Italia, K., R. Colah, and K. Ghosh, *Experimental animal model to study iron overload and iron chelation and review of other such models*. Blood Cells Mol Dis, 2015. **55**(3): p. 194-9.
231. Heming, N., et al., *Efficacy and toxicity of intravenous iron in a mouse model of critical care anemia\**. Crit Care Med, 2012. **40**(7): p. 2141-8.
232. Cooksey, R.C., et al., *Oxidative stress, beta-cell apoptosis, and decreased insulin secretory capacity in mouse models of hemochromatosis*. Endocrinology, 2004. **145**(11): p. 5305-12.
233. Chen, W., et al., *Skeletal muscle hemojuvelin is dispensable for systemic iron homeostasis*. Blood, 2011. **117**(23): p. 6319-25.
234. Xu, A. and G. Sweeney, *Emerging role of autophagy in mediating widespread actions of ADIPOQ/adiponectin*. Autophagy, 2015. **11**(4): p. 723-4.
235. Cen, W.J., et al., *Iron overload induces G1 phase arrest and autophagy in murine preosteoblast cells*. J Cell Physiol, 2017.
236. Chen, G., et al., *Induction of autophagic cell death in the rat brain caused by iron*. Am J Med Sci, 2013. **345**(5): p. 369-74.
237. Russell, R.C., H.X. Yuan, and K.L. Guan, *Autophagy regulation by nutrient signaling*. Cell Res, 2014. **24**(1): p. 42-57.
238. Ganley, I.G., et al., *ULK1.ATG13.FIP200 complex mediates mTOR signaling and is essential for autophagy*. J Biol Chem, 2009. **284**(18): p. 12297-305.
239. Jung, C.H., et al., *ULK-Atg13-FIP200 complexes mediate mTOR signaling to the autophagy machinery*. Mol Biol Cell, 2009. **20**(7): p. 1992-2003.
240. Hosokawa, N., et al., *Nutrient-dependent mTORC1 association with the ULK1-Atg13-FIP200 complex required for autophagy*. Mol Biol Cell, 2009. **20**(7): p. 1981-91.
241. Shioi, T. and Y. Inuzuka, *Aging as a substrate of heart failure*. J Cardiol, 2012. **60**(6): p. 423-8.
242. Shih, H., et al., *The aging heart and post-infarction left ventricular remodeling*. J Am Coll Cardiol, 2011. **57**(1): p. 9-17.
243. Despres, J.P., *Body fat distribution and risk of cardiovascular disease: an update*. Circulation, 2012. **126**(10): p. 1301-13.
244. Lehnart, S.E., *Understanding the physiology of heart failure through cellular and in vivo models-towards targeting of complex mechanisms*. Exp Physiol, 2013. **98**(3): p. 622-8.
245. Doenst, T., T.D. Nguyen, and E.D. Abel, *Cardiac metabolism in heart failure: implications beyond ATP production*. Circ Res, 2013. **113**(6): p. 709-24.
246. Lavandero, S., et al., *Cardiovascular autophagy: concepts, controversies, and perspectives*. Autophagy, 2013. **9**(10): p. 1455-66.
247. McCormick, J., et al., *Autophagy in the stress-induced myocardium*. Front Biosci (Elite Ed), 2012. **4**: p. 2131-41.
248. Dutta, D., et al., *Contribution of impaired mitochondrial autophagy to cardiac aging: mechanisms and therapeutic opportunities*. Circ Res, 2012. **110**(8): p. 1125-38.
249. De Meyer, G.R., G.W. De Keulenaer, and W. Martinet, *Role of autophagy in heart failure associated with aging*. Heart Fail Rev, 2010. **15**(5): p. 423-30.
250. Pan, W., et al., *MiR-30-regulated autophagy mediates angiotensin II-induced myocardial hypertrophy*. PLoS One, 2013. **8**(1): p. e53950.

251. Georgescu, S.P., et al., *Decreased metalloprotease 9 induction, cardiac fibrosis, and higher autophagy after pressure overload in mice lacking the transcriptional regulator p8*. *Am J Physiol Cell Physiol*, 2011. **301**(5): p. C1046-56.
252. Nakai, A., et al., *The role of autophagy in cardiomyocytes in the basal state and in response to hemodynamic stress*. *Nat Med*, 2007. **13**(5): p. 619-24.
253. Hariharan, N., et al., *Autophagy plays an essential role in mediating regression of hypertrophy during unloading of the heart*. *PLoS One*, 2013. **8**(1): p. e51632.
254. Oyabu, J., et al., *Autophagy-mediated degradation is necessary for regression of cardiac hypertrophy during ventricular unloading*. *Biochem Biophys Res Commun*, 2013. **441**(4): p. 787-92.
255. Taneike, M., et al., *Inhibition of autophagy in the heart induces age-related cardiomyopathy*. *Autophagy*, 2010. **6**(5): p. 600-6.
256. Liu, Y., et al., *Total and high molecular weight but not trimeric or hexameric forms of adiponectin correlate with markers of the metabolic syndrome and liver injury in Thai subjects*. *J Clin Endocrinol Metab*, 2007. **92**(11): p. 4313-8.
257. Park, M. and G. Sweeney, *Direct effects of adipokines on the heart: focus on adiponectin*. *Heart Fail Rev*, 2013. **18**(5): p. 631-44.
258. Boddu, N.J., et al., *Is the lack of adiponectin associated with increased ER/SR stress and inflammation in the heart?* *Adipocyte*, 2014. **3**(1): p. 10-8.
259. Hu, P., et al., *Minimally invasive aortic banding in mice: effects of altered cardiomyocyte insulin signaling during pressure overload*. *Am J Physiol Heart Circ Physiol*, 2003. **285**(3): p. H1261-9.
260. Symons, J.D., et al., *Knockout of insulin receptors in cardiomyocytes attenuates coronary arterial dysfunction induced by pressure overload*. *Am J Physiol Heart Circ Physiol*, 2011. **300**(1): p. H374-81.
261. Eguchi, M., et al., *Ischemia-reperfusion injury leads to distinct temporal cardiac remodeling in normal versus diabetic mice*. *PLoS One*, 2012. **7**(2): p. e30450.
262. Eguchi, M., et al., *Diabetes influences cardiac extracellular matrix remodelling after myocardial infarction and subsequent development of cardiac dysfunction*. *J Cell Mol Med*, 2012. **16**(12): p. 2925-34.
263. Shen, D., et al., *Novel cell- and tissue-based assays for detecting misfolded and aggregated protein accumulation within aggregates and inclusion bodies*. *Cell Biochem Biophys*, 2011. **60**(3): p. 173-85.
264. Liu, Y., et al., *Adiponectin corrects high-fat diet-induced disturbances in muscle metabolomic profile and whole-body glucose homeostasis*. *Diabetes*, 2013. **62**(3): p. 743-52.
265. Kimura, N., et al., *Expression of autophagy-associated genes in skeletal muscle: an experimental model of chloroquine-induced myopathy*. *Pathobiology*, 2007. **74**(3): p. 169-76.
266. Liao, Y., et al., *Exacerbation of heart failure in adiponectin-deficient mice due to impaired regulation of AMPK and glucose metabolism*. *Cardiovasc Res*, 2005. **67**(4): p. 705-13.
267. Kanamori, H., et al., *The role of autophagy emerging in postinfarction cardiac remodelling*. *Cardiovasc Res*, 2011. **91**(2): p. 330-9.
268. Billia, F., et al., *PTEN-inducible kinase 1 (PINK1)/Park6 is indispensable for normal heart function*. *Proc Natl Acad Sci U S A*, 2011. **108**(23): p. 9572-7.

269. Bugger, H. and E.D. Abel, *Mitochondria in the diabetic heart*. Cardiovasc Res, 2010. **88**(2): p. 229-40.
270. Mihaylova, M.M. and R.J. Shaw, *The AMPK signalling pathway coordinates cell growth, autophagy and metabolism*. Nat Cell Biol, 2011. **13**(9): p. 1016-23.
271. Yamauchi, T. and T. Kadowaki, *Physiological and pathophysiological roles of adiponectin and adiponectin receptors in the integrated regulation of metabolic and cardiovascular diseases*. Int J Obes (Lond), 2008. **32 Suppl 7**: p. S13-8.
272. Okada, K., et al., *Prolonged endoplasmic reticulum stress in hypertrophic and failing heart after aortic constriction: possible contribution of endoplasmic reticulum stress to cardiac myocyte apoptosis*. Circulation, 2004. **110**(6): p. 705-12.
273. Kouroku, Y., et al., *ER stress (PERK/eIF2alpha phosphorylation) mediates the polyglutamine-induced LC3 conversion, an essential step for autophagy formation*. Cell Death Differ, 2007. **14**(2): p. 230-9.
274. Benjamin, E.J., et al., *Heart Disease and Stroke Statistics-2018 Update: A Report From the American Heart Association*. Circulation, 2018. **137**(12): p. e67-e492.
275. Heusch, G., et al., *Cardiovascular remodelling in coronary artery disease and heart failure*. Lancet, 2014. **383**(9932): p. 1933-43.
276. Jahng, J.W., E. Song, and G. Sweeney, *Crosstalk between the heart and peripheral organs in heart failure*. Exp Mol Med, 2016. **48**: p. e217.
277. Kumada, M., et al., *Association of hypoadiponectinemia with coronary artery disease in men*. Arterioscler Thromb Vasc Biol, 2003. **23**(1): p. 85-9.
278. Frystyk, J., et al., *Serum adiponectin is a predictor of coronary heart disease: a population-based 10-year follow-up study in elderly men*. J Clin Endocrinol Metab, 2007. **92**(2): p. 571-6.
279. Becker, B., et al., *Renal insulin resistance syndrome, adiponectin and cardiovascular events in patients with kidney disease: the mild and moderate kidney disease study*. J Am Soc Nephrol, 2005. **16**(4): p. 1091-8.
280. Matsushita, K., et al., *Comparison of circulating adiponectin and proinflammatory markers regarding their association with metabolic syndrome in Japanese men*. Arterioscler Thromb Vasc Biol, 2006. **26**(4): p. 871-6.
281. Schulze, M.B., et al., *Adiponectin and future coronary heart disease events among men with type 2 diabetes*. Diabetes, 2005. **54**(2): p. 534-9.
282. Ding, G., et al., *Adiponectin and its receptors are expressed in adult ventricular cardiomyocytes and upregulated by activation of peroxisome proliferator-activated receptor gamma*. J Mol Cell Cardiol, 2007. **43**(1): p. 73-84.
283. Hardie, D.G., *AMP-activated/SNF1 protein kinases: conserved guardians of cellular energy*. Nat Rev Mol Cell Biol, 2007. **8**(10): p. 774-85.
284. Nishida, K., et al., *The role of autophagy in the heart*. Cell Death Differ, 2009. **16**(1): p. 31-8.
285. Yan, L., et al., *Autophagy in chronically ischemic myocardium*. Proc Natl Acad Sci U S A, 2005. **102**(39): p. 13807-12.
286. Rothermel, B.A. and J.A. Hill, *Myocyte autophagy in heart disease: friend or foe?* Autophagy, 2007. **3**(6): p. 632-4.
287. Kanamori, H., et al., *Autophagy limits acute myocardial infarction induced by permanent coronary artery occlusion*. Am J Physiol Heart Circ Physiol, 2011. **300**(6): p. H2261-71.

288. Sciarretta, S., et al., *Trehalose-Induced Activation of Autophagy Improves Cardiac Remodeling After Myocardial Infarction*. J Am Coll Cardiol, 2018. **71**(18): p. 1999-2010.
289. Hamacher-Brady, A., N.R. Brady, and R.A. Gottlieb, *Enhancing macroautophagy protects against ischemia/reperfusion injury in cardiac myocytes*. J Biol Chem, 2006. **281**(40): p. 29776-87.
290. Zhu, H., et al., *Cardiac autophagy is a maladaptive response to hemodynamic stress*. J Clin Invest, 2007. **117**(7): p. 1782-93.
291. Matsui, Y., et al., *Distinct roles of autophagy in the heart during ischemia and reperfusion: roles of AMP-activated protein kinase and Beclin 1 in mediating autophagy*. Circ Res, 2007. **100**(6): p. 914-22.
292. Lu, L., et al., *Adriamycin-induced autophagic cardiomyocyte death plays a pathogenic role in a rat model of heart failure*. Int J Cardiol, 2009. **134**(1): p. 82-90.
293. Wang, Y., et al., *Restoring diabetes-induced autophagic flux arrest in ischemic/reperfused heart by ADIPOR (adiponectin receptor) activation involves both AMPK-dependent and AMPK-independent signaling*. Autophagy, 2017. **13**(11): p. 1855-1869.
294. Sung, H.K., et al., *Iron induces insulin resistance in cardiomyocytes via regulation of oxidative stress*. Sci Rep, 2019. **9**(1): p. 4668.
295. Havranek, F., *[Which stage of the menstrual cycle is best suited for the insertion of IUD?]*. Cesk Gynekol, 1978. **43**(6): p. 447.
296. Vasquez, K.O. and J.D. Peterson, *Early Detection of Acute Drug-Induced Liver Injury in Mice by Noninvasive Near-Infrared Fluorescence Imaging*. J Pharmacol Exp Ther, 2017. **361**(1): p. 87-98.
297. Palanivel, R., et al., *Globular and full-length forms of adiponectin mediate specific changes in glucose and fatty acid uptake and metabolism in cardiomyocytes*. Cardiovasc Res, 2007. **75**(1): p. 148-57.
298. Song, E., et al., *Holo-lipocalin-2-derived siderophores increase mitochondrial ROS and impair oxidative phosphorylation in rat cardiomyocytes*. Proc Natl Acad Sci U S A, 2018. **115**(7): p. 1576-1581.
299. Chan, Y.K., et al., *Lipocalin-2 inhibits autophagy and induces insulin resistance in H9c2 cells*. Mol Cell Endocrinol, 2016. **430**: p. 68-76.
300. Shibata, R., et al., *Adiponectin accumulates in myocardial tissue that has been damaged by ischemia-reperfusion injury via leakage from the vascular compartment*. Cardiovasc Res, 2007. **74**(3): p. 471-9.
301. Lutgens, E., et al., *Chronic myocardial infarction in the mouse: cardiac structural and functional changes*. Cardiovasc Res, 1999. **41**(3): p. 586-93.
302. Yang, F., et al., *Myocardial infarction and cardiac remodelling in mice*. Exp Physiol, 2002. **87**(5): p. 547-55.
303. Sung, H.K., et al., *Lipocalin-2 (NGAL) Attenuates Autophagy to Exacerbate Cardiac Apoptosis Induced by Myocardial Ischemia*. J Cell Physiol, 2017. **232**(8): p. 2125-2134.
304. Ma, X., et al., *Impaired autophagosome clearance contributes to cardiomyocyte death in ischemia/reperfusion injury*. Circulation, 2012. **125**(25): p. 3170-81.
305. Liu, Y. and B. Levine, *Autosis and autophagic cell death: the dark side of autophagy*. Cell Death Differ, 2015. **22**(3): p. 367-76.
306. Levine, B. and J. Yuan, *Autophagy in cell death: an innocent convict?* J Clin Invest, 2005. **115**(10): p. 2679-88.

307. Essick, E.E., et al., *Adiponectin modulates oxidative stress-induced autophagy in cardiomyocytes*. PLoS One, 2013. **8**(7): p. e68697.
308. Rose, R.A., et al., *Iron overload decreases CaV1.3-dependent L-type Ca<sup>2+</sup> currents leading to bradycardia, altered electrical conduction, and atrial fibrillation*. Circ Arrhythm Electrophysiol, 2011. **4**(5): p. 733-42.
309. Das, S.K., et al., *Iron-overload injury and cardiomyopathy in acquired and genetic models is attenuated by resveratrol therapy*. Sci Rep, 2015. **5**: p. 18132.
310. Borgna-Pignatti, C., et al., *Survival and complications in patients with thalassemia major treated with transfusion and deferoxamine*. Haematologica, 2004. **89**(10): p. 1187-93.
311. Murphy, M.P., *How mitochondria produce reactive oxygen species*. Biochem J, 2009. **417**(1): p. 1-13.
312. Okada-Iwabu, M., et al., *A small-molecule AdipoR agonist for type 2 diabetes and short life in obesity*. Nature, 2013. **503**(7477): p. 493-9.

## Appendix A: Copyright Permission

### OXFORD UNIVERSITY PRESS LICENSE TERMS AND CONDITIONS

Feb 15, 2020

---

This Agreement between York University -- James Won Suk Jahng ("You") and Oxford University Press ("Oxford University Press") consists of your license details and the terms and conditions provided by Oxford University Press and Copyright Clearance Center.

License Number 4744471093860

License date Jan 08, 2020

Licensed content publisher Oxford University Press

Licensed content publication Journal of Molecular Cell Biology

Licensed content title Adiponectin, the past two decades

Licensed content author Wang, Zhao V.; Scherer, Philipp E.

Licensed content date Mar 30, 2016

Type of Use Thesis/Dissertation

Institution name

Title of your work EXAMINING MECHANISMS AND FUNCTIONAL SIGNIFICANCE OF ADIPONECTIN STIMULATED AUTOPHAGY IN CARDIOMETABOLIC DISEASES

## REVIEW

# Crosstalk between the heart and peripheral organs in heart failure

James Won Suk Jahng, Erfei Song and Gary Sweeney

Mediators from peripheral tissues can influence the development and progression of heart failure (HF). For example, in obesity, an altered profile of adipokines secreted from adipose tissue increases the incidence of myocardial infarction (MI). Less appreciated is that heart remodeling releases cardiokines, which can strongly impact various peripheral tissues. Inflammation, and, in particular, activation of the nucleotide-binding oligomerization domain-like receptors with pyrin domain (NLRP3) inflammasome are likely to have a central role in cardiac remodeling and mediating crosstalk with other organs. Activation of the NLRP3 inflammasome in response to cardiac injury induces the production and secretion of the inflammatory cytokines interleukin (IL)-1 $\beta$  and IL-18. In addition to having local effects in the myocardium, these pro-inflammatory cytokines are released into circulation and cause remodeling in the spleen, kidney, skeletal muscle and adipose tissue. The collective effects of various cardiokines on peripheral organs depend on the degree and duration of myocardial injury, with systematic inflammation and peripheral tissue damage observed as HF progresses. In this article, we review mechanisms regulating myocardial inflammation in HF and the role of factors secreted by the heart in communication with peripheral tissues.

*Experimental & Molecular Medicine* (2016) 48, e217; doi:10.1038/emm.2016.20; published online 11 March 2016

## INTRODUCTION

### Heart failure and the role of inflammation

Cardiovascular diseases are the leading cause of death worldwide, and heart failure (HF) is an important contributor to this statistic.<sup>1</sup> When the heart is under stress or injured, it undergoes structural and functional changes termed cardiac remodeling.<sup>2</sup> These include cardiac hypertrophy, fibrosis, apoptosis and altered metabolism.<sup>3</sup> When an individual suffers from myocardial ischemia, it is intuitively important to re-perfuse the damaged area and re-establish the supply of blood to the damaged area. However, it has also been realized that some cellular events which occur during reperfusion may lead to worse outcomes, a phenomenon termed myocardial ischemia/reperfusion (I/R) injury.<sup>4</sup>

The various mechanisms underlying the detrimental effects of ischemia and subsequent reperfusion are complex and are not fully understood. Nevertheless, a number of clinical and animal studies suggest that inflammation is a key contributor to adverse myocardial remodeling.<sup>4</sup> Broadly speaking, inflammation is a wound-healing process mediated by innate immune cells that recognize microbial and non-microbial sources of danger/stress. Inflammation triggered in the absence of infection is termed 'sterile inflammation'. Multiple studies have highlighted the importance of targeting sterile

inflammation in HF.<sup>5-7</sup> Sterile inflammation involves the secretion of inflammatory cytokines and recruitment of innate immune cells, such as neutrophils and monocytes/macrophages. However, prolonged exposure to inflammatory cytokines will exacerbate adverse remodeling and enhance myocardial damage.<sup>8</sup> Importantly, in addition to local adverse effects on cardiac remodeling, ischemia- or I/R-induced inflammation in the heart releases pro-inflammatory cytokines, such as interleukin (IL)-1 $\beta$  and IL-18, into circulation. These, and other so-called cardiokines, can have significant endocrine effects on other tissues, leading to damage in multiple peripheral organs.<sup>9</sup> For example, prolonged exposure to IL-1 $\beta$  and IL-18 can lead to caspase-1-dependent cell death via pyroptosis.<sup>10,11</sup> Thus, crosstalk from the heart to other tissues can dictate multi-organ damage as a consequence of ischemia-induced inflammation.<sup>9</sup> This review highlights the current knowledge of inflammasome activation in the heart and its consequences on other organs.

### Mechanisms regulating cardiac inflammation in HF, focus on the NLRP3 inflammasome

The nucleotide-binding oligomerization domain-like receptors with pyrin domain (NLRP3) inflammasome is a cytoplasmic protein complex composed of NLRP, apoptosis-associated

Department of Biology, York University, Toronto, ON, Canada  
Correspondence: Dr G Sweeney, Department of Biology, York University, Toronto, ON, Canada M3J 1P3.  
E-mail: gsweeney@yorku.ca  
Received 20 November 2015; revised 10 December 2015; accepted 11 December 2015

speck-like protein containing CARD (ASC), a caspase recruitment domain and pro-caspase-1.<sup>12,13</sup> NLRP is composed of C-terminal leucine-rich repeats, a central nucleotide domain (NACHT) and N-terminal effector pyrin domain. Upon recognizing patterns, either from a pathogenic source (pathogen-associated molecular patterns) or from a non-pathogenic source (danger/damage-associated molecular patterns, DAMPs), NLRP will recruit ASC, which, in turn, recruits pro-caspase 1, which will then get activated.<sup>14</sup> Inflammasomes are classified based on NLRPs, which recognize or sense different stimuli.<sup>15</sup> The NLRP3 inflammasome is the most widely studied to date due to its ability to recognize various cellular stressors and its strong relationship with diseases such as HF.<sup>16</sup> The key consequence of inflammasome activation is maturation of pro-inflammatory cytokines, in particular IL-1 $\beta$  and IL-18. The generation of active forms of IL-1 $\beta$  and IL-18 is regulated at two steps: expression of pro-IL-1 $\beta$  and pro-IL-18 is mediated by nuclear factor kappa-light chain enhancer of activated B cells (NF- $\kappa$ B), and processing to the mature form of IL-1 $\beta$  and IL-18 is mediated by active caspase-1 in the inflammasome.<sup>14</sup>

Multiple DAMPs have been found to activate NLRP3 inflammasomes, including monosodium urate, calcium phosphate crystals, cholesterol crystals, amyloid  $\beta$ , hyaluronan, islet amyloid polypeptide, asbestos and silica.<sup>14</sup> However, in

HF, we suggest that mitochondria have a critical role in initiating inflammasome activation.<sup>17,18</sup> In HF-associated inflammasome activation, the three main triggers are adenosine triphosphate (ATP), mitochondrial DNA (mtDNA), and reactive oxygen species (ROS) (see Figure 1). When cells undergo death they release ATP. Multiple studies have suggested that ATP directly activates the NLRP3 inflammasome.<sup>19,20</sup> High extracellular ATP levels activate P2X<sub>7</sub> purinergic receptors to cause potassium efflux. Low intracellular levels of potassium promote the assembly of NLRP3 and ASC. In addition, it has been suggested that low intracellular potassium will also promote pannexin-1 membrane pore formation, further easing the access of inflammasome activating agents.<sup>21</sup> mtDNA has been established as a DAMP when liberated into the extracellular space.<sup>22,23</sup> It was shown<sup>24</sup> that the translocation of mtDNA to the cytosol was associated with subsequent inflammasome activation. A DNase treatment reduced secretion of IL-1 $\beta$  in macrophages. It has also been reported<sup>25</sup> that mitochondrial dysfunction and oxidized mtDNA directly activate the NLRP3 inflammasome. Macrophages lacking mtDNA or treated with the oxidized nucleoside 8-OH-dG to confer competitive inhibition had severely attenuated IL-1 $\beta$  secretion. Mitochondrial marker and NLRP3 inflammasome colocalization and a significant activation of NLRP3

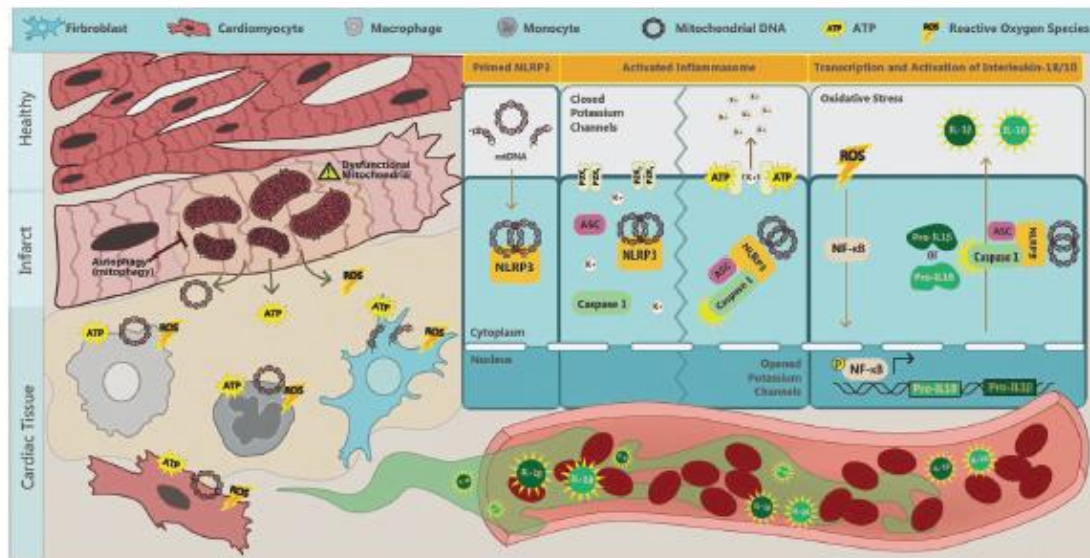


**Figure 1** Mechanisms of NLRP3 inflammasome activation in heart failure. Myocardial infarction (MI), ischemia or ischemia/reperfusion (I/R) injury induces cardiomyocytes to release ROS, ATP and mtDNA. ROS mediates autocrine and paracrine activation and nuclear translocation of NF- $\kappa$ B, which regulates the transcription of pro-IL-1 $\beta$  and pro-IL-18. mtDNA directly primes NLRP3 and ATP via binding to P2X<sub>7</sub> receptors and leads to potassium efflux, a trigger for the assembly of NLRP3 inflammasome. These collective effects result in activation of the NLRP3 inflammasome-associated caspase-1, which processes pro-IL-1 $\beta$  and pro-IL-18 into mature IL-1 $\beta$  and IL-18 and can exacerbate local inflammation. It can also be released into circulation to mediate endocrine effects. ATP, adenosine triphosphate; mtDNA, mitochondrial DNA; NF- $\kappa$ B, nuclear factor kappa-light-chain-enhancer of activated B cells; NLRP3, NLR family, pyrin domain containing 3; ROS, reactive oxygen species; K<sup>+</sup>, potassium.

inflammasome upon mitochondrial membrane disruption have been shown.<sup>26</sup> It was reported<sup>27</sup> that activation of the NLRP3 inflammasome in macrophages occurred due to an ATP-mediated ROS-dependent activation of phosphoinositide 3 kinase signaling. ROS stimulates the activation of NF- $\kappa$ B and increases the expression of pro-IL-1 $\beta$  and pro-IL-18.<sup>21</sup>

#### Mitochondrial regulation by autophagy in the heart

Because all the mediators discussed above (ATP, mtDNA and ROS) may come from mitochondria, our hypothesis is that this organelle has a vital role in inflammasome activation. Thus, mitochondrial integrity is a key limiting factor for NLRP3 inflammasome activation. Furthermore, this may be especially relevant in the heart where cardiomyocytes have a higher mitochondrial content relative to other cell types. Overall, the heart is likely to be highly susceptible to mitochondria-derived DAMPs. Thus, effective regulation of damaged mitochondria is critical. Autophagy is a quality control system mediating degradation of protein aggregates and damaged organelles. Multiple studies have documented the importance of mitochondrial regulation by autophagy, specifically referred to as mitophagy, in HF.<sup>28</sup> Multiple studies have also now established a strong association between autophagy and inflammasome activation. First, stimulating autophagy in macrophages using rapamycin can directly target precursors of IL-1 $\beta$  for degradation. Mice pretreated with rapamycin showed reduced circulating levels of IL-1 $\beta$  following a challenge with an inflammatory stimulus.<sup>29</sup> Using ATG16L1-deficient cells, it was shown that autophagy was involved in endotoxin (lipopolysaccharide)-induced inflammasome activation and increased IL-1 $\beta$  and IL-18 secretion.<sup>30</sup> Another study<sup>31</sup> reported that inflammasomes can be directly sequestered into autophagosomes and destined for autophagic degradation. Nakahira *et al*<sup>24</sup> reported on the regulation of mtDNA-driven inflammasome activation by autophagy. They deleted genes encoding key autophagy proteins LC3B and Beclin1, and found a significant enhancement in caspase-1 activation and secretion of IL-1 $\beta$  and IL-18. Thus, defective autophagy-mediated quality control mechanisms resulted in enhanced inflammasome activation via the accumulation of damaged mitochondria and reduced inflammasome clearance in both *in vitro* and *in vivo* settings.

#### Distinct roles of cardiomyocytes, fibroblasts and immune cells in cardiac inflammasome activation

Numerous studies have now established a strong association between inflammasome activation and adverse remodeling in HF. For example, both ASC-KO and caspase-1-KO mice exhibited a significant reduction in infarct zone and fibrosis, as well as improved cardiac function after myocardial I/R injury.<sup>32</sup> As highlighted in Figure 1, it has been proposed that activation of the inflammasome occurs via cell-to-cell communication within heterogeneous cell populations of heart tissue, including cardiomyocytes, fibroblasts and innate immune cells.<sup>6,33</sup> Kawaguchi *et al*<sup>32</sup> identified that both hematopoietic and non-hematopoietic cells are responsible

for secreting IL-1 $\beta$  after myocardial I/R injury, because only chimeric mice with ASC-KO bone marrow on an ASC-KO background showed reduction in infarct zone. They followed up with *in vitro* experiments in which hypoxia/reoxygenation stimulated inflammasome activation in cardiac fibroblasts, but not in cardiomyocytes. This notion was supported by studies in adult cardiomyocytes in which NLRP3 inflammasome activation was inhibited using either siRNA or pharmacological inhibitors. This resulted in fewer cell deaths but not IL-1 $\beta$  secretion.<sup>34</sup> Upon permanent myocardial ischemia in both murine and rat models, myocardial fibroblasts were shown to be the primary source of IL-1 $\beta$  secretion in response to ATP released from damaged neighboring cells.<sup>35</sup> Further work<sup>36</sup> has also supported the notion of non-immune cell-mediated IL-1 $\beta$  and IL-18 secretion. This work concluded that mitochondrial ROS from cardiomyocytes acts as a trigger to prime the NLRP3 inflammasome. Taken together, the data suggest that cardiomyocytes, cardiac fibroblasts and infiltrating immune cells contribute via different roles toward inflammation and cardiac remodeling in myocardial infarction (MI) (Figure 1).

#### CROSSTALK BETWEEN THE HEART AND ADIPOSE TISSUE

##### Alterations in adipokine profiles influence the development of HF

There is a well-documented association between obesity and HF.<sup>2</sup> Adipose tissue is clearly an important contributor to inflammation in HF. Multiple studies have established both pro- and anti-inflammatory effects of adipokines.<sup>37,38</sup> In obesity, adipose tissue undergoes changes induced by metabolic stress. It releases more pro-inflammatory cytokines, including IL-6, IL-8, monocyte chemoattractant protein-1 (MCP-1), and less of the anti-inflammatory cytokines, including IL-10 and adiponectin.<sup>39-41</sup> Visceral fat is the most important depot, which responds to metabolic stress in this way. There is a well-established positive correlation between visceral fat levels and HF.<sup>42</sup> However, it is interesting to note that epicardial and pericardial fat depots exhibit a similar phenotype to visceral fat and have been strongly correlated with the progression of adverse cardiac remodeling.<sup>43</sup> McKenney *et al*<sup>44</sup> observed increased epicardial adipose tissue after MIs, which correlated with a reduced adiponectin level after MI. In their study they compared pigs with or without adipoectomy subjected to MI. They observed that the progression of adverse remodeling after the MI was attenuated, and the infarct zone size was diminished in adipoctomized animals. This correlates with a previous observation in which a pig with myocardial I/R injury developed improved cardiac function, reduced infarct size and less tumor necrosis factor alpha (TNF $\alpha$ ) production with a greater production of IL-10 after intracoronary administration of adiponectin.<sup>45</sup> In summary, whereas it is generally accepted that in obesity, the profile of adipokines from various fat depots mediates detrimental effects on the myocardium, the obesity paradox suggests that these adipokines can confer beneficial effects during post-MI stages of remodeling.<sup>2</sup>

Extensive epidemiological and clinical data suggest that type 2 diabetes increases the risk for HF independently of other risk factors, such as hypertension.<sup>46,47</sup> One potential mechanism is that type 2 diabetes, often associated with obesity, leads to myocardial lipotoxicity that contributes to cell death, and thus, to cardiac dysfunction. Diabetic cardiomyopathy is also characterized by interstitial and perivascular fibrosis. A significant increase in collagen deposition was found around intramural vessels and between myofibers in heart biopsies in patients with diabetes.<sup>48-50</sup> Given that fibrosis is one consequence of inflammation, IL-1 $\beta$  and other inflammatory markers, such as fibrosis, signal the onset and progression of HF in this way.<sup>51-54</sup>

#### Cardiokine and endocrine effects on peripheral tissues in HF

In recent years, there has been an increased realization of endocrine effects mediated by factors produced and secreted by the heart.<sup>55</sup> Collectively, these are referred to as cardiokines. Ischemic stress results in a substantial change in the profile of cardiokines secreted from the myocardium.<sup>9,55</sup> In particular, upon activation of the inflammasome and infiltration of splenocytes in the infarct zone, the heart will release more pro-inflammatory cytokines.<sup>9</sup> Cardiac fibroblasts have been proposed as the principal source of inflammatory signals in pathological conditions, although cardiomyocytes also contribute to the pro-inflammatory environment in the myocardium by producing different cytokines and chemokines.<sup>56,57</sup> Injured cardiac cells release damage-associated molecular pattern molecules, such as high-mobility group box 1, DNA fragments, heat-shock proteins and matricellular proteins, which instruct surrounding healthy cardiomyocytes to produce inflammatory mediators. These mediators, mainly IL-1 $\beta$ , IL-18, IL-6, MCP-1 and TNF $\alpha$ , in turn activate versatile signaling networks within surviving cardiomyocytes and trigger leukocyte activation and recruitment.

Evidence for myocardial production of TNF $\alpha$  has been controversial.<sup>58,59</sup> However, it is now clear that TNF $\alpha$  can be produced by isolated cardiomyocytes under certain conditions, such as treatment with lipopolysaccharide.<sup>60-63</sup> Similarly, increased expression of TNF $\alpha$  in cardiac myocytes and fibroblasts isolated from failing hearts suggests that if exposed to pathophysiological stimuli, the heart has the capacity to produce TNF $\alpha$ .<sup>64,65</sup> IL-6 can be produced in most cells in the heart, including cardiomyocytes<sup>66,67</sup> and fibroblasts.<sup>68,69</sup> A lipopolysaccharide treatment or hypoxia-reoxygenation stimulated the production of IL-1 $\beta$  in isolated cardiac fibroblasts, while isolated cardiomyocytes did not respond to either treatment.<sup>32</sup> A co-culture of cardiomyocytes with fibroblasts induced by an angiotensin-II treatment secreted much greater levels of IL-6 and TNF $\alpha$  than cultures of fibroblasts alone, indicating that a paracrine action has a vital role in the production of pro-inflammatory cytokines.<sup>70</sup>

Another good example of a cardiokine is atrial natriuretic peptide (ANP), which is produced mainly in the myocardium. Its expression is enhanced during myocardial stretching.<sup>71</sup> ANP

has a beneficial role in cardiac remodeling by acting in an autocrine or paracrine manner. For example, treatment with cultured cardiac myocytes with an antagonist of ANP receptor HS-142-1 increased expression of contractile protein genes, such as skeletal-actin and beta-myosin heavy chain, as well as the size of cardiomyocytes.<sup>72</sup> ANP also contributes to oxytocin-induced protection in myocardial ischemia-reperfusion injury by reducing lipid peroxidation in a nitric oxide-dependent mechanism.<sup>73</sup>

ANP receptors are found in adipose tissue and mediate effects, including enhanced lipolysis and energy expenditure, as well as altering adipokine production and release.<sup>74-76</sup> Thus, natriuretic peptides can definitely influence peripheral metabolism by acting on adipose tissue. Therapeutically targeting ANP action may confer metabolic and cardiovascular benefits in the future.<sup>74</sup>

#### CROSSTALK BETWEEN THE HEART AND SPLEEN: THE CARDIO-SPLENIC AXIS

Neutrophil activation and leukocyte infiltration in the heart are prominent features of MIs that exacerbate inflammatory cytokine release and tissue damage.<sup>77</sup> Indeed, the mononuclear phagocyte network undergoes extensive remodeling after MI. There are different subpopulations of monocytes residing in mice. These are converted from one to another upon inflammatory responses after an MI. Monocytes are generally classified into two categories: migratory monocytes with inflammatory characteristics, which express high levels of Ly6C and CC chemokine receptor CCR2 and low levels of fractalkine receptor CX3CR1 (Ly-6C<sup>hi</sup>, CCR2<sup>hi</sup>, CX3CR1<sup>low</sup>), and reparative monocytes with anti-inflammatory profiles (Ly-6C<sup>low</sup>, CCR2<sup>low</sup>, CX3CR1<sup>high</sup>).<sup>78</sup> The exact mechanism of how each phenotype of monocytes regulates the inflammatory response during an MI is complicated and is not resolved.<sup>79</sup> However, under acute MI conditions, monocyte recruitment to the heart is very dynamic and largely dependent on the spleen. The spleen is one of most important lymphoid tissues. It has a role in filtering blood and regulating immune responses to circulating agents.<sup>80</sup> The spleen contains large pools of undifferentiated monocyte reservoirs<sup>80,81</sup> that can undergo splenic hematopoiesis, increasing motility and pro-inflammatory characteristics (Ly-6C<sup>hi</sup>).<sup>81</sup> Recruitment of reparative monocytes (Ly-6C<sup>low</sup>) ultimately helps resolve inflammation and promote tissue healing.<sup>81,82</sup>

Dendritic cells (DCs), specialized for presenting antigens to T cells, also have an important role in the immune response to an MI.<sup>83</sup> In an acute MI, both DCs and monocytes/macrophages have been shown to positively contribute to tissue healing. Upon an initial cardiac inflammatory response, DCs infiltrate the infarcted area to confer a protective role. This is demonstrated with DC-ablated mice exhibiting greater adverse cardiac remodeling after an MI.<sup>84</sup> In these mice, there was sustained expression of pro-inflammatory cytokines, IL-1 $\beta$ , IL-18 and TNF $\alpha$ , yet reduced IL-10 expression.<sup>84</sup>

Interestingly, under chronic MI conditions, the protective roles of splenocytes become detrimental. Mice with a long-term

MI (8 weeks) showed profound splenic remodeling with a prolonged existence of pro-inflammatory monocytes (Ly-6C<sup>hi</sup>) and increased expression of alarmins.<sup>85</sup> A splenectomy was performed to investigate the role of splenocytes (splenic monocytes/macrophages and DCs) in the progression of HF-associated inflammation and post-MI remodeling. Intriguingly, mice without spleens showed less cardiac dysfunction. This was associated with attenuated monocytes/DC infiltration in the heart.<sup>85</sup> When splenocytes from the mice with an MI were injected into normal mice, the recipient mice developed left ventricle (LV) dilation, cardiac hypertrophy, systolic dysfunction, myocardial apoptosis and fibrosis.<sup>85</sup> However, the recipient mice did not reveal changes in pro-inflammatory cytokines in circulation, indicating that the adverse cardiac remodeling in chronic MI model was specifically due to splenocytes. Therefore, there is a clear sequential activation of inflammatory responses depending on the duration of MI via splenocyte-mediated crosstalk to the heart (Figure 2).

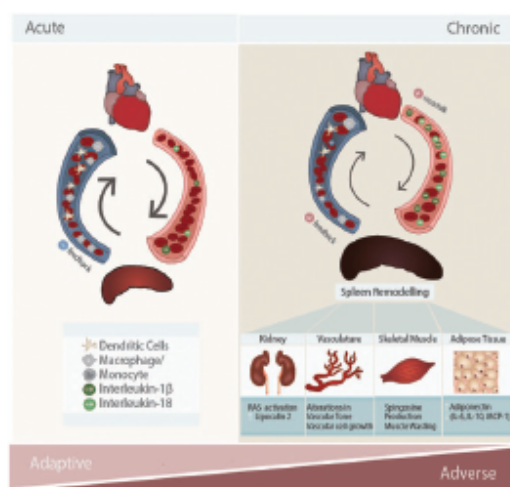


**Figure 2** Crosstalk mechanisms in the cardio-splenic axis in heart failure, and their functional consequences on peripheral tissues. In acute myocardial infarction (MI), splenocytes (splenic monocytes/macrophages and dendritic cells) migrate to the heart and mediate protective effects during the inflammatory response. In chronic MI, cardiokines induce dramatic changes in the spleen, such that splenocytes develop inflammatory profiles. This exacerbates existing inflammation in the heart and promotes adverse cardiac remodeling leading to cardiac dysfunction. Inflammatory splenocytes also lead to peripheral organ damage. For example, kidney inflammation results in enhanced activation of the renin-angiotensin system (RAS) and release of lipocalin-2. In vasculature, inflammation results in adverse alterations in vascular tone and vascular cell proliferation. Skeletal muscle is also strongly affected by heart failure, at least in part via inflammation resulting in cellular changes, such as sphingosine accumulation and muscle wasting. In adipose tissue, inflammation results in reduced adiponectin levels and further increased levels of pro-inflammatory adipokines (IL-6, MCP-1, IL-10, IL, interleukin; MCP-1, monocyte chemoattractant protein 1).

### CROSTALK BETWEEN THE HEART AND KIDNEY: CARDIO-RENAL AXIS

Multiple clinical studies have suggested that patients with chronic kidney disease experience extremely high mortality rates following acute MI.<sup>86-89</sup> This suggests that there is a strong crosstalk between the kidneys and heart. The association between end-stage renal disease and cardiovascular disease is often termed cardio-renal syndrome.<sup>90</sup> The renin-angiotensin system (RAS), a signaling cascade responsible for regulating blood pressure, has a well-established critical role in cardio-renal syndrome.<sup>91</sup> Ogawa *et al*<sup>92</sup> reported that nephrectomy in mice with an MI influenced cardiac remodeling after the MI. The combination of nephrectomy and MI resulted in deteriorated left ventricular remodeling and RAS activation, oxidative stress and MCP-1. This observation was similar to transgenic mice overexpressing renin and angiotensinogen after a coronary artery ligation (CAL) surgery.<sup>92</sup> This correlates with previous findings that cardiomyocytes increase the expression of TNF $\alpha$  and IL-1 family through activation of NF- $\kappa$ B and activator protein 1 transcription factor in response to angiotensin II.<sup>93-95</sup>

Other than RAS, a new biomarker has been identified that strongly correlated with cardio-renal syndrome. HF patients with declined renal function exhibit elevated levels of neutrophil gelatinase-associated lipocalin (also known as lipocalin-2)<sup>96</sup>. Neutrophil gelatinase-associated lipocalin levels are strongly correlated with inflammation and cardiac remodeling in HF patients with renal dysfunction.<sup>96</sup> Pro-inflammatory effects of lipocalin-2 are also known to induce endothelial dysfunction<sup>97,98</sup> and promote apoptosis in cardiomyocytes.<sup>99,100</sup>

In addition, cardiokines, such as ANP, can mediate endocrine effects on the kidney.<sup>101</sup> They have effects on electrolyte balance and water excretion in the kidney by increasing glomerular permeability and filtration rate. ANP also antagonizes the deleterious effects of the renin-angiotensin-aldosterone system activation.<sup>101-103</sup> Furthermore, crosstalk between the heart and kidney are evident from the observation that worsening renal function manifests only in end-stage HF and is strongly related to mortality.<sup>104</sup> Although cardio-renal interactions in HF are well established, many questions, especially mechanistic, remain unanswered.

### CROSTALK BETWEEN THE HEART AND SKELETAL MUSCLE

We now appreciate that HF is strongly associated with skeletal muscle wasting, which is typically not associated with general weight loss.<sup>105,106</sup> Skeletal muscle in congestive HF patients shows increased fatigability as well as decreased endurance and exercise capacity.<sup>105,106</sup> Changes evident in muscle include metabolic imbalance, increased degradation of myofibrils and myocyte apoptosis. The signals mediating crosstalk from the heart need to be comprehensively identified.<sup>107,108</sup> One possibility is that generation of TNF $\alpha$  from the failing heart has a detrimental effect on several processes in skeletal muscle. NF- $\kappa$ B is rapidly activated by TNF $\alpha$  in differentiated skeletal

muscle cells, which directly induces skeletal muscle protein loss.<sup>109</sup> Another proposed mechanism is that TNF $\alpha$  induces sphingosine production, which then leads to induction of apoptosis in these cells.<sup>110</sup> In addition, exercise attenuates the local expression of TNF $\alpha$ , IL-1 $\beta$  and inducible Nitric Oxide Synthase (iNOS) in skeletal muscle and decreases the catabolic wasting process in HF patients.<sup>34,111,112</sup> Angiotensin-II is also produced by the heart under conditions of stress and contributes to cardiac hypertrophy and fibrosis.<sup>113</sup> Studies have shown that there is a catabolic effect of angiotensin-II on skeletal muscle, suggesting its role in muscle wasting in HF.<sup>114,115</sup>

### THERAPEUTIC APPROACHES TARGETING INFLAMMATION IN HF

As outlined above, myocardial inflammation in HF is often detrimental to peripheral tissues. There have been several studies addressing consequences of manipulating HF-associated inflammation.<sup>116</sup> Targeting TNF $\alpha$  has been extensively studied in numerous clinical trials. Patients who already have severe inflammatory conditions, such as rheumatoid arthritis (RA), were treated with TNF $\alpha$  inhibitors (etanercept, infliximab and adalimumab), which effectively reduced the inflammatory activity and reduced the prevalence of HF complications.<sup>117</sup>

The data from two-large-scale trials with more than 2000 HF patients showed that etanercept treatment reduced the risk of mortality or morbidity in HF.<sup>64</sup> Indeed, the US Food and Drug Administration has issued a directive concerning the use of etanercept in the population with HF.<sup>118</sup> However, targeting TNF $\alpha$  using a neutralizing antibody (infliximab) showed no improvement and perhaps even worsened the clinical condition of patients with chronic HF.<sup>119</sup> Other studies indicated that patients treated with high-dose infliximab continued to show a worse outcome compared with other groups.<sup>5,7,120</sup> Several other agents have also been suggested to have potential as therapeutic tools for chronic HF because of their inhibitory effect on TNF $\alpha$ , including the glutamic acid derivative thalidomide.<sup>121</sup> Thalidomide prevents the accumulation of TNF $\alpha$  by inducing the degradation of TNF $\alpha$  messenger ribonucleic acid transcripts, and thus, protein production.<sup>121</sup> The xanthine derivative pentoxifylline has also been reported to have a role in therapeutic TNF $\alpha$  modulation. Reduced TNF $\alpha$  in the serum of patients treated with pentoxifylline was observed. This correlated with improved peripheral vasodilation and blood hemodynamics.<sup>122</sup> Other studies demonstrated a significant improvement in NYHA functional class in patients treated with pentoxifylline.<sup>123,124</sup> However, the results were not reproduced by another group,<sup>125</sup> suggesting that the significance of

**Table 1** Cytokines/chemokines involved in crosstalk between the heart and peripheral organs

Cytokines/Chemokines	Effect	Reference
IL-1 $\beta$ , IL-18 <sup>9,32-35</sup>	Neutrophil activation and leukocyte infiltration [@Spleen] increasing mobility and inflammatory characteristics of monocytes, and infiltration of DCs to heart [@Heart] autocrine production of IL-6, TNF $\alpha$ Prolonged exposure led to pyroptosis	77 78,80-82 71 148,149
IL-6, IL-8, MCP-1 <sup>60,67-69</sup>	Pro-inflammatory cytokines	60,67-69
DAMPs, HMGB1, DNA fragments, heat shock proteins, matricellular protein <sup>9,55-57</sup>	[@Heart] autocrine effects to produce pro-inflammatory cytokines; IL-1 $\beta$ , IL-18, IL-6, MCP-1, TNF $\alpha$	56,57
TNF $\alpha$ <sup>8,59</sup>	Prolonged exposure led to pyroptosis [@Skeletal Muscle] muscle wasting, sphingosine production, induction of apoptosis	64,65 109,110
ANP <sup>71</sup>	Paracrine effect: oxytocin production, reducing lipid peroxidation with NO-dependent mechanism [@Heart] autocrine effect on heart by increasing expression of contractile protein, actin and myosin, and induce hypertrophy [@Adipose Tissue] enhancing lipolysis and increasing energy expenditure, adipokines production [@Kidney] increasing glomerular permeability and filtration rate, antagonizing RAS activation	73 72 75,76,150 101-103
IL-6, IL-8, MCP-1 <sup>37,38</sup>	Pro-inflammatory cytokines	39-41
IL-10 <sup>37,38</sup>	Anti-inflammatory cytokines	39-41
Adiponectin <sup>37,38</sup>	[@Heart] reducing TNF $\alpha$ production, increasing IL-10 production, reducing infarct size	45,55
Alamins <sup>85</sup>	[@Heart] worsening cardiac dysfunction, inducing myocardial apoptosis, fibrosis	85
Angiotensin-II <sup>91</sup>	[@Heart] inducing cardiac hypertrophy/fibrosis, increasing expression of TNF $\alpha$ , IL-1 family cytokines [@Skeletal Muscle] muscle wasting	70,93,94,113 114,115
Lipocalin-2 <sup>95</sup>	endothelial dysfunction, cardiomyocyte apoptosis	97-100

Abbreviations: ANP, atrial natriuretic peptide; DAMPs, danger/damage-associated molecular patterns; DCs, dendritic cells; HMGB1, high-mobility group box 1; IL, interleukin; MCP-1, monocytes chemoattractant protein-1; NO, nitric oxide; TNF $\alpha$ , tumor necrosis factor alpha.

targeting TNF $\alpha$  is controversial and requires further exploration.<sup>126</sup> This may be because pleiotropic TNF $\alpha$  effects may be involved in many beneficial physiologic, as well as pathologic, processes. For example, TNF $\alpha$  provides endogenous cyto-protective signals that prevent cardiomyocyte apoptosis following ischemic injury.<sup>127</sup> Additionally, TNF type 1 receptor deficiency was associated with accelerated myocardial death.<sup>128</sup> Overall, the cardiomodulatory effects of TNF $\alpha$  and other cytokines likely depend on factors such as cell type and timing and extent of inhibition.

We propose that IL-1 $\beta$  is a major mediator between HF and peripheral tissues. In fact, multiple studies have targeted IL-1 $\beta$ . Canakinumab, a neutralizing antibody against IL-1 $\beta$ , and anakinra, a recombinant IL-1 receptor antagonist, were shown to exert beneficial effects on acute MI in animal models.<sup>129,130</sup> Several clinical trials identified therapeutic benefits by blocking IL-1 $\beta$ .<sup>131,132</sup> Anakinra successfully reduced adverse remodeling in patients with an MI and reduced the level of C-reactive protein, a common biomarker used to determine the severity of inflammation.<sup>133,134</sup> Patients diagnosed with HF were treated with Anakinra and subjected to exercise performance testing. Two weeks of the Anakinra treatment significantly increased oxygen consumption, decreased carbon dioxide retention and exercise performance with significant reduction in IL-1 $\beta$ , C-reactive protein and IL-6 serum profiles.<sup>135</sup> These correlated with a previous study in which patients with RA treated with Anakinra had improved cardiac function. A single injection of Anakinra resulted in increased blood flow in 3 h.<sup>136</sup> The commercial usage of Anakinra was approved by Food and Drug Administration in 2001. However, it was for treating patients with RA not chronic HF, although multiple studies demonstrated cardiac benefits of Anakinra in treating RA.<sup>137–139</sup>

There also have been therapeutic efforts to target IL-18 and inflammasome activation. A recombinant human IL-18 binding protein and neutralizing antibody for IL-18 have been developed, and initial clinical trials to treat patients with RAs are ongoing.<sup>140,141</sup> In subjects with moderate to severe RA, IL-18 binding protein shows a favorable safety profile and is well tolerated in healthy volunteers. Because IL-18 binding protein stays in circulation much longer than any other inhibitors previously described, it has attracted a lot of attention.<sup>141,142</sup> Antagonists targeting P2X<sub>7</sub> receptors have also been tested to potentially block inflammasome activation. Many successful cases have been shown; they limit neuronal damage and lung, liver and kidney injury in several animal models.<sup>143–146</sup> Currently, the safety and efficacy of P2X<sub>7</sub> receptor antagonists are being investigated and have progressed to phase 2 clinical trials. However, their main use is to target inflammatory bowel disease, RA and chronic obstructive airway disease.<sup>147</sup>

#### CONCLUDING REMARKS

Myocardial ischemia- and I/R-induced inflammation involve NLRP3 inflammasome activation. One principal trigger for inflammasome activation is the recognition of mitochondrial

DAMPs. This results in the production and secretion of pro-inflammatory cytokines, including IL-1 $\beta$  and IL-18 (Table 1). These and other factors produced by the heart during inflammation can have local effects. They can also crosstalk with other peripheral tissues via endocrine effects. For example, HF is associated with dramatic changes in the spleen, skeletal muscle wasting, alterations in adipose metabolism and kidney function. The extent and significance of bidirectional crosstalk between the heart and other organs may have been underappreciated, but is now becoming more established and may represent a logical focus of therapeutic interventions in the future.

#### CONFLICT OF INTEREST

The authors declare no conflict of interest.

#### ACKNOWLEDGEMENTS

Related research in the author's laboratory is funded by the Canadian Diabetes Association, the Heart & Stroke Foundation of Canada and the Canadian Institutes of Health Research. We thank Lesia Szyca for the excellent graphic illustration of Figures 1 and 2.

- 1 Nabel EG, Braunwald E. A tale of coronary artery disease and myocardial infarction. *N Engl J Med* 2012; **366**: 54–63.
- 2 Abel ED, Litwin SE, Sweeney G. Cardiac remodeling in obesity. *Physiol Rev* 2008; **88**: 389–419.
- 3 Heusch G, Libby P, Gersh B, Yellon D, Bohm M, Lopaschuk G et al. Cardiovascular remodelling in coronary artery disease and heart failure. *Lancet* 2014; **383**: 1933–1943.
- 4 Mozaffari MS, Liu JY, Abebe W, Baban B. Mechanisms of load dependency of myocardial ischemia reperfusion injury. *Am J Cardiovasc Dis* 2013; **3**: 180–196.
- 5 Chen GY, Nunez G. Sterile inflammation: sensing and reacting to damage. *Nat Rev Immunol* 2010; **10**: 826–837.
- 6 Nakayama H, Otsu K. Translation of hemodynamic stress to sterile inflammation in the heart. *Trends Endocrinol Metab* 2013; **24**: 546–553.
- 7 Takahashi M. NLRP3 inflammasome as a novel player in myocardial infarction. *Int Heart J* 2014; **55**: 101–105.
- 8 Marchant DJ, Boyd JH, Lin DC, Granville DJ, Garmaroudi FS, McManus BM. Inflammation in myocardial diseases. *Circ Res* 2012; **110**: 126–144.
- 9 Doroudgar S, Glembocki CC. The cardiokine story unfolds: ischemic stress-induced protein secretion in the heart. *Trends Mol Med* 2011; **17**: 207–214.
- 10 Zheng Y, Gardner SE, Clarke MC. Cell death, damage-associated molecular patterns, and sterile inflammation in cardiovascular disease. *Arterioscler Thromb Vasc Biol* 2011; **31**: 2781–2786.
- 11 Bergsbaken T, Fink SL, Cookson BT. Pyroptosis: host cell death and inflammation. *Nat Rev Microbiol* 2009; **7**: 99–109.
- 12 Lu A, Wu H. Structural mechanisms of inflammasome assembly. *FEBS J* 2015; **282**: 435–444.
- 13 Lechtenberg BC, Mace PD, Riedl SJ. Structural mechanisms in NLR inflammasome signaling. *Curr Opin Struct Biol* 2014; **29**: 17–25.
- 14 Latz E, Xiao TS, Stutz A. Activation and regulation of the inflammasomes. *Nat Rev Immunol* 2013; **13**: 397–411.
- 15 de Zoete MR, Palm NW, Zhu S, Flavell RA. Inflammasomes. *Cold Spring Harb Perspect Biol* 2014; **6**: a016287.
- 16 Abderazak A, Syrovets T, Couchie D, El Hadri K, Friguet B, Simmet T et al. NLRP3 inflammasome: from a danger signal sensor to a regulatory node of oxidative stress and inflammatory diseases. *Redox Biol* 2015; **4**: 296–307.
- 17 Rosca MG, Tandler B, Hoppel CL. Mitochondria in cardiac hypertrophy and heart failure. *J Mol Cell Cardiol* 2013; **55**: 31–41.

- 18 Hollander JM, Thapa D, Shepherd DL. Physiological and structural differences in spatially distinct subpopulations of cardiac mitochondria: influence of cardiac pathologies. *Am J Physiol Heart Circ Physiol* 2014; **307**: H1–H14.
- 19 Franchi L, Eigenbrod T, Nunez G. Cutting edge: TNF- $\alpha$  mediates sensitization to ATP and silica via the NLRP3 inflammasome in the absence of microbial stimulation. *J Immunol* 2009; **183**: 792–796.
- 20 Bauernfeind FG, Horvath G, Stutz A, Alnemri ES, MacDonald K, Speert D et al. Cutting edge: NF- $\kappa$ B activating pattern recognition and cytokine receptors license NLRP3 inflammasome activation by regulating NLRP3 expression. *J Immunol* 2009; **183**: 787–791.
- 21 Kanneganti TD, Lamkanfi M, Kim YG, Chen G, Park JH, Franchi L et al. Pannexin-1-mediated recognition of bacterial molecules activates the cytosolic inflammasome independent of Toll-like receptor signaling. *Immunity* 2007; **26**: 433–443.
- 22 Zhou R, Tardivel A, Thorens B, Choi I, Tschopp J. Thioredoxin-interacting protein links oxidative stress to inflammasome activation. *Nat Immunol* 2010; **11**: 136–140.
- 23 Zhang Q, Raouf M, Chen Y, Sumi Y, Sursal T, Junger W et al. Circulating mitochondrial DAMPs cause inflammatory responses to injury. *Nature* 2010; **464**: 104–107.
- 24 Nakahira K, Haspel JA, Rathinam VA, Lee SJ, Dolinsky T, Lam HC et al. Autophagy proteins regulate innate immune responses by inhibiting the release of mitochondrial DNA mediated by the NALP3 inflammasome. *Nat Immunol* 2011; **12**: 222–230.
- 25 Shimada K, Crother TR, Karlin J, Daggedoij J, Chiba N, Chen S et al. Oxidized mitochondrial DNA activates the NLRP3 inflammasome during apoptosis. *Immunity* 2012; **36**: 401–414.
- 26 Zhou R, Yazdi AS, Menu P, Tschopp J. A role for mitochondria in NLRP3 inflammasome activation. *Nature* 2011; **469**: 221–225.
- 27 Cruz CM, Rinna A, Forman HJ, Ventura AL, Persechini PM, Ojcius DM. ATP activates a reactive oxygen species-dependent oxidative stress response and secretion of proinflammatory cytokines in macrophages. *J Biol Chem* 2007; **282**: 2871–2879.
- 28 Shires SE, Gustafsson AB. Mitophagy and heart failure. *J Mol Med (Berl)* 2015; **93**: 253–262.
- 29 Harris J, Hartman M, Roche C, Zeng SG, O’Shea A, Sharp FA et al. Autophagy controls IL-1 $\beta$  secretion by targeting pro-IL-1 $\beta$  for degradation. *J Biol Chem* 2011; **286**: 9587–9597.
- 30 Saitoh T, Fujita N, Jiang MH, Uematsu S, Yang BG, Satoh T et al. Loss of the autophagy protein Atg16L1 enhances endotoxin-induced IL-1 $\beta$  production. *Nature* 2008; **456**: 264–268.
- 31 Shi CS, Shenderov K, Huang NN, Kabat J, Abu-Asab M, Fitzgerald KA et al. Activation of autophagy by inflammatory signals limits IL-1 $\beta$  production by targeting ubiquitinated inflammasomes for destruction. *Nat Immunol* 2012; **13**: 255–263.
- 32 Kawaguchi M, Takahashi M, Hata T, Kashima Y, Usui F, Morimoto H et al. Inflammasome activation of cardiac fibroblasts is essential for myocardial ischemia/reperfusion injury. *Circulation* 2011; **123**: 594–604.
- 33 Shinde AV, Frangogiannis NG. Fibroblasts in myocardial infarction: a role in inflammation and repair. *J Mol Cell Cardiol* 2014; **70**: 74–82.
- 34 Mezzaroma E, Toldo S, Farkas D, Seropian IM, Van Tassell BW, Salloum FN et al. The inflammasome promotes adverse cardiac remodeling following acute myocardial infarction in the mouse. *Proc Natl Acad Sci USA* 2011; **108**: 19725–19730.
- 35 Sandanger O, Ranheim T, Vinje LE, Bliksoen M, Alfsnes K, Finsen AV et al. The NLRP3 inflammasome is up-regulated in cardiac fibroblasts and mediates myocardial ischaemia-reperfusion injury. *Cardiovasc Res* 2013; **99**: 164–174.
- 36 Bracey NA, Geshkovich B, Chun J, Vilaysane A, Meljndert HC, Wright JR Jr. et al. Mitochondrial NLRP3 protein induces reactive oxygen species to promote Smad protein signaling and fibrosis independent from the inflammasome. *J Biol Chem* 2014; **289**: 19571–19584.
- 37 Park M, Sweeney G. Direct effects of adipokines on the heart: focus on adiponectin. *Heart Fail Rev* 2013; **18**: 631–644.
- 38 Turer AT, Hill JA, Elmquist JK, Scherer PE. Adipose tissue biology and cardiomyopathy: translational implications. *Circ Res* 2012; **111**: 1565–1577.
- 39 Romacho T, Elsen M, Rohrborn D, Eckel J. Adipose tissue and its role in organ crosstalk. *Acta Physiol (Oxf)* 2014; **210**: 733–753.
- 40 Rutkowski JM, Stern JH, Scherer PE. The cell biology of fat expansion. *J Cell Biol* 2015; **208**: 501–512.
- 41 Sun K, Kusminski CM, Scherer PE. Adipose tissue remodeling and obesity. *J Clin Invest* 2011; **121**: 2094–2101.
- 42 Amato MC, Giordano C. Visceral adiposity index: an indicator of adipose tissue dysfunction. *Int J Endocrinol* 2014; **2014**: 730827.
- 43 Britton KA, Fox CS. Ectopic fat depots and cardiovascular disease. *Circulation* 2011; **124**: e837–e841.
- 44 McKeeney ML, Schultz KA, Boyd JH, Byrd JP, Alloosh M, Teague SD et al. Epicardial adipose excision slows the progression of porcine coronary atherosclerosis. *J Cardiothorac Surg* 2014; **9**: 2.
- 45 Kondo K, Shibata R, Unno K, Shimano M, Ishii M, Kito T et al. Impact of a single intracoronary administration of adiponectin on myocardial ischemia/reperfusion injury in a pig model. *Circ Cardiovasc Interv* 2010; **3**: 166–173.
- 46 Boudina S, Abel ED. Diabetic cardiomyopathy, causes and effects. *Rev Endocr Metab Disord* 2010; **11**: 31–39.
- 47 Wilson PW. Diabetes mellitus and coronary heart disease. *Am J Kidney Dis* 1998; **32**(5 Suppl 3): S89–S100.
- 48 Boudina S, Sena S, Theobald H, Sheng X, Wright JJ, Hu XX et al. Mitochondrial energetics in the heart in obesity-related diabetes: direct evidence for increased uncoupled respiration and activation of uncoupling proteins. *Diabetes* 2007; **56**: 2457–2466.
- 49 Regan TJ, Lyons MM, Ahmed SS, Levinson GE, Oldewurtel HA, Ahmad MR et al. Evidence for cardiomyopathy in familial diabetes mellitus. *J Clin Invest* 1977; **60**: 884–899.
- 50 Shimizu M, Umeda K, Sugihara N, Yoshio H, Ino H, Takeda R et al. Collagen remodeling in myocardia of patients with diabetes. *J Clin Path* 1993; **46**: 32–36.
- 51 Maedler K, Dhamadhikari G, Schumann DM, Storz J. Interleukin-1 $\beta$  targeted therapy for type 2 diabetes. *Expert Opin Biol Ther* 2009; **9**: 1177–1188.
- 52 Bujak M, Frangogiannis NG. The role of IL-1 in the pathogenesis of heart disease. *Arch Immunol Ther Exp (Warsz)* 2009; **57**: 165–176.
- 53 Mori MA, Bezy O, Kahn CR. Metabolic syndrome: is Nlrp3 inflammasome a trigger or a target of insulin resistance? *Circ Res* 2011; **108**: 1160–1162.
- 54 Fuentes-Antras J, Ioan AM, Tunon J, Egido J, Lorenzo O. Activation of toll-like receptors and inflammasome complexes in the diabetic cardiomyopathy-associated inflammation. *Int J Endocrinol Metab* 2014; **2014**: 847827.
- 55 Shimano M, Ouchi N, Walsh K. Cardiokines: recent progress in elucidating the cardiac secretome. *Circulation* 2012; **126**: e327–e332.
- 56 Aoyagi T, Matsui T. The cardiomyocyte as a source of cytokines in cardiac injury. *J Cell Sci Ther* 2011; **2012**: 003.
- 57 Pugh PJ, Jones RD, Jones TH, Channer KS. Heart failure as an inflammatory condition: potential role for androgens as immune modulators. *Eur J Heart Fail* 2002; **4**: 673–680.
- 58 Espel E, Garcia-Sanz JA, Aubert V, Menoud V, Sperisen P, Fernandez N et al. Transcriptional and translational control of TNF- $\alpha$  gene expression in human monocytes by major histocompatibility complex class II ligands. *Eur J Immunol* 1995; **26**: 2417–2424.
- 59 Trede NS, Geha RS, Chatila T. Transcriptional activation of IL-1 $\beta$  and tumor necrosis factor- $\alpha$  genes by MHC class II ligands. *J Immunol* 1991; **146**: 2310–2315.
- 60 Alefi G, Zetoune FS, Herron TJ, Jalife J, Bosmann M, Al-Aref R et al. Complement dependency of cardiomyocyte release of mediators during sepsis. *FASEB J* 2011; **25**: 2500–2508.
- 61 Song X, Kusakari Y, Xiao C-Y, Kinsella SD, Rosenberg MA, Scherer-Cosbly M et al. mTOR attenuates the inflammatory response in cardiomyocytes and prevents cardiac dysfunction in pathological hypertrophy. *Am J Physiol Cell Physiol* 2010; **299**: C1256–C1266.
- 62 Comstock KL, Krown KA, Page MT, Martin D, Ho P, Pedraza M et al. LPS-induced TNF- $\alpha$  release from and apoptosis in rat cardiomyocytes: obligatory role for CD14 in mediating the LPS response. *J Mol Cell Cardiol* 1998; **30**: 2761–2775.
- 63 Kapadia S, Torre-Amione G, Yokoyama T, Mann DL. Soluble TNF binding proteins modulate the negative inotropic properties of TNF- $\alpha$  in vitro. *Am J Physiol* 1995; **268**(2 Pt 2): H517–H525.
- 64 Coletta AP, Clark AL, Banerjee P, Cleland JG. Clinical trials update: RENEWAL (RENAISSANCE and RECOVER) and ATTACH. *Eur J Heart Fail* 2002; **4**: 559–561.
- 65 Yokoyama T, Sekiguchi K, Tanaka T, Tomaru K, Arai M, Suzuki T et al. Angiotensin II and mechanical stretch induce production of tumor

- necrosis factor in cardiac fibroblasts. *Am J Physiol* 1999; **276**(6 Pt 2): H1968-H1976.
- 66 Atefi G, Zetoune FS, Herron TJ, Jalife J, Bosmann M, Al-Aref R et al. Complement dependency of cardiomyocyte release of mediators during sepsis. *Faseb J* 2011; **25**: 2500-2508.
- 67 Yamauchi-Takahara K, Ihara Y, Ogata A, Yoshizaki K, Azuma J, Kishimoto T. Hypoxic stress induces cardiac myocyte-derived interleukin-6. *Circulation* 1995; **91**: 1520-1524.
- 68 Fredj S, Bescond J, Louault C, Potreau D. Interactions between cardiac cells enhance cardiomyocyte hypertrophy and increase fibroblast proliferation. *J Cell Physiol* 2005; **202**: 891-899.
- 69 Shiota T, Matsumori A, Kihara Y, Inoko M, Ono K, Iwanaga Y et al. Increased expression of interleukin-1 beta and monocyte chemoattractant and activating factor/monocyte chemoattractant protein-1 in the hypertrophied and failing heart with pressure overload. *Circ Res* 1997; **81**: 664-671.
- 70 Sarkar S, Velaichamy E, Young D, Sen S. Influence of cytokines and growth factors in ANG II-mediated collagen upregulation by fibroblasts in rats: role of myocytes. *Am J Physiol Heart Circ Physiol* 2004; **287**: H107-H117.
- 71 Koller KJ, Goeddel DV. Molecular biology of the natriuretic peptides and their receptors. *Circulation* 1992; **86**: 1081-1088.
- 72 Horio T, Nishikimi T, Yoshihara F, Matsuo H, Takishita S, Kangawa K. Inhibitory regulation of hypertrophy by endogenous atrial natriuretic peptide in cultured cardiac myocytes. *Hypertension* 2000; **35**: 19-24.
- 73 Houshmand F, Faghihi M, Zehediast S. Role of atrial natriuretic peptide in oxytocin induced cardioprotection. *Heart Lung Circ* 2015; **24**: 86-93.
- 74 Gruden G, Landi A, Bruno G. Natriuretic peptides, heart, and adipose tissue: new findings and future developments for diabetes research. *Diabetes Care* 2014; **37**: 2899-2908.
- 75 Szabo T, Postrach E, Mahler A, Kung T, Turhan G, von Haehling S et al. Increased catabolic activity in adipose tissue of patients with chronic heart failure. *Eur J Heart Fail* 2013; **15**: 1131-1137.
- 76 Fenzl M, Schnitzer W, Aebli N, Schlegel C, Villiger B, Disch A et al. Release of ANP and fat oxidation in overweight persons during aerobic exercise in water. *Int J Sports Med* 2013; **34**: 795-799.
- 77 Bujak M, Dobaczewski M, Chatila K, Mendoza LH, Li N, Reddy A et al. Interleukin-1 receptor type 1 signaling critically regulates infarct healing and cardiac remodeling. *Am J Pathol* 2008; **173**: 57-67.
- 78 Si Y, Tsou CL, Croft K, Charo IF. CCR2 mediates hematopoietic stem and progenitor cell trafficking to sites of inflammation in mice. *J Clin Invest* 2010; **120**: 1192-1203.
- 79 Frangogiannis NG. Regulation of the inflammatory response in cardiac repair. *Circ Res* 2012; **110**: 159-173.
- 80 Cesta MF. Normal structure, function, and histology of the spleen. *Toxicol Pathol* 2006; **34**: 455-465.
- 81 Swirski FK, Nahrendorf M, Eitzrodt M, Wildgruber M, Cortez-Retamozo V, Panizzi P et al. Identification of splenic reservoir monocytes and their deployment to inflammatory sites. *Science* 2009; **325**: 612-616.
- 82 Nahrendorf M, Pittet MJ, Swirski FK. Monocytes: protagonists of infarct inflammation and repair after myocardial infarction. *Circulation* 2010; **121**: 2437-2445.
- 83 Mahrike K, Schmitt E, Bonifaz L, Enk AH, Jonuleit H. Immature, but not inactive: the tolerogenic function of immature dendritic cells. *Immunol Cell Biol* 2002; **80**: 477-483.
- 84 Anzai A, Anzai T, Nagai S, Maekawa Y, Naito K, Kaneko H et al. Regulatory role of dendritic cells in postinfarction healing and left ventricular remodeling. *Circulation* 2012; **125**: 1234-1245.
- 85 Ismail MA, Hamid T, Bansal SS, Patel B, Kingey JR, Prabhu SD. Remodeling of the mononuclear phagocyte network underlies chronic inflammation and disease progression in heart failure: critical importance of the cardiosplenic axis. *Circ Res* 2014; **114**: 266-282.
- 86 Smolina K, Wright FL, Rayner M, Goldacre MJ. Determinants of the decline in mortality from acute myocardial infarction in England between 2002 and 2010: linked national database study. *BMJ* 2012; **344**: d8059.
- 87 Tonelli M, Munther P, Lloyd A, Manns BJ, Klarenbach S, Pannu N et al. Risk of coronary events in people with chronic kidney disease compared with those with diabetes: a population-level cohort study. *Lancet* 2012; **380**: 807-814.
- 88 Anavekar NS, McMurray JJ, Velazquez EJ, Solomon SD, Kober L, Rouleau JL et al. Relation between renal dysfunction and cardiovascular outcomes after myocardial infarction. *N Engl J Med* 2004; **351**: 1285-1295.
- 89 Szummer K, Lundman P, Jacobson SH, Schon S, Lindback J, Stenestrand U et al. Influence of renal function on the effects of early revascularization in non-ST-elevation myocardial infarction: data from the Swedish Web-System for Enhancement and Development of Evidence-Based Care in Heart Disease Evaluated According to Recommended Therapies (SWEDEHEART). *Circulation* 2009; **120**: 851-858.
- 90 Go AS, Chertow GM, Fan D, McCulloch CE, Hsu CY. Chronic kidney disease and the risks of death, cardiovascular events, and hospitalization. *N Engl J Med* 2004; **351**: 1296-1305.
- 91 Bock JS, Gottlieb SS. Cardiorenal syndrome: new perspectives. *Circulation* 2010; **121**: 2592-2600.
- 92 Ogawa M, Suzuki J, Takayama K, Senbonmatsu T, Hirata Y, Nagai R et al. Impaired post-infarction cardiac remodeling in chronic kidney disease is due to excessive renin release. *Lab Invest* 2012; **92**: 1766-1776.
- 93 Ruiz-Ortega M, Ruperez M, Lorenzo O, Esteban V, Blanco J, Mezzano S et al. Angiotensin II regulates the synthesis of proinflammatory cytokines and chemokines in the kidney. *Kidney Int Suppl* 2002; **82**: S12-S22.
- 94 Kalra D, Sivasubramanian N, Mann DL. Angiotensin II induces tumor necrosis factor biosynthesis in the adult mammalian heart through a protein kinase C-dependent pathway. *Circulation* 2002; **105**: 2198-2205.
- 95 Moriyama T, Fujibayashi M, Fujiwara Y, Kaneko T, Xia C, Imai E et al. Angiotensin II stimulates interleukin-6 release from cultured mouse mesangial cells. *J Am Soc Nephrol* 1995; **6**: 95-101.
- 96 Siasos G, Tousoulis D, Michalek S, Oikonomou E, Vavuranakis M, Athanasiou D et al. Novel biomarkers assessing renal function in heart failure: relation to inflammatory status and cardiac remodeling. *Curr Med Chem* 2014; **21**: 3976-3983.
- 97 Song E, Fan P, Huang B, Deng HB, Cheung BM, Feletoiu M et al. Deamidated lipocalin-2 induces endothelial dysfunction and hypertension in dietary obese mice. *J Am Heart Assoc* 2014; **3**: e000837.
- 98 Liu JT, Song E, Xu A, Berger T, Mak TW, Tse HF et al. Lipocalin-2 deficiency prevents endothelial dysfunction associated with dietary obesity: role of cytochrome P450 2C inhibition. *Br J Pharmacol* 2012; **165**: 520-531.
- 99 Xu G, Ahn J, Chang S, Eguchi M, Ogler A, Han S et al. Lipocalin-2 induces cardiomyocyte apoptosis by increasing intracellular iron accumulation. *J Biol Chem* 2012; **287**: 4808-4817.
- 100 Sung H, Choi JY, Lee SA, Lee KM, Han S, Jeon S et al. The association between the preoperative serum levels of lipocalin-2 and matrix metalloproteinase-9 (MMP-9) and prognosis of breast cancer. *BMC Cancer* 2012; **12**: 193.
- 101 Theilig F, Wu Q. ANP-induced signaling cascade and its implications in renal pathophysiology. *Am J Physiol Renal Physiol* 2015; **308**: F1047-F1055.
- 102 O'Tierney PF, Komolova M, Tse MY, Adams MA, Pang SC. Altered regulation of renal interstitial hydrostatic pressure and the renal renin-angiotensin system in the absence of atrial natriuretic peptide. *J Hypertens* 2008; **26**: 303-311.
- 103 Abu-Amara I, Balment RJ. Vascular, renal, and endocrine responses to low-dose atrial natriuretic peptide in the fluid-balanced New Zealand genetically hypertensive rats with and without endogenous arginine vasopressin. *Can J Physiol Pharmacol* 1999; **77**: 102-110.
- 104 Damman K, Testani JM. The kidney in heart failure: an update. *Eur Heart J* 2015; **36**: 1437-1444.
- 105 Ebner N, Elsner S, Springer J, von Haehling S. Molecular mechanisms and treatment targets of muscle wasting and cachexia in heart failure: an overview. *Curr Opin Support Palliat Care* 2014; **8**: 15-24.
- 106 von Haehling S, Steinbeck L, Doehner W, Springer J, Anker SD. Muscle wasting in heart failure: an overview. *Int J Biochem Cell Biol* 2013; **45**: 2257-2265.
- 107 Mazzei E, Calvani R, Cesari M, Buford TW, Lorenzi M, Behrke BJ et al. Mitochondrial dysfunction and sarcopenia of aging: from signaling pathways to clinical trials. *Int J Biochem Cell Biol* 2013; **45**: 2288-2301.
- 108 Sakuma K, Aoi W, Yamaguchi A. Current understanding of sarcopenia: possible candidates modulating muscle mass. *PLoS Arch* 2015; **467**: 213-229.

- 109 Li YP, Schwartz RJ, Waddell ID, Holloway BR, Reid MB. Skeletal muscle myocytes undergo protein loss and reactive oxygen-mediated NF-kappaB activation in response to tumor necrosis factor alpha. *FASEB J* 1998; **12**: 871-880.
- 110 Dalla Libera L, Sabbadini R, Renken C, Ravara B, Sandri M, Betto R et al. Apoptosis in the skeletal muscle of rats with heart failure is associated with increased serum levels of TNF-alpha and sphingosine. *J Mol Cell Cardiol* 2001; **33**: 1871-1878.
- 111 Gielen S, Adams V, Mobius-Winkler S, Linke A, Erbs S, Yu J et al. Anti-inflammatory effects of exercise training in the skeletal muscle of patients with chronic heart failure. *J Am Coll Cardiol* 2003; **42**: 861-868.
- 112 Adams V, Spate U, Krankel N, Schulze PC, Linke A, Schuler G et al. Nuclear factor-kappa B activation in skeletal muscle of patients with chronic heart failure: correlation with the expression of inducible nitric oxide synthase. *Eur J Cardiovasc Prev Rehabil* 2003; **10**: 273-277.
- 113 Crowley SD, Gurley SB, Herrera MJ, Ruiz P, Griffiths R, Kumar AP et al. Angiotensin II causes hypertension and cardiac hypertrophy through its receptors in the kidney. *Proc Natl Acad Sci USA* 2006; **103**: 17985-17990.
- 114 Sukhanov S, Semprun-Prieto L, Yoshida T, Michael Tabony A, Higashi Y, Galvez S et al. Angiotensin II, oxidative stress and skeletal muscle wasting. *Am J Med Sci* 2011; **342**: 143-147.
- 115 Delafontaine P, Akao M. Angiotensin II as candidate of cardiac cachexia. *Curr Opin Clin Nutr Metab Care* 2006; **9**: 220-224.
- 116 Sarena A, Russo I, Frangogiannis NG. Inflammation as a therapeutic target in myocardial infarction: learning from past failures to meet future challenges. *Transl Res* 2016; **167**: 152-166.
- 117 Listing J, Strangfeld A, Kerkow J, Schneider M, Kapelle A, Wassenberg S et al. Does tumor necrosis factor alpha inhibition promote or prevent heart failure in patients with rheumatoid arthritis? *Arthritis Rheum* 2008; **58**: 667-677.
- 118 Behnam SM, Behnam SE, Koo JY. TNF-alpha inhibitors and congestive heart failure. *Skinmed* 2005; **4**: 363-368.
- 119 Chung ES, Packer M, Lo KH, Fasanmade AA, Willerson JT. Randomized, double-blind, placebo-controlled, pilot trial of infliximab, a chimeric monoclonal antibody to tumor necrosis factor-alpha, in patients with moderate-to-severe heart failure: results of the anti-TNF Therapy Against Congestive Heart Failure (ATTACH) trial. *Circulation* 2003; **107**: 3133-3140.
- 120 Pugh PJ, Jones TH, Channer KS. Acute haemodynamic effects of testosterone in men with chronic heart failure. *Eur Heart J* 2003; **24**: 909-915.
- 121 Moreira AL, Sampaio EP, Zmuidzinas A, Frindt P, Smith KA, Kaplan G. Thaldomide exerts its inhibitory action on tumor necrosis factor alpha by enhancing mRNA degradation. *J Exp Med* 1993; **177**: 1675-1680.
- 122 Schandené L, Vandenbussche P, Crusiaux A, Allègre ML, Absamowicz D, Dupont E et al. Differential effects of pentoxifylline on the production of tumor necrosis factor-alpha (TNF-alpha) and interleukin-6 (IL-6) by monocytes and T cells. *Immunology* 1992; **76**: 30-34.
- 123 Silwa K, Skudicky D, Candy G, Wisenbaugh T, Sarelli P. Randomised investigation of effects of pentoxifylline on left-ventricular performance in idiopathic dilated cardiomyopathy. *Lancet* 1998; **351**: 1091-1093.
- 124 Skudicky D, Silwa K, Begemann A, Candy G, Sarelli P. Reduction in Fas/ APO-1 plasma concentrations correlates with improvement in left ventricular function in patients with idiopathic dilated cardiomyopathy treated with pentoxifylline. *Heart* 2000; **84**: 438-441.
- 125 Bahrman P, Hengst UM, Rihartz BM, Figulla HR. Pentoxifylline in ischemic, hypertensive and idiopathic dilated cardiomyopathy: effects on left-ventricular function, inflammatory cytokines and symptoms. *Eur J Heart Fail* 2004; **6**: 195-201.
- 126 Fildes JE, Shaw SM, Yonan N, Williams SG. The immune system and chronic heart failure: is the heart in control? *J Am Coll Cardiol* 2009; **53**: 1013-1020.
- 127 Misa A, Haudek SB, Kneufelmann P, Vallejo JG, Chen ZJ, Michael LH et al. Nuclear factor-κB protects the adult cardiac myocyte against ischemia-induced apoptosis in a murine model of acute myocardial infarction. *Circulation* 2003; **108**: 3075-3078.
- 128 Monden Y, Kubota T, Inoue T, Tsutsumi T, Kawano S, Ide T et al. Tumor necrosis factor-α is toxic via receptor 1 and protective via receptor 2 in a murine model of myocardial infarction. *Am J Physiol Heart Circ Physiol* 2007; **293**: H743-H753.
- 129 Hwang MW, Mabumori A, Furukawa Y, Ono K, Okada M, Iwasaki A et al. Neutralization of interleukin-1beta in the acute phase of myocardial infarction promotes the progression of left ventricular remodeling. *J Am Coll Cardiol* 2001; **38**: 1546-1553.
- 130 Abbate A, Salloum FN, Vecile E, Das A, Hoke NN, Straino S et al. Anakinra, a recombinant human interleukin-1 receptor antagonist, inhibits apoptosis in experimental acute myocardial infarction. *Circulation* 2008; **117**: 2670-2683.
- 131 Dinarello CA, Simon A, van der Meer JW. Treating inflammation by blocking interleukin-1 in a broad spectrum of diseases. *Nat Rev Drug Discov* 2012; **11**: 633-652.
- 132 Dinarello CA, van der Meer JW. Treating inflammation by blocking interleukin-1 in humans. *Semin Immunol* 2013; **25**: 469-484.
- 133 Abbate A, Van Tassel BW, Blondi-Zoccali G, Kontos MC, Grizzard JD, Spillman DW et al. Effects of interleukin-1 blockade with anakinra on adverse cardiac remodeling and heart failure after acute myocardial infarction [from the Virginia Commonwealth University-Anakinra Remodeling Trial (2) (VCU-ART2) pilot study]. *Am J Cardiol* 2013; **111**: 1394-1400.
- 134 Abbate A, Van Tassel BW, Seropian IM, Toldo S, Robati R, Varma A et al. Interleukin-1beta modulation using a genetically engineered antibody prevents adverse cardiac remodeling following acute myocardial infarction in the mouse. *Eur J Heart Fail* 2010; **12**: 319-322.
- 135 Van Tassel BW, Arena RA, Toldo S, Mezzaroma E, Azam T, Seropian IM et al. Enhanced interleukin-1 activity contributes to exercise intolerance in patients with systolic heart failure. *PLoS ONE* 2012; **7**: e33438.
- 136 Ikonomidis I, Lekakis JP, Nikolaou M, Paraskevaidis I, Andreadou I, Kaplanoglou T et al. Inhibition of interleukin-1 by anakinra improves vascular and left ventricular function in patients with rheumatoid arthritis. *Circulation* 2008; **117**: 2662-2669.
- 137 Clark W, Jobanputra P, Barton P, Burls A. The clinical and cost-effectiveness of anakinra for the treatment of rheumatoid arthritis in adults: a systematic review and economic analysis. *Health Technol Assess* 2004; **8**: iii-iv, ix-x, 1-105.
- 138 Briesnhan B, Cobby M. Clinical and radiological effects of anakinra in patients with rheumatoid arthritis. *Rheumatology (Oxford)* 2003; **42** (Suppl 2): ii22-ii28.
- 139 Furst DE. Anakinra: review of recombinant human interleukin-1 receptor antagonist in the treatment of rheumatoid arthritis. *Clin Ther* 2004; **26**: 1960-1975.
- 140 Plater-Zyberk C, Joosten LA, Helsen MM, Sattoumet-Roche P, Sieghard C, Alouani S et al. Therapeutic effect of neutralizing endogenous IL-18 activity in the collagen-induced model of arthritis. *J Clin Invest* 2001; **108**: 1825-1832.
- 141 Tak PP, Bacchi M, Bertolino M. Pharmacokinetics of IL-18 binding protein in healthy volunteers and subjects with rheumatoid arthritis or plaque psoriasis. *Eur J Drug Metab Pharmacokinet* 2006; **31**: 109-116.
- 142 Marchetti C, Chojnacki J, Toldo S, Mezzaroma E, Tranchida N, Rose SW et al. A novel pharmacologic inhibitor of the NLRP3 inflammasome limits myocardial injury after ischemia-reperfusion in the mouse. *J Cardiovasc Pharmacol* 2014; **63**: 316-322.
- 143 Gourine AV, Poputnikov DM, Zhemosek N, Melenchuk EV, Gerstberger R, Spyer KM et al. P2 receptor blockade attenuates fever and cytokine responses induced by lipopolysaccharide in rats. *Br J Pharmacol* 2005; **146**: 139-145.
- 144 Csölle C, Sperlagh B. Peripheral origin of IL-1beta production in the rodent hippocampus under in vivo systemic bacterial lipopolysaccharide (LPS) challenge and its regulation by P2X(7) receptors. *J Neuroimmunol* 2010; **219**: 38-46.
- 145 Riteau N, Gasse P, Fauconnier L, Gombault A, Couegnet M, Fick L et al. Extracellular ATP is a danger signal activating P2X7 receptor in lung inflammation and fibrosis. *Am J Respir Crit Care Med* 2010; **182**: 774-783.
- 146 Sugiyama T, Oku H, Shibata M, Fukuhara M, Yoshida H, Ikeda T. Involvement of P2X7 receptors in the hypoxia-induced death of rat retinal neurons. *Invest Ophthalmol Vis Sci* 2010; **51**: 3236-3243.
- 147 Arulkumaran N, Unwin RJ, Tam FW. A potential therapeutic role for P2X7 receptor (P2X7R) antagonists in the treatment of inflammatory diseases. *Expert Opin Investig Drugs* 2011; **20**: 897-915.

- 148 He J, Lu Y, Xia H, Liang Y, Wang X, Bao W *et al*. Circulating Mitochondrial DAMPs Are Not Effective Inducers of Proteinuria and Kidney Injury in Rodents. *PLoS ONE* 2015; **10**: e0124469.
- 149 Bergsbaken T, Cookson BT. Macrophage activation redirects yersinia-infected host cell death from apoptosis to caspase-1-dependent pyroptosis. *PLoS Pathog* 2007; **3**: e161.
- 150 Gruden G, Thomas S, Burt D, Zhou W, Chusney G, Grudl L *et al*. Interaction of angiotensin II and mechanical stretch on vascular endothelial growth factor production by human mesangial cells. *J Am Soc Nephrol* 1999; **10**: 730–737.



This work is licensed under a Creative Commons Attribution-NonCommercial-NoDerivs 4.0 International License. The images or other third party material in this article are included in the article's Creative Commons license, unless indicated otherwise in the credit line; if the material is not included under the Creative Commons license, users will need to obtain permission from the license holder to reproduce the material. To view a copy of this license, visit <http://creativecommons.org/licenses/by-nc-nd/4.0/>

## **Appendix C: Statement of Contribution**

Chapter 2 – “Iron overload inhibits late stage autophagy flux leading to insulin resistance.” Won Suk Jahng designed and conducted all experiments with contributions from co-authors, wrote the initial draft and performed all revisions for final publication. It is published in EMBO Reports on August 2019.

Chapter 3 – “Pressure Overload-induced cardiac dysfunction in aged male adiponectin knockout mice is associated with autophagy deficiency.” Won Suk Jahng designed and conducted all experiments with contributions from co-authors, wrote the initial draft and performed all revisions for final publication. It is published in Endocrinology on July 2015.

Chapter 4 – “Disrupted autophagy flux in adiponectin knockout mice exacerbates ischemia-induced cardiomyocyte cell death.” Won Suk Jahng designed and conducted all experiments with contributions from co-authors, wrote the initial draft. Currently, this chapter is in preparation for publication.

Appendix B – “Crosstalk between the heart and peripheral organs in heart failure.” Won Suk Jahng wrote the draft with Dr. G Sweeney. It is published in Experimental & Molecular Medicine on March 2016.